FACULDADE DE CIÊNCIAS E TECNOLOGIA
UNIVERSIDADE NOVA DE LISBOA

Molecular mobility of *n*-ethylene glycol dimethacrylate glass formers upon free radical polymerization

María Teresa Viciosa Plaza

(Graduated in Physics)

Dissertation presented to obtain a PhD. Degree in Chemical Physics

Supervisors: Dr[a]. Madalena Dionísio Andrade (U.N.L. – Portugal)
Dr. José Luis Gómez Ribelles (U.T.V. – Spain)

Examiners:

Dr. Manuel Luís de Magalhães Nunes da Ponte

Dr. José Narciso Marat Mendes

Dr. Joaquim José de Azevedo Moura Ramos

Dr. João Filipe Colardelle Luz Mano

Dr. Simone Capaccioli

Lisbon
2007

Ao António,

aos meus pais,

aos meus irmãos.

“Tudo o que se acaba e não contenta Deus, é nada e menos que nada.”

Sta. Teresa de Ávila

“Bem podem chegar ao cume da vossa actividade profissional, alcançar os triunfos mais retumbantes, como fruto da livre iniciativa com que exercem as actividades temporais; mas se abandonarem o sentido sobrenatural que tem de presidir todo o nosso trabalho humano, enganaram-se lamentavelmente no caminho.”

S. Josemaria Escrivá

REPORTS BY EXTERNAL ASSESSORS

Ph.D. THESIS EVALUATION FORM

Candidate: María Teresa Viciosa Plaza

''Molecular mobility of *n*-ethylene glycol dimethacrylate glass formers upon free radical polymerization.''

by María Teresa Viciosa Plaza,

Faculdade de Ciencias e Tecnologia da Universidad Nova de Lisboa, Portugal.

Report by External Assessor, Professor Graham Williams, Emeritus Professor of Chemistry, University of Wales, Swansea SA2 8ES, United Kingdom.

1. Quality of the written document in terms of its organization, structure and clarity

The research contained in this thesis is of very high quality and makes a substantial contribution to knowledge in the field of molecular mobility in monomeric and polymeric glass-forming materials. The thesis reads extremely well and contains excellent diagrams and figures. It is well-organised and allows the reader to assimilate the aims and achievements of the thesis, whose content ranges over several inter-related topics in the physical chemistry of materials, polymer science and dielectrics science. The descriptions and molecular interpretations of these complex, wide-ranging investigations are made with clarity, originality of thought and with an authority that clearly shows the candidate has an exceptional command and understanding of her results and the subject under study.

2. Innovative character of the work developed

The thesis is concerned with studies, using modern broadband dielectric spectroscopy (BDS) and scanning calorimetric (DSC) techniques, of molecular mobility in monomeric dimethacrylates (DMA) before, during and after their bulk free-radical polymerizations. In addition, the crystallization behaviour of a dimethacrylate monomer is followed using real-time BDS.
These innovative investigations are of current interest since they provide direct, detailed and quantitative information on how molecular mobility, as manifested dielectrically in multiple relaxation regions, changes as a bifunctional monomer is transformed into a solid network-polymer as polymerization proceeds. Such information is new, difficult to obtain by other techniques and will be of considerable interest to international groups that work in both fundamental and applied aspects of polymer science.

3. Scientific quality of the work produced and its scientific impact

The molecular dielectric relaxation processes in these materials have been studied over an exceptionally wide range of frequency (10^{-1} to 10^{+6} Hz) and sample temperature. Also dielectric studies have been made of systems during polymerization and bulk-crystallization. This is made possible using (i) the modern dielectric equipment (Novocontrol Alpha-N Analyzer) in the laboratory of Professor Dionísio. And (ii) two differential scanning calorimeters (DSC), one being a temperature-modulated machine that allowed both thermochemical and thermodynamic information to be obtained as a material underwent both chemical reactions (bulk thermopolymerization) and an apparent phase-change from liquid to glass (and vice-versa) The samples were in the form of thin films (for dielectric) and drops (for calorimetry), so information on the molecular dynamics, thermochemistry and thermodynamic states of these materials could be obtained with high precision for small samples, avoiding uncertainties due to temperature gradients within bulk samples.

All data were processed using modern numerical-fitting procedures available as software with the BDS and DSC instruments. Extensive use was made of deconvolution procedures to separate complex dielectric spectra into component dynamical processes.
The multiple relaxation processes in the monomers, reacting systems and product network polymers were captured by the BDS studies and quantified systematic changes in the apparent dynamic glass-transition (α-process) and local motional processes (β, γ) as monomers transformed into a network-polymer. The DSC data, obtained in parallel, describe and quantify the courses of the polymerizations in each case (including the Tromsdorff autoacceleration/heating effect) and also show, in the case of methyl acrylate/dimethacrylate copolymerizations, how the glass transition region of the copolymer broadens dramatically as the dimethacrylate (DM) component is raised – this is complemented in the BDS data, which show an increasing breadth of the dielectric α-process as the DM component is raised.

The candidate has obtained dielectric and DSC data of high quality for monomers, reacting systems and the product network-polymers. These have been processed to reveal quantitative details of the multiple component relaxation processes in each case. Through determinations of the real-time changes in relaxation strengths, frequency-temperature locations and shapes of these processes during polymerization, the candidate has obtained a clear understanding of how the dynamics of the monomeric species (seen as α, β and γ dielectric processes) change systematically as the system transforms to a solid network polymer for each monomer. In the experiments concerning the crystallization of the monomer EGDMA, both isothermal and cold crystallization methods were studied by the dielectric method. The Avrami exponents for the crystallization kinetics thus determined were compared with those predicted by theories of nucleation-assisted-crystallization.

4. Global comment (use as many pages as necessary)

It is appropriate at this point to summarize my overall assessment of this thesis.

First, the research is multidisciplinary, involving, *inter alia*, aspects of organic chemistry/polymer chemistry (bulk free radical polymerization of dimethacrylates),

physical chemistry/chemical physics/polymer science (molecular dipole relaxation processes, thermodynamics of amorphous systems, glass transition phenomena) and dielectric/electrical and scanning calorimetric measurements of glass-forming materials and their interpretation in terms of molecular processes.

This study of the behaviour of dimethacrylate monomers and their polymerizing systems involved many experimental variables (including different monomers, different polymerization conditions, presence/absence of oxygen; dielectric measuring frequencies, sample temperatures; DSC heating/cooling rates & modulation conditions; ….). The studies were made systematically and with great attention being paid to detail. Hence reproducible results of the highest quality were obtained

Chapter 1 covers the theoretical background relevant to the thesis i.e. glass-transition, structural relaxation, crystallization, multiple relaxation processes in polymers and glass-formers, dielectric relaxation. It is a substantial yet concise, account that covers a wealth of information in its 64 pages and has a extensive list of up-to-date references. Chapter 2 summarizes the dielectric (BDS) and DSC techniques employed in the thesis. Chapter 3 presents BDS and DSC data for three dimethacrylate monomers, which demonstrate the quality of data now obtainable using modern dielectric instrumentation (figs.3.4, 3.5, 3.17) and DSC (figs.3.12, 3.13), while Chapter 4 investigates the real-time BDS and DSC studies of triEGDMA for samples in N_2 and in air – where it is shown how O_2 in the latter case has a large inhibiting effect on the kinetics of the radical polymerization. Chapters 5 and 6 report BDS and DSC studies of DEGDMDA, TrEGDMA, TeEGDMA and TrEGDMA/methylacrylate copolymers, while in Chapter 7 BDS and DSC are used to determine the crystallization kinetics of EGDMA monomer under isothermal and ‘’cold crystallization conditions.

As mentioned above, the dielectric data revealed (i) multiple relaxation regions in both the monomers and polymerizing systems and (ii) how they changed in real-time during the polymerizations. Each relaxation region covers broad frequency ranges so the deconvolution of total dielectric spectra into component α, β and γ processes at each measurement temperature and each time of polymerization required broadband data of high quality and much skill by the candidate in the implementation of the deconvolution procedures. All the BDS and DSC results have been analyzed using contemporary theories of :
(i) mechanisms for local and global motions of chains and how these change as a network-polymer is formed.
(ii) the dynamical nature of apparent glass transitions (Tg) in monomers and network polymers, the Angell concept of the fragility of glasses, the influence of heterogeneity on the breadth of Tg in a network polymer.
(iii) nucleation-assisted crystallization of glass-formers (Chapter 7).
The thesis work has led, at this time, to six substantial papers in leading journals and there are a further nine publications that include Ms Viciosa as a coauthor on work that developed from the thesis.

It is clear from the above that the candidate has conducted work of the highest quality in this thesis, which advances our knowledge of the nature of molecular mobility in monomeric and polymeric systems and how mobility changes, with time, during free-radical-induced polymerizations.

The candidate is to be congratulated on the many fine achievements in this thesis.

My Global evaluation of the thesis is ''Excellent''.

I include below, as an Annexe, some comments that occurred to me on reading through the thesis.

Annexe

Chapter1 Excellent introduction to the nature of the glass-transition and the apparent glass transition temperature Tg.

p.5, 4 up, the dipole moment acts as the molecular probe, thus dielectric relaxation is related to molecular structure and its dynamics.

p.21-22, last lines, the nature of α, β and αβ processes are also considered in refs .42 and 39 (by G Williams) and were defined originally by Williams (see G. Williams Adv. Polymer Science 1979, 33, 59-92).

p.28, for recent use of BDS and real-time BDS, and the Avrami eqn. for crystallization in polymers, see review by G. Floudas Ch.8 in ref.42, especially the papers by TA Ezquerra (refs.82 and 83); see also G. Williams in Adv. Polymer Science 1979, 33, 59-92 for real-time BDS studies of the crystallization of polyethylene terephthalate. For real-time BDS studies of crystallization of low molar mass glass-formers see G Williams et al (i) Faraday Transactions, 1998, 94, 387 and (ii) J Phys Chem B, 1999, 103, 4197.

p.34-40 Clear account of the essentials of free-radical bulk polymerizations.

p.40-59. Good account of basic dielectric theory. I would have wished to see more on the role of molecular dipole moments in the dielectric relaxation theory.

Chapter 2, p.71-86, succint but adequate account of the BDS and DSC instruments used plus theory of complex heat capacity.

Chapter 3, excellent dielectric data for three monomers, as typified by figs.3.4 and 3.17. Deconvolution reveals three processes, fig.3.5, and good discussion of their origins.

The KWW and HN functions give different loss contours so the Colmonero theory can only be approximate, as is found in table 3.1.

A Comment. Compare Tables 3.2 (BDS) and 3.5 (DSC). As found in other studies there are large differences between the {E,m} results of these techniques for the α-process in glass-formers. The apparent activation energies E and fragility values ''m'' from DSC are about 0.5 of those from BDS for the same process. The reason is as follows.

Values from DSC are obtained using eqn.3.5, which only applies to a single relaxation time process. For α-relaxations, plots of the observable (dielectric loss, specific heat) vs. log f/Hz or (1/T) are broadened by the apparent distribution of relaxation times. The variable $(\omega\tau)$ becomes $(\omega\tau)^{\beta}$ in those cases. Thus $\log\omega\tau$ becomes $\log(\omega\tau)^{\beta} = \beta\log\omega + \beta\log\tau$. For temperature variations, as in the DSC scanning experiments,

$$\beta\log\tau = \beta\log\tau_0 + \beta E/RT \qquad \text{..... (1)}$$

so in eqn.3.5 we replace ΔH^* by βE. Since β is about 0.5 this has the effect of doubling the E and m values in table 3.5, bringing them into agreement with those from BDS in table 3.2.

I am not sure if this approach is already known or used in the literature for DSC data. Previous references to the use of eqn.(1) above are to Thermally Stimulated Current

measurements by G Williams et al, Trans. Faraday Soc II, 1973, 69, 1785 for a glass-former and J van Turnhout 'Thermally Stimulated Discharge of Polymer Electrets' p.72.
This analysis may be useful for future work.

Chapter 4. Excellent account of BDS and DSC behaviour during reactions and hence information obtained on different factors affecting the polymerizations.
p.126, these DSC traces show how complex the reaction kinetics become with variation in t_{polym} and with the presence/absence of O_2 (fig.4.8). Also the modulation amplitude affects the kinetics in a complicated way (fig.4.7).
The large apparent ionic conductivities are likely to be due to small amounts of ionic impurities plus initiator in the samples. Nevertheless, the BDS data presented as complex modulus M* provides evidence of a step change in the structure of the polymerizing systems (figs.4.12 and 4.13) so theis use of BDS may have useful applications in monitoring bulk polymerizations in practical systems.
A comment regarding the possibility of phase-separation during these polymerizations. It might be useful to monitor, in parallel, the intensity of scattered light from systems undergoing these reactions.
Chapter 5, excellent description of a highly-detailed and searching study by BDS and DSC of changes in mobility when the three monomers are polymerized. Multiple relaxations are resolved quantitatively and the BDS signature of monomers is detected, and characterized, in the network polymers. Outstanding results (e.g. figs.5.13 and table 5.3).
Chapter 6. Again a wealth of data of high quality (e.g. fig.6.1) for a series of dimethacrylate/methyl acrylate copolymers made as a part of this thesis. Multiple relaxation regions are extracted from the overall BDS curves and their dielectric parameters obtained. The marked shift in the position of the α-peaks to higher temperatures as the dimethacrylate (DMA) content is raised (see the relaxation map (fig.6.6)) reflects the lower local mobility of crosslinked DMA units. The data show that the dielectric α-process in the copolymers is very broad (table 6.3). The DSC data, fig.6.7, shows how Tg increases as DMA content is raised and, significantly, how the transition region broadens remarkably for MA40 to MA10, in accord with the BDS data.
The candidate analyses these results in terms of changes in intra- and inter-molecular interactions in the copolymer networks.
Fig.6.7. The precision given to the values of Tg in fig.6.10 for materials MA40 to MA10 is, in my view, probably too high. In view of the very broad range for the Tg process (being at least 50 ^{0}C in fig.6.7) it appears that the definition of Tg needs re-examination for MA40 to MA10 and that comparison with the predictions of the Fox eqn. would need further consideration.
Chapter 7. For recent use of real-time BDS and Avrami eqn. for crystallization in polymers see review by G. Floudas Ch.8 in ref.42 and in low molar mass glass-formers by G Williams et al (i) Faraday Transactions, 1998, 94, 387 and (ii) J Phys Chem B, 1999, 103, 4197).
The data in the thesis (e.g. figs.7.1 and 7.5) give direct information on the crystallization behaviour with time (e.g. fig.7.6). The Avrami plots are excellent (fig.7.7) and are a further fine achievement in this thesis. Available theories for nucleation-assisted crystallization do not appear to adequately-describe the data – a result also found in other studies thus raising a need to improve theories of crystallization in the bulk.

Also the BDS spectra are able to recognise differences between crystallized samples, and this has been investigated in some detail. With several BDS loss regions being deconvoluted from the overall BDS spectra (e.g. fig.7.13), I found the account to be complicated and difficult to follow. The deconvolution of loss curves shown in fig.7.13 is a difficult task. At -80^0C I might have made the α-process larger, thus lowering the strength of the α' process. At -70 and -60^0C the curves are so broad that several difgferent fittings are possible, so error bounds were desirable on the fits obtained. At -40^0C two MWS curves are suggested, which is difficult to understand for this material.
Regarding the α' process, earlier preliminary BDS studies by Williams and Tidy (see G. Williams in Adv. Polymer Science 1979, 33, 59-92) and, later, more substantial BDS studies by TA Ezquerra for bulk polymers showed that as the strength of the α process decreased during crystallization, a new process, the α' process appeared, due to constrained α-type motions within the growing spherulite polymer crystals. This may be of relevance to the Discussion on p.238 and 253 of the thesis for the present low molar mass glass-former.
There are some additional comments. (i) Add: the times of crystallization on the curves in fig.7.5. (ii) fig.7.15, include in the caption the name of the process (I think is the α-process? (iii) it was not clear in the text why the melt-crystallized curve (open circles) was at significantly higher frequencies than the other curves.

On , the 9th day of December of 2007 .

Signature:

Professor Graham Williams BSc, PhD, DSc, CChem, FRSC,

Emeritus Professor of Chemistry,

University of Wales, Swansea, Swansea SA2 8PP, United Kingdom.

All correspondence should be sent to my home address :-

8 Royal Oak Road, Sketty, Swansea SA2 8ES, United Kingdom.

g.williams6013@ntlworld.com

UNIVERSIDAD POLITECNICA DE VALENCIA

EVALUATION FROM OF THE DRAFT OF THE Ph.D. THESIS WHICH DATA ARE INDICATED IN THE FOLLOWING

DEPARTMENT IN CHARGE: Chemistry Department, Faculdade de Ciências e Tecnologia, Universidade Nova de Lisboa

AUTHOR OF THE Ph.D. THESIS: María Teresa Viciosa Plaza

TITLE OF THE Ph.D. THESIS: ***Molecular mobility of n-ethylene glycol dimethacrylate glass formers upon free radical polymerization***

ADVISERS: Dra. Madalena Dionísio and Dr. José Luís Gómez Ribelles

Dr. José Mª Meseguer Dueñas, selected as external evaluator of the Ph.D. Thesis described before, provides the current evaluation form, upgraded with the speficications in the attachment and concluded as follows:

The Thesis is approved as it is.

València, the 5th of december of 2007 .

Signature: José M. Meseguer Dueñas.

Specifications of the Evaluation Form

1. Existence of concrete objectives and interest in the subject of the Thesis:

The objectives are clearly specified in the Thesis. The study of the molecular mobility in the supercooled liquid and in the glassy state of low-molecular weight glass-formers and the effect on this mobility of the molecular weight, the polymerization to form polymer networks and its vitrification, and the analysis of phase separation as polymerization progresses are objectives of great interest for the field, ambitious enough for a PhD Thesis

2. Existence of a methodologic strategy suited to the proposed objectives:

The methodological approach is based in the study of the properties of a series of n-ethylene glycol dimethacrylates, nEGDMA, using dielectric relaxation spectroscopy, DSR, and temperature modulated differential scanning calorimetry, TMDSC, is very adequate due to the broad frequency interval of the former that allows characerizing very precisely the relaxation processes originated by the different molecular groups, a series of processes that most of the times overlaps in the frequecy and temperature domains. The high sensibility of TMDSC allows to study vitrification of the monomers during polymerization and correlate these data with the DRS results.

3. Interest of the achieved results and conclusions:

A very complete characterization of the dielectric relaxation spectra of the nEGDMA series has been presented. The influence of the length of the ethyleneglycol moiety on the main relaxation process associated to the glass transition of these low-molecular weight glass formers has been elucidated. The polymerization reaction of these monomers has been followed determining the temperature depedence of the conversion at which the system vitrifies and ascribing the phenomenology found to a phase separation between a swollen polymer network and unreacted monomer. The mobility of the residual monomer has been characterized by DRS as polymerization progresses, as well as the secondary relaxation of the growing polymer network. The effect of the presence of a simpler comonomer, methyl acrylate, in the vecinity to the nEGDMA monomeric units has been studied analysing the DRS spectra of MA-nEGDMA random copolymers. On the other hand the crystallization process of EGDMA has been followed using DRS and DSC showing characteristics of the molecular mobility in semicrystalline low-molecular weight substances.

4. Formal characteristics of the doctoral memory:

The formal characteristics of the Thesis memory: its structure, writing, literature references, figures and plots... are adequate for an easy reading and understanding of the work. The organization of the text in several self contained chapters in which some conclusions are reached is a good election to present a so extensive work and numerous experimental results.

5. Observations (use as many as blank pages as necessary):

Finally I want to express my congratulations to the author of this work, Mª Teresa Viciosa, and to her supervisors Dra. Madalena Andrade Dionisio and Dr José L. Gómez Ribelles, for this excellent work.

6. Global evaluation

☐ *Excellent*

València, the 5th of december of 2007 .

Signature: José M. Meseguer Dueñas.

RESUMO

Quando um líquido evita a cristalização durante o arrefecimento, diz-se que entra no estado sobrearrefecido. Se a temperatura continuar a diminuir, o consequente aumento da viscosidade reflecte-se na mobilidade molecular de tal maneira que os tempos característicos se tornam da mesma ordem de grandeza que os tempos acessíveis experimentalmente. Se o arrefecimento continuar, o líquido altamente viscoso acaba por vitrificar, *i.e.* entra no estado vítreo onde apenas os movimentos locais são permitidos. Os monómeros da família n-etileno glicol dimetacrilato (n-EGDMA, para n = 1 até 4, que constituem o objecto deste estudo, facilmente evitam a cristalização, sendo pois bons candidatos para estudar a mobilidade molecular nos estados sobrearrefecido e vítreo. A Espectroscopia de Relaxação Dieléctrica (DRS) foi a técnica escolhida para obter informação detalhada sobre a sua dinâmica molecular (Capítulos 1 e 2).

A primeira parte deste trabalho consistiu na caracterização dieléctrica dos processos de relaxação existentes acima e abaixo da temperatura de transição vítrea (T_g), a qual aumenta com o aumento do peso molecular (M_w), sendo este resultado confirmado por Calorimetria Diferencial de Varrimento (DSC). No que respeita ao processo cooperativo α, associado à transição vítrea, e ao processo secundário β, observa-se uma dependência com M_w, enquanto que o outro processo secundário, γ, aparenta ser independente deste factor (Capítulo 3).

Nos capítulos seguintes, foram levadas a cabo diferentes estratégias com o objectivo de clarificar os mecanismos que estão na origem destas duas relaxações secundárias (β e γ), assim como conhecer a sua respectiva relação com a relaxação principal (α).

Do estudo, em tempo real, da polimerização isotérmica via radicais livres do TrEGDMA por Calorimetria de Varrimento Diferencial com Modulação de Temperatura (TMDSC), levado a cabo a temperaturas abaixo da T_g do polímero final, concluem-se entre outros, dois importantes aspectos: *i*) que a vitrificação do polímero em formação conduz a graus de conversão relativamente baixos, e *ii*) que o monómero que está por reagir é expulso da rede polimérica que se forma, dando lugar a uma clara separação de fases (Capítulo 4). Com base nesta informação, o passo seguinte foi estudar separadamente a polimerização isotérmica do di-, tri- e tetra-EGDMA, dando

especial atenção às alterações de mobilidade do monómero ainda por reagir. Com as restrições impostas pela formação de ligações químicas, as relaxações α e β detectadas no monómero tendem a desaparecer no novo polímero formado, enquanto que a relaxação γ se mantém quase inalterada. Os diferentes comportamentos que aparecem durante a polimerização permitiram a atribuição da origem molecular dos processos secundários: o processo γ foi associado ao movimento *twisting* das unidades etileno glicol, enquanto que a rotação dos grupos carboxilo foi relacionada com a relaxação β (Capítulo 5).

No que respeita ao próprio polímero, um processo de relaxação adicional foi detectado, β_{pol}, no poly-DEGDMA, poly-TrEGDMA e poly-TeEGDMA, com características similares ao encontrado nos poli(metacrilato de n-alquilo). Este processo foi confirmado e bem caracterizado aquando do estudo da copolimerização do TrEGDMA com acrilato de metilo (MA) para diferentes composições (Capítulo 6).

Para finalizar, o EGDMA, o elemento mais pequeno da família de monómeros estudada, além de vitrificar apresenta uma marcada tendência para cristalizar quer a partir do estado líquido ou do estado vítreo. Durante a cristalização, a formação de uma fase rígida afecta principalmente o processo α, cuja intensidade diminui sem no entanto se observarem modificações significativas na dependência do tempo de relaxação característico com a temperatura. Por outro lado, o processo secundário β torna-se melhor definido e mais estreito, o que pode ser interpretado em termos de uma maior homogeneidade dos micro-ambientes associados aos movimentos locais (Capítulo 7).

Palavras chave: transição vítrea, relaxação dieléctrica, formadores de vidro, polimerização radicalar, TMDSC, n-etileno glicol dimetacrilato.

ABSTRACT

When a liquid upon cooling avoids crystallization, it enters the supercooled state. If the temperature continues to decrease, the consequent increase of viscosity is reflected in the molecular mobility in such a way that the characteristic relaxation times of cooperative motions become of the same order of the experimentally accessible timescales. Further cooling finally transforms the highly viscous liquid into a glass, in which only local motions are allowed. The monomers n-ethylene glycol dimethacrylate (n-EGDMA) for $n=1$ to 4, that constitutes the object of this study, easily circumvent crystallization, being good candidates to study the molecular mobility in both supercooled and glassy states. Dielectric Relaxation Spectroscopy (DRS) was the technique chosen to obtain detailed information about their molecular mobility (Chapters 1 and 2).

The first part of this work consisted in the dielectric characterization of the relaxation processes present above and below the glass transition temperature (T_g), which shifts to higher values with the molecular weight (M_w), result confirmed by Differential Scanning Calorimetry (DSC). While the cooperative α-process associated to the glass transition, and the secondary β process, depend on M_w, the other found secondary process, γ, seems to be independent from this factor (Chapter 3).

In the next Chapters different strategies were carried out in order to clarify the mechanisms in the origin of these two secondary relaxations (β and γ), and to learn about its respective relation with the main α relaxation.

Monitoring the real time isothermal free radical polymerization of TrEGDMA by Temperature Modulated Differential Scanning Calorimetry (TMDSC), carried out at temperatures below the T_g of the final polymer network, we shown among others two important features: *i*) the vitrification of the polymer in formation leads to relatively low degrees of conversion, and *ii*) the unreacted monomer is expelled from the highly cross-linked network originating a clear phase separation (Chapter 4).

Knowing that phase separation occurs upon the polymerization reaction, the next step was the separate study of the isothermal polymerization of di-, tri- and tetra-EGDMA, giving special attention to the changes in the unreacted monomer's mobility. With the restrictions imposed by the formation of chemical bonds, the α and β relaxations detected in bulk monomers tend to vanish in the newly formed polymer

network, while the secondary γ relaxation kept almost unaffected. The high sensitivity of the β relaxation to low contents of unreacted monomer was used as a probe of the reaction's advance. These different behaviours shown under polymerization allowed the assignment of the molecular origin of the secondary processes: the γ relaxation associated to the ethylene glycol twisting motions, while the rotation of the carboxyl groups seems to be related to the β relaxation (Chapter 5).

In what concerns the polymer itself, an additional secondary process was found, β_{pol}, namely in poly-DEGDMA, poly-TrEGDMA and poly-TeEGDMA, with similar characteristics to the one found in poly(n-alkyl methacrylates). This process was confirmed and well characterized when the copolymerization of TrEGDMA with methyl acrylate (MA) was studied varying its composition (Chapter 6).

Finally, EGDMA, the smaller monomer of this family, apart from vitrifying, also shows a high tendency to crystallize by coming from both melt and glassy states. The formation of a rigid phase affects mainly the α-process whose intensity decreases without suffering significant changes in the temperature dependence of the characteristic relaxation time. On the other hand, the secondary β process becomes very well defined and narrowest, indicating a more homogeneous environment around the local-motions (Chapter 7).

Keywords: glass transition, dielectric relaxation, glass-formers, free radical polymerization, TMDSC, n-ethylene glycol dimethacrylate.

AGRADECIMENTOS

Agora, no final deste percurso, quando o pensamento principal é "tenho que acabar isto já duma vez!" é difícil pensar nos agradecimentos, e muito fácil lembrar-se só do que se passou nos últimos tempos esquecendo o resto. Contudo, tentando parar para pensar, o primeiro que percebo é quanta pouca coisa teria feito sem ajuda. Uma ajuda que vem de muitos lados e de muitas maneiras.

A todas as pessoas com as que partilhei o lugar de trabalho, uns momentos de conversa, uns almoços… as que prefiro não nomear particularmente para não me esquecer dalguma. De um modo especial a aquelas com as quais já não só se aplica o adjectivo de *colegas*, com as que a partilha ultrapassou o laboratório. Quando a família e os amigos de sempre estão um bocadinho longe o lugar do trabalho é algo mais do que um sítio para *fazer coisas*, também é um lugar para grandes amizades. A elas, também peço desculpas por não ter-lhes dedicado mais atenção ou não ter ajudado com mais empenho. Espero no entanto poder fazê-lo a partir de agora!

A Natália duma forma particular, quem até perdeu o sono pela minha causa! ... como estaria esta tese sem a tua contribuição! Será que algum dia te poderei retribuir este esforço? Graças por estar ao meu lado!

Aos amigos que aqui em Lisboa *ganhei*, às muitas "Luisas" que me acompanham constantemente, à família e amigos de Espanha com os quais a distância nunca foi um problema.

Ao professor Graham Williams, a quem não conheço directamente, mas a quem devo a escolha dos materiais estudados, e os interessantes resultados que deles derivam, (não houve medida que não se aproveitara!!).

A José Luís, por aceitar ser o co-orientador deste trabalho, pelas suas sugestões, para quem qualquer pequena coisa serve para abrir novos caminhos na investigação, mas sobretudo pela sua forma de ser, na qual a simplicidade no trato e a naturalidade são umas constantes.

E especialmente a Madalena, à PROFESSORA Madalena (que ninguém confunda o eu ter-lhe tratado sempre por "tu" com falta de respeito!). Longe ficam nos dias em que comecei a trabalhar com ela, e tantas coisas passaram entretanto que dificilmente poderia esquecer-me dela. Aprendi muito desde um ponto de vista científico sem dúvida ao seu lado, e espero que dalguma forma isso tenha um reflexo neste trabalho. Mas isso, se calhar poderia tê-lo apreendido com outras pessoas… É como ela é o que não poderia ter aprendido de mais ninguém. Sempre me senti afortunada de trabalhar contigo, e sou consciente de ter falado da "minha professora" com certo orgulho, também com admiração, mas sobretudo com carinho. Me sinto afortunada por estes anos contigo e por eles, dou graças a Deus. Oxalá tenha sido capaz de retribuir nem que seja um bocadinho. *Gracias*!

Só Deus sabe porque algumas pessoas são postas ao nosso lado, porque sem apercebermos com elas partilhamos tantas coisas boas no dia a dia e só pontualmente reparamos nisso. Hoje, agradeço vos e agradeço-Lhe por isso!

I would like to thank to **Fundação para a Ciência e a Tecnologia** for the financial support by means of the grant SFRH/BD/6661/2001.

To the **Chemistry Department of FCT – UNL (Portugal)** where most of the work was developed and to **Biomaterials Center of UPV (Spain)** for receiving this student and its research.

GENERAL INDEX

CHAPTER 1 | GENERAL INTRODUCTION: THEORETICAL ASPECTS

CHAPTER 8| CONCLUSIONS

ANNEXES|

FIGURE INDEX

CHAPTER 1 | GENERAL INTRODUCTION: THEORETICAL ASPECTS

SCHEME INDEX

CHAPTER 1 | GENERAL INTRODUCTION: THEORETICAL ASPECTS

CHAPTER 5 | CHANGES IN THE MOLECULAR MOBILITY UPON POLYMERIZATION

CHAPTER 6 | TrEGDMA/MA COPOLYMERS

TABLE INDEX

CHAPTER 1 | GENERAL INTRODUCTION: THEORETICAL ASPECTS

CHAPTER 2 | EXPERIMENTAL

CHAPTER 3 | MOLECULAR MOBILITY IN N-ETHYLENE GLYCOL DIMETHACRYLATE MONOMERS

CHAPTER 1 GENERAL INTRODUCTION: THEORETICAL ASPECTS

1.1. Introduction

It is well known that the macroscopic properties of the materials depend strongly on their chemical structures. Nevertheless, there are other factors that also influence the macroscopic behavior such as the **mobility in a microscopic scale**, or the temperature and pressure conditions.

This work is mainly dedicated to the characterization of the microscopic mobility in both low molecular weight materials and macromolecules in highly viscous states. It is interesting to note that materials with very different chemical structures exhibit molecular mobility with similar features. In the molten state, one of the characteristics of the equilibrium liquid is the high rate of molecular or segmental (in the case of polymeric chains) mobility, the material presenting both translational and rotational mobility. This dynamical behavior suffers drastic changes with the temperature decrease and the liquid will lose or retain different degrees of freedom depending on the transformations suffered upon cooling as well illustrated in the scheme proposed by R. Brand and co-workers [1] here reproduced.

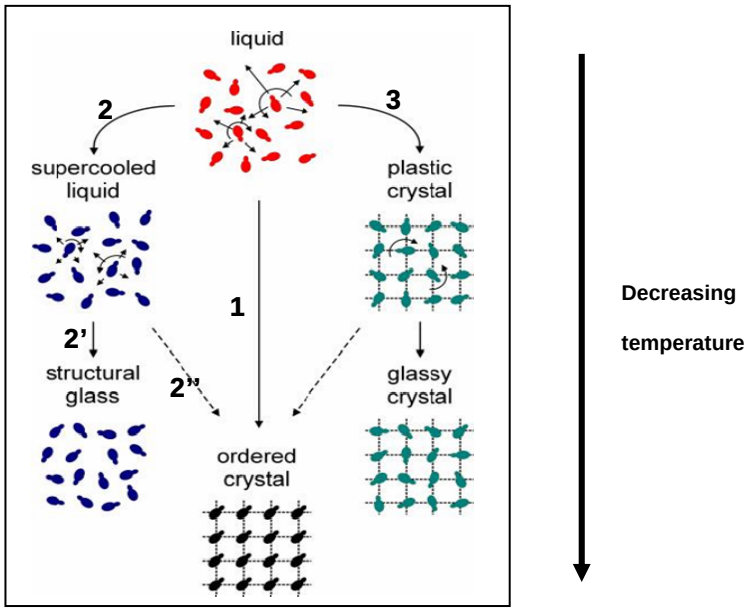

Figure 1.1 Schematic representation of some possible transitions of a liquid of dipolar molecules (represented by asymmetric dumbbells) into a structural glass, an ordered crystal, or a glassy crystal. Reproduced from reference 1.

Mainly, when a liquid is cooled below its freezing temperature it can follow three different pathways: *i*) crystallizing (path 1) loosing translational and rotational degrees of freedom since molecules are fixed in three-dimensional lattices with both positional and orientational order; *ii*) entering an intermediate metastable state (path 2) between liquid and solid keeping translational and rotational degrees of freedom; or *iii*) suffering a transition to a plastic crystal retaining rotational disorder [2] (path 3) or to a liquid crystal (not illustrated in Figure 1.1) with some positional disorder [3], however these type of phenomena were not investigated in the present work. A different possibility, not illustrated, is the transition to a liquid-crystalline mesophase where the material exhibits anisotropic properties between the liquid and crystalline states.

Upon further cooling of the supercooled liquid, the material can crystallize (path 2') in an ordered crystal, or vitrify (path 2'') in a disordered solid with large conformational mobility being frozen although localized reorientational mobility persist (the plastic crystal would freeze to a glassy or ordered crystal).

The reason why crystallization can follow path 2-2' instead of path 1 is due to the complex nature of this process that takes place in two stages: nucleation (the formation of stable crystals germs) and crystal growth. The stability of crystal nucleus is determined by thermodynamic criteria that prove that, in some cases, a stable crystal germ can be formed only at temperatures below the equilibrium melting temperature. When this happens, on cooling, the liquid exists until temperatures significantly below the equilibrium melting beginning to follow path 2. Then crystallization starts provided that there is enough molecular regularity in the material (path 2' from scheme above). Sometimes, the crystallization kinetics is so slow that avoids the establishment of a crystalline phase, especially when the material is rapidly cooled (in this case, molecular arrangements are slower than the cooling rate impairing the build up of a crystalline phase). In some cases crystallization is even unattainable, as in the case of atactic polymers (*i.e.* polymers with random stereochemistry), because the chemical structure of the molecules makes impossible that they fit in a regular crystalline lattice.

Following paths 2 and 2'', the viscosity that determines the dynamical behavior is tuned by temperature changes. However, another form of altering the molecular mobility is to induce the formation of irreversible chemicals bonds that, in the present work, is achieved through the **polymerization** of the initial monomers.

In either case, it will be necessary to obtain information about the **time scale** that characterizes the different molecular events and how it changes under the different conditions: glass formation, crystallization and polymerization.

Macroscopic response of the material can be originated by very different microscopic motions. In the low molecular weight substances for example, simple movements can consist in rotations or in very limited translations of the whole molecule. Complex movements will require cooperative motions with neighbor molecules. In the case of a polymer, the simplest motions can be related to local motions involving rotations around the covalent bonds that link side groups to the main chain or within either side chains or the main chain of the polymer (intramolecular motions). On the other hand, segmental dynamics of the polymer chain is a cooperative motion in which a large number of polymer segments pertaining to different polymer chains participate (intermolecular motions). Other relaxation processes involve large or complete polymeric segment [4] (Rouse dynamics or reptation) as illustrated in the following Figure 1.2.

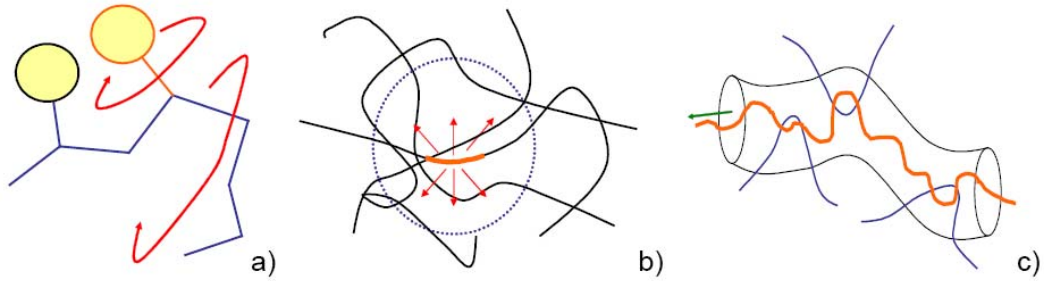

Figure 1.2 Molecular motions that may be found in polymeric systems: a) local mobility, assigned to relaxations occurring in the glassy state; b) cooperative segmental mobility, assigned to glass transition dynamics; c) slower processes, attributed to motions of chain segments between entanglements. Reproduced from reference 4.

In the present work, the main technique used to obtain detailed information about the time scales required for every type of molecular motion, is the broadband dielectric spectroscopy. This method occupies a special place among the numerous modern methods used for physical and chemical analysis of materials, because it enables investigation of dielectric relaxation processes in an extremely wide range of characteristic times (10^{4} - 10^{-12}) s. It offers important and sometimes unique information about the dynamic and structural properties of substances, though it does not allow to assign a given relaxation to a part of the molecular structure, or to inform about the

geometry [5] (jump angles, order parameter,…) of the dynamic process, *i.e.*, it lacks molecular resolution. This information may be obtained through other techniques, such as solid-state NMR, not explored in this work, but covering a very limited time range (order of ms).

As a second technique, differential scanning calorimetry (DSC) was employed. Besides its contribution in the determination of the glass transition temperature of several systems, DSC was especially important in the monitoring of both *i*) polymerization, where it allowed us to investigate the auto-acceleration effect, onset of vitrification under isothermal conditions, and to analyze the influence of several parameters as mass and temperature, and *ii*) crystallization allowing to quantify the degree of crystallization and to extract kinetic information.

1.2. Glass transition: general aspects

If the liquid circumvents crystallization following path 2 as illustrated above, it enters in a metastable state; the liquid in such a state is said to be supercooled (or underercooled). If the temperature continues to decrease, the supercooled liquid will solidify becoming a glass. The evolution from supercooled liquid to a glassy solid is called glass transition, however is a kinetic process, not a proper thermodynamic transition, produced by the impossibility of the material to reach the equilibrium state when the temperature decreases. Thus the glassy state is an out-of-equilibrium state in which the material lacks any molecular order, *i.e.* the material in this sense continues to be a liquid, but the conformational mobility is mostly frozen [6]. As a consequence the substance presents a mechanical behavior similar to that of solid materials, while keeping a disorder typical of liquids, *i.e.* without long-range order (see Figure 1.3).

Far from being an exceptional situation, there are many materials that easily form a supercooled liquid and a glass, thus designated as glass formers. Also in ordinary life, it is common to find situations where the glassy state is crucial. The preservation of life under extremes of cold dehydration and stabilization of labile biochemicals [7], the processing on foods [8,9,10], the improvement of bioavailability in pharmaceutical products [11] are some of several examples in which the glassy state plays an important role.

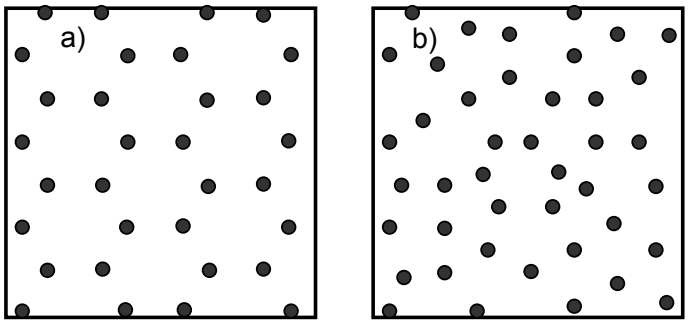

Figure 1.3 Schematic sketches of atomic arrangements in (a) a crystalline solid and (b) an amorphous solid.

This "transition" (we already state that is not a real transition) between liquid and glass takes place in a wide temperature interval (see Figure 1.4). Thus, it is more correct to provide a temperature range instead of a specific temperature; nevertheless, it is common to use the term **glass transition temperature**, T_g, to localize this temperature range (though it will be necessary to specify the method and conditions used to obtain it as we will show further in the text).

A fundamental difference between the crystal or the equilibrium liquid on the one side and the supercooled liquid on the other is the character of metastability that the later presents. The concept of metastable state was introduced by Ostwald [12] to indicate that in this state, although small displacements of the thermodynamic state result in an increase of the free energy of the system, certain large displacements could bring a decrease in the free energy moving the material to a new equilibrium state.

On the other hand, while supercooled regime is an equilibrium situation, in the glassy or vitreous state the material exhibits a new, more "limited kind of metastability" when compared with that of the normal supercooled liquid [13] being unable to establish a equilibrium state within a time range set by the experimental conditions [14]. From a microscopic point of view, the supercooled state is associated to a continuous slowing down of the molecular motions (the characteristic **molecular relaxation time** changes several orders of magnitude from around 10^{-12} to 100 s). This continuous arrest of molecular mobility until vitrification due to an enormous increase of viscosity, can be the result of a temperature decrease or the formation of covalent bonds between individual molecules as already mentioned. Changing the pressure is an example of another pathway for getting a glass [15].

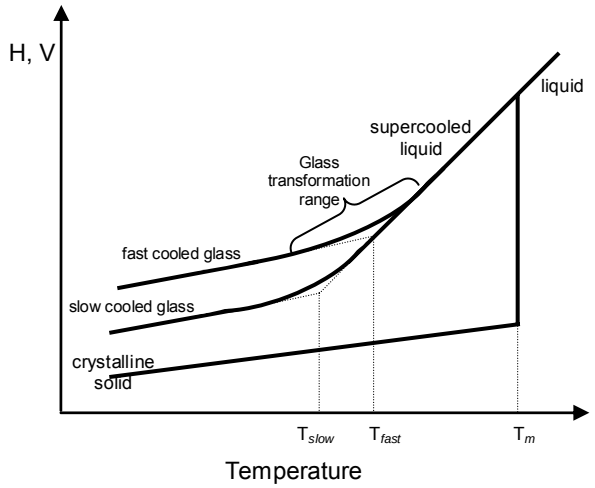

Figure 1.4 Schematic representation of the specific enthalpy or volume as a function of temperature for a liquid that can both crystallize (T_m = melting temperature) or vitrify in two different ways depending on the cooling rate.

Theoretically, nearly all materials can, if cooled fast enough and far enough, be prepared as amorphous solids [16,17], which is to say, if the necessary time to molecular rearrangements is higher than the rate of cooling, the crystallization will not occur. The greater or smaller easiness of a material to vitrify, *i.e.* the *ability* of forming a glass, can also depend on the molecular structure, nevertheless completely structurally different materials as silicates [18], numerous organic liquids as glycerol [19,20], ibuprofen [21], fructose [22] and some polymers [23], circumvent crystallization under moderate cooling rates. As general criteria, a material is considered a glass former if crystallization is avoided even at cooling rates lower than 1 $K.s^{-1}$ [24]. By this way, there is no doubt about the kinetic nature of this process and it is easy to conclude that the attainment of a glass depends on the thermal (or mechanical) history from which it proceeds, being possible to get different glassy states at a given temperature from the same material (see Figure 1.4).

The time scale for molecular motion increases dramatically as a supercooled liquid is cooled toward T_g due to an abnormal viscosity's variation. Close to T_g it is observed that viscosity, η, is extraordinarily sensible to temperature changes: while viscosity values corresponding to the liquid state, are about 10^{-1}-10^{-2} poise, at the glass transition the viscosity is around 10^{13} poise, implying an increment of 13 to 14 decades that occur by temperature changes less than a factor of two!!. This dynamical behavior leads to a more simpler/general description of vitrification where it is claimed that

solidification occurs by a gradual increase of the viscosity rather than by a phase transition [25].

However, given the kinetic nature of the glass transition, it becomes necessary to specify some criteria for defining a characteristic temperature. Depending on the values used, the glass transition is identified as the temperature at which viscosity takes the value of 10^{12} Pa.s [page 245 in ref. 28] (=10^{13} poise [26]); or the relaxation time[a] limit is of 100 s or the onset temperature of the heat capacity step $C_p(T)$. The two former criteria are connected via Maxwell-Kelvin-Voigt's relation [27]

$$\eta = G_\infty \tau \qquad \text{Equation 1.1}$$

where G_∞ is the instantaneous or infinite–frequency shear modulus; for a solidlike material G_∞ takes the value of 10^{10} N.m^{-2} [28].

In the glassy state, the material falls out of the equilibrium keeping a certain molecular mobility. If the glass is kept at a specific temperature for a long time, the molecular rearrangements will tend to reestablish the equilibrium corresponding to a complex process known as **structural relaxation or physical ageing** [29-31]; we will use hereafter the term structural relaxation to refer to it.

The time spent in the evolution to the equilibrium will depend on how far below T_g is the actual temperature, being longer as lower the temperature.

1.2.1 Glass transition and structural relaxation

Structural relaxation is, thus, the process through which an amorphous material tends to attain equilibrium in the glassy state. To understand the kinetic nature of the glass transition, the following example can be considered [32]. A glass former initially in equilibrium at a temperature close but above the glass transition suffers a sudden temperature jump to a lower temperature that takes it to an out of equilibrium state. The subsequent evolution to a new equilibrium state compatible with the new external conditions, it is the structural relaxation. This process involves a decrease in specific

[a] This definition of the relaxation time is not exactly the same of that corresponding to microscopic motions. Nevertheless, the difference is insignificant for the present work, since it is widely believed that different average relaxation times are roughly identical because they basically measure the rate of "flow events" [6].

enthalpy, volume or entropy with time. From now on without losing generality we pay attention to the changes in enthalpy (remember Figure 1.4). We can imagine an equilibrium situation in such a way that enthalpy is determined univocally by two state variables such temperature and pressure, *i.e.* $h^{eq} = h^{eq}(T_0, p_0)$. At this moment we induce a variation in the system by changing instantaneously the temperature to a value T, keeping constant the pressure. This new situation characterized by T and p_0 is out of equilibrium, and the corresponding enthalpy $h = h(T, p_0)$ will evolve in order to reach the equilibrium corresponding to this situation (this is shown in Figure 1.5). The rate at which the material will approach equilibrium depends on temperature in an exponential form. It is possible to distinguish three situations: *i*) if the temperature is high enough, the time required to reach the equilibrium will be very short and the process of structural relaxation can not be detected experimentally (see Figure 1.5 for T_α); *ii*) for intermediate temperatures, like T_β in Figure 1.5, the time employed will be comparable to that of the experiment and the relaxation to equilibrium will be able to be measured in laboratory; *iii*) finally, if the temperature is too low (T_γ in Figure 1.5), the molecular motions that produce structural relaxation will be so slow that we will not be able to follow them during the time of measurement.

If a value for the time t is chosen and we plot enthalpy against temperature, we observe a curve similar to the one shown in the inset of Figure 1.5. For temperatures higher than the interval of the glass transition, the enthalpy value is approximately that of equilibrium, *i.e.* $h(T,t) \approx h^{eq}(T)$. On the other hand, for temperatures well below this transition, the enthalpy is given by: $h(T,t) \approx h(T,0)$, and the instantaneous response of the material or the glass behavior is observed. And for a narrow temperature range a value of the enthalpy intermediate between that of the instantaneous response and the equilibrium one, is observed. This is the temperature interval in which the glass transition takes place. From this representation, the extrapolation of the liquid and glass curves can lead to a possible definition of the glass transition temperature T_g which will obviously depend on the chosen time for the representation.

The main properties of the structural relaxation (entropy, volume or enthalpy) are non-linearity and non-exponentiality [33]. Non-linearity is revealed by the asymmetry in approaching equilibrium. This occurs as a result of the dependence of the relaxation time in both temperature and structure of the glass, as proposed by Tool [34].

The non-exponentiality is a consequence of the existence of a distribution of relaxation times. The evidence of this distribution of times was demonstrated by Kovacs [35].

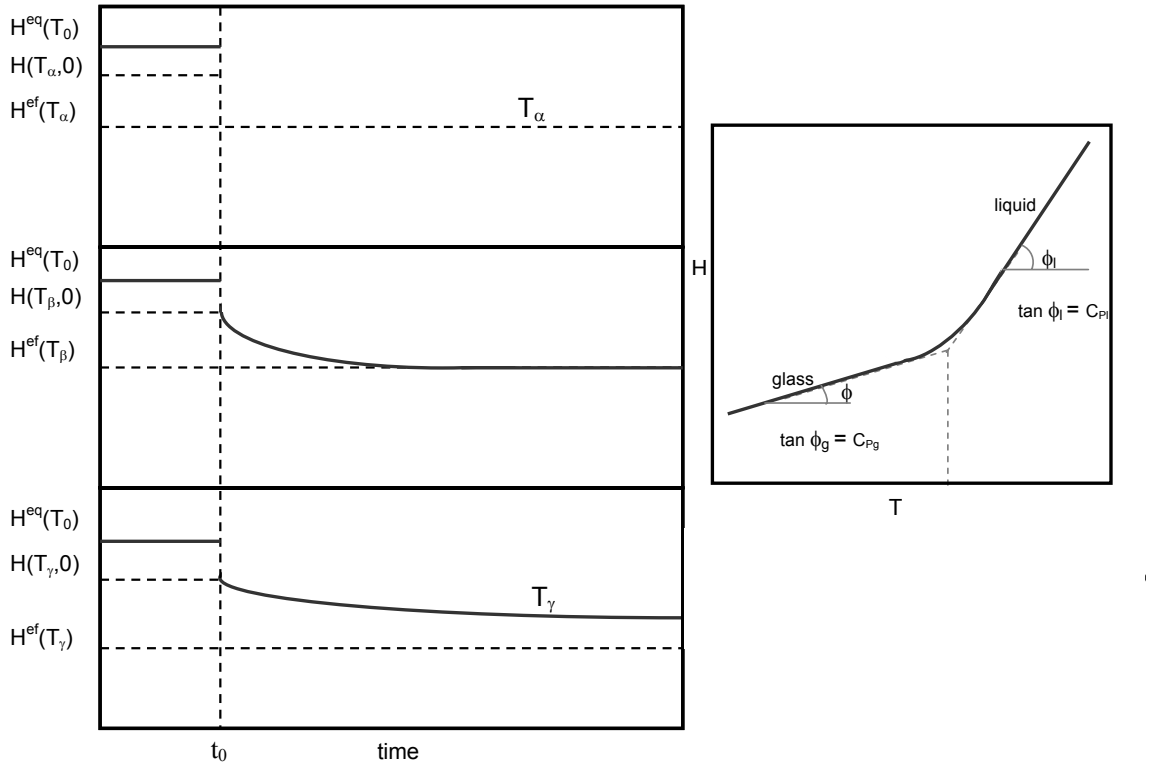

Figure 1.5 Evolution of enthalpy during the structural relaxation process at three temperatures, $T_\alpha > T_\beta > T_\gamma$ (all below T_g). The inset shows the variation of enthalpy *vs.* temperature for a fixed time, t_0 (adapted from reference 32).

Now it is important to emphasize that the glass transition is a translation in a kind of experiment of the existence of the structural relaxation. From this point of view, the physical parameter used to characterize this transition must be specified, since the corresponding sensibility will be different. In other words, using the specific enthalpy or volume, the mechanical module, the dielectric permittivity, or the refraction index will lead to different relaxation times and consequently different glass transition temperatures, though perhaps keeping a correlation (unknown until now) between all of them.

1.2.2 Molecular mobility in polymers and in low molecular weight liquids

When the state of the material is suddenly changed by the application of an external force or an electric field, the response of the material can also be monitored by the time evolution of the appropriate macroscopic properties such as the elastic modulus or the dielectric permittivity. The change in these macroscopic variables is produced by molecular motions that allow the molecules or chain segments to reorganize looking for a new equilibrium state. This process is called a viscoelastic or dielectric relaxation. In this work we will deal with dielectric relaxation processes.

The conformational mobility (*i.e.* molecular rearrangements able to change the spatial disposition of the molecules) determines the behavior of the material in the liquid state. Upon cooling, with the viscosity increase, the molecular mobility is continuously decreasing until the glass transition region is reached, where it becomes so reduced that the time available for intermolecular rearrangements becomes comparable to the time scale of the experiment, originating a structural state frozen-in for practical purposes. The slower a liquid is cooled, the longer the time available for configurational sampling at each temperature, and hence the lower the temperature it can achieve before falling out of liquid-state equilibrium (*i.e.* the lower is T_g) [36].

Nevertheless, in the glassy state the already mentioned slow dynamic process due to structural recovery controlled by long-range diffusion motions, although having very long characteristic times, is not completely frozen [37]. Besides this process there are other mechanisms, below the glass transition, due to localized motions that are the origin of the secondary relaxation processes. Nevertheless, during the experimental time scale where the detection of secondary processes is carried out, the slow dynamics does not affect the measurements and thus, we only will consider here the remaining local mobility.

It is usual to classify the detected relaxation processes in order of decreasing temperature. By this way, the first process found is that corresponding to the dynamic glass transition, named α. The secondary processes that appear after that are designated as β, γ and δ…, corresponding successively with decreasing relaxation times and more and more local mobility.

In the next sections they are described individually with more detail and also the region in which they merge.

1.2.2.1 Cooperative motions: main relaxation

The α relaxation process takes place in amorphous polymers and low molecular weight glass-formers in the liquid state, at temperatures above the glass transition temperature. The application of an electric field to the liquid leads to the reorganization of the material through cooperative conformational motions. The molecular motions in the origin of α relaxation are thus the same which produce structural relaxation. At several degrees above T_g the relaxation times of these cooperative motions are just few seconds and rapidly decreases as temperature increases. This is why structural relaxation cannot be detected at temperatures above T_g by dilatometric or calorimetric techniques whose response times are much longer. Nevertheless, dielectric relaxation spectroscopy (with the instrumentation used in this work) can detect motions with relaxation times as small as 10^{-6} seconds what allows to characterize the α relaxation process at temperatures well above the glass transition temperature. In this sense the α relaxation and the glass transition are related to each other through their molecular origins [38]. On cooling, the glass transition detected by dilatometric or calorimetric experiments takes place when the relaxation times of the conformational rearrangements reach a value in the order of 100 seconds, as already mentioned. In dielectric experiments (see below) performed at a given frequency, f Hz, the α relaxation takes place when the relaxation times of the conformational rearrangements in response to the dielectric field reach a value in the order of $(2\pi f)^{-1}$ seconds.

It is important to note that some authors also designate the dielectric α relaxation as structural relaxation (since that relaxation is associated unanimously to the glass transition phenomenon [38]). In order to avoid confusion, the terminology here adopted will be α or main relaxation for the dielectric relaxation appearing at temperatures above T_g and structural relaxation to the time-dependent process detected in the evolution of the thermodynamical variables approaching equilibrium in the glassy state.

The molecular motions involved in the α relaxation as commented in the introduction, can be very different but always showing a common point: a certain degree of cooperativity which means that a specific part moves together with its environment. In polymers is attributed to micro-Brownian motions of the main chain segments (Schönhals in chapter 3, page 88 in ref. 39, Williams in ref. 40) where several monomers rearrange cooperatively. Therefore, the α relaxation can involve both intramolecular (connectivity within the main chain for polymer's case) and intermolecular (coordinated motion with the environment) interactions. In systems with low molecular weight, the cooperativity is understood as the motion of a molecule (*i.e.* a conformational rearrangement from a site to another one) that needs previous or simultaneous motions of other neighbor molecules.

Since the α relaxation is connected to the strong slowing down of the relaxation rate as approaching the glassy state coming from above, the dependence of the characteristic times with temperature is stronger than the typical Arrhenius behavior. Thus this mechanism involves a temperature dependent activation energy as it can be seen in the relaxation map (Figure 1.6). The apparent activation energy is given by

$$E_a(T) = R\frac{d\ln\tau}{d(1/T)} \qquad \text{Equation 1.2}$$

where R is the ideal gas constant, increases dramatically as T_g is approached. The term "apparent activation energy", is used since it does not refer to a true activation barrier: its value is usually much greater than the dissociation energy of the $C-C$ bond, and consequently if it would represent a true activation energy, it will imply the broken of the chemical bond. Therefore it has no physical or chemical meaning, it just reflects the cooperativity of the underlying molecular motions (41, Schönhals in page 245, chapter 7 in ref. 42).

One of the most successful equations for describing the temperature dependent behavior of the relaxation time near and above T_g, mostly in polymers, is the Williams, Landel and Ferry (WLF) equation [43]:

$$\log a_T = \log\frac{\tau(T)}{\tau(T_{ref})} = -\frac{C_1(T-T_{ref})}{C_2+(T-T_{ref})} \qquad \text{Equation 1.3}$$

where a_T is the time-scale shift factor, τ is the relaxation time, T_{ref} is the chosen reference temperature and C_1 and C_2 are constants. It was initially noted that, when $T_{ref} = T_g$, these constants referred as C_{1g} and C_{2g} assumed "universal" values of C_{1g}=17.4 and C_{2g}=51.6 K. This empirical equation is usually valid over the temperature range $T_g < T < T_g + 100$ K [44]. In this equation it is implicit the time-temperature superposition principle that establishes the equivalence between these two variables [44]. Applying this principle, relaxation curves obtained at different temperatures can be superimposed by horizontal shifts along a logarithmic time scale to give a single master curve covering a large range of times.

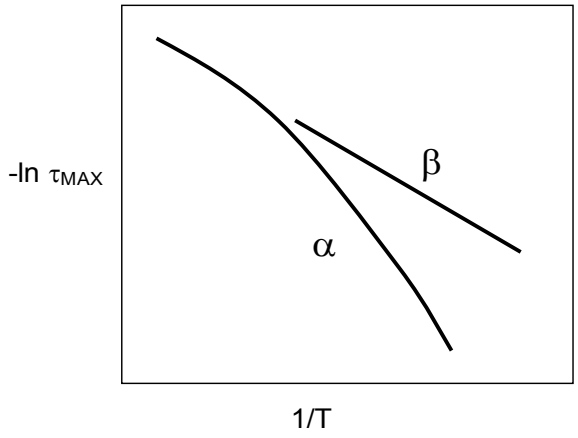

Figure 1.6 Relaxation map: time (or frequency) variation as a function of the reciprocal temperature for the α and β relaxations.

Equation 1.3 is equivalent to the Vogel-Fulcher-Tamman-Hesse equation (VFTH) [45-47],

$$\tau(T) = \tau_0 \exp\left(\frac{B}{T - T_0}\right), T_0 < T_g \qquad \text{Equation 1.4}$$

where τ_0 is a pre-exponential factor corresponding to a time characteristic of molecular vibrations (≈10^{-14} s [48]). τ_0 is seen as a microscopic quantity related to the frequency of attempts to cross some barrier opposing the rearrangement of particles involved in relaxation [49,50], or the time a molecule needs to move into some free space [51,52]. *B* is a constant and T_0 is a temperature that usually is between 30 and 70 ºC below T_g (Schönhals chapter 7 page 245 in ref. 42). This T_0, corresponding to the value where the relaxation time diverges, has been identified with T_K, the "Kauzmann temperature"

[13,53]. T_K is the temperature at which the glass transition must intervene to impede thermodynamic crisis for supercooled liquids[b].

The WLF and the VFTH parameters are related by the following expressions [44]:

$$C_1 = \frac{B}{2.303\left(T - T_{ref}\right)} \qquad \text{Equation 1.5.a}$$

$$C_2 = T_{ref} - T_0 \qquad \text{Equation 1.5.b}$$

The WLF and VFTH equations are the most frequently applied for describing non-Arrhenius behavior, although there exists a wide variety of mathematical representations. In a work of Stickel *et al*. some of the more important formulations are presented and compared [54].

1.2.2.2 Fragility

As mentioned in the previous section, a deviation from thermally activated behavior is a typical feature of the supercooled regime. This reflects in a curvature in the activation plot ($\ln\tau$ *vs.* $1/T$). It becomes useful to evaluate this departure from Arrhenian behavior in order to compare different glass former materials. Angell, based in the T_g-scaled Arrhenius representation of the relaxation time, suggested the classification along a "strong" to "fragile" scale (see Figure 1.7). By this way, a liquid is more fragile the higher is the deviation from the Arrhenius behavior. The fragility index, m, of a substance was defined by Angell as [55,56] the slope at T_g of the curve that describes the dependence between the relaxation time and the temperature reciprocal, *i.e.*

[b] In 1948 Kauzmann pointed out that the entropy of supercooled liquid decreases rapidly on cooling towards the kinetic glass transition temperature, and extrapolates to the entropy of the crystal not far below T_g [13]. Temperature dependence of the entropy of glass intersects that of crystal at so called Kauzmann temperature, T_K. If the entropy of the supercooled liquid becomes lower than that of the stable crystal, it would eventually become negative at sufficiently low temperature, thereby violating the Third Law of Thermodynamics. This situation is named Kauzmann's paradox or entropy crisis. To avoid the entropy crisis, the glass transition must intervene, in order for the entropy of the glass to remain positive, forming an "ideal glass" at T_K.

$$m = \left.\frac{d\log(\tau)}{d(T_g/T)}\right|_{T=T_g} \qquad \text{Equation 1.6}$$

As shown in Figure 1.7, stronger liquids present a fragility value about 16 [56], limit value found for Arrhenius behavior where the pre-exponential factor is about 10^{-13}-10^{-14} s and the relaxation time at T_g is 100 seconds.

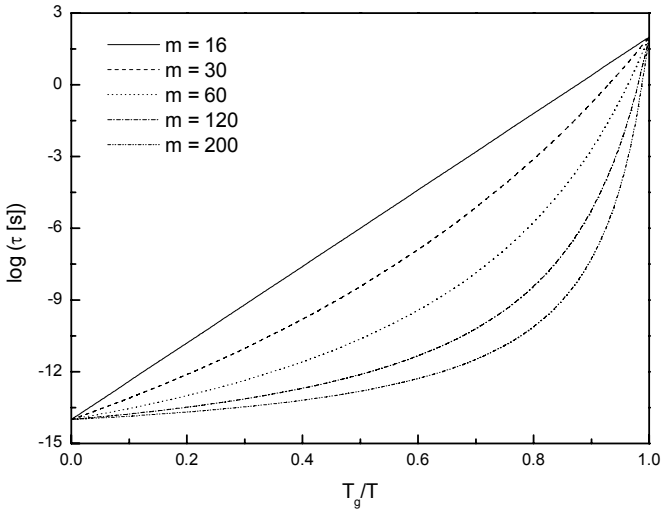

Figure 1.7 Relaxation time as a function of reciprocal temperature normalized to unity at T_g defined for $\tau = 100s$, for materials with different fragilities. The VFTH equation was used to estimate the value of the relaxation time using the m index as independent variable ($\log\tau = \log\tau(T_g) - m_{\min} + m_{\min}^2 (T_g/T)/[m-(m-m_{\min})T_g/T]$) [57].

The physical meaning of the fragility index is related to the complex topology of the potential energy surfaces (see chapter 4, page 305 in ref. 28). The set of available minima of potential energy (connected between them) for a given temperature, allows the system to change the structural configuration only as a consequence of small oscillations of temperature. If the density of minima is high and their depth is relatively low [58], the material will present a high sensibility to temperature changes that corresponds to a fragile material. On the other hand, if the density of minima is low, the liquid will not change easily its conformational structure with increasing temperature, being classified as strong. In other words, strong materials possess a rigid structure that tends to keep the short and intermediate order when heating above T_g, whereas in

fragile ones the temperature increase, easily induces the loss of this order, the larger the jump in C_p observed at the glass transition [20].

Thus, fragility is a central parameter in glassy state physics reflecting the stability of the structure to temperature changes in the supercooled regime.

The structure associated to typical strong liquids consist in a three-dimensional network of covalent bonds [59], while fragile liquids [60] must be related to molecules that present tendency to form only weakly directional or even nondirectional bonds and noncovalent interactions.

Although being the most commonly used method, the tentative to capture in a single number the relative behavior of liquids in the glass transition region does not end with the Angell's definition of fragility. In fact, it has been noted that this definition implies that small variations in the slope taken at T_g that dependent on the author's subjectivity, lead to relatively big changes in the value of the fragility index [61]. In order to bypass this problem several proposals have been raised; in reference 61 some of them are presented.

1.2.2.3 Local motions: secondary relaxations

The β relaxation (or any secondary relaxation) is usually less intense than the α relaxation. Differently from the later, all secondary processes are simple thermally activated, what means that the temperature dependence of their relaxation times is Arrhenius type (Schönhals in ref. 39):

$$\tau(T) = \tau_0 \exp[E_a / RT] \qquad \text{Equation 1.7}$$

where τ_0 is the relaxation time at infinite temperature, and E_a is the activation energy representing the potential barrier resisting the molecular rearrangement [62]. Whatever the origin of the potential barriers, intermolecular or intramolecular, the associated motions must be much simpler and more local than the α relaxation in order to present an Arrhenius behavior.

Other formalism used to describe the temperature dependence of τ was proposed by Eyring who developed the theory of thermally activated states for giving the relation [63]:

$$\tau = \frac{h}{kT}\exp\left(\frac{\Delta G^{\neq}}{kT}\right) \qquad \text{Equation 1.8}$$

where *h* and *k* are respectively the Planck and Boltzmann constants, and $\Delta G^{\neq}$ is the Gibbs free energy, which is related to the activation enthalpy ($\Delta H^{\neq}$) and activation entropy ($\Delta S^{\neq}$) by:

$$\Delta G = \Delta H - T\Delta S \qquad \text{Equation 1.9}$$

By algebraic manipulation it is possible to relate the parameters from previous equation:

$$\Delta H^{\neq} = E_a - kT \qquad \text{Equation 1.10.a}$$

$$\frac{\Delta S^{\neq}}{k} = -\ln\tau_0 + \ln\frac{h}{kT} - 1 \qquad \text{Equation 1.10.b}$$

The fact that secondary relaxations involve independent molecular motions is reflected in the Eyring formalism [63] by a nearly null activation entropy which leads to a τ_0 value of the order of 10^{-14} s for T = 273 K (Equation 1.10.b). For truly activated processes τ_0 should be of the order of 10^{-13} to 10^{-14} seconds. If this parameter is lower than those values, other factors like activation entropy must contribute to the process (page 86 in ref. 39).

For the particular case of polymeric systems, the secondary processes correspond to either limited in-chain movements or hindered rotations of side groups about the bond linking it to the main chain (or of its subunits) that can occur independently of the backbone movements, or even conformational changes in cyclic side groups (chapter 5 in ref. 38). For main-chain motions in hydrocarbon based polymers the Schatzki crankshaft mechanism (Figure 1.8) is thought to play an

important role [64]. The author showed that eight CH_2 units could be lined up in a way that the motion about the two collinear bonds 1 and 7 and the carbon atoms between bonds 1 and 7 move in a manner of crankshaft.

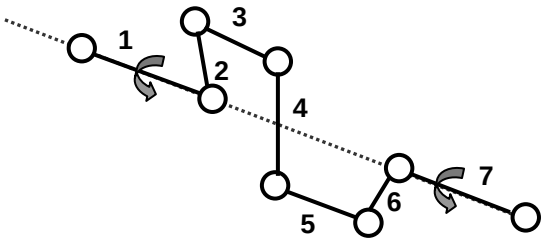

Figure 1.8 Schatzki crankshaft mechanism. Reproduced from reference 64.

Heijboer [65] suggested that the β relaxation time is determined by a local barrier within the molecule, assumption reasonable in the case of polymers. In low molecular weight materials as the epoxy resin cresyl glycidyl ether (CGE), the secondary relaxation (γ) has been assigned to the most mobile dipolar group, *i.e.* the ether group [66]. In the diglycidyl ether of bisphenol-A (DEGBA) epoxy resins, two secondary relaxations are found [66]: a β process assigned to the molecular moiety containing an hydroxyl group, that could be rather weak because it is only present in one in ten molecules, and the more intense γ process with the same molecular origin as the γ relaxation found in CGE.

Nevertheless, the molecular origin of the β relaxation is not completely understood, being observed in a variety of materials other than polymers, including glass-forming liquids made of simple molecules that do not have internal modes of motion [67,68,69,70,71] as is the case of ionic liquids [72]. It seems then to be a near-universal feature of the amorphous state, as proposed by Goldstein and Johari [67], thus called the Johari-Goldstein process, envisaging the motion of the molecule as a whole.

1.2.2.4 αβ splitting region

As mentioned before, the relaxation times of α process show strong temperature dependence, described by the VFTH equation, while the temperature dependence of the secondary processes follows an Arrhenius-type behaviour. Therefore, in a logarithmic

plot of the relaxation time *vs*. the reciprocal of temperature (activation plot), the α process corresponds to a curved line, while the β process is a straight line (as previously shown in Figure 1.6). At temperatures well above T_g the time scales of both relaxation processes tend to converge, because $\log(\omega_\alpha)$ increases faster than $\log(\omega_\beta)$ with the temperature increase. Consequently, with increasing temperature, the two process α and β come close together and eventually merge in a single process. Many authors named this merged process as $\alpha\beta$ but this notation may induce in error leading to identify this process as a simple junction of α and β. Since it was proven that this could not be true it has been proposed to call it a. The region where the separation occurs is designed by $\alpha\beta$ *splitting* or in a more general way as *crossover region*, due to the possibility of defining more than one merging region when multiple secondary processes are detected. Corezzi *et al.* [73] named this region as *the temperature-frequency region where changes take place in the dynamic behaviour of the system*.

Recently the interest in understanding the crossover region is growing up given that it is thought that it plays an important role in the complex phenomenon dynamic of the glass transition [74]. Questions like at which temperature and frequency does the cooperative α dynamic sets in for a given material or does the development of the cooperative process influence the local relaxation, seem to be intimately related with the convergence scenario for main and secondary relaxations.

The characteristic relaxation time values at the merging temperature ($\tau_{\alpha\beta}$) has been given for several glass-forming liquids in a typical range from 10^{-6} to 10^{-8} s [75]. The temperature interval where crossover effects are felt is about ($1.2T_g$ - $1.4T_g$), but large variances occur for different substances (see ref [76] where Beiner *et al.* compiled data for 38 different glasses).

However, the crossover region between α and β processes presents different profiles. In Figure 1.9 the two principal profiles are schematized in accordance with Schönhals [39] and Garwe [77, 78].

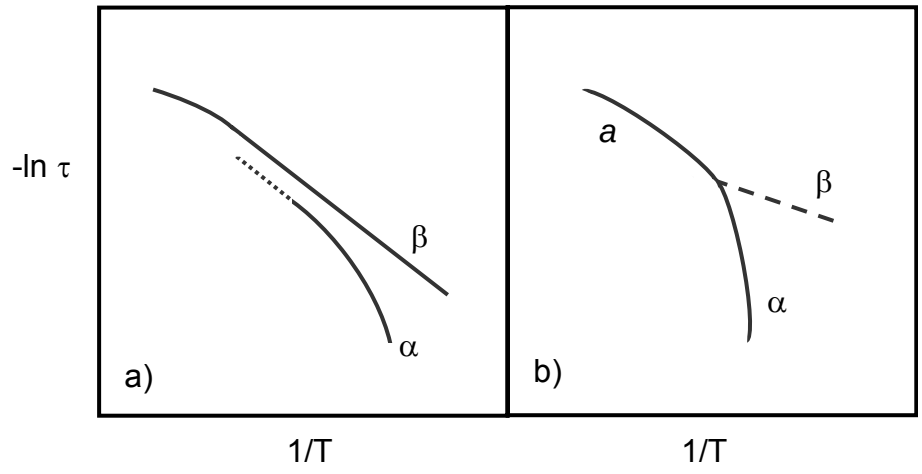

Figure 1.9 Two general scenarios suggested for the splitting region in the Arrhenius diagram schematically (adapted from reference 78).

In scenario (a), an extrapolation of the low temperature behavior of τ_α and τ_β shows that the two processes are always separated, *i.e.* the relaxation time of the α process is always higher than the corresponding to the β process. The slope of the β process trace in the Arrhenius diagram does not change significantly when the α approaches. The separate α onset (*i.e.* the starting temperature for this process) can possibly be characterized by a minimal cooperativity for the α process that can not be continued by a local, non-cooperative process [77,78,79]. The poly(*n* butyl methacrylate) [77] and the low molecular weight epoxy resin EPON828 [80] are two well structurally different materials presenting a separate onset according to the topology of Figure 1.9.a. Even in crosslinked PBMA with 10% w.t. of EGDMA this scenario is kept [81].

This behavior was also predicted by Schultz [82] that considered the β process as a Johari-Goldstein relaxation, supporting the idea that this process is generated by a second process which is partially independent from main relaxation processes.

Anyway, this landscape does not admit that the a process is a simple continuation of the α, but it is strongly determined by the β relaxation.

In scenario (b), the main feature in this landscape is that at a certain temperature the trace of the a process changes in such a way that two new processes are originated, the α and β. This clear differentiation between a and α has been perceived as an indication of the onset of the intermolecular cooperativity [83] and in accordance with

Sokolov [75], it is a demonstration of the non monotonic nature of the glass transition. Also some recent studies, in which a derivative data evaluation method [54] is used, show that the temperature T_B (crossover temperature defined by the intersection of two VFTH laws) is very close to that corresponding to τ_β (the time where structural and secondary processes approach each other). In other words, the coupling of the secondary relaxation leads to changes in the cooperativity. This differentiation between the processes below and above τ_β was already noted by G. Williams in 1966 [84] for poly(ethyl methacrylate). Measurements made with heat capacity spectroscopy for example in PnHMA, also confirm that the main relaxation consists of two calorimetrically distinct parts [85]. Because of this, the application of temperature-time superposition holding below $\alpha\beta$ splitting region can not be recommended for the characterization of the high temperature a process above the crossover region [86].

An open and debated question is whether the trace of the process a follows a VFTH or an Arrhenius behavior. Goldstein and Johari [67,69], for example, considered that above a certain temperature (higher than T_g) no cooperative rearrangement is required [87] and the activation energy of the merged process was the same as the β one. Garwe *et al.* [78] found also an Arrhenius behavior in poly(ethyl methacrylate) (PEMA), but with larger activation energy than that of the β process. The later seemed to act as a precursor of the cooperativity of the α process, what was interpreted as an indication of a locally coordinative mobility in the origin of the β process. Studies carried on alkyl acrylates and alkyl methacrylates interpenetrating polymer networks also shown this coalescence scenario where the secondary β relaxation and the main α process merge to a single process [88,89].

On the other hand, some studies do not support this possibility (chapter 4 in ref. 42), and only accept the VFTH law for the high temperature process.

1.2.3 Molecular mobility in light of the Adam Gibbs theory

Theories of the glass transition fall essentially into two categories each with its own approach: thermodynamic and kinetic. The most famous theories in the first category are from Adam and Gibbs [49] using the entropy as fundamental variable, and that from Doolittle [90] based in the concept of free volume.

Since the work presented in this thesis is mainly experimental we choose to describe in detail only the Adam Gibbs theory that seems to be gaining strength and popularity in recent years.

Adam and Gibbs assuming the relation VFTH for describing the dramatic increase in the relaxation times near T_g, developed a thermodynamic theory in order to attribute a physical meaning to parameters appearing in that empirical equation.

In this theory the new concept of cooperatively rearranging regions (*CRR*) arises and it is used to define the smallest region inside a material that allows a transition to a new configuration without requiring a configurational change outside its boundary [49]. When a liquid is supercooled, the size of these regions increases as a consequence of the increase in the number of unities that moves in a cooperative manner. This increased cooperativity is a reflection of the loss of configurational entropy due to the decrease in the number of minima of potential energy that are available. The Adam-Gibbs theory establishes a link between configurational entropy and the molecular relaxation time.

The temperature-dependent relaxation times in liquids are determined by the average probability of cooperative rearrangements, $\overline{W(T)}$, *i.e.*

$$\tau(T) \alpha \frac{1}{\overline{W}(T)} \qquad \text{Equation 1.11}$$

In order to determine this transition probability the macroscopic system is considered as a set of *N* equivalent and independent subsystems, from which, *n* (*n*<*N*) allow cooperative transitions. Every of these subsystems contain *z* molecules (or monomeric unities) at temperature *T* and pressure *P*. Using the statistical-mechanical formalism, the average probability of transition results:

$$\overline{W(T)} \approx \overline{A} \exp\left(-\frac{z^* \Delta\mu}{kT}\right) \qquad \text{Equation 1.12}$$

where $\Delta\mu$ represents the potential energy hindering the cooperative rearrangement per monomeric unity. This equation indicates that the majority of the cooperative transitions occur in regions with the minima size allowed, z^*. In other words, z^* monomeric

unities must rearrange in order to allow a transition between two states inside a *CRR*. This value depends on the available conformations at the corresponding *CRR*,

$$z^*(T) = \frac{N_A s_c^*}{S_c(T)} \qquad \text{Equation 1.13}$$

with N_A the Avogadro's number and $s_c^* = k \ln \Omega^*$ is the configurational entropy for the smallest *CRR* (Ω^* is the number of available states for this *CRR*), and $S_c(T)$ is the macroscopic configurational entropy.

Thus, the Adam and Gibbs's theory leads to the next relation for the relaxation time:

$$\tau = \tau_0 \exp\left(\frac{z^* \Delta\mu}{k\,T}\right) = \tau_0 \exp\left(\frac{B}{TS_c(T)}\right) \qquad \text{Equation 1.14}$$

showing that upon vitrification, a decrease in the number of available configurations to the system is associated to an amazing increase in the characteristic relaxation times. In terms of the new concept of *CRR*, the molecular motions in a liquid are characterized by an increase in the size of this region or in other words, an increase in the cooperative length, $\xi(T)$ (see Figure 1.10).

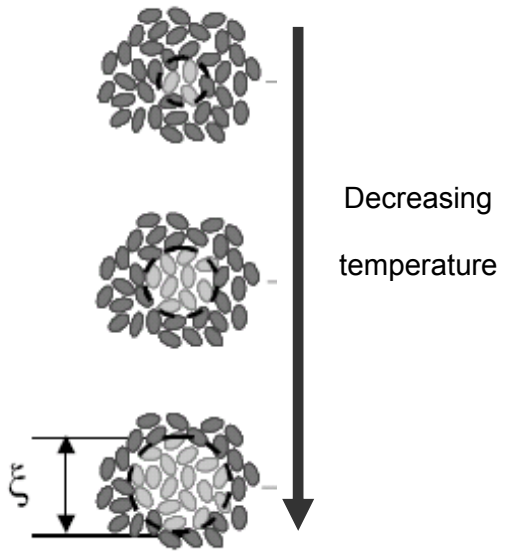

Figure 1.10 Schematic representation for the increasing cooperative region with decreasing T near the glass transition (reproduced from ref. 111).

Finally, the macroscopic configurational entropy, $S_c(T)$, can be calculated in a thermodynamic equilibrium state assuming that the conformational specific heat capacity is equal to the difference between the heat capacity of the liquid and glassy states, ΔC_p, *i.e.* the glass transition is exclusively due to conformational rearrangements and in the glassy state this parameter is null. Also it is accepted in accordance with Gibbs and DiMarzio [91] theory that the configurational entropy in equilibrium at temperature T_0 is null. Taking in account these assumptions, the next relation (for equilibrium) is obtained:

$$S_c(T) = \int_{T_0}^{T} \frac{\Delta C_p}{T} dT \qquad \text{Equation 1.15}$$

Now, taking up again the convergence scenarios described in section 1.2.2.4, we will try to relate them with the Adam and Gibbs formalism in a qualitative manner.

The concept of *CRR* introduced by Adam and Gibbs has been largely used to explain changes in mobility near T_g. Fredickson in 1988 [92] described the supercooled liquids as possessing strong constrains on the dynamics of the individual atoms or molecules. In this scenario a particular molecule is trapped by its neighbors in a "cage", in which it may persist for long period of times. The idea of cage is based in the concept of cooperative rearranging region.

At high temperatures, successive steps of molecules escaping from the interior of the cage give rise to long-range diffusion. The free volume existing in the cage, facilitates the molecular motions in order to create a hole for the molecule to escape (see Figure 1.11). Approaching the crossover region, the decrease in temperature jointly with the increase in density lead to a progressive trapping of the molecule in the cage. At a certain temperature, this type of diffusion and consequently the associated processes, a, vanishes.

Cooperativity starts when the process a splits in two different processes, α and β. From this point, the behavior can be described by using the concept of cooperatively rearranging regions. Initially, the homogeneous liquid is composed by equivalent systems. With time, this picture evolves by diffusion effects also generated by cage escape, but now conditioned to molecules near defects. In this situation, the α process corresponds to this constrained diffusion [93] different from that at higher temperatures

(see Figure 1.11). Here, the necessity of defining a cooperative distance, $\xi(T)$, similar to the average size of the *CRR*, naturally arises.

Below T_g, the cooperative diffusion extinguishes and only localized motions around the free volume existing in the proximity of the defects persist. This interpretation reconciles the Johari's island of mobility picture [94] with the concept of *CRR*, where the β process is assumed to be a localized motion in the inner, less dense and more mobile part of the *CRR* (Figure 1.11).

Theoretical developments [95] within the so-called coupling model (CM) introduced by Ngai and co-workers [96] seem to point in the direction of a universal slow β relaxation closely connected to the glass transition process; in this context the term 'slow' is used to distinguish from 'fast' β process, predicted by the mode coupling model (MCT), ascribed to fast relaxations and observed in a variety of glass formers in the GHz region (97 and refs. cited therein).

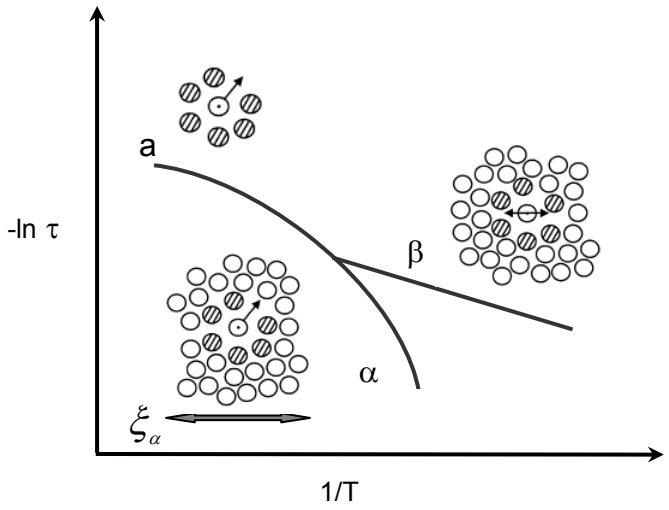

Figure 1.11 Schematic molecular pictures for the diffusive high temperature **a** process (cage escape), the diffusive low-temperature α process (cooperatively-assisted cage escape), and the finite β process (adapted from ref. 93).

More recently, a special relevance has be given to the quantitative determination of the number of molecules or monomeric units in a cooperatively rearranging region, N_α, and its dependence with the temperature. Calorimetric parameters obtained from heat capacity spectroscopy (HCS) has been used to calculate N_α as the ratio between the volume of the *CRR*, $V_\alpha = \xi_\alpha^3$, and the mean volume of one molecule

[98,99,79,100]. In PPGE and DGEBA for example, the N_α was estimated around 75 and 110 molecules in the proximity of their respective T_g [73], corresponding to cooperative lengths of 3.3 and 3.8 nm for PPGE and DGEBA respectively.

Using the Adam-Gibbs formalism a cooperativeity length at the glass transition temperature of 2-3 nm was found for PVAc as reported in reference 101.

This parameter becomes very useful in the study of the crossover region because it allows the estimation of the temperature at which the cooperativity starts, from the extrapolation for $N_\alpha(T) \to 0$. The representation of N_α *vs.* T is usually [102] fitted by the relationship $N_a^{0.5} = A(1-x)/x$, where A is constant typically between 2 and 15 [103], and x a reduce temperature taking values between the Vogel temperature ($x = 0$) and a formal cooperativity-onset temperature ($x \to 1, N_\alpha^{0.5} \to 0$).

1.2.4 Crystallization

Since the formation of a glass material depends on the cooling rate, it is easy to find circumstances in which crystallization can superimpose to vitrification. Obviously, if this happens and the temperature continues decreasing, the incipient crystallization will be arrested. In the final product, the crystalline and amorphous phases will coexist, and the corresponding molecular mobility can be different from the totally amorphous or crystalline (no mobility) material. Since in this work one of the monomers presents this behavior, it was considered important to describe crystallization with some detail [104,105].

1.2.4.1 Mechanisms and conditions for crystallization

The crystallization of a homogeneous liquid does not occur in the whole volume at once, but it starts by discrete centers that arise in a random way, after which they extend for the whole volume. Keeping this in mind, during crystallization process two different stages must be considered:

a) Nucleation: it consists in the formation of point ordered regions. These points appear and disappear in accordance with structural fluctuations induced by thermal oscillations. When this ordered points reach a fixed size (critical size), they become a real focus of development of the crystalline phase, and after this moment, they will be named nuclei.

If the initial phase is structural, chemical and energetically identical in all its points, the appearance of nuclei will be completely random. The existence of inhomogeneities (as is the case of impurities) originates regions whose required energy for the nuclei formation is lower, and the process is not more randomized.

b) Growth: when the nuclei are already formed, molecules or polymer segments from the liquid phase near to the crystal surface start to add in a progressive way.

In order to determine the kinetic of crystallization, two magnitudes must be defined: the number of nuclei produced by time and volume unity that is the nucleation rate (*I*); and the rate at which these particles grow, known as growing rate (*u*). Both are temperature dependent as shown in Figure 1.12.

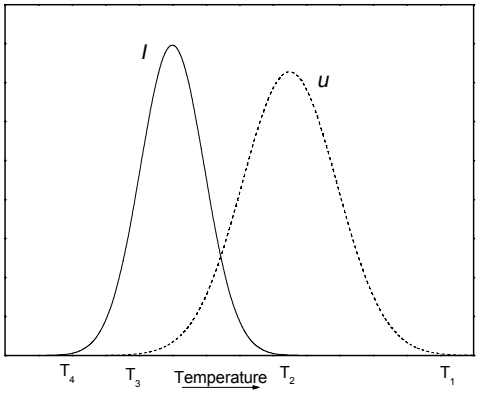

Figure 1.12 General profiles for nucleation (I) and growing rate (u) during crystallization (adapted from reference 105).

To determine if a liquid will crystallize upon cooling it is necessary to pay especial attention at the critical region comprised between T_2 and T_3, *i.e.* the temperature interval in which the curves overlap and also the absolute values of the rates I and u in this region. If this region is narrow, or crystallization and nucleation rates are small or even both things happen, the crystallization will not be possible or, it occurs in a nearly imperceptible manner. In contrast, if the rates I and u are high and the overlapping region large, the total crystallization can easily be reached. In intermediate situations, a partially crystallized material will be obtained.

1.2.4.2 Classical theory of homogeneous nucleation

The classical theory for homogeneous crystallization starts from a principal assumption: the existence of a thermodynamic barrier of nucleation and the statement of conditions for a rate of nucleation in a stable state, determination of the temperature dependence and the liquid nature.

The simplest model was proposed by Volmer and Weber [106], and Becker e Döring [107], and it assumes as starting point that the aggregates that are in the origin of the formation of stable nuclei present identical properties and composition, and the only difference is in shape and size.

On the other hand, as a first approximation, the shape's aggregate is spherical, avoiding differences originated by several crystallographic orientations. By this way, the size will only depend on the conditions imposed by the thermodynamic stability.

From Figure 1.13, at the melting temperature, T_f, the free molar energy (G) of liquid and crystalline phases are equal. If the material passes through the supercooled or superheated states, it will have an increase in the free molar energy (per volume), (Δg_v), negative in the first situation and positive in the last one.

With nuclei or embryo formation, an interface arises whose free energy per volume can be estimated, (Δg_s). Therefore, for spherical nuclei, the free energy associated to the formation of one of them will be:

$$\Delta g_r = \frac{4}{3}\pi r^3 \Delta g_v + 4\pi r^2 \Delta g_s \qquad \text{Equation 1.16}$$

Calculating the maximum for this free energy as a radius function, it is possible to determine a critical radius, $r^* = -\frac{2\Delta g_s}{\Delta g_v}$, and from this, to estimate the minimum energy for the formation of a stable nucleus, $\Delta g_r = W^*$, and consequently the number of molecules contained in the corresponding volume minima.

The temperature dependence of r^* and W^* can be written in terms of "supercooled degree", *i.e.* the difference between the equilibrium melting temperature and the nucleation temperature, $\Delta T = T_f - T$, obtained from thermodynamic equations.

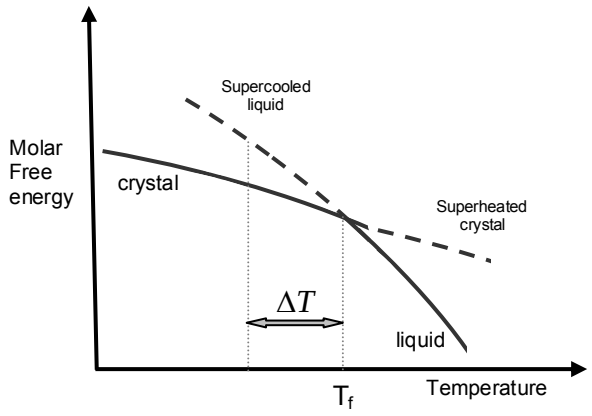

Figure 1.13 Variation of the molar free energy with temperature.

In order to determine the rate of nuclei formation (I) it is necessary take into account the random character of size and distribution of nuclei, and also the free energy of activation ($\Delta G'$) needed for molecules to add to the nucleus in formation, by diffusion mechanisms.

The growth rate (u) on the other hand, will be dependent of both the tax with which the molecules spread on the surface of the crystal and also the way they pass through the interface.

1.2.4.3 Kinetic criteria for crystallization

Taking into account that crystallization depends on both, growth of interface and diffusion of atoms to crystalline phase, it is possible to determine the critical speed to glass formation.

With analytical expressions for the nucleation rate (I) and the growth rate (u), the crystal formation can be quantified from the limit values for the kinetic barrier for nucleation ($\Delta G'$) and the free energy barrier for transferring atoms in the direction liquid to crystal ($\Delta G''$).

The minimum values were estimated by Turnbull and Cohen [108] as being 1 nucleus.cm^3.s^{-1} for $I_{\min}$ and 10^{-5} interatomic distances.s^{-1} for $u_{\min}$. Above these values the crystallization is unavoidable. As a consequence, it was established that crystallization can be avoided if either it is not possible to find a temperature T' below the melting temperature, T_f, for which nucleation rate is superior to $I_{\min}$, or if this temperature T' exists, the growth rate u always remains less than $u_{\max}$. If these

conditions are fulfilled, the kinetic barrier for nucleation ($\Delta G'$) and the free energy barrier for transferring atoms in the direction liquid to crystal ($\Delta G''$) will correspond to values higher than $20RT_f$.

In what concerns the nature of glass-formers, it is generally accepted that a high viscosity at the melting point and a rapid increase in viscosity as the temperature falls below the melting point, are crucial for obtaining a glass. A simple relation between the glass transition (T_g) and the melting temperature (T_f) was found by Sakka [109] being useful to predict the glass transition temperature of organics liquids and molten oxides: $T_g/T_f \sim 2/3$.

For the case of polymers, this situation becomes quite complex. Polymers that have a linear architecture and a regular chemical constitution, in principle, may fit in a three dimensional lattice, and hence, crystallize. A number of inhomogeneities are present in real polymeric chains including molecular weight distribution, branching, entanglements, and others, that cannot be included in the sites of the crystalline lattice. On the other hand, polymer chains require a longer time to complete the disentangling required for crystallization in comparison with low-molecular weight substances.

It is important to note that during the cooling process from the melting, the chains that can be stretched and incorporated to the growing crystal are separated from chains parts near to entanglements or chain imperfections which are moved to the amorphous regions. By this way, two unmixed phases are obtained: one ordered and another disordered.

It is necessary to emphasize that the structure formation is governed principally by kinetic criteria and not by equilibrium thermodynamics. Therefore the structure which develops at a given temperature is that with the maximum growth rate rather than that with the lowest free energy. As a consequence, kinetical considerations have to be required for explaining crystallization process.

The polymer networks that are the subject of this work are fully amorphous due to their structure of highly cross-linked networks and also because they are atactic. Even in the cases where linear chains are formed (in the methyl acrylate sequences of P(MA-co-TrEGDMA) copolymers) free radical polymerization situates randomly the side-chain groups of the methyl acrylate monomeric units one side or the other of the

polymer chains. The lack of regularity along the main chains or the crosslinks in the case of the networks avoids the formation of any long-range order in these polymers.

1.2.4.4 Molecular mobility in semicrystalline materials

The molecular mobility associated with the amorphous phase in partially crystalline systems, can be different of that found when the same material is in a fully amorphous state. It seems a general fact that the former are much less uniform than the later and this will be reflected in the relaxation modes. Principally, two effects can be distinguished:

i) The amorphous part "trapped" in the crystalline structure behaves in a similar way of confined systems. Taking up again the idea of the cooperative rearranging regions introduced by Adam and Gibbs [49], it is expected that when the dimensions of the geometry imposed by the crystals becomes comparable to the *CRR*'s size (or the cooperativity length, $\xi_\alpha(T)$) the molecular dynamics around the glass transition will change relatively to that of the bulk behavior. Thought the main relaxation is sensitive to this situation does not mean that it is always identically influenced. For example, Pissis *et al.* [110] shown that the α relaxation in the confined propylene glycol becomes faster than in the bulk, leading to a lower T_g when the pore dimensions is about 10 nm. The opposite effect is found when propylene glycol is confined to smaller pores due to adsorption (page 205, chapter 6 in ref. 42). Other authors [111] confined PMMA in films with layer of different thickness and they found a situation where the α process even disappeared when the thickness was about 5 nm. The suppression of T_g is rationalized in terms of a minimal length-scale for cooperativity for the glass transition to occur. Thus, the vanishing of the glass transition occurs when this critical length-scale becomes comparable to the confinement dimensions (page 207 chapter 6 in ref. 42).

The situation of the amorphous phase in semicrystalline polymers is more complicated since there is a strong interaction between the polymer segments in the amorphous phase and the crystals. In fact some of the polymer chains pertain both to the crystallites and the amorphous phase. Thus there are covalent bonds between amorphous and crystalline segments. This imposes strong restriction to the amorphous material in the inter-lamellae spaces, which is frequently called rigid amorphous phase to differentiate it of the amorphous polymer situated far from the crystals. Several

studies have found two glass transitions in semicrystalline polymers such as poly(ethylene terephtalate [112] or polylactide [113]; in the later two alpha processes were detected corresponding to the relaxation of the amorphous phase: a rigid or constrained fraction adjacent to stiff crystalline walls, and the other one presenting bulk-like behavior [114].

Concerning the influence of the confinement in the secondary relaxations, in poly(isobutyl vinylether) studies show that it is almost uninfluenced (page 202, chapter 6 in ref. 42).

ii) The existence of crystalline structures will promote the evolving of new processes inside the crystalline regions or the loss of mobility of the existing processes between different crystalline regions. An example of the first situation is current in the polyethylene, whose simple and flexible structure leads to the appearance of a new relaxation, localized between the glass transition and the melting temperatures. This process seems to be related to rotational motions within the crystalline lamellae (Boyd and Liu in ref. 39, 115). A 180º flip in a molecular segment occurs at a given place and propagates in screw-like motions through the crystal.

This remaining mobility existing in the supercooled and glassy state in samples that posses crystalline stable nuclei, can induce, at a constant temperature, a higher degree of crystallinity. Consequently, the glass transition dynamics will probably change during crystallization as the amorphous phase is progressively confined within the crystalline structures that are being formed. This apparent simple fact must be taken into account for practical purposes, since long period of time under supercooled conditions or even in the glassy state, can provoke undesired structural changes (this is for example the case of storage of pharmaceutical products) [11].

1.2.5 Free radical polymerization

There are a multitude of chemical reactions and associated monomer types that can produce polymer chains with the simple requirement that each molecule of monomer must be capable of being linked to two or more other similar molecules by chemical reaction, *i.e.* monomers must present a functionality of two (or higher) [116-118].

The classification more frequently used is due to Carothers and is based upon comparison of the molecular formula of a polymer with that of the monomer(s) from which it was formed.

Condensation polymerizations are those which yield polymers with repeating units having fewer atoms than the monomers from which they were formed. This usually arises from chemical reactions which involve the elimination of a small molecule. *Addition polymerizations* are those which yield polymers with repeat units having identical molecular formulae to those of the monomers from which they are formed.

A better basis for classification is provided by considering the underlying polymerizations mechanisms, which are of two general types: *i*) polymerizations in which the polymer grows step-wise by reactions that can occur between any two molecular species that are known as *step polymerizations*, and *ii*) polymerizations in which a polymer chain grows only by reaction of monomer with a reactive end-group on the growing chain and that are known as *chain polymerizations*. *Free-radical polymerization* is the most widely practiced method of chain polymerization and since it is the one considered in this work, it will be described in detail below.

Free radical polymerizations are initiated by radicals, which possesses an unpaired electron, and propagated by macro-radicals. It is possible to find situations where the radicals are formed from monomers themselves, but normally they are produced from initiators deliberately introduced. The decomposition of initiators can be induced thermal, photochemical or electrochemically, and for this work only thermal one will be considered.

An important requirement for initiators is a high reactivity. Nevertheless, for considering the effective number of radicals responsible for initiating the polymerization reaction, it is necessary to take into account secondary reactions where initiators will be involved and that imply a diminution in the useful number of radicals. Among these reactions, we should include those between two radicals already formed, which will influence the rate of formation, the rate of propagating chains and the rate of initiator decomposition. In this work the thermal initiator used was

N,*N*-azo*bis*isobutyronitrile (AIBN), which efficiency is decreased when suffers secondary reactions, the three most important shown in Scheme 1.1.

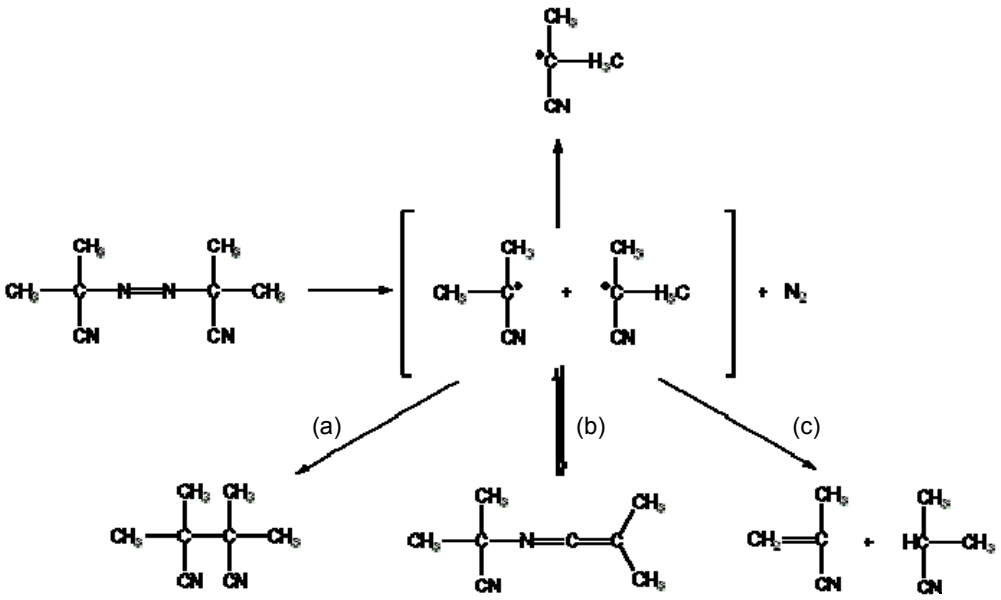

Scheme 1.1 Decomposition of *N*,*N*-azo*bis*isobutyronitrile (AIBN) in two isobutyronitrile radicals (in the middle) and secondary reactions: a) between two radicals, b) termination by primary radicals and c) with transfer to initiator.

Polymerization follows according three stages: initiation, propagation and termination. In the initiation path, the free radicals generated from the initiator, I, (and not involved in secondary reactions) add to monomer's double bond. The monomer-radical formed in this way ($I-M^*$) is responsible for the initiation of the polymerization (note that initiator are covalently linked to monomer). This reaction depends on both monomer and radical structures, however its rate constant is always very high (10^3-10^7 l mol^{-1}s^{-1}) [116-118] and thus, the polymerization rate will be controlled by the decomposition constant of initiator k_d.

The action of the free radical depends on temperature and usually also on the solvent and the presence of monomer and polymer [119], and it is characterized by an activation energy E_d. For the particular case of AIBN, Table 1.1 presents these constants for several temperatures and solvents:

Solvent	**E_d (kJ.mol^{-1})**	**$t_{1/2}$ (h)**		
		40 ºC	70 ºC	110 ºC
Dibutyl phthalate	122.2	303	5.0	0.057
Benzene	125.5	354	6.1	0.076
Styrene	127.6	414	5.7	0.054

Table 1.1. Values of activation energy, E_d, and half-lifes, $t_{1/2}$, for the decomposition of AIBN at several temperatures and solvent conditions [119].

During the next stage, propagation, molecules of monomer add quickly to monomer-radical unities formed in the initiation path. In the addition of every monomer, the free radical moves to the end of the chain. These reactions are usually very fast, with rate constant higher than 100 l.(mol.s)$^{-1}$.

In these two stages it is important do not forget that oxygen is an efficient scavenger and acts over both initiating and propagating species, so care must be taken to exclude oxygen from polymerization or to minimize its effects [117].

In the last step, termination, the growth of the chain finishes when two polymeric radicals recombine or when hydrogen is transferred from a chain to another. In the first case, named head-to-head, the chain obtained is a result of the sum of the two precedent, M_{n+m}, and contains two fragments of initiator in the extremes. In the second one, called desproportionation, one of the participating chains gives the unpaired electron to the other one, and the result are two closed chains, M_n and M_m. The difference between these two final chains is in that the one that gives the electron, gains a double bond $C=C$, inducing an instable character to this chain, whereas the other, that accepted the electron, finishes with a simple bond, $C-C$, a perfectly stable chain.

$$\bullet M_n + M_m^{\bullet} \rightarrow M_n + M_m \quad (k_{tc})$$
$$\bullet M_n + M_m^{\bullet} \rightarrow M_n + M_m \quad (k_{td})$$

At this moment it is accepted that termination reactions are controlled by diffusion of radical-carrying segments. This diffusion is at the same time influenced by the size of the macroradicals and the viscosity of the system [116-118,120-123]. The effect is reflected in the decrease of the average value of the constants k_{tc} and k_{td}.

The molecular weight of polymers obtained by this type of reactions is usually high, in spite of the propagation rate being much smaller than the termination one, due to the fact that concentration of the two active radicals that is extremely low (10^{-8}-10^{-6} mol.l^{-1}).

The rate of polymerization via radicals is expressed by:

$$-\frac{dM}{dt} = k_p\left(\frac{2fk_d[I]}{k_t}\right)^{1/2}[M] \qquad \text{Equation 1.17}$$

where [M] and [I] are respectively the monomer and initiator concentrations, k_d, k_p and k_t are, respectively, the initiator, radical's propagation and termination constant, and f is the efficiency factor of initiator. This equation was obtained considering that the steady state of radicals is reached: the rate of initiation is equal to that of termination. By integrating it is achieved that:

$$\ln\frac{[M_0]}{[M]} = 2k_p\left(\frac{2f[I_0]}{k_t k_d}\right)^{1/2}\left[1-\exp\left(\frac{-k_d t}{2}\right)\right] \qquad \text{Equation 1.18}$$

And for low times of reaction, this last equation can be brought by:

$$\ln\frac{[M_0]}{[M]} = k_p\left(\frac{2f[I_0]k_d}{k_t}\right)^{1/2} t \qquad \text{Equation 1.19}$$

A large diversity of values for kinetic constants appears in the literature. Equation 1.17 is recommended to obtain $k_p/k_t^{1/2}$ [124].

1.2.5.1 Changes in molecular dynamics upon polymerization

In a qualitative way, this section pretends to give a general point of view of the different stages in the polymerization reaction that are going to induce changes in the molecular dynamics.

Gelation

The presence of monomers with polyfunctionality leads initially to the formation of a branched polymer and ultimately to the formation of a network polymer. The point at which polymer molecules link together into a three-dimensional network of indefinitely large size is named the gel-point. This fact is manifested by a rather abrupt change of the reacting mixture from a viscous liquid to a gel which shows no tendency to flow. Gelation occurs at a specific point in the course of the chemical reaction and depends on functionality, reactivity and stoichiometry of the reactants.

Trommsdorff-Norrish effect

In this type of polymerizations a marked acceleration of the reaction is frequently observed at monomer conversions higher than 15% to 25%. This increase in polymerization rate is accompanied by an increase of the degree of polymerization and the average molecular weight. This auto-acceleration of the reaction, called Trommsdorff-Norrish [125] or gel effect, is generally attributed to the decreased diffusion rate of the chain radicals due to the increased viscosity of the mixture, which reduces the termination rate and thus raises the polymerization rate [116,117]. Since termination constants are already diffusion-controlled at very small monomer conversions, this effect does not seem to be caused by an onset of diffusion control, but by changes in the mechanism originating the diffusion control. It has been suggested that this change of mechanism is related to critical value of concentration of chain entanglements (page 101 in ref. 116). Nevertheless, O'Neil and co-workers [126] through measurements in which they eliminated or delayed the formation of chain entanglements, put in evidence the non existence of correlation of concentration of chain entanglements with the gel effect onset.

Glass effect

When isothermal polymerization is carried out at temperatures below the glass transition temperature of the final network, the reaction can not reach the total degree of conversion. It happens that upon polymerization, the glass transition temperature of the

mixture continuously increases as a result of the changes in the composition of the monomer/polymer mixture. When the glass transition temperature of the mixture approaches the value of the polymerization temperature, the reacting system becomes a glass. The vitrification of the mixture reduces not only the diffusion of macroradicals and the termination reactions but also the diffusion of monomer molecules and thus the chain propagation. The polymerization rate approaches to zero, and consequently the monomer can no longer be fully polymerized.

Plasticization

The existence of a small content of small molecules (for instance water) or the mixing with a low glass transition polymer can plasticize a polymeric material, increasing conformational mobility. This has a reflection in the decreases of the glass transition temperature. Typically, one percent plasticizer lowers the glass transition temperature by a few Kelvins [83]. This shifts in T_g also affects the frequency temperature position of the crossover region. Typical crossover features like the separate α onset in dielectric data are unaffected. Main α relaxation and crossover are significantly shifted by very small amounts of plasticizer.

Another strategy to lower the T_g in high crosslinked polymer is to blended it or copolymerize with another polymer having a lower T_g (this aspect will be described in more detail in chapters 3 and 4).

1.3. Polarization and Dielectric Relaxation Spectroscopy

The interaction between an electric field and matter can be measured by dielectric relaxation spectroscopy (DRS) in a large range of frequencies (10^{-6}-10^{11} Hz). The variation of the dielectric constant with frequency and temperature is very useful for obtaining information about dipolar reorientational motions and electric conduction that arises from translational motions of charge carriers. With this information it is possible to infer about the molecular structure and dynamic of molecular reorientation.

Since 1927, when Debye established the relationship between the dielectric relaxation and the orientational motions of molecular dipoles [127], the technique of DRS has been gaining progressively interest within the scientific community.

As this work is based in its majority in results acquired with this technique, it seems vital to develop with some depth the basic concepts and theory that support it.

1.3.1 Polarization

Since matter is constituted by electric charges, when an electric field is applied, an interaction is produced. If the material is a conductor, that interaction is translated in a charge movement that originates the conduction phenomena. On the other hand, if the material is a dielectric, that movement of long range is not possible (or only in a weak way), nevertheless, the electric field is able to induce a deformation in the charge distribution. This displacement, with low intensity, is in the origin of polarization. At microscopic level, three different mechanisms can induce polarization in a dielectric material when it is subjected to an electric field: electronic, atomic and orientational [128].

Electronic polarization: it happens when the electrons suffer a displacement with respect to the nucleus by the action of the electric field. The intensity of the electric field inside the atom ($\sim 10^{11}$ $V.m^{-1}$) is higher than those applied in the experiments ($\sim 10^{8}$ $V.m^{-1}$); this difference induces usually a weak polarization.

Atomic polarization: It is the result of the modification in the relative positions of atomic nuclei inside the molecule or in an atomic network. Here are included movements like bending, twisting or stretching of molecules. All these movements are slower than those that originate the electronic polarization.

Orientational polarization: only appears in materials which possess molecular or ionic dipole moments, and it is a result of the preferential orientation of these dipoles in the direction of the applied electric field.

At this moment, it is important to emphasize that the time of response of the three types of polarization are very different: around 10^{-17} and 10^{-14} s for electronic, 10^{-13} to 10^{-12}s for atomic polarization, and between 10^{-5} e 10^{-12} s for orientational one.

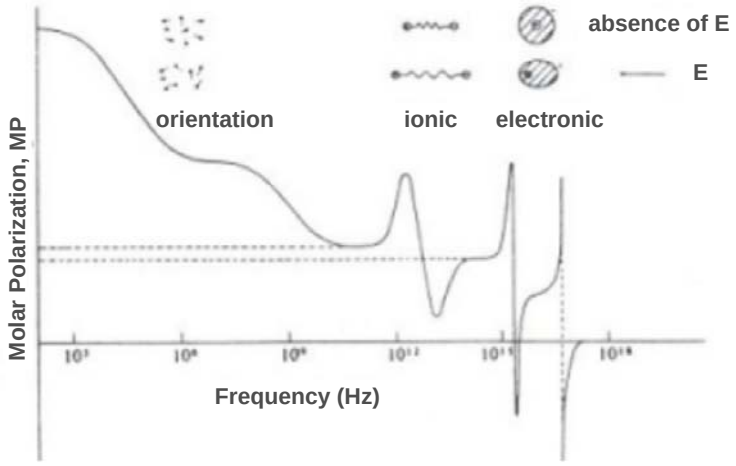

Figure 1.14 Schematic distribution of the molar polarization with frequency (reproduced from reference 129).

Figure 1.14 shows the frequency-dependent loss of polarization upon application of an oscillating electric field, putting in evidence several facts: *i*) the location of the different mechanisms involved in the polarization; *ii*) the difference in the intensity of the various processes; and *iii*) the width of the bands that in orientational polarization is higher due to the resistance that the medium puts up to the dipole's motion [130] being far from an instantaneous response as the other two polarization mechanisms.

Upon removal of the electric field, the electronic and atomic polarizations (also designed by induced polarization) disappear immediately. In contrast, the orientational polarization falls down slowly (comparatively to those ones). This lag is due to the internal friction of the material, and it depends on viscosity. Keeping this in mind, naturally arise the necessity of define a parameter that describes the polarization loss when the electric field is turned off. This parameter is the characteristic time, known by **relaxation time** (required time to polarization decreases a factor $1/e$ from its initial value).

Dielectric relaxation spectroscopy is precisely based in the measure of this loss of polarization (*i.e.* dielectric relaxation) after removal of a sinusoidal electric field at a certain temperature. The way as these dipoles relax will be rationalized in terms of molecular mobility existing in the system.

1.3.2 Phenomenological description of dielectric measurement

In this section we will start describing in general the response of a material to a stimulus (not specified) considering that the relation between them are included in the linear theory (*i.e.* when the strength of the stimulus is small, the response is proportional to that [128]). After this, we will particularize this description to the situation where the stimulus is a sinusoidal electric field and the response is the dielectric displacement, related to polarization.

To obtain the general expression for a linear response, let us start by considering the stimulus as a infinitely short pulse, that can be described in mathematical terms by using the Dirac's delta function, $\delta(t)$, which is zero for all values except for t, where it diverges ($\int_{-\infty}^{\infty}\delta(t)dt=1$). The stimulus can be expressed as $\varphi(t)=\varphi_0\delta(t)$. The primary response function $\mu(t)$ produced by this stimulus describes the time-dependent response, also called generally "displacement" (that is zero for $t=0$ and 1 for $t\to\infty$).

$$\mu(t)=-\frac{d\phi(t)}{dt}=\Phi(t) \qquad \text{Equation 1.20}$$

When the intensity of the stimulus is small, it is possible to apply the theory of linear response to the system that establishes a general expression between the cause and the corresponding effect:

$$x(t)=\varphi_0\mu(t) \qquad \text{Equation 1.21}$$

At this moment if we consider the arbitrary stimulus as the sum of a sequence of several pulses with adjusted heights (that is possible by application of superposition

principle of Boltzmann for systems where it is possible to verify the hypothesis of linearity[c] and causality[d]), the response $x(t)$ will be written by:

$$x(t) = \int_{-\infty}^{t} \mu(t-t')\varphi(t')dt' \qquad \text{Equation 1.22}$$

In dynamics experiments the application of an oscillatory stimulus $\varphi(t) = \varphi_0 \exp(i\omega t)$ leads to a "displacement" in the form $x(t) = x_0 \exp(-i\delta)\exp(i\omega t)$, where the parameter δ expresses the delay between stimulus and response. Making these substitutions in Equation 1.22 it is obtained:

$$x(t) = x_0 e^{-i\delta} e^{i\omega t} = \int_{-\infty}^{t} \mu(t-t')\varphi_0 e^{i\omega t'} dt' \qquad \text{Equation 1.23}$$

that can be rewritten by:

$$\frac{x_0 e^{-i\delta}}{\varphi_0} = \int_{-\infty}^{t} \mu(t-t') e^{i\omega(t-t')} dt' \qquad \text{Equation 1.24}$$

where the right term is characteristic of dynamic experiments and is named general dynamic susceptibility, $\alpha^*(\omega)$. By this way, $\alpha^*(\omega)$ and $\mu(t)$ are related by Fourier transform function:

$$\alpha^*(\omega) = \alpha'(\omega) - i\alpha''(\omega) = \int_{-\infty}^{t} \mu(t-t')\exp[-i\omega(t-t')]dt' \qquad \text{Equation 1.25}$$

The real component of $\alpha^*(\omega)$ is proportional to the reversible exchanged work (component in phase with stimulus applied), being a measure of the stored energy. On

[c] The linearity principle was stated by Galileo as: "joint causes operate each as though the others were not present" (Steiner, M., *The Applicability of Mathematics as a Philosophical Problem*, Harvard University Press, Cambridge, 1998, p. 30).

[d] In accordance with Born (1949) the causality statement can be enunciated as: "there are laws by which the occurrence of an entity B of a certain class depends on the occurrence of an entity A of another class", "the cause must be prior to the effect" and they "must be in spatial contact or connected by a chain of intermediate things in contact".

the other hand, α'' is related to dissipated energy during the process (out-of-phase component).

Dielectric relaxation spectroscopy is a particular case where the experiments are developed in the linear response regime. Here the stimulus is an electric field $E(t)$, and the response is the dielectric displacement $D(t)$. When the electric filed is static, the dielectric displacement resulting at $t = 0$ is:

$$D(t) = \varepsilon_0 [\varepsilon_\infty + (\varepsilon_S - \varepsilon_\infty)\Phi(t)]E \qquad \text{Equation 1.26}$$

where ε_0 is the vacuum permittivity, ε_∞ is the permittivity of induced polarization and ε_S is the static permittivity The first term, $\varepsilon_0 \varepsilon_\infty E$, represents the instantaneous response of dielectric material to the field, and the second term, $\varepsilon_0(\varepsilon_S - \varepsilon_\infty)\Phi(t)E$, is related to dipolar polarization, including the dielectric function $\Phi(t)$, that describes the polarization response after switching off the electric field (note that in equilibrium the orientational polarization will decay to zero at long times, so that $\Phi(t \to \infty) = 0$). The decrease of polarization after removing the electric field can be expressed by decay function, related to $\Phi(t)$ by $\phi(t) = 1 - \Phi(t)$.

If the applied electric field is not static, the variation in $D(t)$ produced by the increment dE at $t = u$ is:

$$dD(t) = \varepsilon_0 \varepsilon_\infty dE + \varepsilon_0(\varepsilon_S - \varepsilon_\infty)\Phi(t-u)dE \qquad \text{Equation 1.27}$$

where with the application of Boltzmann's principle leads to:

$$D(t) = \varepsilon_0 \varepsilon_\infty E(t) + \varepsilon_0(\varepsilon_S - \varepsilon_\infty)\int_{-\infty}^{t} \Phi(t-u)\frac{dE(u)}{du}du \qquad \text{Equation 1.28}$$

Making the substitution $t' = t - u$ and integrating it is obtained

$$D(t) = \varepsilon_0 \varepsilon_\infty E(t) + \varepsilon_0 (\varepsilon_S - \varepsilon_\infty) \int_0^\infty E(t - t') \left[- \frac{d\phi(t')}{dt'} \right] dt' \qquad \text{Equation 1.29}$$

In a typical dielectric experiment the stimulus consists in applying a harmonic electric field $E(t) = E_0 \exp(i\omega t)$. Inserting this into the last equation one obtains as the response:

$$\frac{D(t)}{\varepsilon_0 E(t)} = \varepsilon_\infty + (\varepsilon_S - \varepsilon_\infty) \int_0^\infty \exp(-i\omega t') \left[- \frac{d\phi(t')}{dt'} \right] dt' \qquad \text{Equation 1.30}$$

where $\varepsilon^*(\omega)$ is identified with $\frac{D(t)}{\varepsilon_0 E(t)}$ and is named permittivity. The dependence of ε^* with the frequency is given by:

$$\frac{\varepsilon^*(\omega) - \varepsilon_\infty}{\varepsilon_S - \varepsilon_\infty} = \int_0^\infty \exp(-i\omega t) \left[- \frac{d\phi(t)}{dt} \right] dt \qquad \text{Equation 1.31}$$

When a relaxation happens this can be detected either as a peak in the imaginary part or as an inflexion in the curve of the real part of the permittivity. That means that the two components are not independent (Kramers-Kronig relations described this connection [131]).

1.3.3 Debye model and related empirical models

1.3.3.1 Debye relaxation

Debye in 1945 presented a work on dielectric properties of polar liquids [132] where he proposed that for a system in non-equilibrium, relaxation takes place with a rate that increases linearly with the distance from equilibrium.

This statement can be written by a first order differential equation such as:

$$\frac{dP(t)}{dt} = -\frac{P(t)}{\tau_D} \qquad \text{Equation 1.32}$$

where τ_D is a characteristic relaxation time. Three assumptions were made: *i*) non interaction between dipoles, *ii*) only one process leads to the equilibrium (*i.e.* either a transition above a potential barrier either a rotation with friction) and *iii*) all the dipoles can be considered equivalents, this is, all of them relax in average with one only characteristic time.

The solution of Equation 1.32 leads to an exponential decay for the correlation decay function $\Phi(t)$:

$$\Phi(t) = \exp\left[-\frac{t}{\tau_D}\right] = -\frac{d\phi(t')}{dt'}\ P(t) = P_0 \exp\left(-\frac{t}{\tau_D}\right) \qquad \text{Equation 1.33}$$

This relaxation function can be introduced in Equation 1.31 to obtain the next relation for the complex permittivity:

$$\varepsilon^* = \varepsilon'(\omega) - i\varepsilon''(\omega) = \varepsilon_\infty + \frac{\varepsilon_0 - \varepsilon_\infty}{1 + i\omega\tau} = \left(\varepsilon_\infty + \frac{\varepsilon_0 - \varepsilon_\infty}{1 + (\omega\tau)^2}\right) - i\left(\frac{(\varepsilon_0 - \varepsilon_\infty)\omega\tau}{1 + (\omega\tau)^2}\right) \qquad \text{Equation 1.34}$$

This is the well-known Debye dispersion equation. Plots of the characteristics shapes of real and imaginary parts of $\varepsilon^*(\omega)$ against $f = \omega/2\pi$ (f is the frequency of the outer electrical field) for this model are shown in Figure 1.15.a. The imaginary part exhibits a symmetric peak whose maximum value occurs at $\omega_{\max}\tau = 1$ and has an amplitude of $\varepsilon''_{\max} = \frac{\varepsilon_S - \varepsilon_\infty}{2}$. The breadth of the peak at half the height is constant at 1.44 decades of frequency [38]. The real part shows dispersion falling from ε_0 to ε_∞ with increasing frequency. The mean relaxation time of the process, $\langle\tau\rangle$, is defined as the inverse of ω_{MAX} ($\langle\tau\rangle = (2\pi f_{MAX})^{-1}$).

The Debye behavior is observed in very few materials among which are organic liquids [133-135] and liquid crystals [136]. For more complex systems as it is the case of polymers, this model is not well succeeded (nevertheless, PnLMA [137] comes out as an exception).

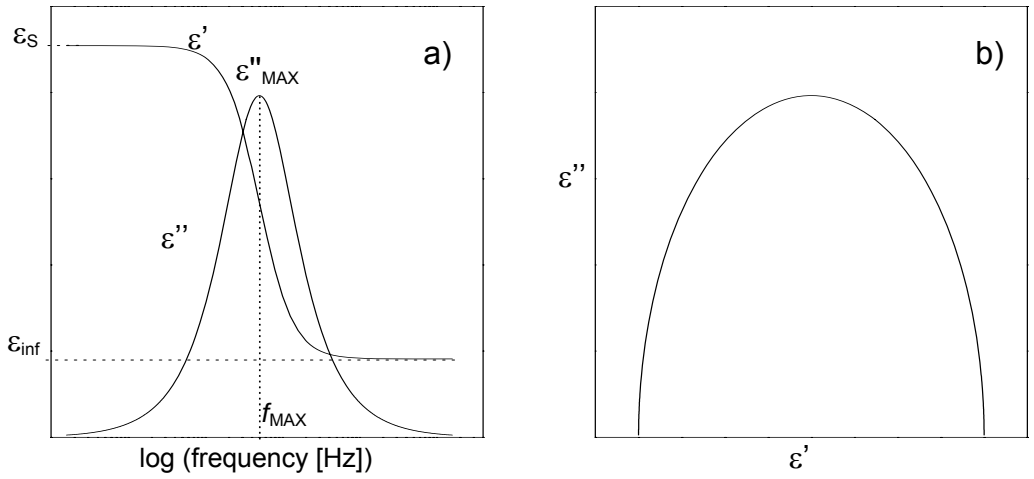

Figure 1.15 (a) Frequency dependence of the real, ε', and imaginary, ε'', parts of permittivity in a simple Debye process. (b) Imaginary part *vs.* real part of ε^*.

It is also useful construct the plot of imaginary part *vs*. real part of permittivity, known by Cole-Cole plot. In this representation, the Debye model corresponds to a symmetric arc (see Figure 1.15.b).

1.3.3.2 Complex systems: distribution of relaxation times

In real systems, typical decay functions are far from exponential. The loss of polarization are not satisfactorily described by one only characteristic time, this is, the shape of $\varepsilon''(\log f)$ appears much broader than the value defined by Debye. For interpreting this non-Debye behavior two approaches arise: the first one state that due to the complexity of molecular motions, the relaxation from a molecular point of view is not intrinsically exponential, or in other words, the material is interpreted as a homogeneous medium in which all molecules relax in a similar nonexponential manner. The other one considers that there are several entities relaxing every one characterized by one relaxation time and with an exponential decay. This assumption leads to visualize the material as a set of heterogeneous environments. By this way, the decay global function is defined by the superposition of all relaxation processes [25].

This distribution of relaxation times that correspond to an enlargement in the response is written in terms of a probability density function of $\rho(\ln\tau)$ (obeying the normalization condition $\int_0^\infty \rho(\ln\tau)d\ln\tau = 1$):

$$\phi(t) = \int_{-\infty}^{+\infty} e^{-t/\tau}\rho(\ln\tau)d\ln\tau \qquad \text{Equation 1.35}$$

The quantity $\rho(\ln\tau)d\ln\tau$ acts as a weighting term corresponding to the fraction of relaxation processes with relaxation times between $\ln\tau$ and $(\ln\tau + d\ln\tau)$ (the integral representation instead of the sum, is more convenient to reflect a continuous distribution of relaxation times). From Equation 1.35 it is concluded that the decay function is in mathematic terms related to a distribution of relaxation times. Qualitatively, the mean value of this distribution function should be linked to the inertia of the relaxing dipole moment, while the standard deviation can be associated to the degree of interaction and/or disorder between the relaxing entities [138].

In frequency domain:

The existence of this distribution of relaxation times, in the frequency domain, transforms the Equation 1.31 in:

$$\frac{\varepsilon^*(\omega) - \varepsilon_\infty}{\varepsilon_S - \varepsilon_\infty} = \int_{-\infty}^{+\infty} \frac{\rho(\ln\tau)}{1 + i\omega\tau} d\ln\tau \qquad \text{Equation 1.36}$$

The Debye situation is established when $\rho(\ln\tau)$ is a Dirac function.

The first modification to Debye theory was that of Cole and Cole [139] who introduced a shape parameter, α_{CC}, in order to broad the peaks though keeping the symmetry $(\omega_{MAX}\tau_{CC} = 1)$ as follows (see upper part in Figure 1.16):

$$\varepsilon^*(\omega) = \varepsilon_\infty + (\varepsilon_S - \varepsilon_\infty)\frac{1}{1 + (i\omega\tau_{CC})^{1-\alpha_{CC}}},\ 0 < \alpha_{CC} < 1 \qquad \text{Equation 1.37}$$

The shape parameter can be directly obtained for the Cole-Cole diagram, ε'' *vs* ε', by measuring the angle subtending the radius of the circle to the horizontal axis and equalling to $\alpha_{CC}\pi/2$.

Another important tentative to improve Debye's model was presented in 1950 by Davidson and Cole [140] (see lower part in Figure 1.16). Davidson and Cole function presents de maximum loss not at $\omega\tau = 1$, but at $\omega_{MAX}\tau_{DC} = \tan\left[\pi/2\left(1+\beta_{DC}\right)\right]$. The empirical equation is:

$$\varepsilon^*(\omega) = \varepsilon_\infty + (\varepsilon_S - \varepsilon_\infty)\frac{1}{(1+i\omega\tau)^{\beta_{DC}}},\ 0 < \beta_{DC} \leq 1 \qquad \text{Equation 1.38}$$

At limiting high frequencies, the approach of the arc towards the abscissa in Cole-Cole representation becomes a straight line, with an angle between the line and abscissa equal to $\beta_{DC}\pi/2$.

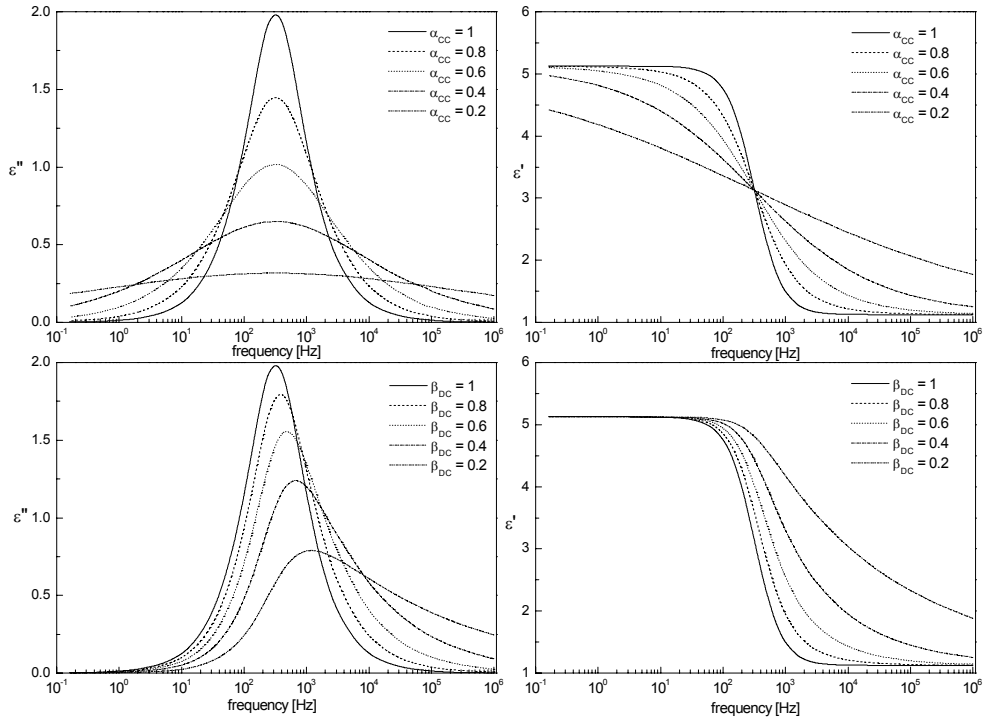

Figure 1.16 Real and imaginary parts of complex dielectric permittivity for the Cole-Cole and Davidson-Cole functions in top and bottom respectively ($\Delta\varepsilon = 4$ and $\tau = 5\times10^{-4}$ s). (For $\alpha_{CC} = 1$ and $\beta_{DC} = 1$ both functions coincide with the Debye model)

In the actuality, the most widely relaxation function used for data treatment in frequency domain combines both shape parameter related to broadness and asymmetry.

This empirical relation was introduced by Havriliak and Negami in 1966 [141] and reads:

$$\varepsilon^*(\omega) = \varepsilon_\infty + \frac{\varepsilon_S - \varepsilon_\infty}{\left[1 + (i\omega\tau_{HN})^{\alpha_{HN}}\right]^{\beta_{HN}}},\ 0 < \beta_{HN}, \alpha_{HN}\beta_{HN} \leq 1 \qquad \text{Equation 1.39}$$

Its shape parameters, α_{HN} and β_{HN}, describe the slopes of the ε'' peak at low and high frequencies relative to that corresponding to ε''_{MAX}: $\alpha_{HN} = \partial \log \varepsilon'' / \partial \log \omega$ for $\omega << 1/\tau_{HN}$, and $\alpha_{HN}\beta_{HN} = -\partial \log \varepsilon'' / \partial \log \omega$ for $\omega >> 1/\tau_{HN}$.

The characteristic relaxation rate, ω_{MAX} or relaxation time $\tau_{MAX} = \omega_{MAX}^{-1}$, can easily be obtained from τ_{HN} using Equation 1.40 [142], usually preferred because it is a model-independent parameter.

$$\omega_{MAX} = 2\pi f_{MAX} = \frac{1}{\tau_{MAX}} = \frac{1}{\tau_{HN}}\left[\sin\left(\frac{\alpha_{HN}\pi}{2+2\beta_{HN}}\right)\right]^{\frac{1}{\alpha_{HN}}}\left[\sin\left(\frac{\alpha_{HN}\beta_{HN}\pi}{2+2\beta_{HN}}\right)\right]^{\frac{-1}{\alpha_{HN}}} \qquad \text{Equation 1.40}$$

The distributions of relaxation times associated to these relationships, calculated from Fourier transform are presented in Table 1.2 [38,128].

Name	Distribution function
Debye	$\delta(\tau)$
Cole-Cole	$\frac{1}{2\pi}\frac{\sin(\pi\alpha_{CC})}{\cosh[(1-\pi\alpha_{CC})u] - \cos(\pi\alpha_{CC})}$
Cole-Davidson	$\frac{\sin(\beta_{DC}\pi)}{\pi}\left(\frac{\tau}{\tau^* - \tau}\right)^{\beta_{DC}}$ for $\tau \leq \tau^*$ 0 for $\tau > \tau^*$
Havriliak-Negami	$\frac{1}{2\pi}\frac{x^{\beta_{HN}(1-\alpha_{HN})}\sin(\beta_{HN}\theta)}{\left[x^{2(1-\alpha^{HN})} + 2x^{(1-\alpha_{HN})}\cos(\pi(1-\alpha_{HN})) + 1\right]^{\beta_{HN}/2}}$

Table 1.2 Distribution functions. The distribution variable is $u = \ln(\tau/\tau^*)$, where τ^* represents the more probable value of the relaxation time. $x = e^u = \tau/\tau^*$ and $\theta = arctg[\sin(\pi(1-\alpha_{HN}))/(x + \cos(\pi(1-\alpha_{HN})))]$.

These were the principal proposals to take into account deviation from the Debye model in the frequency domain. On the other hand, in time domain, special attention must be paid in the empirical distribution established by Kohlrausch [143] applied later to dielectric relaxation by Williams and Watts [144]. Accordingly, the decay function is described by a stretched exponential by the form:

$$\phi(t) = \exp\left[-\left(\frac{t}{\tau_{KWW}}\right)^{\beta_{KWW}}\right],\ 0 < \beta_{KWW} \leq 1 \qquad \text{Equation 1.41}$$

where τ_{KWW} is a characteristic time and β_{KWW} is a parameter that describes the non-exponential behaviour of the decay function. A decrease of β_{KWW} may be related to a broadening of the distribution of relaxation times, which also presents an asymmetric shape (see Figure 1.17 where it is compared the shape for distribution function for Debye model and *KWW* proposed for $\beta_{KWW} = 0.5$). This parameter can be rationalized in terms of degree of interaction between dipole moments [138].

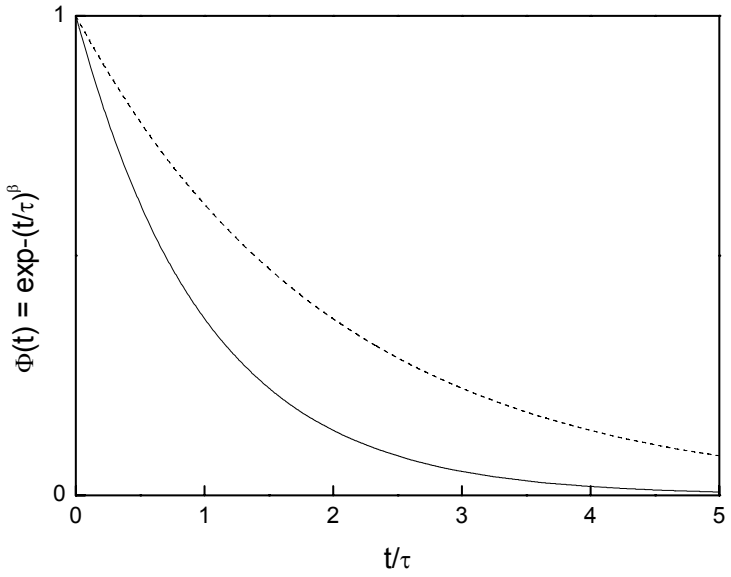

Figure 1.17 The decay relaxation function for a single exponential function when $\beta = 1$ related to Debye model (solid line), and for $\beta = 0.5$ corresponding to a stretched exponential function proposed by *KWW* (dot line).

A disadvantage of *KWW* equation is that since it is defined in time domain, its study in function of frequency involves the determination of the Fourier transform, for which does not exist an analytical expression [145]. Different numerical approximations

have been made and an example largely used is that suggested by Hamon [146] who related angular frequency to time by expression $\omega t = 0.2\pi$. Figure 1.18 shows several ε'' curves obtained by transforming Equation 1.41 to the corresponding frequency dependent data in accordance with Hamon approximation and taking into account that $\varepsilon''(\omega) = \gamma(t)\omega^{-1}$ for $\gamma(t) = -\frac{d\phi(t)}{dt}$ [144].

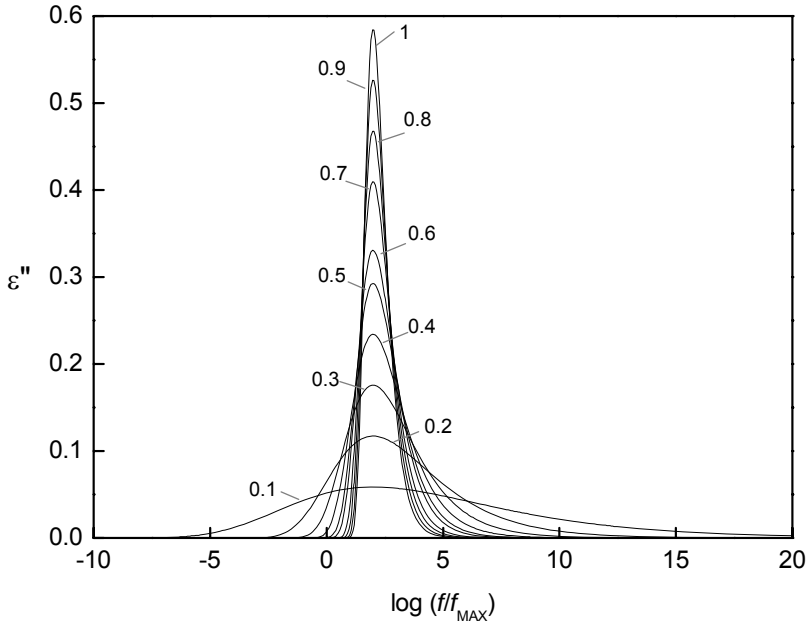

Figure 1.18 Imaginary component of the permittivity, calculated using the *KWW* model (Equation 1.41) and the Hamon approximation [144], obtained at different β_{KWW} values (shown in the figure) for $\tau_0 = 10^{-3}$ s.

Even though a distribution of relaxation times has not been introduced in this model, this decay function would correspond to a particular distribution [144].

The simultaneous utilization of both *KWW* and *HN* equations (in the respective domains) to analyze the dielectric data and the good results obtained, suggested the existence of a relation between them. With the objective of finding this relation, an important work made by Alegría and co-workers [145] using numeric methods to solve the Fourier transform of the *KWW* equation, leaded to the following approximation:

$$\ln\left[\frac{\tau_{HN}}{\tau_{KWW}}\right] \approx 2.61(1-\beta_{KWW})^{0.5}\exp(-3\beta_{KWW}) \qquad \text{Equation 1.42}$$

leading to the following equation that relates by a simple manner the shape parameters of the two models:

$$\alpha_{HN}\beta_{HN} = \beta_{KWW}^{1.23} \qquad \text{Equation 1.43}$$

Nevertheless, it must be noted that while the *HN* function uses two shape parameters, the *KWW* employs only one. This fact jointly to the empirical approximation from the frequency to the time domain will lead to the lost of some information.

1.3.4 Dielectric strength: from Onsager to Fröhlich-Kirkwood

From the analysis of the dielectric loss peak an important obtainable parameter is the dielectric strength, $\Delta\varepsilon$, which is related to the effective dipole moment. Onsager gave the first derivation of the static dielectric constant for a condensed phase of dipole moment [147].

The fundamental point in Onsager's theory is the way he computes the electric field E, that acts upon a rigid dipole located in the center of a spherical cavity inserted in a dielectric medium. He considers the interaction between the dipole moment of the molecule and the dielectric (isotropic) surrounding, understanding this as a continuum, *i.e.* without any differentiation between all molecules that surround it (volume of the liquid equals the sum of the volumes of the molecules).

When computing the total electric field it arises the term known by 'reaction field', which is the field acting upon a dipole due to electric displacements induced by its own presence in the system.

The polarization per volume unit depends on the mean of the total electric moment, $P = N\overline{m}/V$ (N is the whole number of dipoles). This moment is the sum of the permanent and the induced dipole moments, $m = \mu_0 u + \alpha E$, where u denotes a unit vector in the direction of the dipole axis, μ_0 permanent electric moment in vacuum, α the polarizability and E, the electric field. To compute the mean moment Onsager uses Boltzmann's formula considering all the possible orientations of the molecule in respect

to the electric field (being θ the angle describing that orientation). The result is the following equation:

$$\mu_0^2 = \frac{9kT}{4\pi N}\frac{(\varepsilon - \varepsilon_\infty)(2\varepsilon + \varepsilon_\infty)}{\varepsilon(\varepsilon_\infty + 2)^2} \qquad \text{Equation 1.44}$$

This result allows calculating the dipole moment of a molecule from the dielectric constant of the pure liquid, if ε_∞ and the density are known.

Although Equation 1.44 is in good agreement with results obtained for pure polar liquids, when one considers systems where there are correlations between the molecular orientations of neighbors, such hydrogen bonds, the theory fails (see reference 148).

Kirkwood [149,150] based in the theory of Onsager for the estimation of μ, introduced a purely empirical term, the correlation function, g_K, for taking into account the interaction between nearest molecules. The so-called Kirkwood correlation function, accounts for specific dipole-dipole orientations (for parallel or anti-parallel correlations between neighboring dipoles, $g_K > 1$ or $0 < g_K < 1$, respectively, while for a random orientation distribution of dipoles, $g_K = 1$). Later on, Fröhlich [151] developed a theory similar to Onsager but considering at the starting point the deformation of the polarization jointly with the correlation factor introduced by Kirkwood. The concept of local approximation was replaced by a region containing the molecule and its *z* nearest neighbors; γ_i is the angle between the dipole moment of the central molecule and the dipole moments of the molecules in the vicinity. The result is an analytical expression similar to that of Kirkwood but that can be easily reduced to Onsager expression for non-reacting molecules (in this particular case $g_K = 1$). The correlation factor introduced is equal to $g_K = \frac{\mu^{*2}}{\mu^2} = 1 + \sum_{i=1}^{\infty} z_i \langle \cos\gamma_i \rangle$, giving a measure of the restriction to the rotation exerted by a central molecule over the surrounding ones and μ^* the effective dipole moment in the liquid phase. The final Kirkwood - Fröhlich expression is:

$$\Delta\varepsilon = \varepsilon_s - \varepsilon_\infty = g_K \frac{\mu_0^{\,2}}{9kT\varepsilon_0}\frac{N}{V}\frac{\varepsilon_s(\varepsilon_\infty + 2)^2}{2\varepsilon_s + \varepsilon_\infty} \qquad \text{Equation 1.45}$$

where ε_0 is the vacuum permittivity as already defined, μ_0 the dipole moment of the moving unit in vacuum ($\mu_0(\varepsilon_\infty + 2)/3 = \mu$ is the permanent dipole moment of a dipole laying in cavity surrounded by other dipoles as defined by Onsager), T the temperature, k the Boltzmann constant, N/V the volume density of dipoles.

1.3.5 Conductivity; Electric Modulus

Since dielectric absorption is a measure of the energy dissipated in the material, in addition to the relaxation processes, it is necessary to considerer the contribution of d.c. conductivity, σ. By this way, the total dielectric loss ε'' will be given by:

$$\varepsilon''_{TOTAL}(\omega) = \varepsilon''_{DIPOLAR}(\omega) + \frac{\sigma}{\omega\varepsilon_0} \qquad \text{Equation 1.46}$$

From this expression it can be pointed out that the influence of d.c. contribution can be significant at low frequencies from relatively low temperatures. When conductivity is high, this easily masks the term relative to dipole relaxation and the data analysis by this way becomes complicated. In these situations, the analysis of the complex electric modulus M^*, defined as the reciprocal of the complex permittivity, results more advantageous. This fact is due to the fact that conductivity with pure electronic origin appears in the imaginary part of the modulus as a Debye peak (low frequency peak in Figure 1.19), allowing a better resolution of dipolar processes jointly with the characterization of this d.c. contribution.

It is important to underline that the physical content of both representations, modulus or permittivity, is identical and the principal difference is in which is the relaxational feature that is emphasized with one or another (chapter 4, page 45 in ref. 152).

Originally the consideration of complex reciprocal dielectric constant, M^*, was made by McCrum *et al*. (page 111 in ref. 38) according to the equation:

$$M^* = \frac{1}{\varepsilon^*} = \frac{1}{\varepsilon' - i\varepsilon''} = \frac{\varepsilon'}{\varepsilon'^2 + \varepsilon''^2} + i\frac{\varepsilon''}{\varepsilon'^2 + \varepsilon''^2} = M' + iM'' \qquad \text{Equation 1.47}$$

If $\varepsilon^*(\omega)$ is described by the Debye function, the complex modulus is written as (Williams and Thomas, in ref. 153):

$$M^*(\omega) = M_\infty + \frac{\Delta M}{1 + i\omega\tau_{D-M}} \qquad \text{Equation 1.48}$$

with $\Delta M = M_0 - M_\infty (<0)$, $M_0 = 1/\varepsilon_0$ and $M_\infty = 1/\varepsilon_\infty$. The relaxation time, determined from the modulus, is related to the Debye relaxation time through: $\tau_{D-M} = (\varepsilon_\infty/\varepsilon_0)\tau_D$ and is smaller relative to τ_D because $\varepsilon_0 > \varepsilon_\infty$ (high frequency peak in Figure 1.19). Consequently, a Debye-like relaxation process appears at a higher frequency in the modulus representation when compared to $\varepsilon^*(\omega)$. A recent work from Bello *et al.* [154] showed the comparison of the two formalisms for poly(ε-caprolactone) confirming the utility of this alternative analysis.

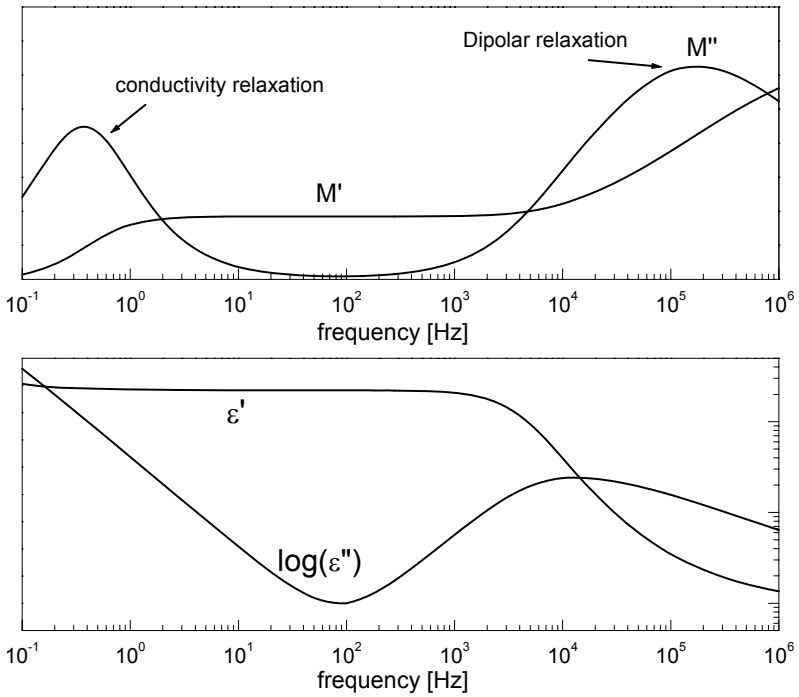

Figure 1.19 Representative data where a peak related to dipolar relaxation is located around 10^4 - 10^5 Hz which is visible in both representations, M'' and ε''; and a pure d.c. conductivity contribution, which is visible as a peak located around 0.5 Hz in M'' and as a linear increase of $\log(\varepsilon'')$ with slope equal to -1.

Besides the free charge transport that is in the origin of pure conductivity (without any contribution in the real part of the permittivity) there are other phenomena related to conductivity.

Between them it is worth highlighting the trapping of charge carriers at interfaces within the bulk of the sample (interfacial Maxwell-Wagner-Sillars polarization [42,155-157]) and the blocking of charge carriers at the interface between the ion-conducting material and the electron-conducting metallic electrode (electrode polarization [158]).

When these effects are present in the sample, the conductivity term added in the HN equation must be slightly changed as:

$$\varepsilon^*(\omega) = -ia\left(\frac{\sigma_0}{\varepsilon_0 \omega^s}\right) + \varepsilon^*_{HN}(\omega) \qquad \text{Equation 1.49}$$

where a has dimensions of $Hz^{-1}(rad.Hz)^s$. The exponent s is used to take into account a low frequency tail that is influenced by either electrode or interfacial polarization. When the conductivity is not pure d.c. $s < 1$, usually $0.5 \leq s < 1$ (Kremer and Różański in chapter 12, in ref. 42) that also affects the real part of the permittivity.

While the conductivity of pure electronic origin corresponds to a Debye peak in the modulus representation, the electrode polarization does not have any contribution in the modulus representation.

This way, by using simultaneously data analysis of ε^* and M^* it is possible to get information about the origin of the conductivity.

The next figure delineates these different contributions.

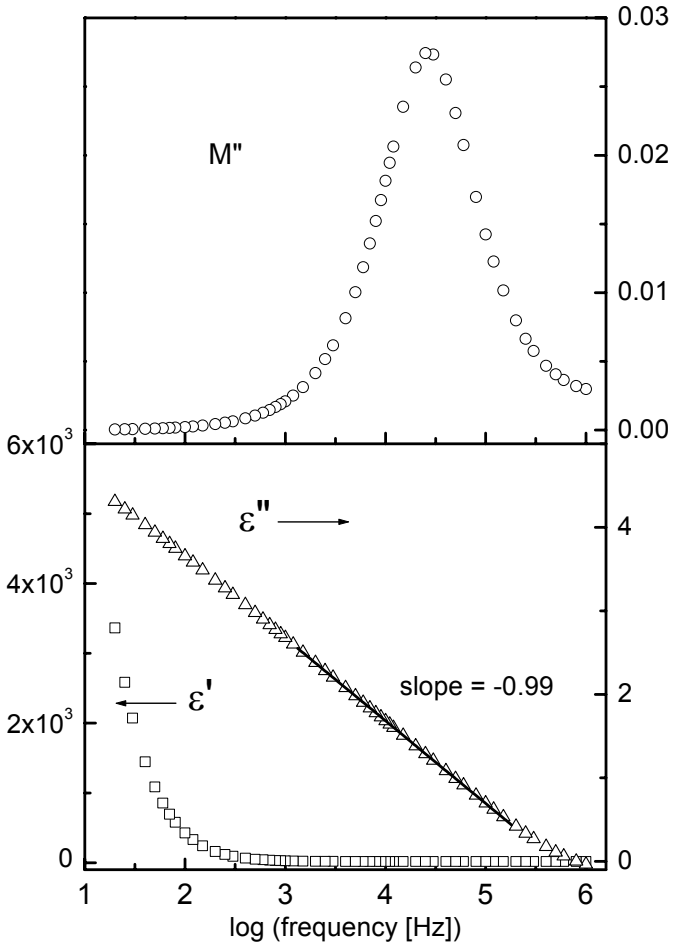

Figure 1.20 Real and imaginary parts of the complex permittivity (bottom graph) of fructose at 90 ºC. The region where the slope in ε'' (on a logarithmic scale) is close to unity is due to d.c. conductivity, as confirmed by the invariance in ε' and the Debye peak (top graph) in M'' (the slight asymmetry on the high frequency side is due to the relaxation process that is starting at the edge of the frequency window). At the lowest frequencies, electrode polarization is influencing ε', lowering the ε'' slope while leaving M'' unaffected (reproduced from reference 159).

1.4. References

[1] R. Brand, P. Lunkenheimer, A. Loidl, J. Chem. Phys. 116(23) (2002) 10386-10401.

[2] M. Dionísio, H.P. Diogo, J.P.S. Farinha, J.J. Moura-Ramos, J. Chem. Ed. 32 (2005) 1335-1359.

[3] P.J. Collings, "Liquid Crystals: Nature's delicate phase of matter", Princenton Univeristy Press, 2nd Edition (2002).

[4] M. Dionísio, N.M. Alves, J.F. Mano, e-polymers 44 (2004).

[5] O. Pascui, M. Beiner, D. Reichert, Macromolecules 36 (2003) 3992-4003.

[6] J. C. Dyre, J. Non-Cryst. Solids 235-237 (1998) 142-149.

[7] J.H. Crowe, J.F. Carpenter, L.M. Crowe, Ann. Rev. Physiol. 60 (1998) 73-103.

[8] P. Walstra, "Physical Chemistry of Food", chap. XVI, Marcel Dekker Inc., New York (2003).

[9] "The Glassy State in Foods", J.M.V. Blanshard, P. Lillford, Nottingham Univ. Press, Nottingham (1993).

[10] S. Kasapis, Drying Technology 23(2005) 731-757.

[11] B.C. Hancock, G. Zografi, J. Pharm. Sci. 86(1) (1997) 1-12.

[12] W. Ostwald.: "Lehrbuch der allgemeinen Chemie", vol II/1, p.514. W. Engelmann, Leipzig (1910).

[13] W. Kauzmann, Chem. Rev. 43 (1948) 219–256.

[14] R. Richert, C. A. Angell, J. Chem. Phys. 108(21) (1998) 9016-9026.

[15] C.A. Angell, Science 267 (1995) 1924-1935; Proc. Natl. Acad. Sci. USA 92 (1995) 6675-6682.

[16] D. Turnbull, Contemp. Phys. 10 (1969) 473-488.

[17] C.A. Angell, J. Non-Cryst. Solids 102 (1988) 205-221.

[18] C.A. Angell, J. Non-Cryst. Solids 131-133 (1991) 13-31.

[19] M.R. Carpentier, D.B. Davies, A.J. Matheson, J. Chem. Phys. 46(7) (1967) 2451-2454.

[20] C.A. Angell, J. Res. Natl. Inst. Stand. Technol. 102 (1997) 171-185.

[21] A.R. Brás, A.M.M. Antunes, M.M. Cardoso, J.P. Noronha, M. Dionísio, N.T. Correia, submitted.

[22] E. Tombari, C. Cardelli, G. Salvetti, G.P. Johari, J. Mol. Struct. 559 (2001) 245-254.

[23] W.H. Wang, C. Dong, C.H. Shek, Materials Science and Engineering R 44 (2004) 45-89.

[24] "Disorderd Effects on Relaxation Processes", R. Richert, A. Blumen, Springer-Verlag, Berlin (1994).

[25] M.D. Ediger, C.A. Angell, S.R. Nagel, J. Phys. Chem. 100(31) (1996) 13200-13212.

[26] C.A. Angell, in: Relaxations in Complex Systems, eds. K. Ngai and G.B. Wright (National Technical Information Service, US Department of Commerce, Springfield, VA 1985) p.1.

[27] J.C. Maxwell, Philos. Trans. R. Soc. London 157 (1867) 49-88.

[28] P.G. Debenedetti, "Metastable Liquids", Princeton University Press, Princeton (1996).

[29] R.O. Davies, G.O. Jones, Adv. Phys. 2(7) (1953) 370-410.

[30] I.M. Hodge, J. Non-Cryst. Solids 169(3) (1994) 211-266.

[31] L.C.E. Struik, "Physical Ageing in Amorphous Polymers and Other Materials", Elsevier, Amsterdam (1978).

[32] J.L. Gómez Ribelles, "Lecture Notes", Universidad Politécnica de Valencia (2000).

[33] J.M. Hutchinson, Prog. Polym. Sci. 20(4) (1995) 703-760.

[34] A.Q. Tool, J. Am. Cer. Soc. 29 (1946) 240-253.

[35] A.J. Kovacs, Fortschr. Hochpolym. Forsch. 3 (1963) 394-394.

[36] P.G. Debenedetti, F. H. Stillinger, Nature, 410 (2001) 259-267.

[37] A. Alegría, E. Guerrica-Echevarría, L. Goitiandía, I. Tellería, J. Colmenero, Macromolecules 28(5) (1995) 1516-1527.

[38] N.G. McCrum, B.E. Read, G. Williams, "Anelastic and Dielectric effects in Polymeric Solids", Wiley, New York (1967) (reprinted by Dover, New York 1991).

[39] J.P. Runt, J.J. Fitzgerald, "Dielectric Spectroscopy of Polymeric Materials", American Chemical Society, Washington (1997).

[40] E. Riande, "Keynote Lectures in Selected Topics of Polymer Science", CSIC, Madrid (1995).

[41] G.P. Johari, J. Chem. Phys 58(4) (1973) 1766-1770.

[42] "Broadband dielectric spectroscopy", Eds. A. Schönhals, F. Kremer, Springer-Verlag, Berlin (2003).

[43] M.L. Williams, R.F. Landel, J.D. Ferry, J. Am. Ceram. Soc. 77 (1955) 3701-3707.

[44] J.D. Ferry, "Viscoelastic Properties of Polymers", Wiley, New York (1970).

[45] H. Vogel, Phys. Z. 22 (1921) 645-646.

[46] G.S. Fulcher, J. Am. Ceram. Soc. 8 (1925) 339-355.

[47] G. Tammann, W. Hesse, Z. Anorg. Allg. Chem. 156 (1926) 245-257.

[48] P.W. Atkins, "Physical Chemistry", 4th ed. Oxford University Press, Oxford (1990).

[49] G. Adam, J.H. Gibbs, J. Chem. Phys. 43(1) (1965) 139-146.

[50] H. van Damme, J.J. Fripiat, J. Chem. Phys. 62(8) (1978) 3365-3366.

[51] M.H. Cohen, D.J. Turnbull, J. Chem. Phys. 31(5) (1959) 1164-1169.

[52] M.H. Cohen, G.S. Grest, Phys. Rev. B 20(3) (1979) 1077-1098.

[53] W. Kauzmann, Chem. Rev. Lett. 64 (1990) 1549-1552.

[54] F. Stickel, W. Fischer, R. Richert, J. Chem. Phys. 102(15) (1995) 6251-6257.

[55] C.A. Angell, J. Non-Cryst. Solids 131-135 (1991) 13-31.

[56] K.L. Ngai, R.W. Renedll, D.J. Plazek, J. Chem. Phys. 94(4) (1991) 3018-3029.

[57] R. Böhmer, K.L. Ngai, C.A. Angell, D.J. Plazek, J. Chem. Phys. 99 (5) (1993) 4201-4209.

[58] F.H. Stillinger, Science 267 (1995) 1935-1939.

[59] E.H. Fontana, W.A. Plummer, Phys. Chem. Glasses 7 (1966) 139-146.

[60] R.J. Greet, D. Turnbull, J. Chem. Phys. 46(4) (1967) 1243-1251.

[61] R. Ritcher, C.A. Angell, J. Chem. Phys. 108(21) (1998) 9016-9026.

[62] K. L. Ngai, J. Non-Cryst. Solids 275 (2000) 7-51.

[63] H. Eyring, J. Chem. Phys. 4 (1936) 283-291.

[64] T.F. Schatzki, J. Polym. Sci. 57(165) (1962) 337-356.

[65] J. Heijboer, Ann. NY Acad. Sci. 279 (1976) 104-116.

[66] S. Corezzi, S. Capaccioli, G. Gallone, A. Livi, P.A. Rolla, J. Phys.: Condens. Matter 9 (1997) 6199–6216.

[67] G.P. Johari, M. Goldstein, J. Chem. Phys. 53(6) (1970) 2372-2388.

[68] G.P. Johari, M. Goldstein, J. Chem. Phys. 55(9) (1971) 4245-4252.

[69] G.P. Johari, J. Chem. Phys. 58(4) (1973) 1766-1770.

[70] G.P. Johari, K. Pathmanathan, J. Chem. Phys. 85(11) (1986) 6811-6812.

[71] S.H. Chung, G.P. Johari, K. Pathmanathan, J. Polym. Sci. B 24 (1986) 2655-2668.

[72] A. Rivera, E.A. Rössler, Phys. Rev. B, 73 (2006) 212201-212204.

[73] S. Corezzi, M. Beiner, H. Huth, K. Schröter, S. Capaccioli, R. Casalini, D. Fioretto E. Donth, J. Chem. Phys., 117(5) (2002) 2435-2448.

[74] C.A. Angell, K.L. Ngai, G.B. McKenna, P.F. McMillan, S.W. Martin, J. Appl. Phys. 88(6) (2000) 3113-3157.

[75] A. P. Sokolov, J. Non-Cryst. Solids 235–237 (1998) 190-195.

[76] M. Beiner, H. Huth, K. Schröter, J. Non-Cryst. Solids 279(1-3) (2001) 126-135.

[77] F. Garwe, A. Schönhals, M. Beiner, K. Schröter, E. Donth, J. Phys.: Condens. Matter 6 (1994) 6941-6945.

[78] F. Garwe, A. Schönhals, H. Lockwenz, M. Beiner, K. Schrötter, E. Donth, Macromolecules 29 (1996) 247-253.

[79] E. Donth, "Relaxation and Thermodynamics in Polymers, Glass Transition", Akademie-Verlag, Berlin (1992).

[80] R. Casalini, D. Fioretto, A. Livi, M. Luchesi, P.A. Rolla., Physical Review B 56(6) (1997) 3016-3021.

[81] J.M. Meseguer Dueñas, D. Torres Escuriola, G. Gallego Ferrer, M. Monleón Pradas, J.L. Gómez Ribelles, P. Pissis, A. Kyritsis, Macromolecules 34 (2001) 5525-5534.

[82] M. Schultz, Phys. Letter A 251 (1999) 269-272.

[83] M. Beiner, Macromol. Rapid. Commun. 22(12) (2001) 869-895.

[84] G. Williams, Trans. Farad. Soc. 62 (1966) 2091-2102.

[85] M. Beiner, S. Kahle, E. Hempel, K. Schröter, E. Donth, Europhys. Letters, 44 (1998) 321-327.

[86] M. Beiner, J. Korus, E. Donth, Macromolecules 30 (1997) 8420-8424.

[87] G.P. Johari, Ann. New York Acad. Sci. 279(1) (1976) 117-140.

[88] A. Kyritsis, J.L. Gómez Ribelles, J.M. Meseguer Dueñas, N. Soler Campillo, G. Gallego Ferrer, M. Monleón Pradas, Macromolecules 37(2) (2004) 446-452.

[89] A. Espadero Berzosa, J.L. Gómez Ribelles, S. Kripotou, P. Pissis, Macromolecules 37 (2004) 6472-6479.

[90] A.K. Doolittle, J. App. Phys. 22(12) (1951) 1471-1475; A.K. Doolittle, J. App. Phys. 23(2) (1952) 236-239.

[91] J.H. Gibbs, E.A. Dimarzio, J. Chem. Phys. 28 (1958) 373-383.

[92] G. H. Fredrickson, Annu. Rev. Phys. Chem. 39 (1988) 149-180.

[93] S. Kahle, E. Hempel, M. Beiner, R. Unger, K. Schröter, E. Donth, J. Mol. Struct. 479(2-3) (1999) 149–162.

[94] G.P. Johari, E. Whalley, Faraday Symp. Chem. Soc. 6 (1972) 23-41.

[95] K.L. Ngai, Phys. Rev. E 57(6) (1998) 7346-7349.

[96] K.L. Ngai, S. Capaccioli, Phys. Rev. E 69 (2004) 31501-31505. K.L. Ngai, M. Paluch, J. Chem. Phys. 120(2) (2004) 857-873.

[97] U. Schneider, P. Lunkenheimer, R. Brand, A. Loidl, Phys. Rev. E, 59(6) (1999) 6924-6936.

[98] E. Donth, J. Non-Cryst. Solids 53(3) (1982) 325-330.

[99] E. Hempel, G. Hempel, A. Hensel, C. Schick, E. Donth, J. Phys. Chem. B 104(11) (2000) 2460-2466.

[100] M. von Laue, Phys. Z. 18 (1917) 542.

[101] J.L. Gómez Ribelles, A. Vidaurre, J.M.G. Cowie, R. Ferguson, S. Harris, I.J. McEwen, Polymer 40(1) (1998) 183-192.

[102] E. Donth, H Huth, M Beiner, J. Phys.: Condens. Matter 13 (2001) L451–L462.

[103] J. Korus, E. Hempel, M. Beiner, S. Kahle, E. Donth, Acta Polym. 48(9) (1997) 369-378.

[104] G. Strobl, "Condensed Matter Physics", Springer-Verlag, Berlin (2004).

[105] J. Zarzycki, "Glasses and the vitreous state", Cambridge: Cambridge University Press (1991).

[106] M. Volmer, A.Z. Weber, Phys. Chem. 119 (1926) 277-301.

[107] R. Becker, W. Döring, Ann. Phys. 24 (1935) 719-752.

[108] D. Turnbull, M.H. Cohen, J. Chem. Phys. 29(5) (1958) 1049-1054.

[109] S. Sakka, J.D. Mackenzie, J. Non-Cryst. Solids, 6(2) (1971) 145-162.

[110] P. Pissis, A. Kyritsis, G. Barut, R. Pelster, G. Nimtz, J. Non-Cryst. Solids 235-237 (1998) 444-449.

[111] M. Wübbenhorst, V. Lupascu, Proceedings of the ISE-12, Brazil (2005).

[112] N.M. Alves, J.F. Mano, E. Balaguer, J.M. Meseguer Dueñas, J.L. Gómez Ribelles, Polymer 43(15) (2002) 4111-4122.

[113] Y. Wang, J.L. Gómez Ribelles, M. Salmerón Sánchez, J.F. Mano, Macromolecules 38(11) (2005) 4712-4718.

[114] M. Dionísio, M.T. Viciosa, Y. Wang, J.F. Mano, Macromol. Rapid Commun. 26 (2005) 1423-1427.

[115] R.H. Boyd, Polymer 26 (1985) 323-347.

[116] G. Odian, "Principles of Polymerization", Wiley−Interscience, New York (1981).

[117] G. Moad, D.H. Solomon, "The chemistry of free radical polymerization", Pergamon, Oxford, U.K. (1995).

[118] "Controlled Radical Polymerization", K. Matyjaszewski, ACS Symposium Series; Am. Chem. Soc.: Washington D.C. (1997).

[119] H-G. Elias, "An introduction to polymer science", VCH, New York (1997).

[120] M. Buback, C. Kowollik, Macromolecules 32(5) (1999) 1445-1452.

[121] G. A. O'Neil, J. M. Torkelson, Macromolecules 32(2) (1999) 411-422.

[122] G.T. Russell, R.G. Gilbert, D.H. Napper, Macromolecules 25(9) (1992) 2459-2469.

[123] G.T. Russell, R.G. Gilbert, D.H. Napper, Macromolecules 26(14) (1993) 3538-3552.

[124] "Polymer Handbook", 5th Edn. (Eds. J. Brandrup and E.H. Immergut), Wiley, New York (1998).

[125] R.G.W. Norrish, R.R. Smith, Nature 150 (1942) 336-337.

[126] G.A. O'Neil, M.B. Wisnudel, J.M. Torkelson, Macromolecules 29(23) (1996) 7477-7490.

[127] P. Debye, "Polar Molecules", Chem. Catalog. , New York (1929).

[128] C.J.F. Böttcher, P. Bordewijk, "Theory of electric polarization", vol. II-Dielectrics in time-dependent fields, Elsevier, Amsterdam (1978).

[129] A.R. Blythe, "Electrical properties of polymers", Cambridge University Press (1979).

[130] M. Dionísio, "Aplicação de técnicas dieléctricas a estudos de dinâmica molecular e estrutura molecular", Ph.D. Thesis, Inst. Sup. Técnico (Lisboa) (1993).

[131] R. Lovell, J. Phys. C: Solid State Phys. 7(23) (1974) 4378-4384.

[132] P. Debye, "Polar Molecules" Dover Publications: New York (1945).

[133] G. Loveluck, J. Phys. Chem. 64(4) (1960) 385-387.

[134] L-M. Wang, R. Richert, J. Phys. Chem. B 109(18) (2005) 8767-8773.

[135] S.S.N. Murthy, J. Phys. Chem. 100 (1996) 8508-8517.

[136] M.T. Viciosa, A. Nunes, A. Fernandes, P.L. Almeida, M.H. Godinho, M.D. Dionísio, Liquid Crystals 29(3) (2002) 429-441.

[137] G. Floudas, P. Placke, P. Štepánek, W. Brown, G. Fytas, K.L. Ngai, Macromolecules 28 (1995) 6799-6807.

[138] C.J. Dias, Phys. Rev. B 53(21) (1996) 14212-14222.

[139] K.S. Cole, R.H. Cole, J. Chem. Phys. 9 (1941) 341-351.

[140] D.W. Davidson, R.H. Cole, J. Chem. Phys. 18 (1950) 1417-1418.

[141] S. Havriliak, S. Negami, J. Polym. Sci. Part C: Pol. Symp. 14(1) (1966) 99-117.

[142] R. Díaz-Calleja, Macromolecules 33(24) (2000) 8924-8924.

[143] R. Kohlrausch, Pogg. Ann. Phys. 167(1) (1854) 56-82, 167(2) (1854) 179-214; 195(7) (1863) 337-368; 204(5) (1866) 1-20.

[144] G. Williams, D.C. Watts, Trans. Faraday Soc. 60 (1970) 80-85.

[145] F. Alvarez, A. Alegría, J. Colmenero, Phys. Rev. B 44(14) (1991) 7306-7312.

[146] B.V. Hamon, Proc. Inst. Elec. Eng. 99 (1952) part IV, monograph 27.

[147] L. Onsager, J. Amer. Chem. Soc. 58 (1936) 1486-1493.

[148] E. Grunwald, K-C. Pan, A. Efflo, J. Phys. Chem. 80(27) (1976) 2937-2940.

[149] J.G. Kirkwood, J. Chem. Phys. 7 (1939) 911-919; Ann NY Acad. Sci. 40 (1940) 315.

[150] J.G. Kirkwood, Trans. Faraday Soc. 42 (1946) 7-12.

[151] H. Fröhlich, "Theory of dielectrics", Oxford University Press, London (1958).

[152] T. Blochowicz, "Broadband Dielectric Spectroscopy in Neat and Binary Molecular Glass Formers", Ph.D. Thesis, Universität Bayreuth, Bayreuth (2003).

[153] G. Williams, D.K. Thomas, "Phenomenological and Molecular Theories of Dielectric and Electrical Relaxation of Materials", Application Note Dielectrics 3, Novocontrol GmbH (1998).

[154] A. Bello, E. Laredo, M. Grimau, J. Non-Crystal. Solids (2007) in press.

[155] J.C. Maxwell, "Treatise on Electricity and Magnetism", Dover reprint, New York (1892).

[156] K.W. Wagner, Arch. Elektrotech. 2 (1914) 371-387.

[157] R.W. Sillars, J. Inst. Electr. Eng. 80 (1937) 378-394.

[158] P.A. Steeman, F. H. J. Maurer, Polymer 33(20) (1992) 4236-4241.

[159] M. Dionísio, J.F. Mano, "Electric Techniques" in Handbook of Analysis and Calorimetry Edited by Michael Brown (in press).

CHAPTER 2 EXPERIMENTAL

2.1 Introduction

This chapter describes the equipment used to perform the dielectric relaxation spectroscopy (DRS) and differential scanning calorimetry (DSC) experiments. In DRS two impedance analyzer was used, the HP4284A available in Centro de Química-Física Molecular do Instituto superior Técnico and the ALPHA-N from Novocontrol, available in the laboratory 415 of Chemical Department of Faculdade de Ciências e Tecnologia from the New University of Lisbon. Nevertheless, the first one only was employed during the first stage of this work (the monomers characterization) and because of this the detailed description only will be referred to the second one. On the other hand, the DSC experiments were carried out in three different devices: *i*) Setaram DSC131 available in the Chemical Department of University Nova of Lisbon; *ii*) TA of Technical Superior Institute of Lisbon and *iii*) DSC7 Perkin Elmer, available in Centre of Biomaterials of University Polytechnic of Valencia (Spain). Since the principal contribution of this technique to this work is in the study of the free radical polymerization, and this was completely developed in the Centre of Biomaterials of Valencia, the only equipment described in detail will be that used in that laboratory.

Also in this chapter, a presentation of the monomers studied will be done, and the chemical structure of the network formed will be introduced.

2.2 Principles of dielectric spectroscopy

Dielectric relaxation spectroscopy comprises an exceptionally wide frequency range [1] not able to be covered by a single apparatus. Thus, a combination of several equipments/methods is used: frequency-response analysis (10^{-4} to 10^{11} Hz), impedance analysis (10^{2} to 10^{7} Hz), radio frequency-reflectometry (10^{6} to 10^{9} Hz) and network analysis (10^{7} to 10^{12} Hz).

In order to obtain the dielectric information of a material, it is used an electric circuit with several components which simulate the response of the material. This model circuit is known as **equivalent circuit**. The loss part of the dielectric response

is represented by a resistance R_x, while the introduction of a capacitance C_x plays the role of the storage material, i.e. the ability to storage the electric field. In such a way, the overall admittance $Y(\omega)$ and impedance $Z(\omega)$ in a RC circuit is given by the sum of the contributions of both elements:

$$Y(\omega)=\frac{1}{Z(\omega)}=\frac{1}{R_P(\omega)}+i\omega C_P(\omega)=\frac{1}{R_S(\omega)+\frac{1}{i\omega C_S(\omega)}} \qquad \text{Equation 2.1}$$

where sub index P and S correspond to parallel and series circuits respectively, i is $\sqrt{-1}$ and ω is the angular frequency (this equivalence does not apply to d.c. step-function experiments [2]). The measured values will depend on the geometry of the sample. As that is localized between a parallel capacitor the factors to be considered are the plate area A and separation d (with $A>>d$). In order to avoid this influence, the dielectric properties of the material are expressed in terms of dielectric permittivity (eventually, with electric modulus or conductivity) using the relation $\varepsilon^*(\omega)=C^*(\omega)/C_0$. Here, $C_0=A\varepsilon_0/d$ is the vacuum capacitance of the parallel plate capacitor and C^* is the complex capacitance of the same capacitor filled with the material under study. If a sinusoidal electric field is applied, the complex permittivity relates to the impedance through:

$$\varepsilon^*(\omega)=\frac{1}{i\omega Z(\omega)C_0} \qquad \text{Equation 2.2}$$

When one is in presence of a material with a Debye response, i.e. with a relaxation process with a single relaxation time, the simplest equivalent circuit consists in one resistance R_1 associated in series with the capacitance C_1. For describing the instantaneous polarization due to atomic an electronic contributions, a capacitance, C_∞ associated in parallel with those components must be included [3,4] (see Figure 2.1.a). For describing this situation, Equation 2.1 (for series elements) must be introduced in Equation 2.2:

$$\varepsilon^*(\omega)=\frac{C_\infty}{C_0}+\frac{1}{i\omega C_0\left[R_S(\omega)+\frac{1}{i\omega C_S(\omega)}\right]}=\varepsilon_\infty+\frac{1}{i\omega C_0 R_S(\omega)+\frac{C_0}{C_S(\omega)}}=$$

$$=\varepsilon_\infty+\frac{\frac{C_S(\omega)}{C_0}}{i\omega C_S(\omega)R_S(\omega)+1} \qquad \text{Equation 2.3}$$

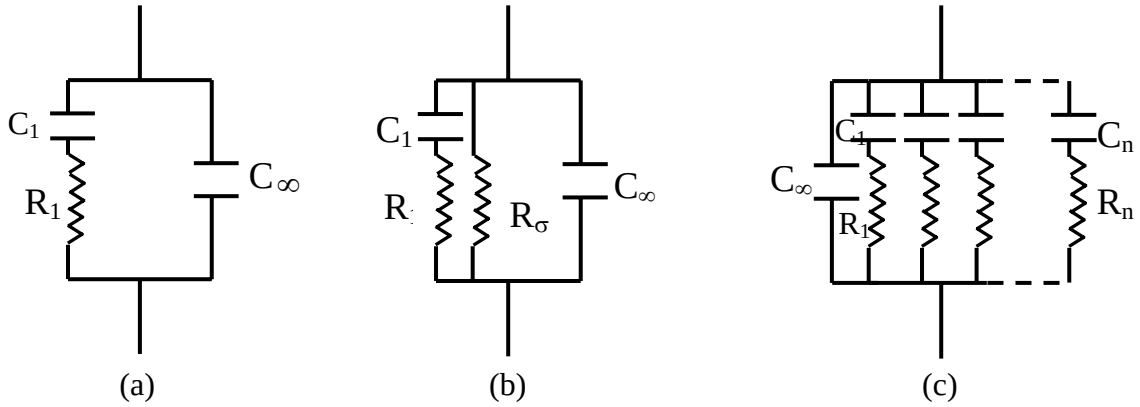

Figure 2.1 Circuit diagrams for a material exhibiting: a) a relaxation process with a single relaxation time and induced polarization, b) a relaxation process with a single relaxation time, conduction and induced polarization and c) a distribution of relaxation times and induced polarization (reproduced from reference 5).

where ε_∞ denotes the quotient C_∞/C_0. In last expression it can be identified the relaxation time of the equivalent RC circuit as $\tau_{RC}=R_S C_S$ and $\varepsilon_0-\varepsilon_\infty$ as the fraction C_∞/C_0. Rewriting Equation 18, we obtain:

$$\varepsilon^*(\omega)=\varepsilon_\infty+\frac{\varepsilon_0-\varepsilon_\infty}{1+i\omega\tau_{RC}} \qquad \text{Equation 2.4}$$

which is a typical representation of complex permittivity for a Debye material.

For a substance that presents a non-Debye behavior, i.e. when it is necessary to considerer a distribution of relaxation times, the equivalent circuit results of a combination of several R_iC_i 's associated in series, as shown in Figure 2.1.c.

Additionally, if translational diffusion of mobile charges occurs, i.e. if the material exhibits conduction the term $1/R_\sigma$ must be introduced in the overall impedance leading to a complex permittivity as:

$$\varepsilon^*(\omega)=\frac{C_\infty}{C_0}+\frac{1}{i\omega C_0\left[R_S(\omega)+\frac{1}{i\omega C_S(\omega)}+\frac{1}{R_\sigma}\right]}=\varepsilon_\infty+\frac{\varepsilon_0-\varepsilon_\infty}{1+i\omega\tau_{RC}}-\frac{i}{\omega C_0 R_\sigma} \quad \text{Equation 2.5}$$

The conduction process appears as a low frequency tail in the plot of ε'', giving a value for $C_0R_\sigma=\varepsilon_0/\sigma_0$, being σ_0 the frequency independent specific conductivity. The equivalent circuit is presented in Figure 2.1.c.

2.3 Alpha High Resolution impedance analyzer and temperature control

The Alpha-N analyzer measures the impedance or complex dielectric function of materials at frequencies between 3 μHz and 10 MHz with high precision. In addition, it can be used in gain phase mode by measurement of two a.c. voltages and their phase relation.

Two major parts are distinguished in this analyzer:

- A frequency response analyzer with a sine wave and d.c. bias generator (this last one was not used in this work) and two a.c. voltage input channels. Each input channel measures the a.c. voltage amplitude of an applied sine wave (more exactly, they measure the amplitude and phase angle of the harmonic base wave component of the signal). The phase shift between the sine waves applied to the both inputs is also detected.

- A dielectric (or impedance) converter with a wide dynamic range current to voltage converter and a set of precision reference capacitors. This dielectric converter is mounted inside the Alpha analyzer mainframe.

For electric material measurements an additional dielectric sample cell is required. The BDS1200 sample cell from Novocontrol was employed for the measurements. It is suitable for low frequency range from DC to 10 MHz. It includes PT100 temperature sensor localized inside the inferior electrode. It can work in the temperature range from -160 ºC to 450 ºC. This cell is connected to the Alpha-N analyzer by two wires BNC. These BNC cables present the disadvantage of limiting the performance at high frequencies (up to MHz).

The alpha analyzer has to be operated under control of a separate host computer by the GPIB IEEE 488 bus.

Principles of operation

The ALPHA analyzer incorporates a digital frequency response analyzer (FRA) with sine wave generator, dc bias generator and two analysis channels. The FRA is used in combination with the dielectric converter. This component measures the response of a system to a harmonic (sinusoidal) excitation. The excitation and the response signals are voltages. The response signal is analyzed by Fourier transform, being of especial interest the amplitude and phase angle of the sinusoidal base wave with respect to the excitation signal.

The ALPHA analyzer contains two independent voltage input channels and correlators as shown in Figure 2.2.

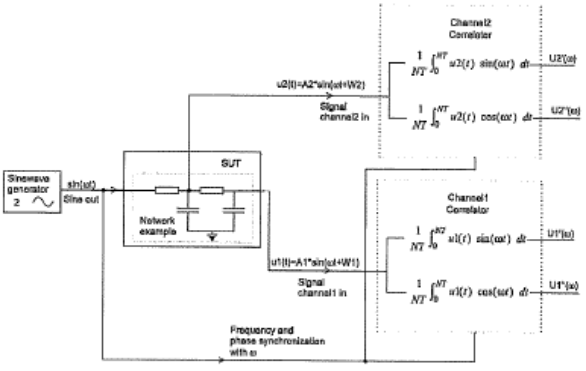

Figure 2.2 Basics of frequency response analysis [6].

A sine wave generator creating the excitation signal is connected to the system under study. In the Figure 2.2, a RC network is shown as example. The input signals $u_1(t)$ and $u_2(t)$ are applied to a correlator performing the Fourier transform. The correlators are phase synchronized to the generator, so that the correlation frequency $\omega/2\pi$ corresponds to the generator frequency and a defined phase relation between the generator and the correlation exists.

The response of the correlator 1 to the signal $u_1(t)$ has two components:

$$U_1'(t) = \frac{1}{NT}\int_0^{NT} u_1(t)\sin(\omega t)dt \qquad \text{Equation 2.6}$$

$$U_1''(t) = \frac{1}{NT}\int_0^{NT} u_1(t)\cos(\omega t)dt \qquad \text{Equation 2.7}$$

Where U_1' is the in phase component and U_1'' the orthogonal component of the harmonic base wave of $u_1(t)$. N is the number of periods with duration $T = 2\pi/\omega$ measured by the correlator.

The amplitude $A_1(\omega)$ and the phase angle $W_1(\omega)$ of the base wave of $u_1(t)$ is calculated from:

$$A_1(\omega) = 2\sqrt{U_1'^2 + U_1''^2} \qquad \text{Equation 2.8}$$

$$W_1(\omega) = \arctan\left(\frac{U_1''}{U_1'}\right) \qquad \text{Equation 2.9}$$

The basic principle of measurement of the internal Alpha current to voltage converter used for impedance measurements is shown in Figure 2.3.

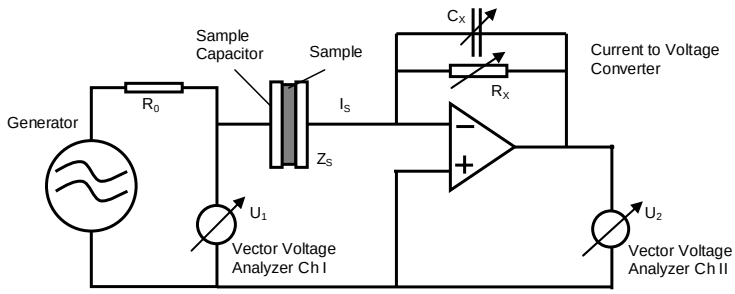

Figure 2.3 Principle of the impedance measurement [6].

The a.c. voltage from the generator is applied to the sample and measured in amplitude and phase as U_1. The resistor R_0 (50 Ω) limits the sample current if the sample impedance becomes to low. The sample current I_S feeds in the inverting input of an operational amplifier which has the variable capacity C_X (100-470 pF) and the resistor R_X (it switches between 30 Ω, 100 Ω and 1 TΩ) in its feed back loop. The Alpha analyzer selects a combination of R_X and C_X in such a way that the output voltage U_2 is in good measurable range of the voltage input channels (3 V – 30 mV). For ideal components, U_2 is related to the sample current I_S by

$$I_S = -\frac{U_2}{Z_X} \qquad \text{Equation 2.10}$$

where $Z_X = \left(R_X - 1 + i\omega C_X\right)^{-1}$ and $\omega = 2\pi f$. For an ideal operational amplifier, the voltage at the input is 0 V with respect to ground and therefore U_1 corresponds to the voltage over the sample capacitor. By this way, the sample impedance Z_S is calculated from

$$Z_S = \frac{U_1}{I_S} = -\frac{U_1}{U_2} Z_X \qquad \text{Equation 2.11}$$

The impedance Z_S relates to the complex dielectric permittivity through the Equation 2.18.

Temperature control

The temperature control was made by the QUATRO modulus also from Novocontrol. This temperature controller is connected to the Alpha-N analyzer as schematized in Figure 2.4.

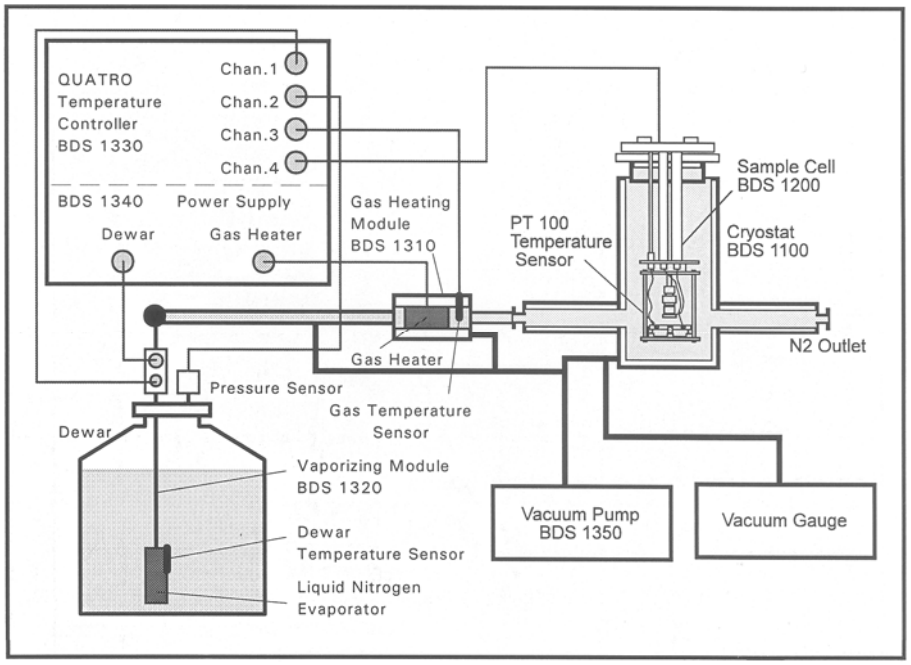

Figure 2.4 Temperature control device and its connection to the sample cell (reproduced from reference 6).

The Quatro controller has four circuits controlling the sample temperature, the gas temperature, the temperature of the liquid nitrogen in the dewar and the pressure in the dewar. The sample temperature is reached by heating the N_2 gas with a precision that can be of ± 0.01 K. All the nitrogen passing circuit is isolated by a vacuum chamber whose pressure is measured.

Both the acquisition data and the temperature control are carried out by the software WinDETA also from Novocontrol.

For the data treatment the software WinFIT from Novocontrol was always used considering the HN fitting functions for the analysis of the real and imaginary parts of $\varepsilon^*(\omega)$.

2.4 Power compensation DSC – Pyris1

The principal results of DSC experiments reported in this work were performed with a Pyris 1 Perkin Elmer differential scanning calorimeter, which is power-compensated DSC [7]. The heat flow exchanged by the sample with their surroundings is practically compensated in the totality by the variation of the heater

electrical power. This equipment is schematically presented in Figure 2.5. The system consists of two individual furnaces, one for the sample and the other for a reference (empty pan), each one with a temperature sensor and a heater. So, the heat fluxes are supplied independently to each furnace. The two furnaces are inserted in a thermostated aluminium block and each one containing a thermometer and a heating resistor.

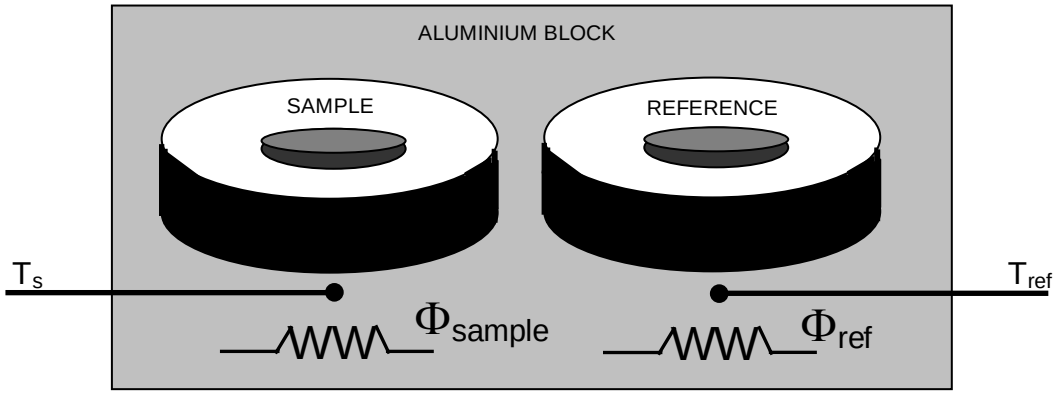

Figure 2.5 Scheme of a power-compensated differential scanning calorimeter (adapted from reference 8).

During the heating run, the programmed temperature profile of both furnaces is maintained by supplying the adequate heat flux to each of them. Thus, heat capacity measurement of a polymer sample is performed from the difference in heat flow supplied to the furnace containing an aluminum sample pan with few milligrams of the polymer when the reference furnace contains just an empty pan. The enthalpy increment in first order transitions such as melting or crystallization can be calculated from the increase or decrease respectively of the heat flow while the transition takes place in the sample. As it is usual in thermodynamics, a heat flow is considered positive when it is absorbed by the sample, given origin to endothermic processes for increments in the heat flow.

How fast the response of the system is depends on the thermal contact between the samples and the heating elements and the furnaces. The response of the compensation DSC is fast ($k_t \approx 2s$), but for very accurate or kinetic measurements, the system's response can be corrected in order to take into account this delay. It is important to point out that the DSC works in the linear response region.

To measure the heat capacity of a material is one of the more usual applications of DSC that allows the calculation of entropy and enthalpy.

In order to obtain the heat capacity the procedure is the following:

- determine the heat flow $\Phi_0(t)$ in the convenient temperature range using two empty pans in the furnaces;

- determine the heat flow $\Phi(t)$ changing one of the pans by the sample;

- for each temperature, calculate $c_p = \frac{K_\Phi(\Phi - \Phi_0)}{qm}$, where q represents the rate of the temperature, m the sample's mass and K_Φ is a calibration factor that keeps constant in the temperature range selected. If this factor changes with temperature, this dependence must be determined from a third measurement with a sample whose heat capacity is known.

Nevertheless, the knowledge of the absolute values of heat capacity is not necessary in most of the studies performed using DSC technique, provided the curvature of the baseline of the instrument (the thermogram measured with an empty pan in each furnace) is small enough. Thus, the enthalpy increment of a first order transition can be determined form the integration of the experimental heat flow measure in the temperature range of the transition drawing an adequate baseline for integration: $\Delta H = A/m.(dT/dt)$, A being the area of the heat flow peak and dT/dt the heating rate. Something similar can be said with respect to the heat absorbed or emitted in chemical reactions such as isothermal polymerization. The increment of heat capacity in the glass transition can be determined from the heat flow trace since it is just the increment of heat flow divided by the mass of the sample and the heating rate of the measurement.

The temperature gradient between the block and the furnaces is high enough to obtain a precise control of the sample temperature, either in heating or cooling experiments or in the isothermal mode. Typical scanning rates for DSC experiments are between 10 and 20 ºC.min^{-1} and the working range is between -170 ºC and 725 ºC, the lower temperature limit depending on the cooling system (liquid nitrogen, "Intracooler", water bath). A purge gas circulates in both furnaces (nitrogen in this case) to improve the temperature control. The accuracy of the temperature reading is ±0.1 ºC, according to Perkin Elmer manufacturers.

In this work only normalized heat flow thermograms (heat flow divided by the mass of the sample) will be presented. The heating scans will be performed at $10^{o}C.min^{-1}$. Temperature calibration was performed at this heating rate with indium and zinc standards, using the onset of the melting peak as the measure of the melting temperature [9]. Heat flow was calibrated with the melting enthalpy of indium. Aluminum pans (capacity = $30\,\mu l$) were used to encapsulate the samples. Other details of the experimental procedures will be given in the results description.

2.4.1 Temperature-Modulated method

In temperature modulated differential scanning calorimetry (TMDSC) the temperature profile imposed to the sample is the superposition of some temperature oscillation in the shape of a sinusoidal or a teeth saw (depending on the instruments) to the conventional DSC isotherm or heating or cooling ramp. In the case of Perkin-Elmer Pyris 1 instrument the modulation programmed is in the shape of a teeth saw, but in fact the sample temperature profile recorded is similar to a sinusoidal if its frequency is not far from 1 Hz due to heat transmission dynamics. As we will describe below the analysis of the measured heat flow oscillation is performed on the basis of the first harmonic of the Fourier transform of the heat flow curve, thus, the description of the equations can be done in any case on the basis of a sinusoidal modulation:

$$T(t) = T_0 + q_0 t + a_T \sin(\omega_0 t) \qquad \text{Equation 2.12}$$

with q_0 the underlying heating/cooling rate, a_T the temperature fluctuation amplitude and $\omega_0 = 2\pi f$ the angular frequency of modulation (the usual frequencies are between 8 and 80 mHz). In this work, TMDSC will be used to study isothermal polymerization, and thus, only the operation in the quasi-isothermal mode will be employed. From Equation 2.12, the imposed heating rate is described by:

$$\dot{T} = \frac{dT}{dt} = q_0 + a_T \omega_0 \cos(\omega_0 t) \qquad \text{Equation 2.13}$$

The heat flow transmitted to the sample under constant pressure is related to the heat capacity through:

$$\Phi = \dot{Q} = \frac{dH}{dt} = C_p \frac{dT}{dt} \qquad \text{Equation 2.14}$$

Applying the Fourier transform of this expression and using the convolution theorem (see ref. 10 for detailed calculations),

$$\Phi(\omega) = C(\omega)T(\omega) \qquad \text{Equation 2.15}$$

where $C(\omega)$ is defined as the complex heat capacity

$$C(\omega) = \int_{-\infty}^{\infty} K(t)\exp(i\omega t)dt = C'(\omega) + iC''(\omega) \qquad \text{Equation 2.16}$$

and $T(\omega)$ is the Fourier transform of the temperature rate $\dot{T}$

$$T(\omega) = \int_{-\infty}^{\infty} \dot{T}(t)\exp(i\omega t)dt = 2\pi q_0 \delta(\omega) + \pi a_T \omega_0 [\delta(\omega - \omega_0) + \delta(\omega + \omega_0)] \qquad \text{Equation 2.17}$$

The usual criterion of signal in physics was used. The inverse Fourier transformation of Equation 2.15 is the heat flow

$$\Phi(t) = \frac{1}{2\pi}\int_{-\infty}^{\infty} \Phi(\omega)\exp(-i\omega t)d\omega = q_0[C'(0) + iC''(0)]$$

$$+ \frac{a_T \omega_0}{2}[C'(-\omega_0)\exp(i\omega_0 t) + C'(\omega_0)\exp(-i\omega_0 t)]$$

$$+ i\frac{a_T \omega_0}{2}[C''(-\omega_0)\exp(i\omega_0 t) + C''(\omega_0)\exp(-i\omega_0 t)] \qquad \text{Equation 2.18}$$

This is a real expression since $C''(0) = 0$, and it is usually written in terms of the heat capacity in absence of temperature oscillations $C_0 = C'(0)$, the modulus $|C|$ and the phase angle between temperature and heat flow oscillations

$$\Phi(t) = C_0 q_0 + a_T \omega_0 [C'(\omega_0)\sin\omega_0 t + C''(\omega_0)\sin\omega_0 t]$$

$$= C_0 q_0 + a_T \omega_0 |C| \cos(\omega_0 t - \varphi) \qquad \text{Equation 2.19}$$

The real and imaginary parts of $C(\omega_0)$ are

$$C' = |C|\cos\varphi$$
$$C'' = |C|\sin\varphi \qquad \text{Equation 2.20}$$

The magnitudes C_0, $|C|$ and φ can be calculated by Fourier transform of the modulated the heat flow. From the first harmonic of the periodic component of the heat flow, H_0 and H_1, of that transformation it is obtained:

$$C_0 = \frac{H_0}{q_0} \qquad \text{Equation 2.21}$$

$$|C| = \frac{|H_1|}{a_T \omega_0} \qquad \text{Equation 2.22}$$

and φ is the argument of the complex value H_1. If the response is not linear, coefficients corresponding to higher harmonics can be arises.

2.5 Materials

Ethyleneglycol dimethacrylate (EGDMA), diethyleneglycol dimethacrylate (DEGDMA), triethyleneglycol dimethacrylate (TrEGDMA) and tetraethyleneglycol dimethacrylate (TeEGDMA) are the four monomers used in the present work. These monomers with ≥95% purity, stabilised with hydroquinone, were purchased from

Aldrich Chemicals. Hydroquinone was eliminated using a column from Aldrich (cat. nr. 306312-1). The general structure of this family of monomers is shown in Figure 2.6 and their properties listed in Table 2.1. All are liquid at room temperature.

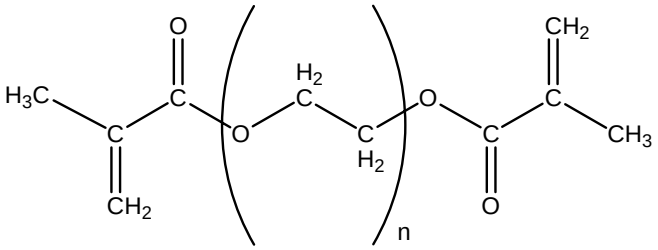

Figure 2.6 Chemical structure of the *n*-ethylene glycol dimethacrylate monomers used in this work.

Free radical polymerization was thermally initiated using AIBN (supplied by Aldrich, with 98% purity). The experimental details of isothermal polymerization of these monomers are described in Chapter 3.

These monomers are low-molecular weight glass-formers, with glass transition temperatures ranging between -85 and -100 ºC. Although some of them can crystallize, as we will see below, all of them easily vitrify just cooling from the equilibrium liquid at moderate cooling rates. Their low glass transition temperatures compared with polymerization temperatures (governed by the decomposition of the initiator) and the glass transition of the polymers, allows to study the evolution of the main dielectric relaxation of the monomer during polymerization with nearly no overlapping of dipolar phenomena related to the growing polymer network.

	EGDMA (98%)	**DEGDMA** (95%)	**TrEGDMA** (95%)	**TeEGDMA** (90%)
Mol. wt ($gr.mol^{-1}$)	198.22	242.30	286.2	330.3
Density ($gr.cm^{-3}$)	1.051	1.082	1.092	1.082
T_{boil}	98-100 °C 5 mmHg	134 ºC 2 mmHg	170-172 ºC 5 mm Hg	------
Supplier	Aldrich	Aldrich	Aldrich	Fluka
CAS number	97-90-5	2358-84-1	109-16-0	109-17-1

Table 2.1 Properties of the four monomers used in the studies (provided by suppliers).

Furthermore, in order to study the influence of the cross-linking density of the network on the molecular mobility, a series of methyl acrylate -co- TrEGDMA random copolymers were also synthesised (the chemical structure of methyl acrylate, MA, is shown in Figure 2.6.b). In this case polymerization was initiated with a 0.2% w.t. of benzoin (Scharlau 98% pure) (structure is shown in Figure 2.7) and took place under UV light.

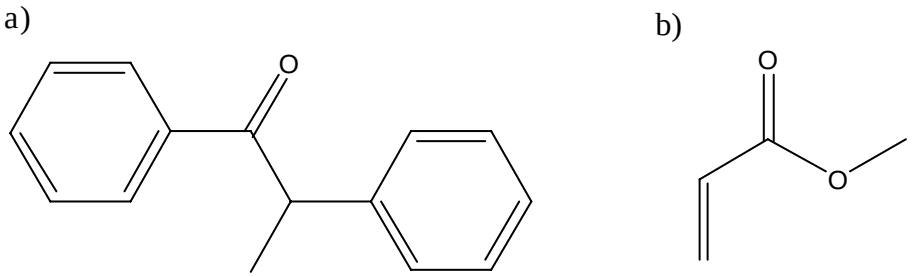

Figure 2.7 Molecular structures of a) benzoin and b) methyl acrylate

2.6 References

[1] U. Schneider, P. Lunkenheimer, R. Brand, A. Loidl, Phys. Rev. E 59(6) (1999) 6924-6936.

[2] G. Williams, D.K. Thomas, "Phenomenological and Molecular Theories of Dielectric and Electrical Relaxation of Materials", Application Note Dielectrics 3, Novocontrol GmbH (1998).

[3] J. Mijovic, B.D. Fitz, "Dielectric Spectroscopy of Reactive Polymers", Application Note Dielectrics 2, Novocontrol GmbH (1998).

[4] F. Kremer, D. Boese, G. Maier, E.W. Fischer, Prog. Colloid. Polym. Sci. 80 (1989) 129-139.

[5] M. Dionísio, J.F. Mano, "Electric Techniques" in Handbook of Analysis and Calorimetry Edited by Michael Brown (in press).

[6] "Alpha high resolution dielectric/impedance anlayzer", Novocontrol (2003).

[7] T. Hatakeyama, F.X. Quinn, "Thermal Analysis: Fundamentals and Applications to Polymer Science", John & Sons: Chichester (1994).

[8] N. Alves, "Study of the glass transition dynamics of polymeric systems by differential scanning calorimetry and mechanical spectroscopy, Universidade do Minho, Braga (2004).

[9] G.W. Höhne, W. Hemminger, H.J. Flammersheim, "Differential Scanning Calorimetry, Springer-Verlag", Springer, Berlin (1996).

[10] C. Torregosa, "Movilidad molecular conformacional de cadenas de polímeros en sitemas heterogéneos: mezclas compatibles y redes interpenetradas", Universidad Politécnica de Valencia, January (2003).

CHAPTER 3 MOLECULAR MOBILITY IN *N*-ETHYLENE GLYCOL DIMETHACRYLATE MONOMERS

3.1 Introduction

In this chapter the results of the dielectric and thermal characterization of the di-, tri- and tetra-ethylene glycol dimethacrylate monomers, respectively DEGDMA, TrEGDMA and TeEGDMA, will be presented. Ethylene glycol dimethacrylate, the first member of this series, will be analyzed separately since it crystallizes implying a different data analysis.

The three relaxations found in each monomer, the one related to the dynamic glass transition and the two remaining secondary relaxations will be analyzed in detail. The molecular origin of the two secondary processes will be only clarified in Chapters 4 and 5 with the help of polymerization results.

The glass transition was also studied by DSC measurements in function of the heating rate. The respective results will be analyzed allowing the estimation of the fragility indexes that are going to be compared, together with the glass transition temperatures of each monomer, with the values determined by dielectric relaxation spectroscopy.

All the results presented in this chapter have already been published [1-3].

3.2 Dielectric characterization

The dielectric properties of the pure monomers were carried out in the HP4284A impedance analyzer covering a frequency range from 20 Hz to 1 MHz. With the acquisition of the ALPHA-N analyzer, the low frequency limit was extended to 0.1 Hz allowing a better detection of the multiple processes. This equipment was used to investigate the dielectric behavior of monomer and AIBN initiator (0.1% w.t.) mixtures, further used to undergoing polymerization (data analyzed in Chapter 4). Since it was proved that unreacted monomer/AIBN mixtures with so low amounts of initiator behave dielectrically as the pure monomers, as it is illustrated in Figure 3.1 for DEGDMA and DEGDMA/AIBN at -76 ºC, data corresponding to fresh mixtures will be taken to characterize the monomers themselves. Thus, from now on, we will refer to *monomer*'s data without specifying the initiator content; only in the next chapter, where the polymerization is described, the amount of AIBN will be indicated.

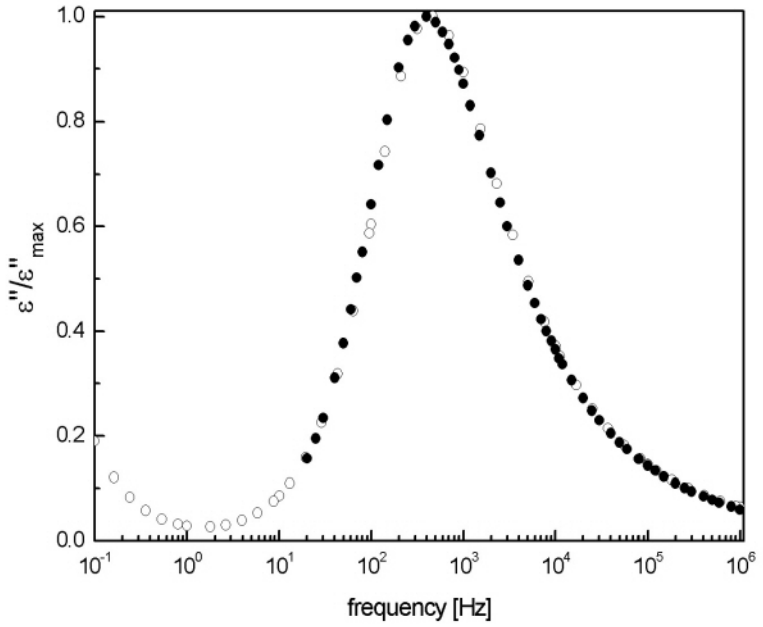

Figure 3.1 Normalized loss curves collected at -76 ºC for DEGDMA comparing data acquired using HP4284A (full symbols - neat DEGDMA) and ALPHA analyzer (open symbols - DEGDMA with 0.1% of AIBN). The superposition reveals that neither the equipment nor the initiator affected the measurements of the pure monomer.

For the data acquisition the monomers were cooled down from room temperature to -120 ºC, and successive frequency sweeps were carried out, isothermally, in increasing temperature steps. For DEGDMA and TeEGDMA data collection started at -115 ºC: from -114 to -50 ºC frequency sweeps were performed every 2 ºC, and from -50 to 25 ºC, every 5 ºC. For TrEGDMA, the frequency scans were performed from -115 to -100º and from -25 to 25 ºC, every 5 ºC, and from -100 to -30 ºC, every 2 ºC. The temperature control was performed within ± 0.5 ºC. The cooling process was done as fast as the equipment allows in order to avoid any crystallization (the average cooling rate further estimated was about -10 ºC.min^{-1}).

The dielectric loss spectra, $\varepsilon''(f)$, for the three monomers are shown in Figure 3.2, in logarithmic scale allowing to present, in the same plot, the different relaxation processes which intensities vary several orders of magnitude.

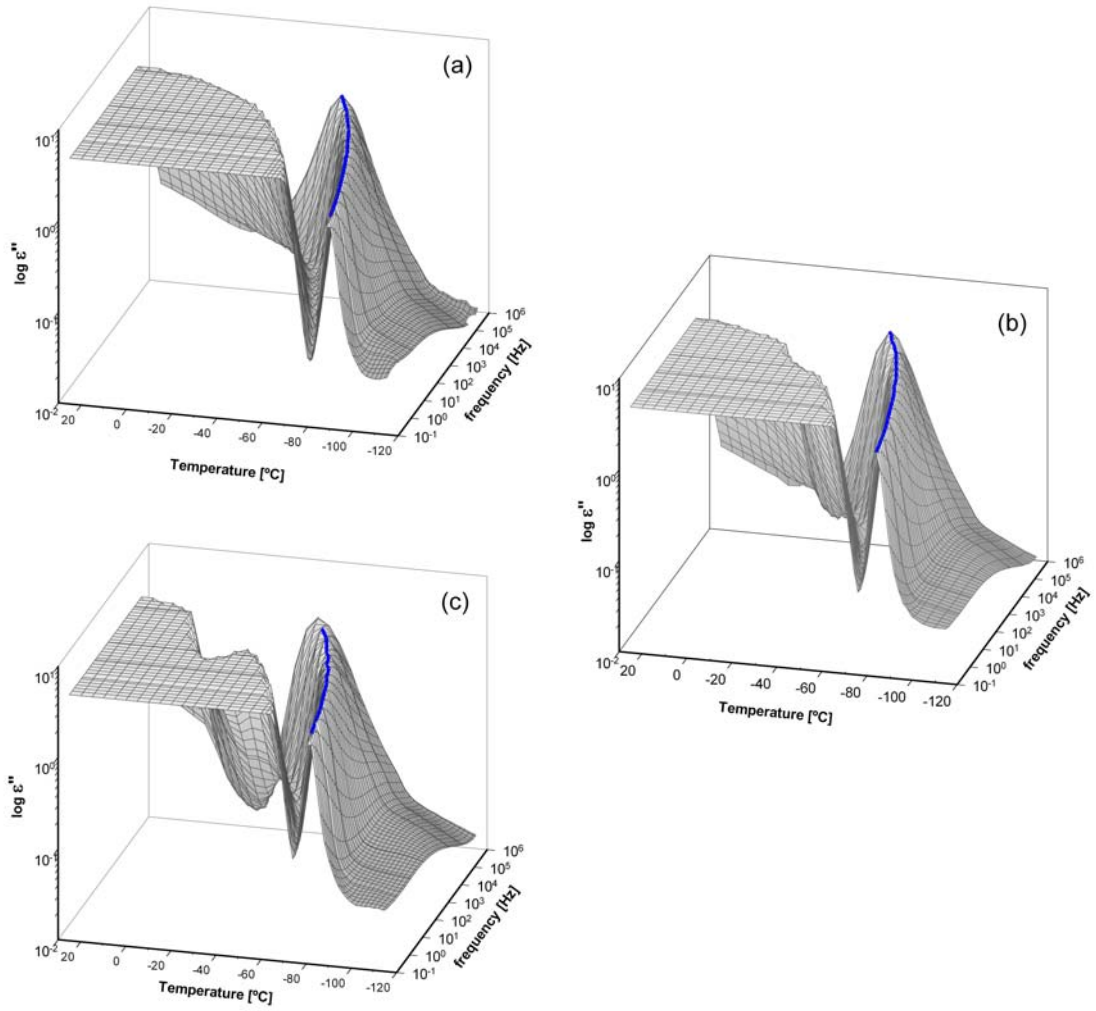

Figure 3.2 Dielectric loss spectra in logarithmic scale for (a) DEGDMA, (b) TrEGDMA and (c) TeEGDMA monomers between -115 ºC and 25 ºC. Data acquired with ALPHA analyzer. The solid blue line acts as a guide indicating the behavior of the maxima of ε'' for the α relaxation.

The three materials present a clear maximum that shifts to higher frequencies with increasing temperature (see solid line in Figure 3.2). The position of this dominating peak is different in each monomer as it is shown in Figure 3.3 where the data at the frequency of 1 kHz are plotted as a function of the temperature. The position of ε''_{max}, moves slightly to higher temperatures with the increases of the number of ethylene glycol unities (n), going from around -75 ºC, for DEGDMA, to -66 ºC for TeEGDMA. The relaxation process observed in this temperature region is related with the glass transition of the monomers, being an α -type process.

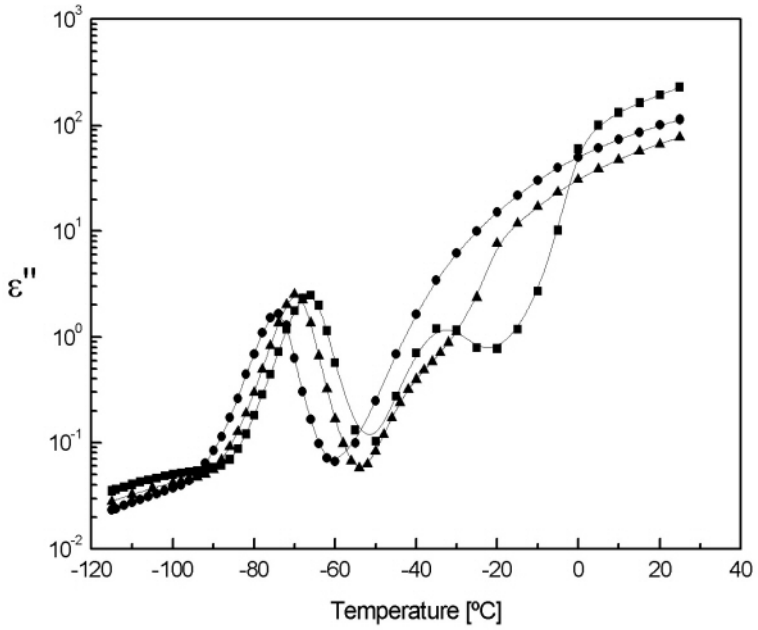

Figure 3.3 ε'' values at 1 kHz, taken from isothermal measurements, for DEGDMA (circles), TrEGDMA (triangles) and TeEGDMA (square).

Due to high intensity of this α process, secondary relaxations are hardly visible in 3D representation. In Figure 3.3 a broad secondary relaxation can be observed in isochronal plots at the lowest temperatures. However, it is necessary to present isothermal spectra at temperatures where the α relaxation has not yet entered in our frequency window, to show without any doubts the existence of a third relaxation process. In Figure 3.4, where the spectra for TeEGDMA monomer is presented only at temperatures between -114 and -86 ºC (the main relaxation only arises as a contribution in the low frequency side at the higher temperatures), the two secondary relaxations are very well defined being designated as γ and β in increasing order of temperature.

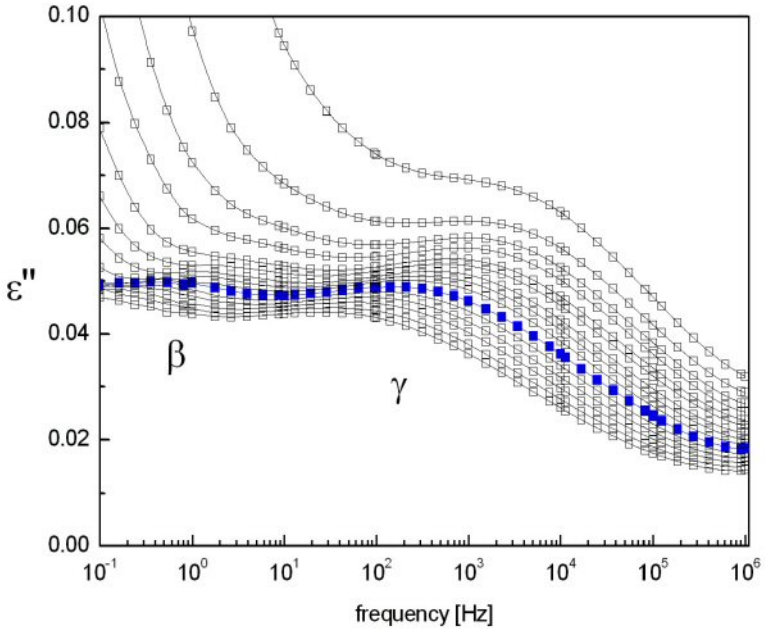

Figure 3.4 Dielectric loss spectra of TeEGDMA between -114 and -86 ºC in steps of 2 ºC, showing two secondary relaxation processes , β and γ (the isotherm collected at -104 ºC is presented in full symbols); the high loss values on the low frequency side for the highest temperatures is due to the incoming of the α relaxation process associated with the glass transition.

For temperatures higher than around -60 ºC, a contribution of the d.c. conductivity arises in the low frequency side. A close inspection of Figure 3.2.b and c (TrEGDMA and TeEGDMA respectively) shows that the increase of this conductivity does not follow a continuous behavior. As we will see later, this irregular temperature dependence of conductivity is related to cold crystallization.

Data treatment was performed using the empirical Havriliak-Negami [4] function described in Chapter 1. The fit of the overall spectrum for each temperature was accomplished by summing two or three individual HN functions. When necessary, a conductivity term ($-i\sigma/\omega^c\varepsilon_0$) was included to obtain a good fit at low frequencies and higher temperatures.

Figure 3.5 illustrates the results of the fitting procedure and the individual functions used, for the three monomers at two different temperatures.

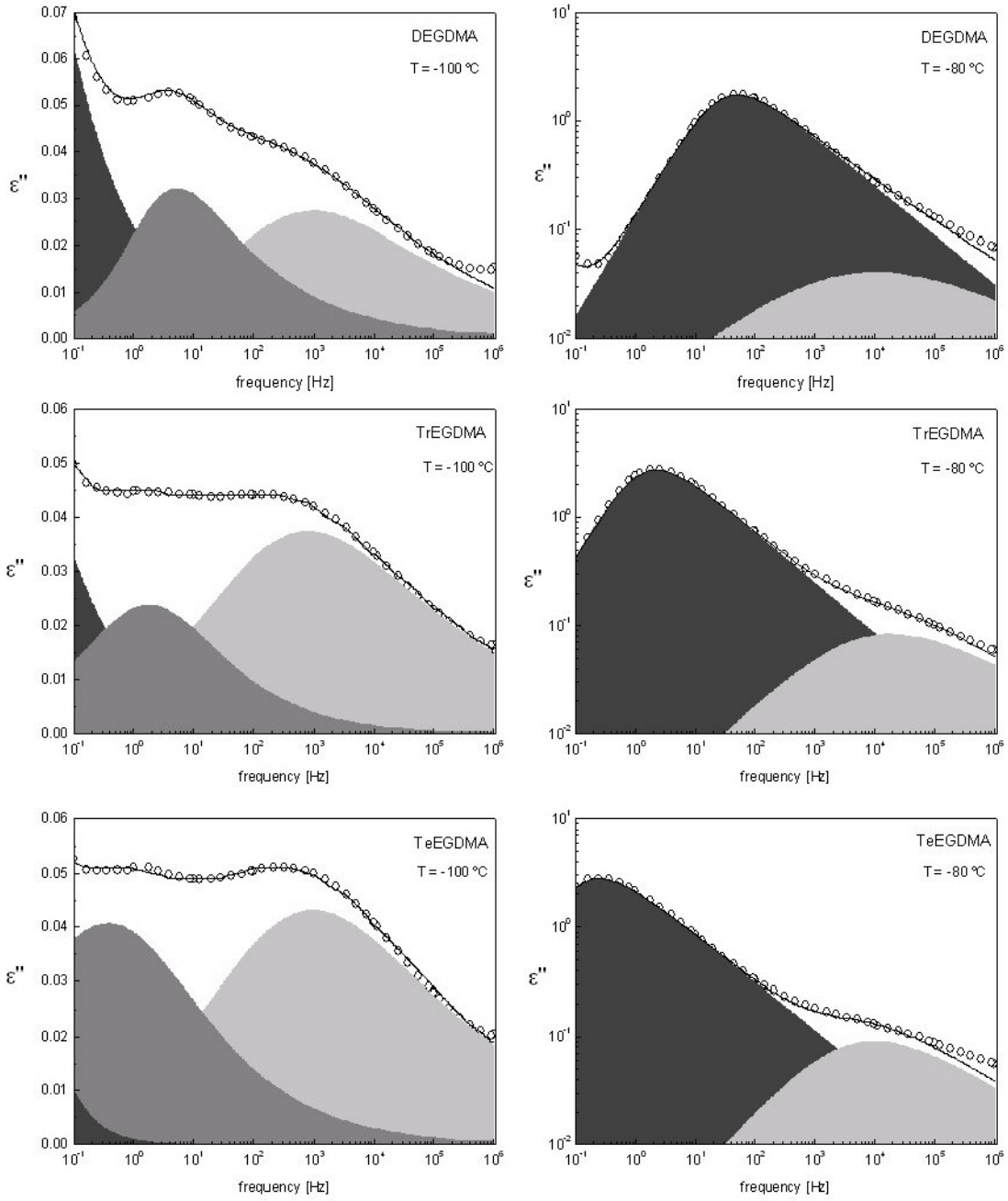

Figure 3.5 Dielectric loss spectra obtained at -100 and -80 ºC for: a) DEGDMA, b) TrEGDMA and c) TeEGDMA. The individual HN curves are represented as filled areas: α (black), β (dark gray) and γ (light gray) processes. The overall fittings are depicted as solid lines.

For the sake of clarity, the analysis of the different parameters obtained form the HN fits will be presented separately for the main and secondary relaxation processes.

3.2.1 The α process

The shape parameters and dielectric strength estimated from the HN fitting for the more intense dominating α-process are plotted in Figure 3.6 for the three monomers (values presented in Annex I); From the figure four features are observed: *i*) the dielectric strength decreases with increasing temperature for the three monomers, and *ii*) increases with the size of ethylene glycol moiety; *iii*) the α_{HN} and β_{HN} shape parameters are almost constant in the temperature range studied, and *iv*) these parameters are almost the same for the three monomers.

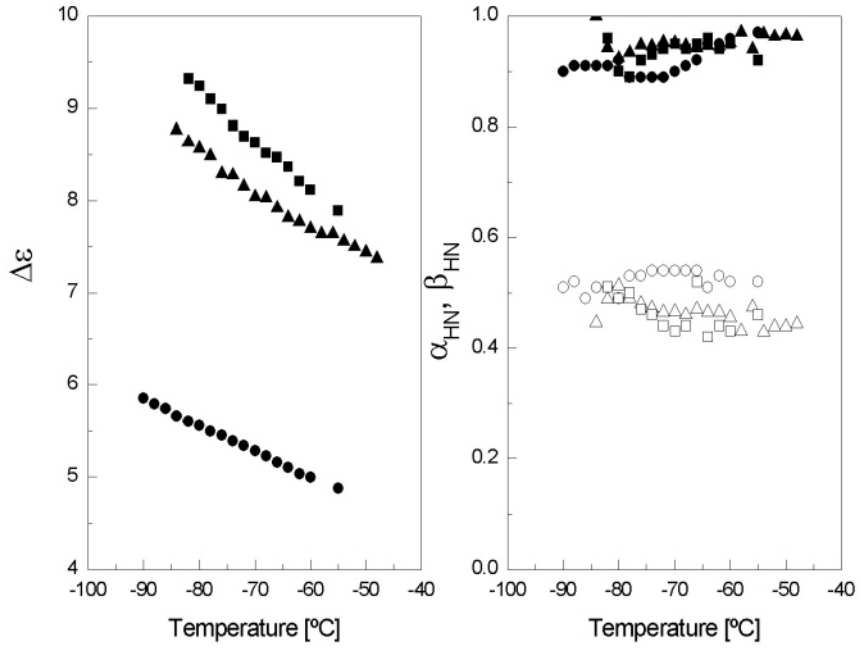

Figure 3.6 Dielectric strength and shape parameters obtained from the HN fitting procedure for the main relaxation process of: DEGDMA (circles), TrEGDMA (triangles) and TeEGDMA (squares). In the right, open symbols correspond to β_{HN} and full symbols to α_{HN}.

The increase of the dielectric strength between consecutive monomers can be rationalized in terms of an increase of the ethylene glycol moiety. On the other hand, the intensity of the α-relaxation decreases almost linearly with the temperature increase as typically found for this process [5-7]. The linear temperature dependence is frequently used to find the temperature of the dielectric onset of the α-process,

$T_{on,\alpha}$ that lies at temperatures higher than the glass transition. The linear extrapolation of $\Delta\varepsilon = 0$ in order to estimate the onset of α process for these monomers, leads to 117, 145 and 92 ºC for DEGDMA, TrEGDMA and TeEGDMA respectively, i.e. values around 200 degrees above T_g. Although these values are not predictable, the weak temperature dependence of $\Delta\varepsilon$ seems to lead to unreasonable values.

Using the values of $\Delta\varepsilon_\alpha$ from HN fitting, it is possible to check the relation proposed by Kirkwood-Fröhlich that predicts an inverse dependence of this parameter with temperature as Equation 3.1 (see chapter 1 section 1.3.4).

$$\Delta\varepsilon \sim F_{onsager}\, g \frac{\mu^2}{kT}\frac{N}{V} \qquad \text{Equation 3.1}$$

According to this equation the product $T\Delta\varepsilon_\alpha$ should be a constant value. In Figure 3.7 where $T\Delta\varepsilon_\alpha$ is plotted versus temperature for the three monomers, the temperature independence observed is the confirmation of the behavior predicted by Kirkwood-Fröhlich, thus data can be described by a law according to $\Delta\varepsilon \sim 1/T$. However, it seems important to point out that in other low molecular systems as dibutyl phthalate [8] and glycerol [9] has been verified a strong deviation of this prediction, where $\Delta\varepsilon$ decreases more than expected with increasing temperature. In these cases, the stronger temperature dependence of $\Delta\varepsilon$ can be related to an increasing influence of the environment over a test dipole with decreasing temperature. In the framework of the cooperativity concept $\Delta\varepsilon_\alpha$ should be related to an effective dipole moment due to the *CRR*. With the temperature decrease the size of *CRR* increases and consequently the effective dipole moment (Schönhals in ref. 10 and chapter 7 in ref. 11).

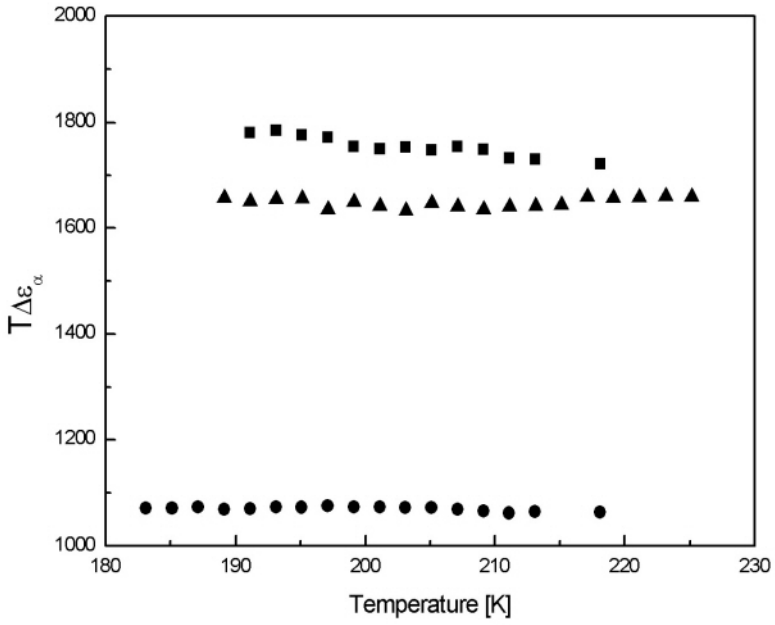

Figure 3.7 Values of $(T\Delta\varepsilon_\alpha)$ *vs.* temperature: circles for DEGDMA, triangles for TrEGDMA and squares for TeEGDMA.

The value of the α_{HN} shape parameter for the three monomers remains almost constant in the temperature region where the loss peaks are detected. The β_{HN} parameter slightly increases with increasing temperature. The fact that the shape parameters of HN equation are nearly temperature independent traduces that the shape of the loss peak does not change with temperature as it is confirmed drawing a master curve in a normalized plot. The master curve for DEGDMA is shown in Figure 3.8.a where the data for temperatures from -80 to -60 are also included. The fitting parameters for the master curves are $\alpha_{HN} = 0.92 \pm 0.04$ and $\beta_{HN} = 0.52 \pm 0.03$ for DEGDMA, $\alpha_{HN} = 0.95 \pm 0.03$ and $\beta_{HN} = 0.46 \pm 0.03$ for TrEGDMA and $\alpha_{HN} = 0.94 \pm 0.03$ and $\beta_{HN} = 0.46 \pm 0.05$ for TeEGDMA. While α_{HN} is nearly the same for the three monomers, β_{HN} is slightly higher for DEGDMA than for the other two. The similar shape of the main relaxation of the three monomers is put in evidence when the normalized loss curves are built at the same temperature giving rise to a good superposition (see Figure 3.8.b where isothermal data at -70 ºC are normalized); nevertheless, the master curve of DEGDMA presents a little less pronounced high frequency tail and thus, higher symmetry, as denoted by the superior value of β_{HN} .

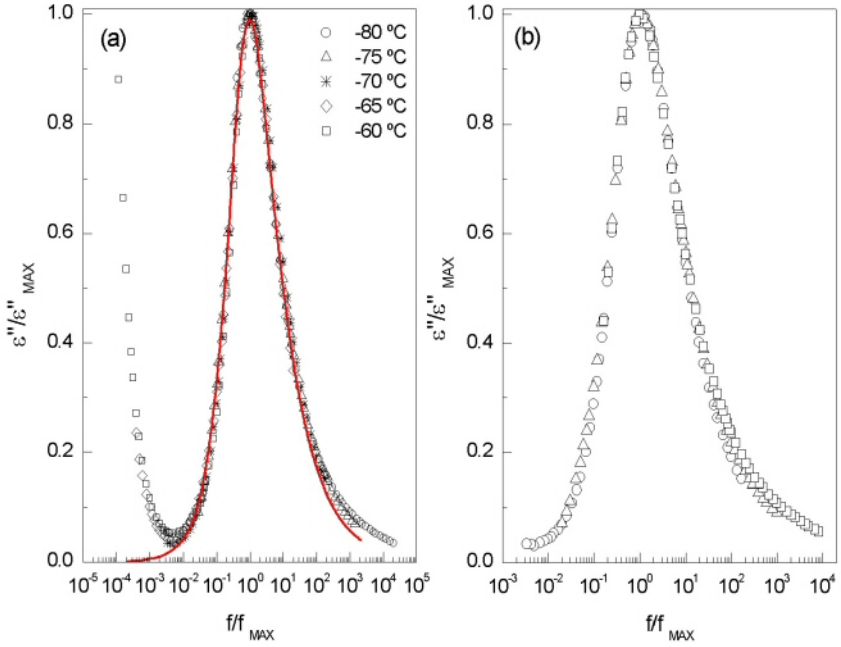

Figure 3.8 (a) Master curve (red line) constructed for DEGDMA at -76 ºC using $\alpha_{HN} = 0.92$ and $\beta_{HN} = 0.52$; data collected between –80 and –60 ºC every 5 ºC (symbols indicated in the figure); (b) normalized curves at -70 ºC for: DEGDMA (circles), TrEGDMA (triangles) and TeEGDMA (squares).

The construction of the master curve for each monomer let us to obtain the stretched exponent β_{KWW}, i.e. to relate the fitting procedure of data collected in the frequency domain with the equivalent data in the time domain. To find the β_{KWW} value that better fits experimental data, we superimposed the theoretical curves obtained from the transformation proposed by Hamon [12] and also from those obtained following the method proposed by Williams *et al.* [13] (based in the series expansion of the relaxation function) to the master curve of each monomer.

The parameters obtained are included in Table 3.1. Figure 3.9 shows data acquired at -76 ºC for TeEGDMA with the best approximation found.

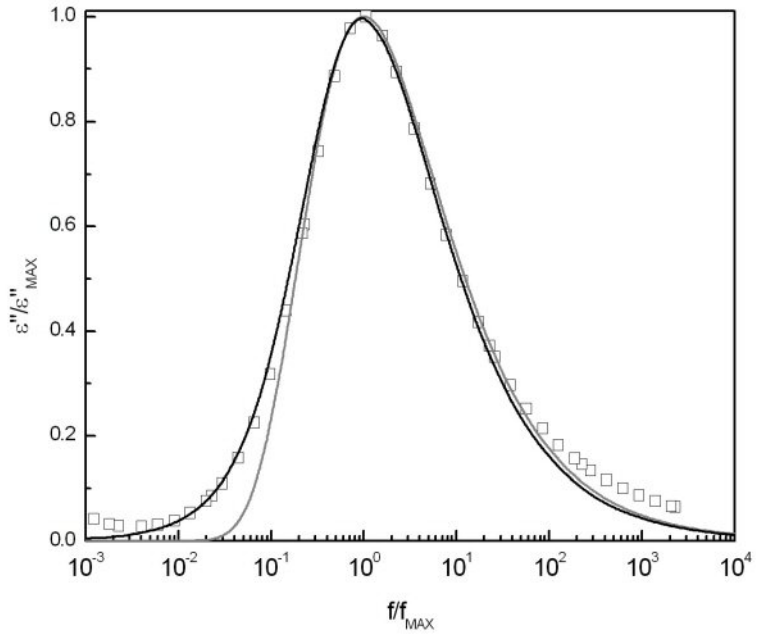

Figure 3.9 Symbols: normalized curve for DEGDMA at -76 ºC; Grey line: ε'' constructed from Hamon approximation with $\beta_{KWW} = 0.56$ in accordance with ref. 12 and black line for $\beta_{KWW} = 0.59$ estimated from a series expansion in accordance with reference 13.

Although the β_{KWW} values obtained from the two approximations are very similar, from Figure 3.9 it is clear that the Hamon method clearly underestimate the values of $\varepsilon''/\varepsilon''_{\max}$ in the low-frequency side of the isotherms. The small discrepancy of *KWW* equation calculated with any of two methods at the high frequency side could be due to the submerged secondary relaxations.

The β_{KWW} obtained by this construction allows us to evaluate the relationship $\alpha_{HN}\beta_{HN} = \beta_{KWW}^{1.23}$, proposed by Alegría and co-workers [14], whose values from the HN parameters are summarized in Table 3.1. Alegria's relation presents in all cases values lower than that evaluated by the previously used approximations.

	α_{HN}	β_{HN}	$\alpha_{HN}\beta_{HN}$	β_{KWW} (ref. 12)	β_{KWW} (ref. 13)	β_{KWW} (ref. 14)
DEGDMA	0.92±0.04	0.52±0.03	0.48±0.03	0.58	0.59	0.55
TrEGDMA	0.95±0.03	0.46±0.03	0.44±0.03	0.59	0.59	0.51
TeEGDMA	0.94±0.03	0.46±0.05	0.43±0.03	0.56	0.59	0.51

Table 3.1 Shape parameters (average values), α_{HN} , β_{HN} and $\alpha_{HN}\beta_{HN}$, for the α-relaxation of the three monomers obtained from HN fittings and β_{KWW} obtained using method proposed by Hamon [12], Williams [13] and the Alegria's relation [14].

Finally the last parameter obtained from the fitting procedure is the relaxation time, τ_{HN}. By using the transformation indicated in Chapter 1, we can derive τ_{MAX}, which is preferably since is a model-independent parameter. The relaxation times so obtained are presented in a logarithmic scale as a function of the reciprocal of temperature in Figure 3.10. This figure includes in gray the τ_{MAX} values obtained from the data collected using the HP4284A. We think interesting include these data because initially [1], the curvature of the $-\ln\tau_{MAX}$ was weak and doubtful for DEGDMA and TrEGDMA, but when the frequency range was enlarged, this behavior was confirmed and better defined.

All curves were fitted by Vogel-Fulcher-Tamman-Hesse equation (see Chapter 1), $\tau = \tau_0 \exp\left(B/\left(T - T_0\right)\right)$. The parameters estimated for B, τ_0 and T_0 are summarized in Table 3.2.

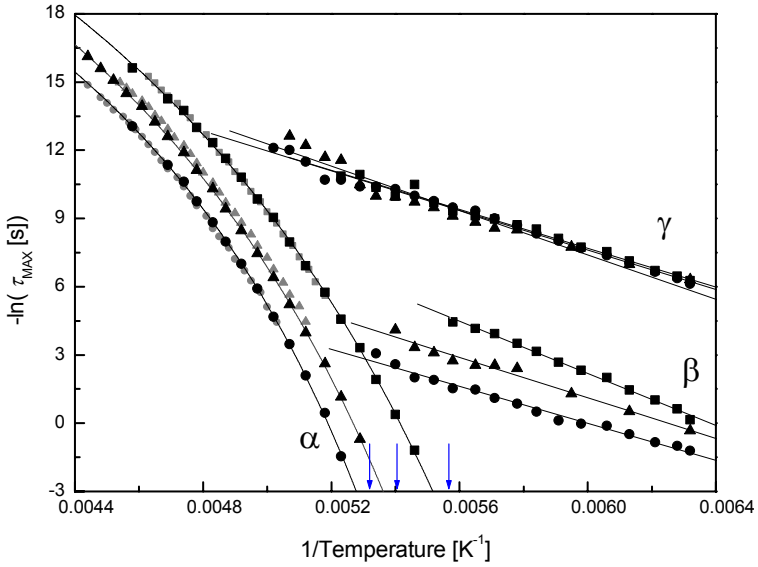

Figure 3.10 Arrhenius plot for all the relaxation processes indicated in figure for: unreacted DEGDMA/AIBN (0.1%) (full circles), TrEGDMA/AIBN (full triangles) and TeEGDMA/AIBN (0.1%) (full squares). Gray symbols correspond to the main relaxation process for pure monomers monitored with HP4284A, showing the correspondence between the different measurements. The arrows indicate the location of the estimated T_g at 100 s.

	τ_0 [s]	B [K]	T_0 [K]	T_g [K]	m	$E_a(T_g)$ [kJ.mol^{-1}]
DEGDMA	$(7\pm4)\times10^{-17}$	1695±97	139±2	179.6 (-93.6 ºC)	80	276
TrEGDMA	$(3\pm1)\times10^{-16}$	1520±52	147±1	184.9 (-88.2 ºC)	85	303
TeEGDMA	$(7\pm4)\times10^{-15}$	1251±87	154±2	187.9 (-85.2 ºC)	90	325

Table 3.2 Values of the VFTH parameters, glass transition temperatures obtained from the VFTH curve at $\tau = 10^2$ s; fragility indexes, m, and apparent activation energy at T_g, $E_a(T_g)$, for the three materials determined by dielectric relaxation spectroscopy.

By replacing the VFTH equation in the activation energy equation defined as:

$$E_a = R\frac{\partial \ln \tau}{\partial(1/T)} \qquad \text{Equation 3.2}$$

it is possible to calculate the temperature dependent activation energy (apparent activation energy):

$$E_a(T) = \frac{RB}{(1-T_0/T)^2} \qquad \text{Equation 3.3}$$

Therefore, the fragility index, defined by Angell [15] and already described in Chapter 1 can also be calculated by:

$$m = \frac{\partial \log \tau}{\partial(T_g/T)_{T=T_g}} = \frac{E_a(T_g)}{\ln 10 RT_g} \qquad \text{Equation 3.4}$$

These values, apparent energy at T_g and fragility index are included in Table 3.2.

3.2.2 The secondary relaxations β and γ

At lower temperatures, two secondary processes precede the main relaxation in the three monomers studied (remember Figure 3.4 and Figure 3.5). The γ relaxation is observed in a large range of temperatures (-115 to about -78 ºC approximately). The β relaxation only can be clearly detected in a shortest interval (never above -86 ºC) becoming sub-merged under the intense α process.

Shape parameters (average values) obtained from the HN fitting procedure are presented in Table 3.3 for γ and β relaxations (the complete list of fitting parameters are included in Annex I).

The γ relaxation presents shape parameters very similar for the three monomers. The β relaxation, differently from the γ relaxation, shows significant changes in the shape parameters while comparing the different monomers. In

TrEGDMA the β process cannot be accurately characterized neither concerning location nor the shape parameters, due to a join effect of low intensity and proximity of the main relaxation. Nevertheless it seems clear that this relaxation in this monomer corresponds to an intermediate location between the DEGDMA and TeEGDMA.

		DEGDMA	**TrEGDMA**	**TeEGDMA**
gamma	α_{HN}	0.45±0.07	0.42±0.06	0.44±0.14
	β_{HN}	0.49±0.07	0.55±0.07	0.49±0.08
	$\alpha_{HN}\beta_{HN}$	0.22±0.03	0.26±0.05	0.22±0.08
beta	α_{HN}	0.78±0.03	0.48±0.07	0.79→0.36
	β_{HN}	0.42±0.02	0.79±0.04	0.40→0.85
	$\alpha_{HN}\beta_{HN}$	0.33±0.01	0.38±0.05	0.34±0.03

Table 3.3 Average values of shape parameters obtained from the HN fitting for the two secondary relaxations, γ and β, detected in all studied systems.

The temperature dependence of the corresponding dielectric strengths is depicted in Figure 3.11 that also includes $\Delta\varepsilon$ values for the α-process for comparison purposes. While $\Delta\varepsilon$ for the main process decreases linearly with increasing temperature, as already discussed, the dielectric strength of secondary relaxations show an overall increase with temperature presenting a significant change of slope through the glass transition.

The marked increase observed for the γ relaxation above T_g is also due to the disappearance of the β relaxation that merges under the incoming α relaxation; the sensitivity of secondary relaxations to the glass transition has been reported in several works [6,16]. It was found for EPON838 [5] that data above and below the glass

transition can be fitted by two different linear equations; the increase of $\Delta\varepsilon$ above T_g was attributed to the coupling of local motions with diffusive motions dominating at temperatures higher than the glass transition.

Thus, the glass transition signature can be seen in these systems through the temperature dependence of the dielectric strength.

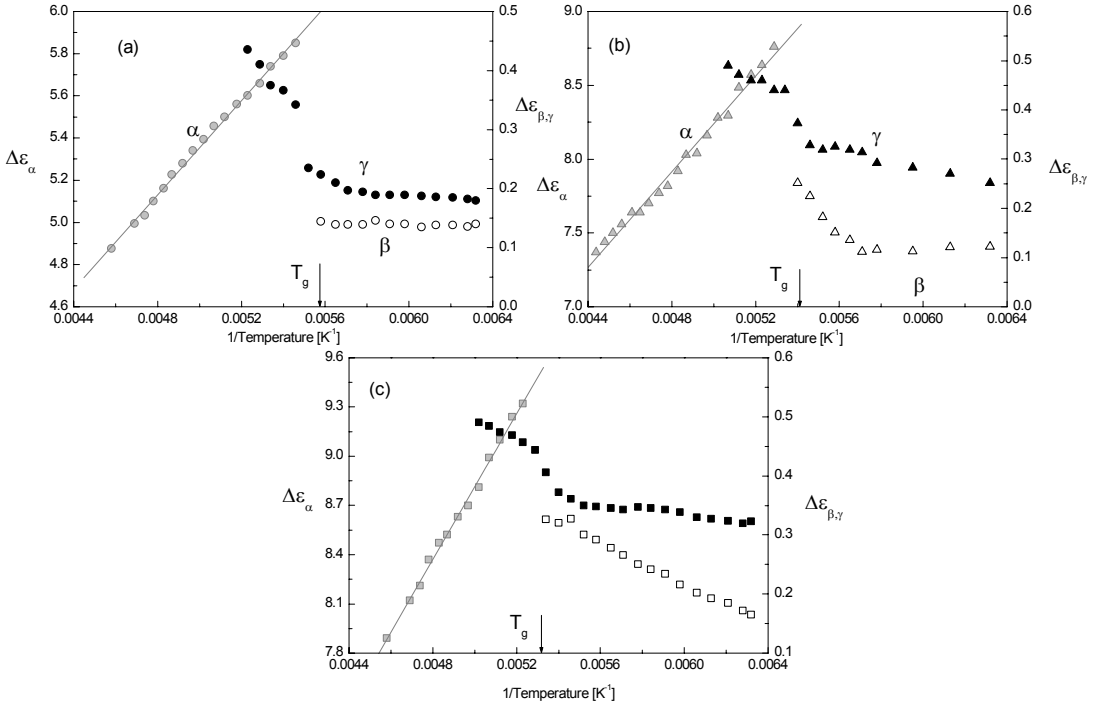

Figure 3.11 Dielectric strengths plotted *vs.* the reciprocal temperature for monomer a) DEGDMA, b) TrEGDMA and c) TeEGDMA: grey symbols for the α relaxation (left axis), open and filled black symbols for, respectively, β and γ relaxations (right axis).

Both relaxation processes show a relaxation time having an Arrhenius temperature dependence, $\tau = \tau_0 \exp(E_a/RT)$, most clearly seen at temperatures well below T_g where the main relaxation process is not present, what allows us a more precise data treatment (remember Figure 3.10 where relaxation times for these processes were also included).

The activation energy and the τ_0 parameters calculated for all the systems are included in Table 3.4. Also the crossover temperatures (i.e. the temperature in which α and the extrapolation of the behaviour of secondary relaxations intercept) were estimated and are presented in Table 3.4. $T_{\alpha\beta}$

	β relaxation			**γ relaxation**		
	E_a [kJ.mol^{-1}]	τ_0 [s]	$T_{\alpha\beta}$ [ºC]	E_a [kJ.mol^{-1}]	τ_0 [s]	$T_{\alpha\gamma}$ [ºC]
DEGDMA	48±1	(3±1)x10^{-17}	-77.3	36±1	(3.2±1.5)x10^{-15}	-64.2
TrEGDMA	38±2	(3±2)x10^{-13}	-75.6	41±2	(1.2±0.9)x10^{-16}	-54.5
TeEGDMA	34±1	(2±1)x10^{-11}	-75.3	37±1	(10±5)x10^{-16}	-49.9

Table 3.4 Activation energy, E_a, pre-exponential factor, τ_0, and intersection temperature with main relaxation process of both secondary relaxations. All linear fittings show a correlation coefficient of 0.99.

3.3 Thermal characterization

The thermal characterization, using Differential Scanning Calorimetry, of the three monomers was carried out in the Centro de Química-Física (Instituto Superior Técnico - Lisboa)[1]. The calorimeter used was a TA Instruments, fitted with a liquid nitrogen cooling accessory. Dry high purity *He* gas with a flow rate of 30 cm^3.min^{-1} was purged through the sample. The baseline was calibrated scanning the temperature domain of the experiments with an empty pan.

The temperature calibration was performed taking the onset of the endothermic melting peak of several calibration standards (see *Experimental* of ref. [17]). The transition from glass to supercooled liquid was recorded in the heating mode for all monomers, from -130 up to 0 ºC. In the assays with different cooling rates, the thermograms for the TeEGDMA monomer were only collected up to -30 ºC in order to avoid crystallization.

[1] The author would like to thank the supervision of Prof. J. J. Moura-Ramos.

The glass transition temperature for each monomer was determined by DSC as the temperature of the onset, T_{on}, of the glass to supercooled liquid transition, obtained with a heating rate of 10 ºC.min^{-1}. Figure 3.12 presents the thermograms thus obtained for the three monomers.

The onset temperatures of the glass transition calorimetric signal are -92, -87 and -83 ºC, respectively, for DEGDMA, TrEGDMA and TeEGDMA, being in close agreement, for all monomers, with the T_g values determined by extrapolating the VFTH fit of the dielectric data to 100 s (remember Table 3.2) leading to -94, -88 and -85 ºC respectively. The glass transition temperature of TeEGDMA is also in agreement with -81.7 ºC of reference [18], being the only value reported in literature concerning these monomers. The heat capacity jumps, ΔC_p, of the calorimetric glass transition, are very high and well defined being equal to 209±19, 256±23 and 316±40 J.(K.mol)$^{-1}$ ethylene glycol dimethacrylate, respectively.

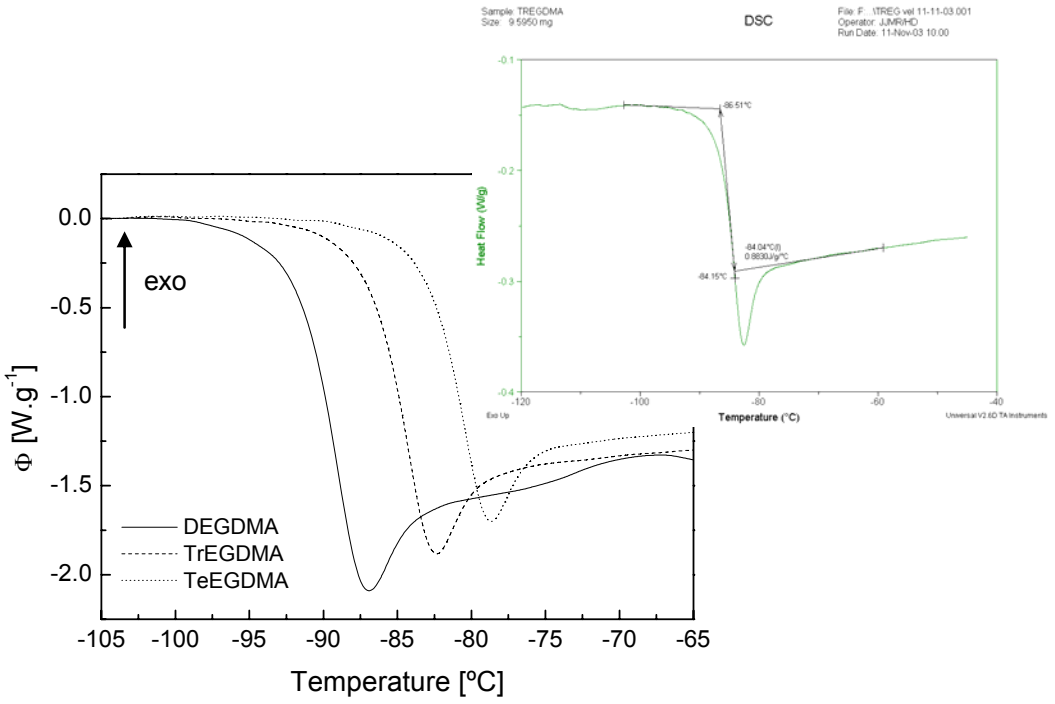

Figure 3.12 DSC heating curves for DEGDMA, TrEGDMA and TeEGDMA obtained at a heating rate of 10 ºC.min^{-1} (the curves were vertically displaced to situate the initial heat flow, Φ, at 0). The inset shows for TrEGDMA, how the onset temperature, T_{on}, is determined.

The differential scanning calorimetry technique can be used for the estimation of the fragility index, since it allows the determination of the activation energy through the dependence of the glass transition temperature on the heating/cooling rate, $|q|$. According Moynihan *et al.* [19,20], the dependence of T_g on $|q|$ is given to a high degree of approximation by

$$\frac{d\ln|q|}{d\left(1/T_g\right)} = \frac{-\Delta H^*}{R} \qquad \text{Equation 3.5}$$

where ΔH^* is the activation energy (more properly, the activation enthalpy) for structural relaxation. Therefore, in order to determine the activation energy for the glass transition process through calorimetric experiments, we performed several assays at different heating rates.

The reason why T_{on} was used to estimate T_g was based in the discussion shown in reference 17 where T_{end} is discarded since is less accurate due to the influence of the overshoot of the structural relaxation obtaining on heating. On the other hand, the choice between T_{on} and T_{mid} is indifferent since both are affected in a similar way by the heating rate.

Figure 3.13 presents the deviation of the glass transition signature with the heating rate that was tested in the range from 5 (upper thermogram) to 20 ºC.min^{-1} for the TrEGDMA monomer. It can be observed that, as expected, the glass transition signal deviates to higher temperatures. The T_{on} dependence on the heating rate for the three monomers is presented in Figure 3.14. The activation energy values calculated from the slope of the activation plot according to Equation 3.5, and fragility indexes (calculated from Equation 3.4 with $E_a\left(T_g\right) = \Delta H^*$), are included in Table 3.5.

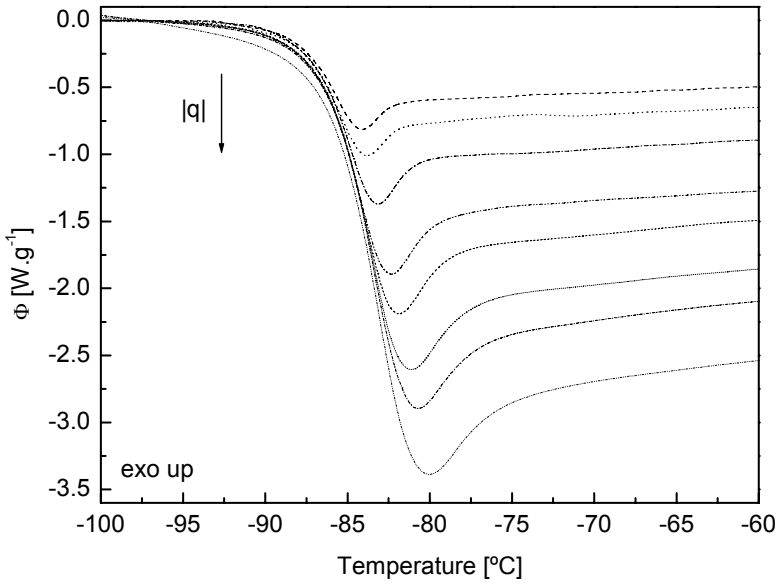

Figure 3.13 DSC signature of the glass transition for TrEGDMA obtained at different heating rates, |q|: 4, 5, 7, 10, 12, 15, 17 and 20 ºC.min^{-1}; the curves were shifted in order to make coincide the initial heat flow, Φ, values.

	E_a [kJ.mol^{-1}]	ΔC_p [J.K^{-1}.mol^{-1}]	m	T_g [K]
DEGDMA	148	209±19	43	181
TrEGDMA	157	256±23	46	187
TeEGDMA	175	316±40	64	190

Table 3.5 Calorimetric parameters of the three monomers: activation energy, E_a, obtained from the influence of the heating rate on the DSC signal (Equation 3.5); heat capacity jump at T_g, ΔC_p; fragility index, m, and onset glass transition temperature, T_g, obtained at heating rate of 10 ºC.min^{-1}.

Finally, the TeEGDMA monomer shows crystallization when heated above the temperature of -20 ºC. Figure 3.15.a shows, in addition to the glass transition, the exothermic peak centered at -30 ºC due to crystallization which was absent in the previous cooling run. The fusion endothermic peak centered at 2.9 ºC for a heating

rate of 12 ºC.min^{-1} is shown in Figure 3.15.b. Due to the large C_p value (37×10^3 J.K^{-1}.mol^{-1}) associated with the crystallization, almost 100 times greater than the C_p value associated with the glass transition, it is not possible to observe both processes in the same heat flow scale.

This particular type of crystallization that occurs when the material is heated from below its glass transition, *i.e.* from the amorphous solid state, rather during cooling from above their melting point, it is known as cold crystallization [21,22].

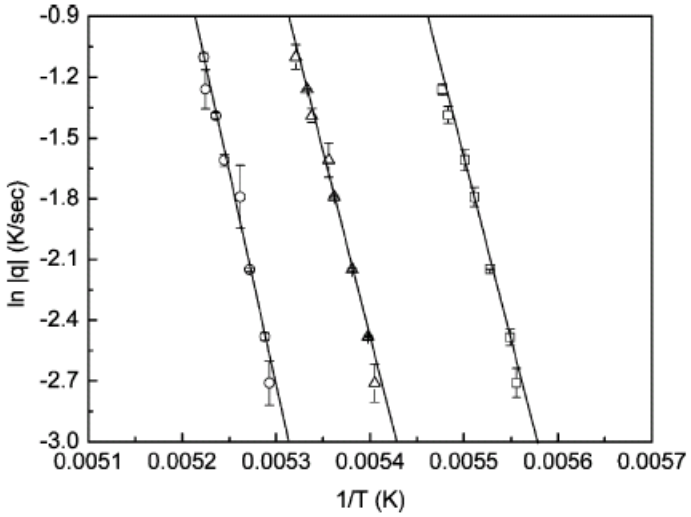

Figure 3.14 Activation plots (logarithm of the heating rate as a function of $1/T_{on}$) of the calorimetric glass transition signal for DEGDMA (●), TrEGDMA (▲) and TeEGDMA (■).

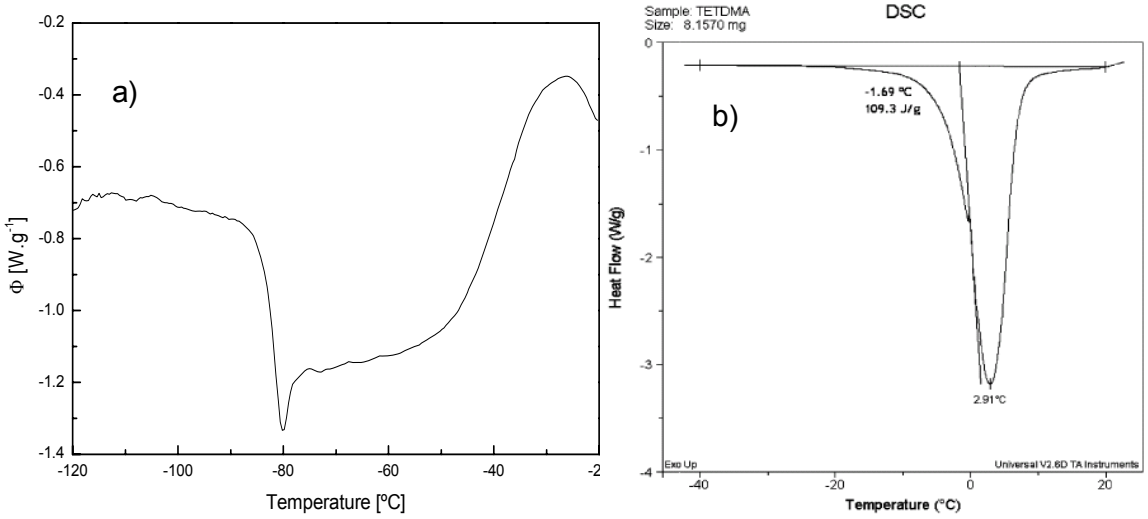

Figure 3.15 (a) Glass transition and exothermic peak of crystallization obtained at 5 ºC.min^{-1}; (b) endothermic peak centered at 2.9 ºC obtained in a subsequent run in heating mode at 12 ºC.min^{-1}, corresponding to the fusion of crystalline TeEGDMA.

3.4 Discussion

The dielectric data revealed a rather intense relaxation process related to the glass transition, for the three monomers studied. The shape of this α process is similar for all the materials making possible to build a master curve. Since the α_{HN} shape parameter is close to 1, the relaxation behavior is nearly equivalent to describe the α peak with the empirical Davidson-Cole equation [23] (HN function with $\alpha_{HN} = 1$). The width parameter ($\alpha_{HN}\beta_{HN}$) maintains almost constant in the three monomers in the temperature range where this relaxation is detected, and it slightly decreases from 0.48 to 0.43 with increasing molecular size (see Table 3.1). Although only a small tendency to increase the width of the α peak (lower $\alpha_{HN}\beta_{HN}$ values) is observed, the fact that it is also accompanied by a fragility increase, is in accordance with the strong correlation between fragility and non exponentiality observed in a large number of supercooled liquids [5,23,24]. Analogously, using the values of fragility index and *KWW* exponent, one can test the broad correlation between m and β_{KWW} proposed by Böhmer *et al.* [5]. This correlation was established from a compilation of data concerning 55 glass formers, which reads:

$$m = 250(\pm 30) - 320\beta_{KWW} \qquad \text{Equation 3.6}$$

From the values of stretching exponent β_{KWW} calculated using the relation proposed by Alegría [14] from the α_{HN} and β_{HN} shape parameters, the fragility indexes estimated with Equation 3.6 are 74 for DEGDMA and 86.8 for TrEGDMA and TeEGDMA which are in good agreement with the values listed in Table 3.2. The fact that data obey to Equation 3.6 indicates that a close correlation exists between non-exponentiality, quantified by the *KWW* exponent, and fragility, in these monomers.

Additionally, by analyzing separately the α_{HN} and β_{HN} values, the low β_{HN} means that the loss curves of this family of monomers present asymmetry in all temperature range, and this is more pronounced with the increase of the size of the

molecule. It has been reported that the overlapping of other relaxations on the high-frequency side of the main relaxation can underestimate the value of the β_{HN} parameter [25] obtained by the fitting procedure for the α-peak at the lowest temperatures. In our case, the presence of two well defined secondary processes allows to obtain accurate values of the shape parameters of the α process in the temperature range of the measurements.

The dielectric strength values for the α-relaxation are quite high due to the dipole moments of both $C=O$ groups and ethyleneglycol moiety, decreasing with increasing temperature in the entire temperature range where this relaxation process was detected. This behavior, observed in all monomers, let determine the onset for the α relaxation strength (very similar for the three systems). No specific range of $T_{on,\alpha}-T_g$ can be given since a quite different set of values can be found in literature: in poly-alkyl methacrylates the difference between the onset of the α-process and the glass transition temperature is around 25-40 ºC, ($T_{on,\alpha}$ | T_g = 9ºC|-18ºC [26], 50ºC|24ºC [27], 110ºC|74ºC [28], respectively in poly(*n*-hexyl methacrylate), poly(*n*-butyl methacrylate) and poly(ethyl methacrylate)) while for PPGE (poly[(phenyl glycidyl ether)-co-formaldehyde] the onset of the α-process lies 133 ºC above T_g ($T_{on,\alpha}$ = 118ºC and T_g =-15 ºC) and for a low molecular weight material as DGEBA (diglycidyl ether of bisphenol-*A*) the difference between the α-onset and T_g is 96 ºC ($T_{on,\alpha}$ =78ºC and T_g =-18ºC) [16].

In spite of such variety, the linear extrapolation to $\Delta\varepsilon_\alpha = 0$ in order to estimate the onset of α process for these monomers, seems to lead to unreasonable temperatures values (more than 200 K above T_g) due to the weak temperature dependence.

This onset has been interpreted as the limit of cooperativity at high temperatures. At temperatures above this temperature segmental mobility would be no longer a cooperative motion [29,30].

On the other hand, the difference of dielectric strength between consecutive monomers in the series can be attributed to the dipolar contribution of each additional ethyleneglycol moiety. This difference is not constant from consecutive monomers.

This cooperative process is more mobile in DEGDMA relatively to TrEGDMA and TeEGDMA monomers, since it has both lower apparent activation

energy, and the relaxation process is deviated to higher frequencies/lower temperatures (see Figure 3.16 and Figure 3.10 with the relaxation map). Consequently, the glass transition occurs at lower temperatures increasing with the increase of the ethylene glycol group. The same behaviour is observed in dielectric measurements of polyalcohols [23], poly(propylene glycol) oligomers [24] and poly(ethylene glycol) methacrylate macromers with *n*=7 and *n*=12 [31], where the dielectric loss peaks of the higher molecular weight materials are located at higher temperatures.

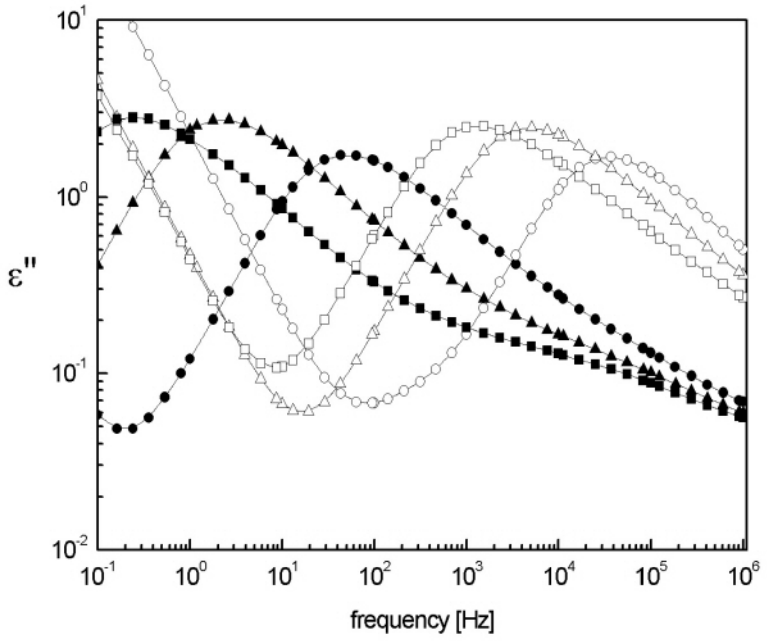

Figure 3.16 Loss curves for the three monomers at -80 ºC (full symbols) and -66 ºC (open symbols) for DEGDMA (circles), TrEGDMA (triangles) and TeEGDMA (squares).

The temperature dependence of the relaxation times also reveals an increasing curvature and, consequently, an increasing activation energy at T_g and fragility values, with increasing *n* (di<tri<tetra). The increase of *m* with the molecular weight is also observed in related materials [24,32,33].

The fragility indexes determined by DRS and DSC listed in Table 3.2 and Table 3.5 differ almost by a factor of 2. This discrepancy was also detected in other systems as PVC [34,35]. This divergence predicting m for more fragile materials by using DSC technique is already described in the literature [19,36]. The non-Arrenhius behaviour near T_g produces a large $\Delta H^* = E_a(T_g)$, which decreases the effect of the

heating rate on T_g, and thus, a greater error is found in the estimation of $E_a(T_g)$ [36]. By this way, we will consider the m values obtained by DRS to compare with other fragile materials as the polyalchol threitol (*m*=79 [32]), *m*-toluidine (*m* = 79 [37], 83 [38]) or sorbitol (*m* = 93 [5]).

On the other hand, in what concerns the T_g values, the accordance is really good between DSC and the extrapolation of VFTH behaviour for $\tau = 100s$ (see Table 3.2 and Table 3.5) putting in evidence the complementarity between the two techniques.

The values of ΔC_p at the glass transition, which are a measure of the degrees of freedom released on heating from the glassy state to the supercooled liquid, are unusually high by comparing with organic glass formers and polymers, being of the same order of ionic liquids that have, in the liquid state, an appreciable mobility [17].

Finally, the higher ethyleneglycol dimethacrylate monomer (TeEGDMA) crystallizes on heating, presenting an exothermal crystallization peak around -26 ºC; the maximum of the endothermic peak associated to the later fusion is close to 3 ºC anticipated by an onset around –10 ºC. The temperature region where crystallization occurs in the calorimetric run agrees with the anomalous behaviour found for this monomer in dielectric measurements (remember Figure 3.2.c) where a jump in ε'', obtained in increasing temperature step, is observed above –30 ºC. This behaviour was also detected in dielectric data of DEGDMA and TrEGDMA (see Figure 3.2.a and b) but with a lower intensity. Since crystallization seems to happen upon heating, the interface formed between the crystalline and the liquid supercooled phases can originate interfacial polarization revealed by the rapid increase detected in the real part of the permittivity, ε'. Whereas ε'' is greatly affected by conductivity that can mask the interfacial polarization, ε' due to its insensitivity to the contribution of pure d.c. conductivity, allows seeing that effect corresponding to an additional capacitance created by the build-up of space charges near the interfaces between the two phases as it happens in inhomogeneous media (chapter 13 in ref. 11).

Anyway, when the system presents a high conductivity and low crystallization degrees, it is difficult to extract information from the analysis of ε'' spectrum.

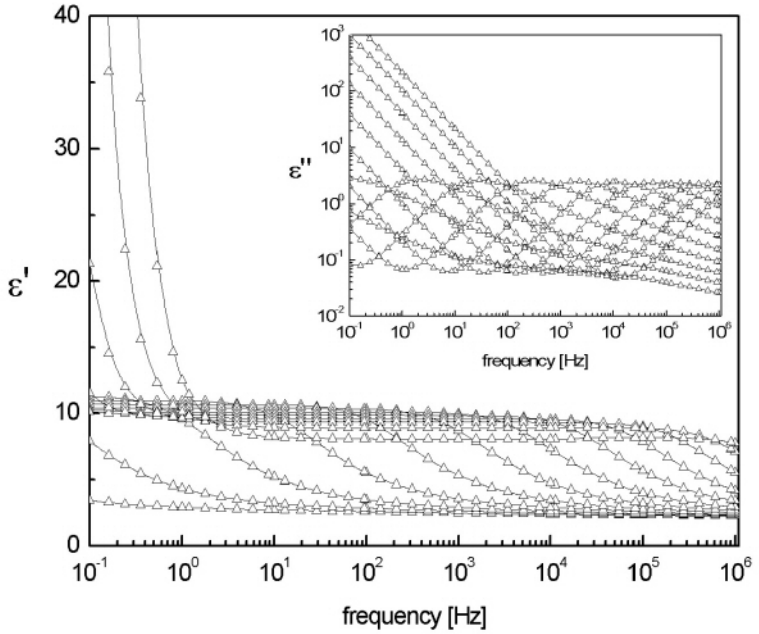

Figure 3.17 Real part, ε', of TrEGDMA corresponding to isothermal data obtained from -88 ºC to -44 ºC every 4 ºC, showing the rapid increase in the low frequency side. In the inset the imaginary part ε'', in the logarithmic scale of the same set of data where the last isothermals show a slight curvature indicating that not only pure conductivity occurs.

Having in mind the shape of the loss peak of the dominating α relaxation processes in logarithmic scale of Figure 3.16, the high frequency side exhibits a shoulder with the aspect of an excess wing, claimed by some authors [39,40] as a universal feature of the glass forming liquids. However in these systems, this flank was resolved in two well-defined peaks at temperatures below T_g, where the main relaxation does not affect the spectra (see loss curves in Figure 3.5 at -100 ºC). Similar results were found in the works reported by Schneider and co-workers [41,42] for low molecular weight glass-formers as ethanol, glycerol and propylene carbonate, where dielectric spectroscopy covering an extended frequency window until 10^{12} Hz provided experimental evidence that the excess wing is caused by a second relaxation peak, submerged under the α peak.

At this time it is not possible to pull completely apart that, at least the origin of one of the two secondary processes, is due to a Johari-Goldstein (JG) relaxation that entails the motion of a molecule as a whole. Anyway, given the chemical structure of monomer molecules, seems to be very plausible to associate these secondary

relaxations to internal modes of motion that clearly remain active when the molecule as a whole is frozen in the glassy state, contrary to the slow JG process found in rigid molecules lacking of internal modes of motion.

In what concerns how these processes affect the main relaxation, from the direct observation of the relaxation map, it seems easy to accept that the β process does not change the trace of the α process, which can be due to the low intensity of this secondary process. In respect to the γ relaxation, the fact that the intersection of the α and γ traces is localized in the limit of our frequency window, jointly with the higher intensity of the α process, do not allow at this moment to confirm the possible deflect of the γ trace when approaches the main relaxation, as observed by others authors in systems as DGEBA and PPGE [16]. However, the present analysis of the relaxation map can be insufficient to conclude about the influence of the secondary processes. In fact, in systems showing two secondary relaxations, each crossover temperature, i.e. $T_{\alpha\beta}$ and $T_{\alpha\gamma}$, seem responsible for different changes: the intersection with the beta trace, $T_{\alpha\beta}$, can be correlated with the Adam Gibbs breakdown (deviation from $\log\tau \propto (S_c T)^{-1}$) showing that above $T_{\alpha\beta}$, the number of unities forming the *CRR* is lower than predicted; on the other hand, the $T_{\alpha\gamma}$ indicates a different kind of dynamic change [16].

Nevertheless, in next chapters, the influence of the α relaxation will be diminished and some lights about the convergence scenario will be added.

3.5 Conclusions

A detailed dielectric characterization of the relaxation process related with the glass transition of DEGDMA, TrEGDMA and TeEGDMA was provided for the first time in literature. At each temperature, the mobility of the cooperative process decreases with the molecular weight, M_w, increase while the width of the relaxation peak, glass transition temperature and fragility increases with the M_w increase.

The temperature dependence of the relaxation times is VFTH type for all the systems as usually found in fragile glass formers. The fragility indexes estimated by both DSC and DRS techniques increase with number of ethylene glycol units, *n,* but

their values do not agree. In spite of the differences between the two techniques, the fragility indexes indicate fragile liquids with m values comparable to *m*-toluidine (m=79 [37]) and sorbitol (m=93 [5]). The ΔC_p, values associated with the calorimetric glass transition are quite high, being comparable with the values found for ionic liquids, which are characterized by a high mobility in the liquid state.

Although the secondary relaxations are well characterized by DRS, their molecular origin could not be completely clarified. The γ relaxation is less sensitive to the monomer weight than the β relaxation. Moreover, the pre-exponential factor τ_0 for the γ relaxation is lower than for the β one; this can be an indication of a higher complexity of the γ process. For example, this relaxation could involve a higher volume of the molecule or even a certain degree of cooperativity. This will be further discussed and elucidated in next chapters.

3.6 References

[1] M.T. Viciosa, M. Dionísio, J. Non-Cryst. Solids 341 (2004) 60-67.

[2] M.T. Viciosa, C.M. Rodrigues, M. Dionísio, J. Non-Cryst. Solids 351 (2005) 14-22.

[3] M.T. Viciosa, A.R. Brás, J.L. Gómez-Ribelles, M. Dionísio, Europ. Polym. J., in press.

[4] S. Havriliak, S. Negami, Polymer 8 (1967) 161-210.

[5] R. Böhmer, K.L. Ngai, C.A. Angell, D.J. Plazek. J. Chem. Phys. 99(5) (1993) 4201-4209.

[6] R. Casalini, D. Fioretto, A. Livi, M. Lucchesi, P.A. Rolla. Phys. Rev. B 56(6) (1997) 3016-3021.

[7] M. Schulz, E. Donth, J. Non-Cryst. Solids 168 (1994) 186-194.

[8] A. Schönhals, Europ. Letter 56(6) (2001) 815-821.

[9] A. Schönhals, F. Kremer, A. Hofmann, E.W. Fischer, E. Schlosser, Phys. Rev. Lett. 70 (1993) 3459-3462.

[10] "Dielectric Spectroscopy of Polymeric Systems", J.P. Runt, J.J. Fitzgerald, ACS Washington (1997).

[11] "Broadband dielectric spectroscopy", A. Schönhals, F. Kremer, Springer-Verlag, Berlin (2003).

[12] G. Williams, D.C. Watts, Trans. Faraday 60 (1970) 80-85.

[13] G. Williams, D.C. Watts, S.B. Dev, A.M. North, Trans. Faraday 67 (1971) 1323-1335.

[14] F. Alvarez, A. Alegría, J. Colmenero, Phys. Rev. B 44(14) (1991) 7306-7312.

[15] C.A. Angell, J. Non-Cryst. Solids 13 (1991) 131-135.

[16] S. Corezzi, M. Beiner, H. Huth, K. Schröter, S. Capaccioli, R. Casalini, D. Fioretto, E. Donth, J. Chem. Phys. 117(5) (2002) 2435-2448.

[17] J.J.M. Ramos, C.A.M. Afonso, L.C. Branco, J. Therm. Anal. Calorim. 71 (2003) 659-666.

[18] D.R. Morgan, S. Kalachandra, H.K. Shobha, N. Gunduz, E.O. Stejskal, Biomaterials 21 (2000) 1897-1903.

[19] C.T. Moynihan, A.J. Easteal, J. Wilder, J. Tucker, J. Phys. Chem. 78(26) (1974) 2673-2677.

[20] C.T. Moynihan, S.K. Lee, M. Tatsumisago, T. Minami, Thermochim. Acta 280/281 (1996) 153-162.

[21] B. Wünderlich, J. Chem. Phys. 29(6) (1958) 1395-1404.

[22] H.P. Diogo, J.J. Moura Ramos, J. Chem. Ed. 83(9) (2006) 1389-1392.

[23] D.W. Davidson, R.H. Cole, J. Chem. Phys. 18(10) (1950) 1417-1418.

[24] I-S Park, K. Saruta, S. Kojima, J. Phys. Soc. Japan 67 (12) (1998) 4131-4138.

[25] N.G. McCrum, B.E. Read, G. Williams, "Anelastic and Dielectric effects in Polymeric Solids", Wiley, New York (1967); reprinted by Dover, New York (1991).

[26] M. Beiner, S. Kahle, E. Hempel, K. Schröter, E. Donth, Macromolecules 31 (1998) 8973-8980.

[27] K. Schröter, R. Unger, S. Reissig, F. Garwe, S. Kahle, M. Beiner, E. Donth, Macromolecules 31(25) (1998) 8966-8972.

[28] F. Garwe, A. Schönhals, H. Lockwenz, M. Beiner, K. Schröter, E. Donth, Macromolecules 29 (1996) 247-253.

[29] M. Beiner, J. Korus, E. Donth, Macromolecules 30 (1997) 8420-8424.

[30] G.P. Johari, J. Chem. Phys. 58(4) (1973) 1766-1770.

[31] K.L. Ngai, J. Phys.: Condens. Matter 15 (2003) S1107-S1125.

[32] A. Döß, M. Paluch, H. Sillescu, G. Hinze, J. Chem. Phys. 117(14) (2002) 6582-6589.

[33] F. Aliotta, G. Di Marco, M.E. Fontanella, M. Lanza, J. Phys.:Condens. Matter 10 (1998) 545-556.

[34] C.G. Robertson, P.G. Santangelo, C.M. Roland, J. Non-Cryst. Solids 275 (2000) 153-159.

[35] E. Bureau, C. Cabot, S. Marais, J.M. Saiter, Europ. Pol. J. 41 (2005) 1152-1158.

[36] K.J. Crowley, G. Zografi, Thermochim. Acta 380 (2001) 79-93.

[37] C.A. Angell, J. Res. Nat. Inst. Stand. Technol. 102(2) (1997) 171-185.

[38] N. Correia, C. Alvarez, J.J. Moura Ramos, M. Descamps, J. Chem. Phys. 113(8) (2000) 3204-3211.

[39] P.K. Dixon, L. Wu, S. R. Nagel, B.D. Williams, J.P. Carini, Phys. Rev. Lett. 65(9) (1990) 1108-1111.

[40] N. Menon, S.R. Nagel, Phys. Rev. Lett. 74(6) (1995) 1230-1233.

[41] U. Schneider, P. Lunkenheimer, R. Brand, A. Loidl, Phys. Rev. E 59(6) (1999) 6924-6936.

[42] R. Brand, P. Lunkenheimer, U. Schneider, A. Loidl, Phys. Rev. B 62(13) (2000) 8878-8883.

CHAPTER 4 REAL TIME POLYMERIZATION OF TREGDMA

4.1 Introduction

In this chapter the polymerization of TrEGDMA monitored by both temperature modulated differential scanning calorimetry, TMDSC, and dielectric relaxation spectroscopy (DRS) will be analyzed (partial data already published in reference 1).

TMDSC has been used to study the polymerization of different polymer systems as it permits the simultaneous measurement of the heat flow released by the exothermal reaction and the heat capacity of the reacting mixture of monomer and growing polymer chains or polymer networks [2-10]. This technique will support the principal results of the isothermal polymerization presented here, since the high conductivity of the reaction mixture only will allow us the qualitative analysis of DRS data using the dielectric modulus.

The isothermal polymerization will be carried out at a temperature that is higher than the T_g of the initial monomer (T_g = -82 ºC from DSC data present in Chapter 3 and ref. 11) but lower than the T_g of the final polymer network, that in our case is very high, around 160 ºC [12]. From these particular conditions, the main feature that we will observe upon polymerization will be the vitrification of the reacting mixture. During polymerization, if the reacting system consists of a homogeneous mixture of the growing polymer chains or polymer network and the unreacted monomer, the glass transition temperature of the mixture continuously increases as a result of the changes in the composition of the monomer/polymer mixture. When the glass transition temperature of the mixture approaches the value of the polymerization temperature, the reacting system becomes a glass, the mobility of the reacting species becomes much more restricted, and the reaction is controlled by diffusion. In many systems the reaction practically stops so that the full conversion is not attained. The change in heat capacity that accompanies this process can be directly measured by TMDSC.

Another interesting feature that was observed and characterized by TMDSC was the appearance of a peak in the real component of the heat capacity during isothermal polymerization. At the beginning of the polymerization process the measured value of C' is that of the monomer. An increase in C' with time during the first stages of polymerization has been reported both in network [2,3] and chain [4]

polymerizations. The heat capacity, C', then goes through a maximum and subsequently it decreases. If the reaction temperature is above the final T_g of the polymer, the system is in the liquid or rubbery state during the whole process and a maximum is clearly observed [5]. If the polymerization temperature is below the final T_g the vitrification of the material produces the fall of C' [6,7] and sometimes it is uncertain whether the maximum observed in *C'* takes place before vitrification [8] or whether it is produced by it [8,9]. Wang and Johari [10] using polymer chain statistics have recently explained the appearance of this peak in C' as a consequence of the balance between two contributions to the configurational component of $C_{p,}$ one of them coming from the fraction of vacancies in the lattice and the other one from the chain flexibility.

The kinetics of free radical addition polymerization is the result of the kinetics of different simultaneous reactions: the decomposition of the initiator which continuously produces free radicals, propagation which consumes the monomer available in the reaction mixture, and the termination reactions. Probably the most important termination mechanism is the interaction of two active chain ends (see for instance references [13,14]); termination rates strongly depend on the viscosity of the medium. An increase in the viscosity of the medium may cause a decrease in the rate of the termination reaction. This produces a rapid increase in the polymerization rate called the Trommsdorff-Norrish or gel effect [13-16].

4.2 Experimental conditions

Commercial TrEGDMA, from Sigma-Aldrich (cat. Nbr. 26,154-8) containing hydroquinone as inhibitor was used in the experiments. Hydroquinone was eliminated using a column also from Aldrich (cat. nr. 306312-1).

4.2.1 Temperature Modulated Scanning Calorimetry

DSC and TMDSC experiments were performed in a Perkin Elmer Pyris1 calorimeter; sealed aluminium pans were used. Quasi-isothermal experiments were performed. The programmed modulation was a teeth saw with varying peak-to-peak

amplitude between 0.2 and 1 ºC (the actual amplitude of the temperature oscillation is lower than the peak to peak temperature increment programmed), and a modulation period between 12 and 48 sec. The DSC was calibrated using indium and zinc standards at a heating rate of 10 ºC.min^{-1}. The TMDSC storage heat capacity, C', was calibrated following a method similar to that proposed in reference [17] (second order calibration). Heat capacity values of TrEGDMA monomer were measured in conventional DSC in the temperature interval of the isothermal TMDSC measurements, using an aluminium oxide standard for heat capacity calibration. The same procedure was used to determine the heat capacity of the polymer networks. The samples used in these measurements were those polymerized in the isothermal TMDSC experiments. A multiplicative calibration factor was obtained by comparing the modulus of the complex heat capacity measured by TMDSC in the monomer and in the polymer with that determined by DSC, ψ_m and ψ_p respectively. The calibration factor for intermediate polymerization times was considered proportional to the polymer fraction according to the conversion *x* (see Equation 4.1 below).

$$\psi(t) = \psi_m + \frac{x(t)}{x(t_{\max})}\left(\psi_p - \psi_m\right) \qquad \text{Equation 4.1}$$

One of the major difficulties in the study of the kinetics of free radical polymerization is the reproducibility of the results. It was determined that the accuracy in the reproducibility of the initiator content in the samples was crucial in this sense. When a series of samples are taken from the same monomer/initiator mixture (with a 0.1% w.t. of AIBN in TrEGDMA) and sealed in nitrogen atmosphere in aluminium pan the reproducibility of the results can be considered acceptable to support the conclusions reached in this work. Figure 4.1 shows the result of two TMDSC experiments conducted on two different samples prepared in this way.

Small differences between the different polymerization thermograms might come from differences in the small amount of oxygen dissolved in the monomer even when it was sealed under nitrogen atmosphere.

After this preliminary studies two solutions were prepared by dissolving 0.1% w.t. of AIBN in TrEGDMA; the fresh mixtures were stored at -18 ºC and used in all

the experiments to ensure no variability in the initiator content of the samples. One of the solutions was prepared in nitrogen atmosphere and nitrogen flushing was continued during sealing. The other solution was prepared and sealed in air to study the influence of oxygen on the reaction kinetics. To check that no polymerization took place in the monomer/initiator mixture during storage at -18 ºC, several samples were encapsulated after several months of storage and some experiments reproduced. No significant deviation of the results from those obtained with the original samples was found.

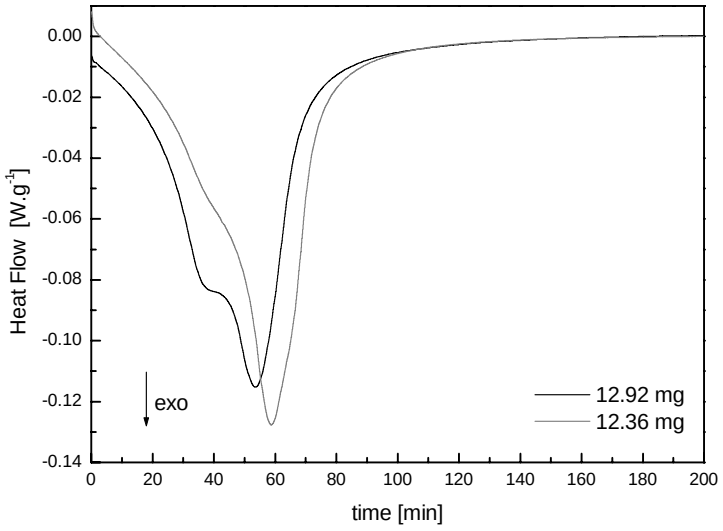

Figure 4.1 Normalized average heat flow measured by TMDSC during isothermal polymerization at 66 ºC of two samples of TrEGDMA/AIBN (0.1% w.t.) prepared under nitrogen atmosphere to show the reproducibility of the experimental results.

4.2.2 Dielectric Relaxation Spectroscopy

The dielectric measurements were carried out using the Alpha-N analyzer from Novocontrol GmbH. Only one solution was prepared in air by dissolving 0.1% w.t. of AIBN in TrEGDMA and it was used in all the samples polymerized using DRS measurements.

To verify that all samples did not polymerize during the storage, these were monitored from room temperature to -120 ºC at a cooling rate of around 8 ºC.min^{-1}

and compared with isochronal data for the TrEGDMA monomer presented in Chapter 3. Figure 4.2 shows this feature.

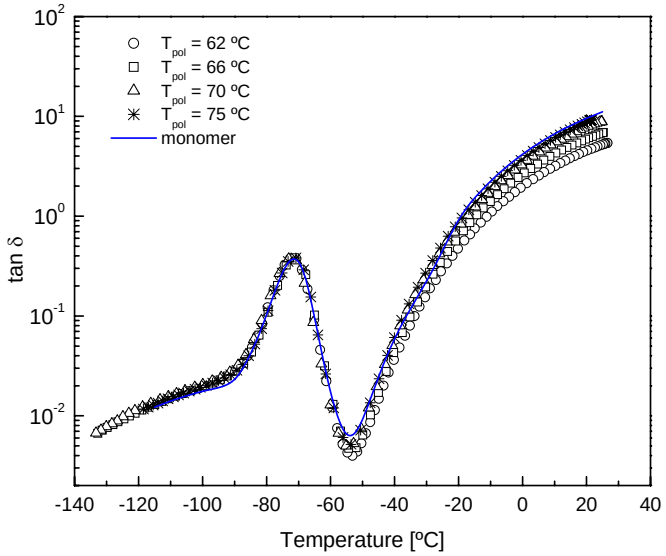

Figure 4.2 Isochronal loss $\tan\delta$ at 1 kHz for data taken on cooling (~-8 ºC.min^{-1}) for samples used afterwards in the isothermal polymerization at the temperatures indicated in figure (for more details see text); data corresponding to TrEGDMA monomer is also included as a line for comparison.

After this cooling scan to -120 ºC, the temperature of the samples was sharply increased to the final polymerization temperature (T_{pol}) (62, 66, 70 and 75 ºC). Dielectric loss spectra were collected isothermally at T_{pol} every 90 seconds, during 2.5 hours for each sample.

The real and imaginary parts of the complex permittivity were measured at 29 frequencies within the range from 0.7 Hz to 1 MHz, in such a way that each loss spectrum was collected in a period of time that does not exceed one minute, assuring that no significant changes occur during every spectrum. The temperature control was performed within ±0.5 ºC.

4.3 Results

4.3.1 TMDSC

4.3.1.1 Samples sealed under nitrogen atmosphere

The average specific heat flow released by the sample during the quasi-isothermal polymerization, $\dot{Q}_u / m$, at different temperatures is shown in Figure 4.3. The peak-to-peak amplitude of the temperature modulation was 0.2 ºC and the period 24 seconds. The sample mass, m, was around 11 mg in all the samples. Experiments were conducted for 200 minutes in the temperature interval ranging from 60 to 75 ºC. In this temperature range one or two exothermal peaks are clearly observed in the underlying heat flow within the experimental time interval.

The AIBN decomposition kinetics determines that at lower temperatures the reaction rate is too slow for the experimental time, and at temperatures above 75 ºC a significant part of the reaction takes place before the stabilization of the calorimeter required to the start temperature modulation. At the lowest temperatures a broad single peak is shown, but as temperature increases, the shape of the heat flow curve becomes more complex, and at the highest temperatures clearly a double peak appears.

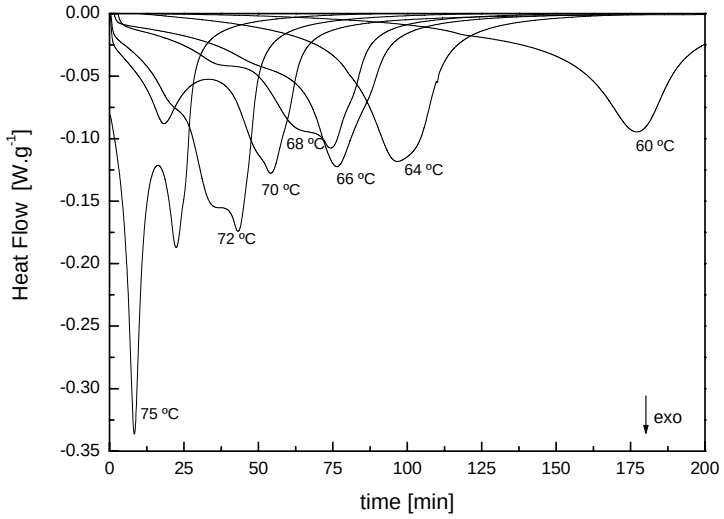

Figure 4.3 Normalized average heat flow measured by TMDSC during isothermal polymerization at the indicated temperatures. Samples were prepared under nitrogen atmosphere.

After each isothermal experiment the sample was cooled from room temperature to -40 ºC and a conventional DSC scan followed until 220 ºC at 10 ºC.min^{-1}. These scans showed an exothermal peak in the temperature range between the polymerization temperature and 200 ºC, corresponding to the polymerization of the unreacted methacrylate $C = C$ bonds (Figure 4.4).

In several polymer networks it was reported that the system can vitrify during this kind of post-curing treatment and more than one heating scan is needed to reach full polymerization [8]. This seems not to be the case of our system at the heating rate of 10 ºC.min^{-1}.

The shape of the exotherm indicates that the system doesn't vitrify during heating, and that the reaction continues up to temperatures in the range of the final glass transition temperature of the network.

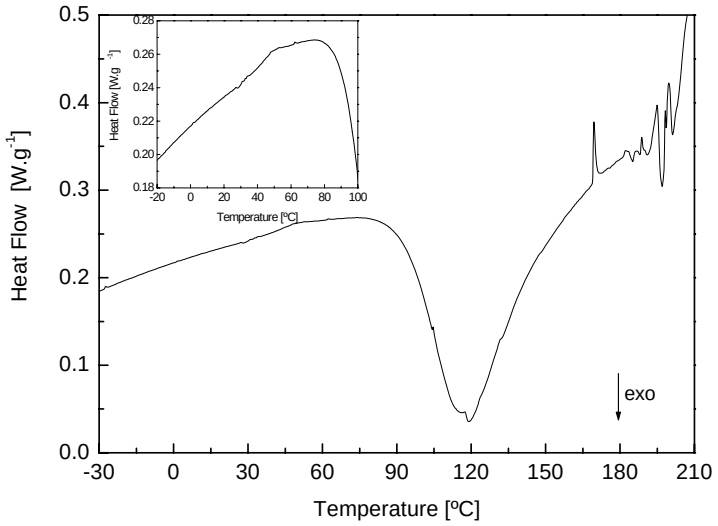

Figure 4.4 Conventional DSC scan obtained from -40ºC to 220ºC at 10ºC.min^{-1} for a representative sample sealed under nitrogen atmosphere and previously polymerized during 200 min at 66 ºC.

The inset enlarges the temperature region where the glass transition of the sample was detected.

The enthalpy increment in the isothermal experiment was determined by the area below the curves shown in Figure 4.3. The sum of the heat released in the isothermal reaction and that measured in the DSC scan was ΔH_{total} = 94 ± 4 kJ per mol of monomer. In spite of the high uncertainty, it can be said that this value is similar to those found in the polymerization of other methacrylate polymers [18,19].

Conversion was determined from the theoretical reaction heat per methacrylate double bond, ΔH_{theor} = 54.8 kJ.mol^{-1} [20]. The conversion x, and the conversion rate were calculated:

$$x = \frac{M}{2\Delta h_{theor}} \int_0^t \frac{\dot{Q}}{m} dt \qquad \text{Equation 4.2}$$

$$\frac{dx}{dt} = M \frac{\dot{Q}}{2m\Delta h_{theor}} \qquad \text{Equation 4.3}$$

where m is the mass of the sample and M the molecular weight of the repeating unit. Plots of conversion rate against conversion are shown in Figure 4.5, corresponding to some characteristic temperatures selected from those of Figure 4.3. The maximum conversion attained depends on the polymerization temperature ranging from around 65% at 64 ºC to 80% at 75 ºC (see the abscissa in the plot of Figure 4.5). Figure 4.6 presents the evolution of the storage heat capacity at different polymerization temperatures.

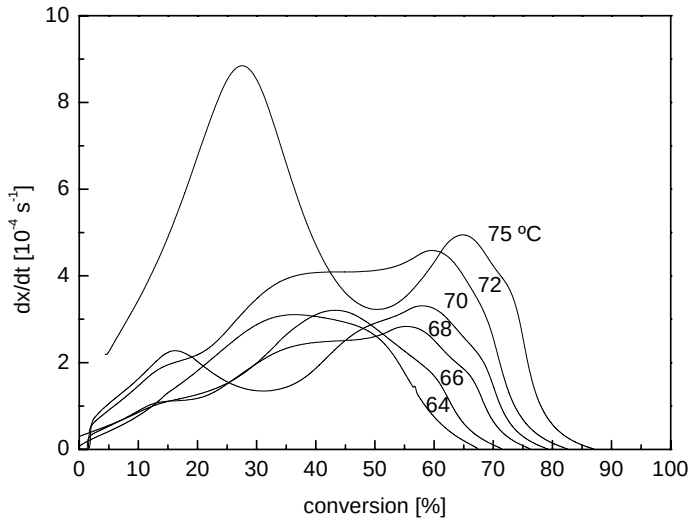

Figure 4.5 Conversion rate versus conversion, x, for the isothermal polymerization at different temperatures (as indicated in the figure). Samples prepared under nitrogen atmosphere.

The influence of some characteristic parameters of TMDSC measurement on results was studied. Figure 4.7 shows the conversion rate *vs.* conversion measured at different modulation amplitudes for polymerization at 70 ºC. The strong dependence of the reaction kinetics on temperature results in a significant dependence of the heat flow on the modulation amplitude. However, the main features of this curve are preserved when increasing the peak-to-peak amplitude from 0.2 to 1 ºC. A conventional DSC heat flow curve is also shown for comparison. The influence of the modulation period in the range between 24 and 96 seconds was found to be irrelevant (results not shown).

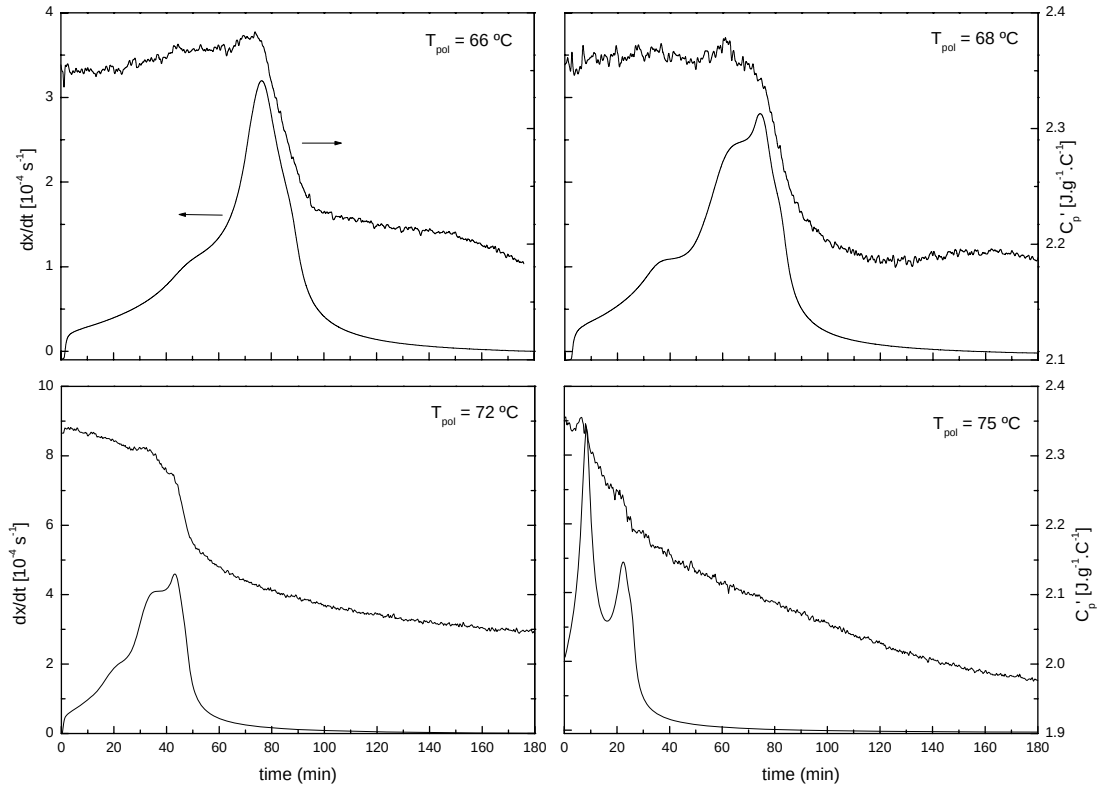

Figure 4.6 Conversion rate (left axis) and storage heat capacity (right axis) against polymerization time for isothermal polymerization at different temperatures.

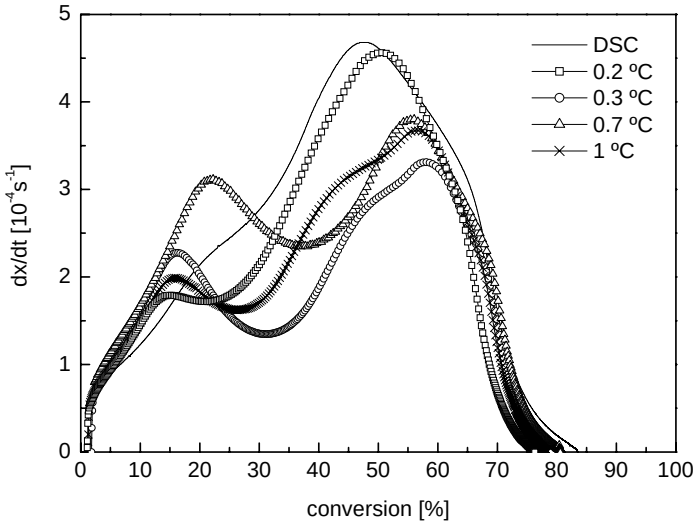

Figure 4.7 Influence of the modulation amplitude on the conversion rate plot. Samples sealed under nitrogen atmosphere.

4.3.1.2 Samples sealed under air atmosphere.

The effect of oxygen inside the sample pan was studied by comparing the polymerization behaviour of samples sealed in air atmosphere with samples sealed in nitrogen atmosphere.

Figure 4.8 shows the delaying effect of oxygen in the polymerization process at 70 ºC by keeping all the other experimental conditions constant. The effect of oxygen inhibition on polymerization is clearly shown by the shift of the peak to higher times for the air sealed TrEGDMA sample.

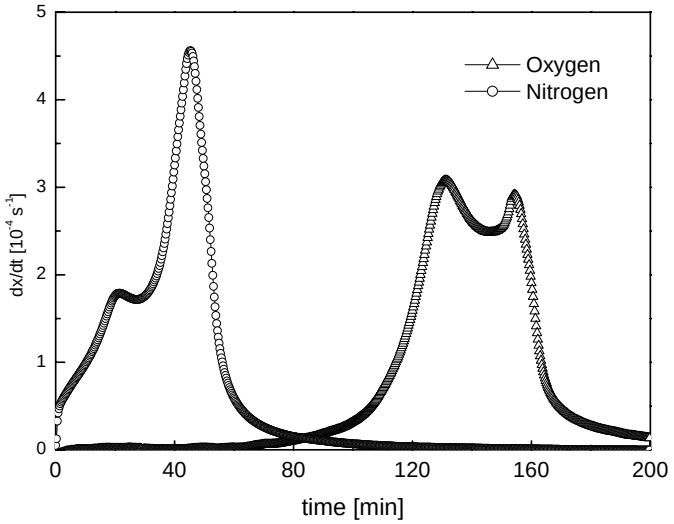

Figure 4.8 Comparison of the conversion rate versus time for samples polymerized under an oxygen and nitrogen atmosphere, and measured under the same conditions (at a temperature of polymerization of 70 ºC, amplitude with a period of modulation of 1 ºC and 24 sec).

On the other hand, the thermogram becomes more complex, with several exotherms, and the evolution of the heat capacity during polymerization in the air-sealed samples presents a clear maximum before vitrification, as shown in Figure 4.9.

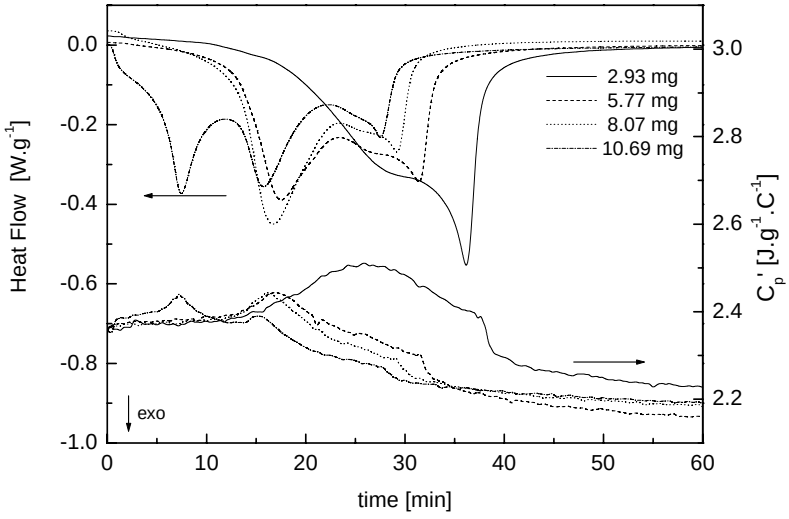

Figure 4.9 Normalized average heat flow (left axis) and storage heat capacity (right axis) for samples sealed under air atmosphere and polymerized at 85 ºC.

Additionally, the influence of sample mass was studied in a number of air-sealed samples with masses ranging from 2 to 23 mg and modulation amplitude 1 ºC. Significant changes in the evolution of heat flow and heat capacity were found when changing the sample mass, as shown in Figure 4.9. Variations in the amount of monomer introduced in the sample pan (always a hermetic 30-microlitre pan) may cause two effects: one of them is to change the amount of oxygen contained in the reaction volume, and the specific surface of monomer exposed to the air inside the sample pan; and the other is to change the amount of heat that must be released from the reacting mixture to the DSC block.

An increase in the mass of the reacting mixture may produce an increase in the local temperature as compared to the temperature measured by the instrument due to the thermal resistance of the sample holder. This increase in the local temperature can speed up the reaction. To check the relative influence of both effects a number of samples with masses varying between 6 and 18 mg were sealed in nitrogen atmosphere and polymerized at 75 ºC. The evolution of the conversion rate (or heat flow profile) is shown in Figure 4.10.

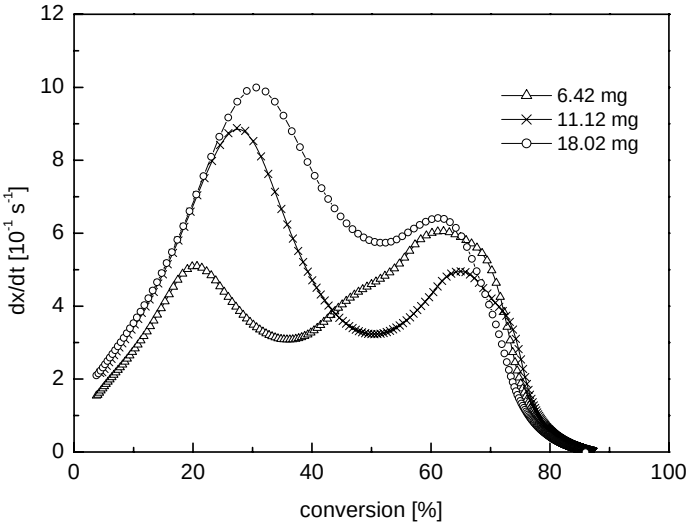

Figure 4.10 Influence of sample mass on the polymerization kinetics monitored at 75 ºC (amplitude and period of modulation of 1 ºC and 24 sec) of samples sealed under nitrogen atmosphere. The sample mass is indicated in the figure.

4.3.2 DRS

Since the TrEGDMA monomer is in the liquid state, the polymerization at high temperatures (about 70 ºC) present a high conductivity. The data collected during the reaction present this contribution during the whole polymerization as shown in Figure 4.11.a. Though the value of ε'' changes until reaching an equilibrium value depending on the polymerization temperature, this is not enough to extract information. Oppositely, the representation of the electric modulus allows a more detailed analysis of underlying changes (see Figure 4.11.b).

Frequency scans show a single peak in the electric modulus loss during all the polymerization time. In this representation, the space charge effects are suppressed and the existing peak reveals an ionic conductivity [21-23]. Using a Havriliak-Negami function, data were fitted considering fixed the $\alpha_{HN} = 1$ and the remaining parameters variable. The characteristic time of this peak changes upon polymerization in accordance with Figure 4.12, where the four samples polymerized are included. In the same way, the intensity of the peak, as shown in Figure 4.11.b, initially keeps almost

constant but at a certain polymerization time suffers an abrupt increase. This change is represented in Figure 4.13.

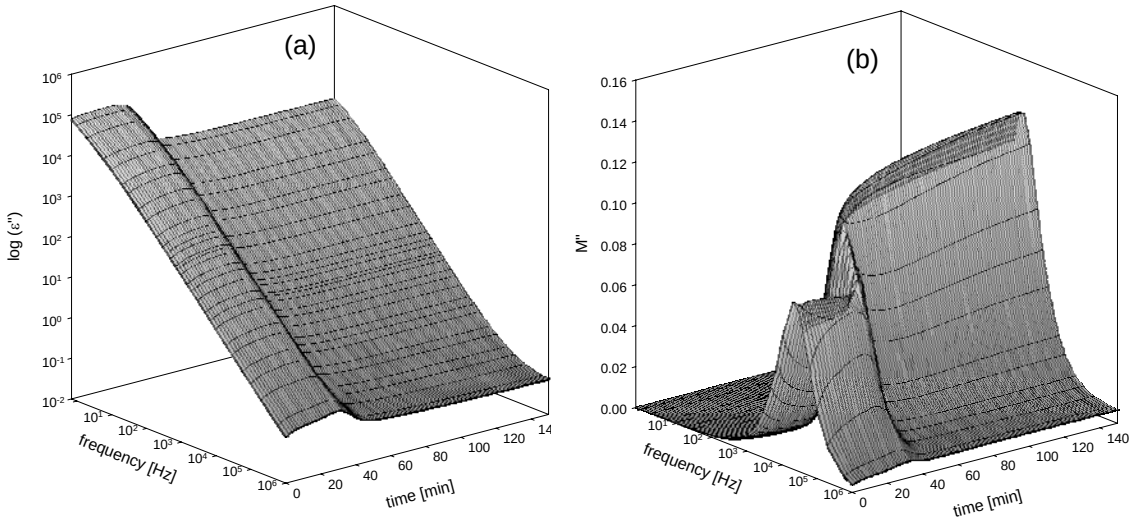

Figure 4.11 (a) 3D dielectric loss spectra and (b) 3D electric modulus, corresponding to TrEGDMA/AIBN during isothermal polymerization at 66 ºC.

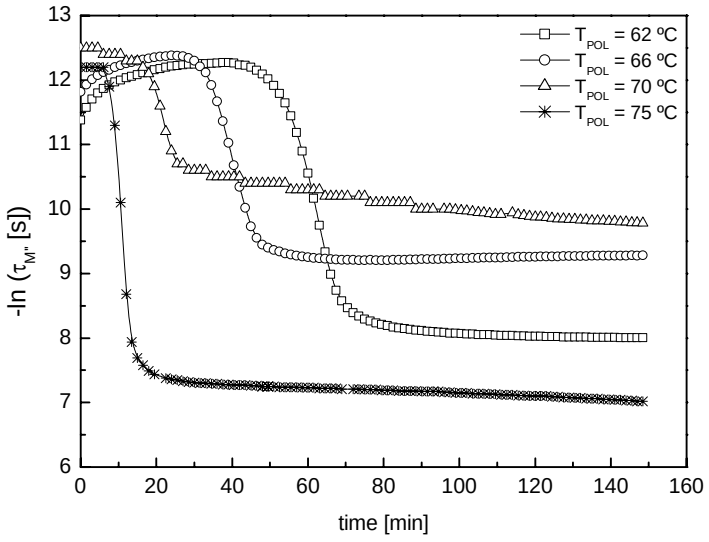

Figure 4.12 Relaxation time, $\tau_{M''}$, of electric modulus loss *vs.* polymerization time.

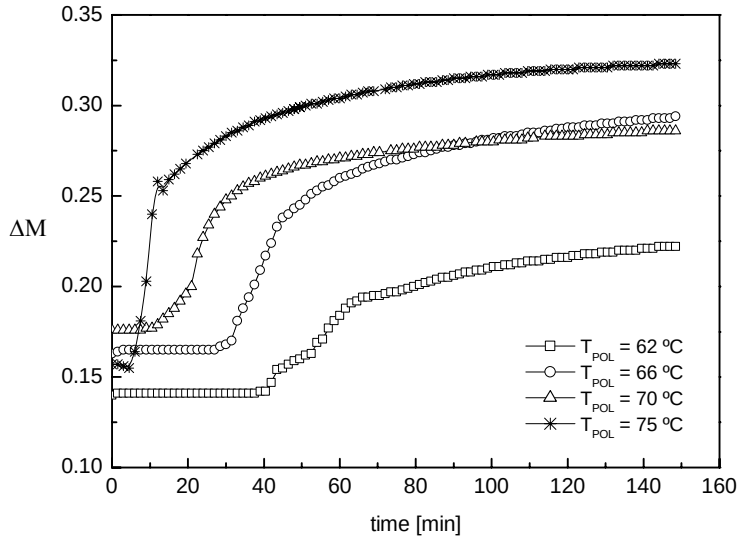

Figure 4.13 Intensity of electric modulus ($\Delta M = M_0 - M_\infty$) *vs.* polymerization time.

After the isothermal polymerization, the sample was cooled down to -120 ºC and next a heating scan at a rate about 10 ºC.min^{-1} was carried up to 220 ºC. This way two important facts could be verified: *i*) the existence of an important quantity of unreacted monomer in all polymerized samples (see Figure 4.14.a) whose glass transition is responsible for the relaxation peak appearing between -80 and -60 ºC, and *ii*) that a second polymerization induced during the heating run until 220 ºC does not lead to a total consumption of the monomer for all the samples (see the isochronal corresponding to the polymerization at 70 ºC in Figure 4.14.b). If data collected after polymerizing at 220 ºC are plotted in $\tan\delta$, no significant differences are observed in the intensities in the final polymer (data not shown). The differences observed in ε'' (Figure 4.14.b) can be thus attributed to some thickness variations and not to different quantities of the unreacted monomer. The relaxation process that lefts over in the produced polymer is located in the same position than the γ process detected in the pure monomer described in the preceding chapter. The sample previously polymerized at 70 ºC, still shows the α monomer's relaxation and a significant conductivity tail when compared with the other samples.

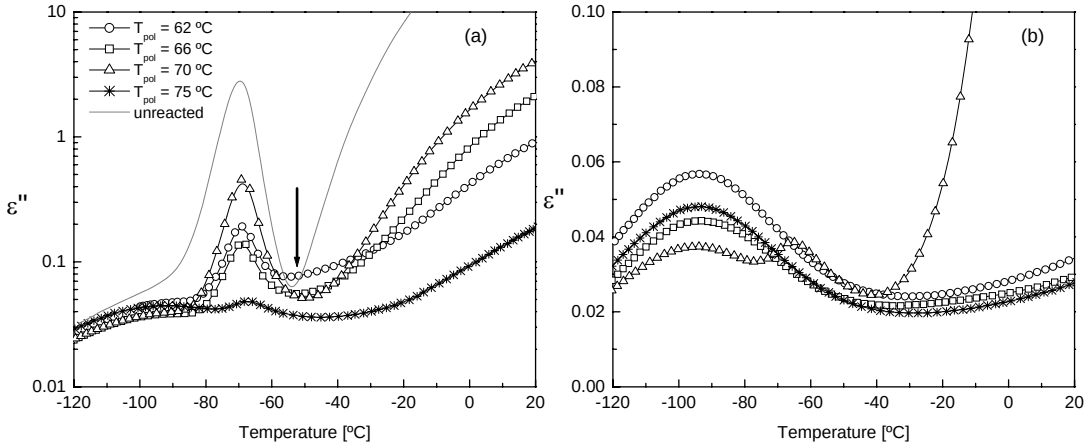

Figure 4.14 (a) Loss factor at 1 kHz obtained after polymerization at the temperatures indicated in the figure and (b) after heating the semi-polymerized samples up to 220 ºC. Data were collected at a cooling rate of around -9 ºC.min^{-1}.

4.4 Discussion

In calorimetric experiments, the presence of double peaks in the conversion rate against time or conversion in the polymerization at the highest temperature, 75 ºC, in nitrogen-sealed samples can be explained by the Trommsdorff-Norrish effect (remember Figure 4.3). The absence of reaction inhibitors (except for the oxygen that could be solved in the monomer) makes the conversion rate increase rapidly at the first instants of the reaction. The conversion rate value is the result of the balance between initiation, propagation and termination reactions that take place simultaneously.

The rate of each reaction changes as polymerization progresses due to the reduction in the amount of monomer and initiator and to the change in mobility due to the increase in the viscosity of the reacting mixture of the different species involved in the reaction. The first peak can be explained by the decrease in the amount of available monomer and initiator molecules.

If the influence of the termination reactions on the conversion rate were not significant with respect to that of the initiation and propagation mechanisms, as has been pointed in some works [16,24], the conversion rate would continue decreasing

until the final stop of the reaction by vitrification. But the presence of the second peak means that the termination reactions play an important role in the conversion rate at this temperature. The increase in viscosity and the network connectivity cause the termination mechanisms involving radicals linked to the growing network to become diffusion controlled. The rate of the termination reactions rapidly decreases and the reaction self-accelerates. The second maximum would be due again to a decrease in the amount of the remaining unreacted monomer, and finally, after 27 minutes, vitrification takes place and the conversion rate rapidly decreases.

As temperature decreases, the conversion rate plot becomes simpler (remember Figure 4.6); nevertheless, between 72 and 68 ºC the overlapping of more than one peak is quite clear. In this temperature range, the high conversion side of the curve shows a more or less sudden slope change that can be ascribed to the onset of vitrification. For temperatures below 68 ºC, only one single peak can be observed.

The reason for this change in behaviour can be found in the fact that initiation and propagation reactions show higher activation energy than that of termination [13,14,15]. The rates of initiation and termination mechanisms become more different from each other as temperature decreases. At low temperatures the kinetics of the polymerization process is governed by the kinetics of initiation and propagation.

The plot of the real part of the complex heat capacity C' against time (Figure 4.6) shows the characteristic drop that can be associated with the vitrification of the system. Nevertheless there are some peculiarities in this system that requires a more detailed analysis. The lower the polymerization temperature is, the longer the time at which the C' step occurs (remember Figure 4.6). To characterize the position of the C' step in the time axis, the time for the mid-point decrease of C' in the step, t_{mp}, will be defined, similarly to the mid-point glass transition temperature in a DSC scan of a glass forming liquid. It is possible to calculate for each polymerization temperature, the conversion at that time, that we call x_{mp}. These values are represented in Figure 4.15. It is worth noting the great dependence of x_{mp} with temperature. In this system the glass transition of the monomer ($T_{gM} = -86^{o}C$) and that of the polymer network ($T_{gN} \approx 156^{o}C$ [12]) are quite different. When the system vitrifies during the polymerization reaction at a temperature in the order of 70 ºC it must consist in a polymer network with a cross-linking density below the

stechiometric one, due to a number of unreacted double bonds in it and some unreacted monomer that acts as a plasticizer. The glass transition of this system is approximately the polymerization temperature, thus, around 100 ºC below the final glass transition temperature of the polymer network. The difference comes both by *i*) the defect in cross-linking density and internal plasticization due to branching and *ii*) the plasticization effect of unreacted monomer.

To analyze the effect of each factor Figure 4.15 shows the glass transition temperature (or the polymerization temperature) of the system after vitrification during the isothermal polymerization against the conversion at time t_{mp}. At the moment of vitrification in the reaction at 64 ºC the conversion of double bonds is $x = 0.51$. Clearly not all the monomer is fixed to the polymer chains since in that case the system would consist in a linear polymer. But an increase in the conversion up to $x = 0.75$ (conversion attained at 75 ºC) only increases the glass transition temperature by 15 ºC. If at this conversion degree most of the monomer is consumed, the additional cross-links produced by the reaction of the remaining double bonds in the network should account for the increase of the T_g of the system from 75 to 156 ºC. To analyze the effect of plasticization, Figure 4.15 shows a rough estimation of the conversion dependence of T_g, assuming that the unreacted monomer and the polymer network form a homogeneous mixture, obtained using Fox equation [25]

$$\frac{1}{T_g + 273.15} = \frac{x}{T_{gN} + 273.15} + \frac{1-x}{T_{gM} + 273.15} \qquad \text{Equation 4.4}$$

with T_{gN} and T_{gM} being the glass transition temperature of the polymer network and the monomer respectively, and x the conversion calculated at time t_{mp}. Changes in the mixture composition that would produce a change in the T_g of the mixture from 60 to 75 ºC (the temperature interval of our experiments) would be very small as shown in Figure 4.15.

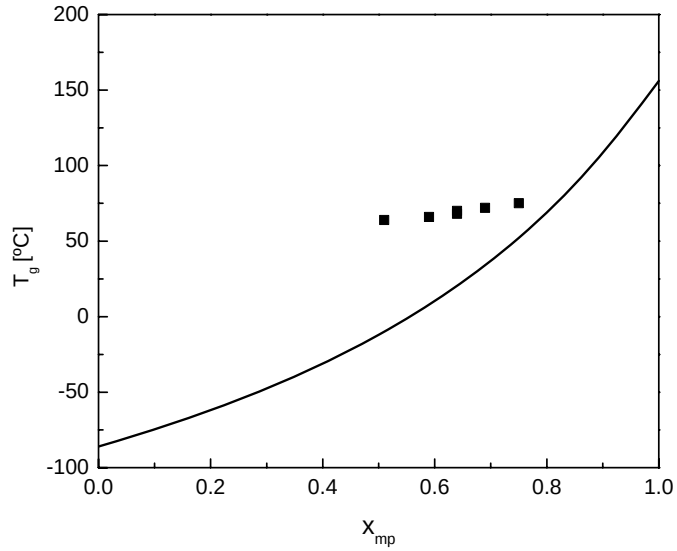

Figure 4.15 Relationship between the glass transition temperature (for each T_{pol}) and conversion at the mid-point of the C' step, corresponding to vitrification. The solid line represents the glass transition temperature of a homogeneous mixture of monomer and the polymer network according to Fox's equation (see text).

The situation does not change significantly if one takes into account that the polymer network actually has a lower T_g due to the discussed deficiency in cross-linking density. None of both effects *i*) or *ii*) or a combination of them satisfactory account for the experimental results. An alternative explanation is that a phase separation takes place in the system as polymerization progresses and the monomer is segregated from the growing network. Once an initiator molecule decomposes and the polymer network starts growing the local monomer/polymer ratio corresponds to the maximum swollen capacity of the polymer network that is smaller than that given by the average conversion. The local glass transition temperature in the growing network becomes higher than the reaction temperature and the heat capacity drops because of the local vitrification although a homogeneous monomer/polymer system with the composition given by the conversion at that time would have a glass transition temperature still lower than the polymerization temperature.

At the moment of the drop in C' the system consists of polymer network domains swollen in the amount of monomer roughly estimated by the Fox equation for a plasticized network, and domains consisting of pure unreacted monomer. The

progress in the reaction follows by the opening of more initiator molecules in the monomer phase or by the diffusion of monomer into the glassy network domains.

The reaction involves the incorporation of the monomeric unit to the glass and thus a transition from the liquid to the glassy states that contributes to a further decrease in the heat capacity of the system. It is interesting to note that according to this interpretation the glass transition of the monomer should be detected in the reacting system even for high conversion states. This fact is in accordance with results of dielectric data collected after polymerization where the main relaxation process of the pure monomer is still detected (see Figure 4.14.a).

If after vitrification the sample is cooled to a temperature low enough to stop any further progress of the reaction and some time is allowed for the diffusion of the monomer into the polymer network, the glass transition temperature measured in a subsequent heating scan is lower than the temperature at which the polymerization takes place, as shown in Figure 4.4 for a sample polymerized at 66 ºC that was stored for a long time at 5 ºC before the DSC heating scan. This sample shows T_g around 45 ºC. If vitrification had taken place in a homogeneous mixture during reaction, the glass transition would be equal to 66 ºC independently of the time delay before the DSC heating scan.

Another interesting feature is that C' does not show a maximum before vitrification (Figure 4.6). According to the work of Wang and Johari [10] this maximum can be expected due to the mixture of monomer and polymer network. The reason why the peak is not present in our system can also be due to the existence of a phase separation that prevents the formation of a homogeneous mixture of monomer and polymer chains. Interestingly enough the peak in *C'* appears clearly and repeatedly in the samples polymerized in aluminium pans sealed in air atmosphere. In that case the reaction is much slower than in the absence of oxygen provided the polymerization temperature is the same. There is more time for monomer to diffuse into the growing network and the segregation of the monomer can occur at longer polymerization times.

Oxygen is a well-known inhibitor in these reactions [26-28] that affects both initiating and propagating species in radical polymerization. In Figure 4.8 the shift of the peaks in the heat flow plot to higher times can be observed for TrEGDMA sealed in air atmosphere.

Two peaks are always present in the heat flow *vs.* time plot of samples sealed in air atmosphere (Figure 4.9), which separate when the sample mass is increased. These can be easily related to the peaks present in the nitrogen-sealed samples. But, in addition a third peak can be observed when the mass is 10.69 mg. Recently Soulé and co-workers [19] observed a similar feature in the free radical isothermal polymerization of isobornyl methacrylate with benzoyl peroxide as initiator. A peak appears in the heat flow trace of the sample polymerized in presence of air which is not present in the case of samples sealed in nitrogen atmosphere; more experiments are necessary to clarify the origin of this peak.

In what concerns to dielectric results, at the polymerization temperature no dipolar dielectric relaxation processes is expected in the initial mixture, where the monomer is in the equilibrium liquid state. Thus, the peak appearing in the imaginary part of M^* for the shortest polymerization times can be ascribed to conduction processes.

From the analysis of the evolution of the relaxation time with polymerization time, obtained from the HN fitting procedure of M'', two principal features are observed (Figure 4.12): *i*) this parameter suffers a sudden decrease at a certain polymerization time t_{pol}, which changes with the polymerization temperature; *ii*) the $\tau_{M''}$ of the final network increases with increasing the polymerization temperature from 62 to 70 ºC, but it decreases for the highest temperature *i.e.* 75 ºC.

The abrupt change in the relaxation time can be related to the vitrification of the formed polymer, clearly detected by TMDSC experiments. During glass transition the conformational rearrangements of the polymer chains becomes frozen and this hinders the motion of space charges. Thus, at the same time that the heat capacity of the sample drops, the relaxation time of the ionic carriers displacement sharply increases. However, it is worth note that conductivity is still high in the glassy state, as can be seen in Figure 4.11.a. In fact the conductivity changes from 10^{-8} S.cm^{-1} in the liquid monomer to 10^{-9} S.cm^{-1} in the final mixture monomer/polymer at 1 kHz and

70 ºC, *i.e.* only one order of magnitude. Only after polymerizing up to 220 ºC, the conductivity falls to 10^{-11} S.cm^{-1}.

This feature can be related with the phase separation described above to explain the polymerization temperature dependence of T_g determined by TMDSC. The presence of a monomer phase permits ionic conduction although decreased in the partially polymerized material since in the swollen polymer phase the displacement of the charge carriers is frozen.

A more detailed analysis of the conductivity in both unreacted mixture and final polymer/monomer mixture shows that the conductivity contribution is not of only pure d.c. origin. This fact is revealed by: *i*) the increase in the low frequency side of the real part of the permittivity, ε' (right axis in Figure 4.16.a and c), which is insensitive to d.c. conduction, and *ii*) a deviation of the slope from -1 in the $\log \varepsilon''$ *vs.* $\log f$ representation (left axis in same plots). In the initial moment, the blocking of charge carriers at the sample/electrodes interfaces is in the origin of this additional contribution, *i.e.* the electrode polarization. On the other hand, after polymerization, two phases coexist, unreacted monomer and polymer network, leading to the accumulation of charges at the internal phase boundaries, which results in the well-known Maxwell-Wagner-Sillars effect [29]. These mechanisms, though presenting similar features are usually different in their intensities as shown in Figure 4.16 where different scales are employed in both ε' and ε'' (Steeman and Turnhout in chapter 13 of ref. 30,31).

Now, putting again the attention in the $\tau_{M''}$ parameter (Figure 4.12), the first observation is the plateau at the end of the polymerization time dependence, that is an indication that the polymerization reaction attained the maximum conversion degree at that T_{pol}. From TMDSC experiments this network is in the glassy state and thus the mobility of the remaining monomer is the main factor that determines $\tau_{M''}$.

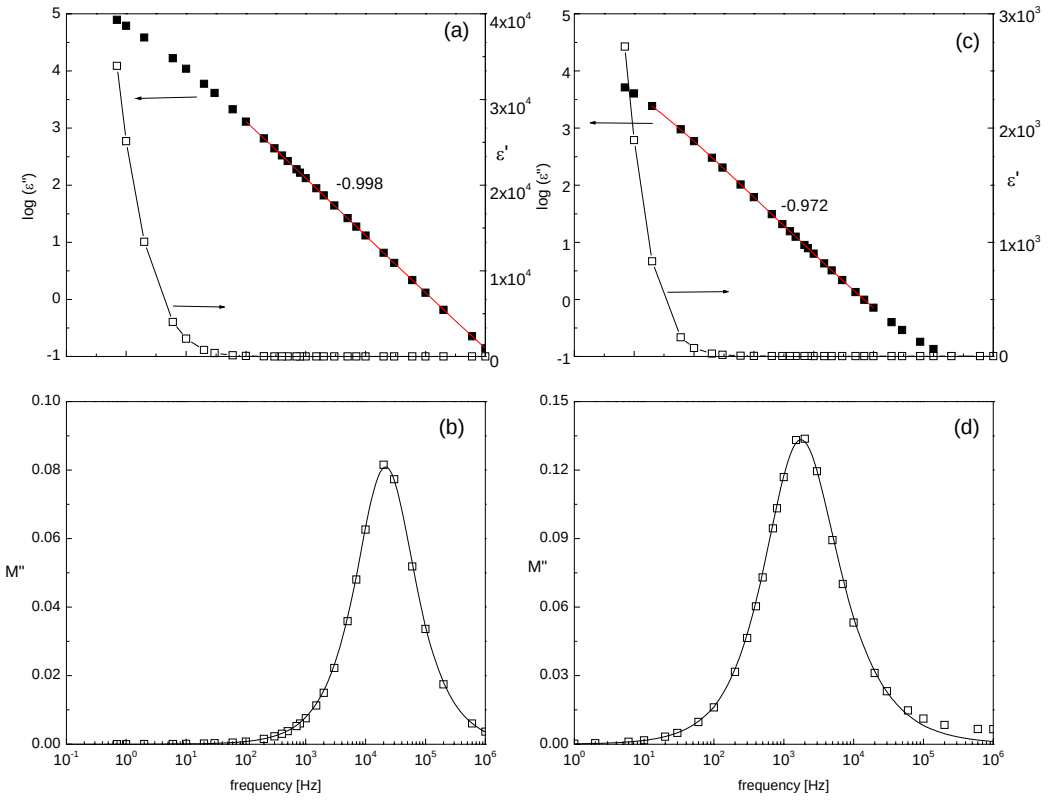

Figure 4.16 Dielectric results for TrEGDMA/AIBN mixture at 66 ºC: (a) and (c) real (right axis) and imaginary (left axis) parts of ε^* for t = 0 min and t =150 min of polymerization; (b) and (d) represent the dielectric modulus and the HN fitting curves for t = 0 min and t =150 min of polymerization.

This mobility can depend on either the cross-linking and conversion degree reached by the polymer and also on the microstructure of the material. The relatively high values of the conductivity show that there are pathways for the charge carriers within the sample, perhaps along defects of grain borders if finally the microstructure of the polymer network consists of an agglomeration of polymer domains. This mechanism of charge transport through a phase consisting in the remaining monomer is also supported by the fact that the dipolar main relaxation of the monomer is still observed in the samples after isothermal polymerization (see Figure 4.14.a). It is also worth note that the values of $\tau_{M''}$ found are higher/lower than expected for the motions of a low molecular weight substance within a homogeneous swollen polymer in the glassy state.

The important dependence of the relaxation time $\tau_{M''}$ at the end of isothermal reaction wit polymerization temperature can be explained by this mechanism. As can be observed in Figure 4.12, vitrification during polymerization at 70 ºC increases the relaxation time from 3.6×10^{-6} to 5.6×10^{-5} s, *i.e.* by a factor of 15, while at 62 ºC the relaxation time in the glassy state is 36 times higher than that at the beginning of polymerization (9.4×10^{-6} to 3.3×10^{-4} s).

It seems that polymerization at 70 ºC that presents the highest $\tau_{M''}$, produces a more dense crosslinked microstructure expelling unreacted free monomer that remains in a higher amount, as confirmed by the superior intensity of the monomer's α process in Figure 4.14.a.

Concerning polymerization at 62 and 66 ºC the differences in $\tau_{M''}$ can not be ascribed to different amounts of remaining unreacted monomer, since the intensities of the respective α peaks are very similar ($\tan\delta$ curves are superimposed in both samples). So, the higher $\tau_{M''}$ in sample polymerized at 66 ºC should be an indication of a different morphology that enhances the mobility of charge carriers, and thus the conductivity contribution, as confirmed by the higher conductivity tail in the high temperature side of Figure 4.14.a. In the sample polymerized at 62 ºC, the percolation path of charge carriers is somehow more hindered, resulting in a lower conductivity tail, possibly due to a higher incorporation of unreacted monomer in the polymer network. If this would be the case, then a higher interfacial polarization effect will be observed. It is not possible at this moment to confirm this fact, however we would like to note that the flank observed between the monomer's α peak and the conductivity in this sample, visible in Figure 4.14.a pointed out by the arrow, is probably related with this effect (in next chapter we will return to this point).

It is worth noting that at 75 ºC the relaxation time at the end of the isothermal polymerization is much longer, probably because the unreacted mobile monomer nearly becomes extinct, as demonstrated by the fact that its α relaxation is significantly reduced, as can be seen in Figure 4.14.a.

4.5 Conclusions

The shape of the heat flow or the conversion rate profile during isothermal polymerization of TrEGDMA measured by TMDSC highly depends on the polymerization temperature. The presence of more than one maximum in the heat flow versus time curves can be caused by the gel effect. The presence of oxygen inside the DSC pan has an inhibiting effect (at the same temperature, the samples polymerized in oxygen atmosphere have a longer induction time than the samples polymerized in nitrogen atmosphere) but at the same time the shape of the heat flow profile gets affected and a new maximum appears.

Vitrification of the polymer-monomer mixture during polymerization is clearly observed both by TMDSC and by dielectric measurements. The great dependence of conversion with the polymerization temperature can be explained if the growing polymer network is accompanied by a phase separation between highly crosslinked domains containing a certain amount of monomer such that their glass transition temperature equals the polymerization temperature, and another phase containing unreacted monomer. This conclusion is further supported by the dielectric experiments that show: *i*) a high mobility of charge carriers at the end of the isothermal reaction, when the polymer network is in the glassy state, and *ii*) the α process of the unreacted monomer.

Before vitrification, the temperature dependence of the real component of the complex heat capacity goes through a maximum in the samples sealed in air atmosphere. This was explained by Wang and Johari by the entropy of mixing of the monomer and the growing polymer network. Nevertheless, this peak is absent in samples sealed in nitrogen atmosphere. The difference between both situations may come from the phase separation mentioned in the former paragraph.

4.6 References

[1] M.T. Viciosa, J. Quiles Hoyo, M. Dionísio, J.L. Gómez Ribelles, J. Thermal Anal. and Cal., on-line (2007).

[2] S. Monserrat, I. Cima, Thermochimica Acta 330 (1990) 189-200.

[3] J.E.K. Schawe, I. Alig, Colloid Polym. Sci. 279 (2001) 1169-1176.

[4] C. Ferrari, G. Salvetti, E. Tombari, G.P. Johari, Phys. Rev. E 54 (1996) R1058-R1061.

[5] E. Tombari, G. Salvetti, G.P. Johari, J. Chem. Phys. 113 (2000) 6957-6965.

[6] G. Cassetari, G. Salvetti, E. Tombari, S. Varonesi, G.P. Johari, J. Polym. Sci. Part B: Polym. Phys. 31 (1993) 199-205.

[7] S. Swier, G. Van Assche, A. Van Hemelrijck, H. Rahier, E. Verdonck, B. Van Mele, J. Thermal Analysis 54 (1998) 585-604.

[8] G. Van Assche, A. Van Hemelrijck, H. Rahier, B. Van Mele, Thermochimica Acta 268 (1995) 121-142.

[9] G. Van Ascche, A. Van Hemelrijck, H. Rahier, B. Van Mele. Thermochimica Acta 304-305 (1994) 317-334.

[10] J. Wang, G.P. Johari, J. Chem. Phys. 116 (2002) 2310-2322.

[11] M.T. Viciosa, M. Dionísio, J. Non-Cryst. Solids 341 (2004) 60-67

[12] value estimated from the extrapolation of the T_g values determined for a set of MA/TrEGDMA copolymers in M.T. Viciosa, N. Rouzé, M. Dionísio, J.L. Gómez Ribelles, Eur. Polym. J. 43 (2007) 1516-1529.

[13] J.M.G. Cowie, "Polymers: Chemistry and Physics of Modern Materials", Blackie Academic & Professional (1991).

[14] G. Odian, "Principles of Polymerization", Wiley (1991).

[15] P.J. Flory, "Principles of Polymer Chemistry", Cornell University (1992).

[16] G. Van Ascche, E. Verdonck, B. Van Mele, Polymer 42 (2001) 2959-2968.

[17] M. Merzlyakov, G.W.H. Hölne, C. Schick, Thermochimica Acta 391 (2002) 69-80.

[18] W.Z. Xia, W.Z. Cook. Polymer 44 (2003) 79-88.

[19] E.R. Soulé, J. Borrajo, R.J.J. Williams, Macromolecules 37 (2004) 1551-1557.

[20] K S. Anseth, C.M. Wang, C.N. Bowman, Polymer 35 (1994) 3243-3250.

[21] Jr. H.W. Starkweather, P. Avakian, J. Polym Sci, Part B: Polym Phys 30 (1992) 637-641.

[22] G.M. Tsangaris, G.C. Psarras, N. Kouloumbi, J. Mater Sci. 33 (1998) 2027-37.

[23] P. Pissis, A. Kyritsis, Solid State Ionics 97 (1997) 105-13.

[24] J.L. Martin, A. Cadenato, J.M. Salla, Thermochimica Acta 306 (1997) 115-126.

[25] T.G. Fox, Bull. Am. Phys. Soc. 1 (1956) 123-135.

[26] J.G. Kloosterboer, Adv. Polym. Sci.84 (1988) 1-61.

[27] T.Y. Lee, C.A. Guymon, E. Sonny Jönsson, C.E. Hoyle, Polymer 45 (2004) 6155-6162.

[28] J.G. Kloosterboer, G.F.C.M. Lijten, C.P.G. Zegers, Polym. Matter. Sci. Eng. 60 (1989) 122-126.

[29] J.C. Maxwell, “Treatise on Electricity and Magnetism”, Dover reprint, New York (1892); K.W.Wagner, Arch. Elektrotech., 2 (1914) 371; R.W. Sillars, J. Inst. Electr. Eng. 80 (1937) 378.

[30] “Broadband dielectric spectroscopy”, Schönhals A, Kremer F, Springer-Verlag, Berlin (2003).

[31] J. Mijovic, B.D. Fitz, “Dielectric Spectroscopy of Reactive Polymers”, Application Note Dielectrics 2, Novocontrol GmbH (1998).

CHAPTER 5 CHANGES IN THE MOLECULAR MOBILITY UPON POLYMERIZATION

5.1 Introduction

n-ethyleneglycol dimethacrylate monomers due to its polyfunctionality have practical interest as precursors of cross linked polymers widely used in the production of coatings, information storage systems, spherical lenses and dental biomaterials [1-3]. Moreover, recently, it was found that they are also promising as matrixes for polymer dispersed liquid crystal devices [4]. In this chapter, the individual polymerization of each monomer (DEGDMA, TrEGDMA and TeEGDMA) without any other materials will be studied, since it seems to be useful to know about it in order to better define their applications. The results here presented are already published in references 5 and 6.

In the previous chapter, the isothermal polymerization of TrEGDMA was followed comprising real time measurements by both calorimetric and dielectric techniques, methods very used in literature as well illustrate by the results of Johari and co-workers [7-10], Williams [11] and Beiner and Ngai [12] among others. In our systems the isothermal polymerizations are carried out at high temperatures relatively to those of monomer's T_g, and a huge conductivity does not allow us extracting information about the dipolar relaxation processes during the formation of the polymer. Consequently, we decided to pay attention in the changes suffered by the remaining/unreacted monomers around their glass transition, where conductivity presents low values. We will continue inducing thermal polymerization but now using different combinations of temperatures and times.

Using the information obtained in the Chapter 4, where it was observed that the degree and the profile of polymerization are sensitive to the polymerization temperature (T_{pol}), we will start polymerizing the TrEGDMA monomer at two different temperatures and also during a heating run until 200 ºC. By this way the influence of the α process of the monomer will be diminish, and this fact will permit us a better characterization of the secondary relaxations already detected in the bulk monomer (Chapter 3).

Then, selecting the more interesting conditions for polymerization, we will proceed to study the changes induced in the reaction by changing the monomers, *i.e.* studying the formation of poly-DEGDMA and poly-TeEGDMA respectively.

Additionally, TeEGDMA will be isothermally polymerized at 70 ºC and the monomer's dielectric loss spectra collected at different polymerization times. This procedure where the progress of the reaction is monitored discontinuously by allowing the monomer to react at a higher temperature followed by the cooling of the partially reacted mixture to a temperature low enough to vitrified it, provides a convenient dielectric fingerprint spectra that reveals the mobility changes during polymerization [13-16].

This thermal cycling polymerization of TeEGDMA let us evaluate the mobility changes occurring upon polymerization on the α relaxation, and principally in the secondary relaxation β, difficult to observe in other polymerization conditions.

The results obtained are rationalized in function of the monomer's structural differences. This cycling polymerization also will become helpful for detecting new relaxation processes that arise upon reaction.

The aim of this study is then to interpret the results in function of the monomer's structural differences, investigate about the origin of the secondary relaxations detected in bulk monomers, and furthermore, to characterize the polymers produced from each monomer.

5.2 Polymerization of TrEGDMA

The monomer was previously passed through a disposable inhibitor remover column from Aldrich, ref. 306312-1EA, in order to eliminate the hydroquinone stabilizer. The polymerization initiator was 2,2'-azo-bis-isobutyronitrile (AIBN) from Aldrich, cat. nbr. 11630, being used as received, in the proportion 0.1% w.t. relative to monomer. The solutions were prepared in air atmosphere. This procedure was followed for all the polymerizations studied in this chapter.

5.2.1 Experimental conditions

5.2.1.1 Dielectric Relaxation Spectroscopy

The dielectric measurements were carried out in different increasing temperature steps from -115 up to 0 ºC (in the temperature range -115 ºC ≤ T ≤ -85 ºC and -55 ºC ≤T ≤ 0 ºC, the dielectric spectra were recorded every 5 ºC; in the remaining temperature region the spectra were recorded every 2 or 3 ºC). As usually, a drop of the monomer/AIBN mixture with two silica spacers 50 μm thick was placed between two gold plated electrodes (diameter 20 mm) of a parallel plate capacitor. The sample cell was mounted on a cryostat and exposed to a heated gas stream being evaporated from a liquid nitrogen Dewar. The temperature control is performed within ±0.5 ºC.

The polymerization essays at 70 and 80 ºC were performed by the following procedure (see Scheme 5.1):

Path 1 - heating a fresh TrEGDMA/AIBN mixture from 25 ºC up to the temperature of polymerization (T_{pol}).

Path 2 - isothermally maintenance of the mixture at T_{pol} during 2.5 hours.

Path 3 - cooling of the mixture down to -115 ºC.

Path 4 - isothermal acquisition of the dielectric spectra of the poly-TrEGDMA partially polymerized in increasing temperature steps from -115 up to 0 ºC.

The samples so obtained will be named accordingly the corresponding polymerization temperature, *i.e.* T_{pol} 70 ºC and T_{pol} 80 ºC.

Additionally, a fresh mixture previously maintained 2.5 hours at 80 ºC was further heated to 120 ºC in increasing steps of 10 ºC, by maintaining it 10 minutes at each temperature (path 5), cooled down to -115 ºC (path 6) and re-measured (path 7 equal to path 4) (see Scheme 5.1). See further on text the reason for this type of procedure; this mixture will be designated as being polymerized at T_{pol} 80+120ºC.

Other fresh sample was polymerized during an heating process that was performed at a rate of 1 ºC.min^{-1} from 25 ºC up to 200 ºC, where it was maintained only 1 minute at the final temperature (200 ºC). Afterwards it was cooled down to

-115 ºC before the acquisition of the dielectric spectra (path 4). This polymerized sample is designated as T_{pol} 200ºC.

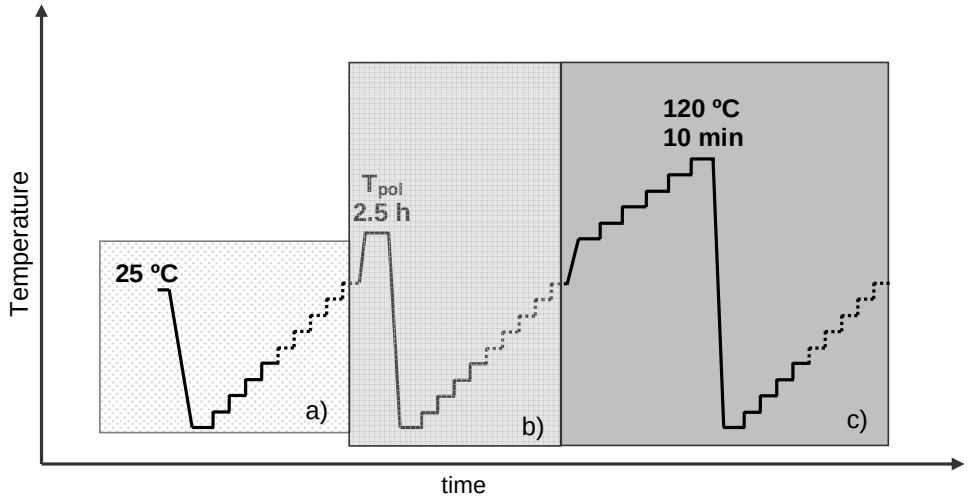

Scheme 5.1 Schematic representation of the temperature protocol followed in dielectric measurements: a) region that corresponds to the acquisition data analyzed in Chapter 3;

b) procedure for isothermal polymerization at T_{pol} - paths from 1 to 4 (see text);

c) protocol for further polymerization (T_{pol} 80+120ºC) - paths from 5 to 7 (see text).

5.2.1.2 Differential Scanning Calorimetry

DSC 121 from Setaram equipment fitted with a liquid nitrogen cooling accessory was used for differential scanning calorimetry experiments. The sample vessels were placed in the sample holder at room temperature and cooled down to -130 ºC. Measurements were performed upon heating, at a rate of 5 ºC.min^{-1}, in two different runs since the heating procedure does not allow covering the entire temperature range in a single run. Therefore, a first thermogram was collected from -130 up to 70 ºC followed by a second run covering the temperature range 25 to 400 ºC. Unsealed aluminium sample vessels were used. The vessels containing the samples were weighted in a precision balance (± 1 μg) before and after the DSC essays.

5.2.2 Results

From results present in Chapter 3, it was established that in the pure monomers, as well as the main relaxation process associated to the glass transition,

two secondary relaxations appear, the β and γ, that were well defined below T_g. The dielectric loss spectra, $\varepsilon''(f)$, of the unreacted monomer (fresh TrEGDMA/AIBN mixture) was shown in Chapter 3, and here the same sample was further polymerized at T_{pol} = 70ºC, that allows a good comparison of the results.

The dielectric loss spectra acquired in path 4 for polymerized samples T_{pol} 70ºC, T_{pol} 80ºC, T_{pol} 200ºC and T_{pol} 80+120ºC (see *Experimental conditions*) are present in Figure 5.1. The loss curve in full symbols, on each figure, corresponds to the temperature of -75 ºC and acts as a guideline to help the reader to perceive the existence of more than one relaxation process.

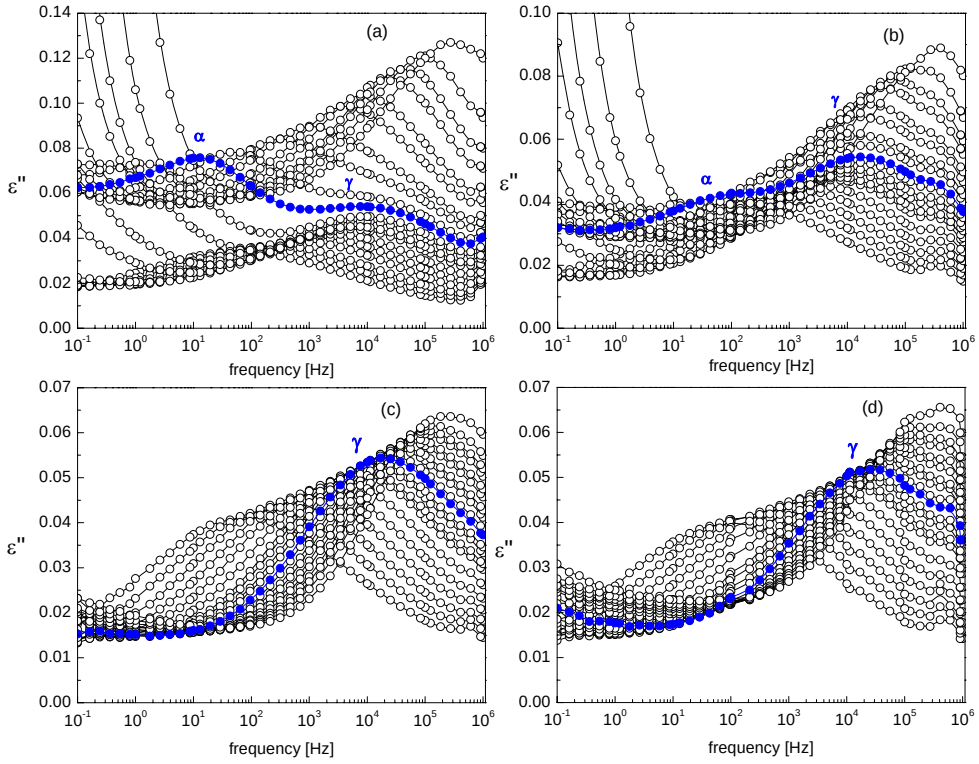

Figure 5.1 Dielectric loss spectra collected from -115 to -45 ºC (see section 5.2.1.1) for the poly-TrEGDMA samples: a) T_{pol} 70ºC, b) T_{pol} 80ºC, c) T_{pol} 200ºC and d) T_{pol} 80+120ºC. In full symbols are presented the corresponding loss curves obtained at -75 ºC.

The results in Figure 5.1 show that the main relaxation process is being depleted with the increase of the polymerization temperature, vanishing for T_{pol} 200ºC and T_{pol} 80+120ºC, while the secondary relaxation γ remains almost unaffected. From

this point of view, it can be said that polymerization allows defining better this secondary process even above T_g, since the influence of the main relaxation process is strongly reduced. The isothermal plots of dielectric loss at -75 ºC shown in Figure 5.2 illustrate more clearly this behavior. Also by the simple observation of Figure 5.2, where the unreacted monomer was included, in a different scale, it is put in evidence the deviation of the main relaxation process to lower frequencies upon polymerization.

Now, in order to distinguish that the γ process belongs uniquely to the monomer or also to the polymer network, we will call it hereafter γ_{pol} relaxation.

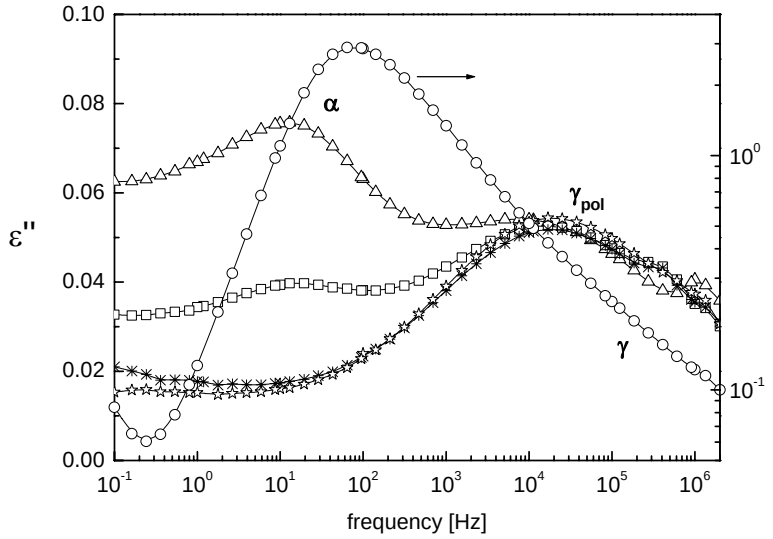

Figure 5.2 Comparison between the loss curves obtained at -75ºC for each poly-TrEGDMA samples: T_{pol} 70ºC – triangles, T_{pol} 80ºC – squares, T_{pol} 80+120ºC – asterisks, T_{pol} 200ºC – stars (left axis). The fresh mixture TrEGDMA/AIBN is included in circles in logarithmic scale (right axis).

Another way to visualize the effect of polymerization on the monomer mobility is through the plot of the dielectric loss at one fixed frequency. Figure 5.3 presents the isochronal plot at 1 kHz, taken from isothermal measurements, in a logarithmic scale to allow a better definition of the γ / γ_{pol} secondary process.

The secondary γ process that was largely merged in the low temperature side of the glass transition relaxation in the unreacted mixture becomes evident with the polymerization.

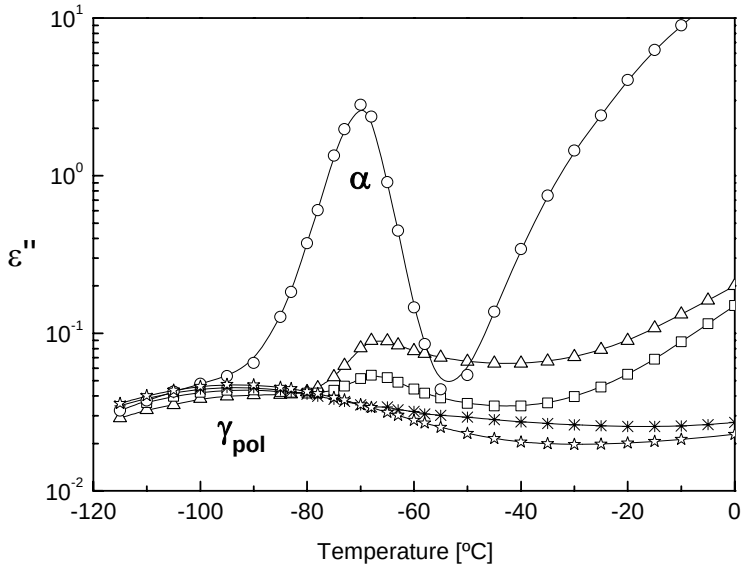

Figure 5.3 Isochronal plot of ε'' at 1 kHz for all polymerized samples of TrEGDMA (same symbols as Figure 5.2 are used).

The loss spectra obtained for the polymerized mixture T_{pol} 80+120ºC (see *Experimental Conditions*) was found to be very similar with the mixture polymerized at 200 ºC (detailed differences will discussed further on). The "final" temperature of 120 ºC was chosen after monitoring $tg\delta\left(=\varepsilon''/\varepsilon'\right)$ at a fixed frequency (1 kHz) during the heating process from 80 ºC (where the mixture stayed 2.5 hours) up to 120 ºC. At each 10 ºC step, $tg\delta$ was measured and no significant changes were found until the 120 ºC temperature was attained. At this temperature, $tg\delta$ showed an abrupt decrease. After 10 minutes at 120 ºC, the dielectric spectra were collected as already explained. Both T_{pol} 80+120 ºC and T_{pol} 200 ºC polymerized films thus obtained were analyzed by differential scanning calorimetry (Figure 5.4). Neither the characteristic exothermal peak originated upon polymerization, nor the glass transition of the monomer were detected in thermograms obtained from -100 up to 400 ºC; the inset in Figure 5.4 shows the thermogram obtained in the first run (see *Experimental*) where no monomer's glass transition was detected. Instead, an endothermic variation was observed for temperatures higher than 225 ºC which is associated with thermal degradation as confirmed by a weight loss in both samples; for thermograms covering a narrower temperature range (-100 to 300 ºC) the weight loss is around 40% whereas

it is higher than 90% when the final temperature is 400 ºC. With these results, we can conclude that for these two samples, the polymerization was completed since no signals of residual monomer were detected.

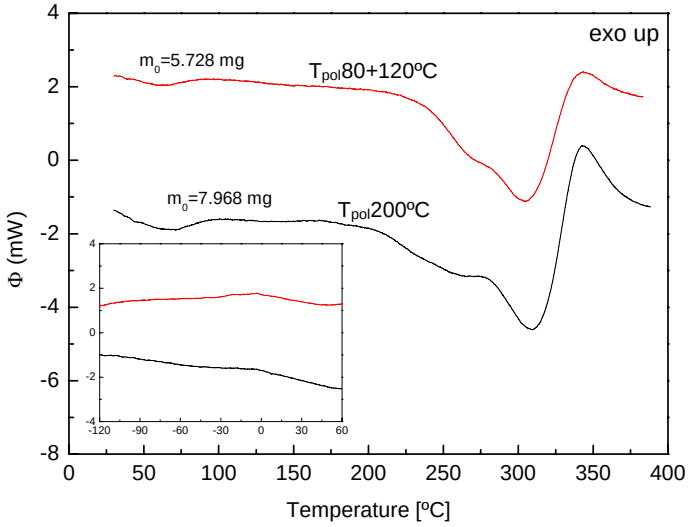

Figure 5.4 DSC thermograms obtained at 5 ºC.min^{-1} from 30 up to 400 ºC for both poly-TrEGDMA samples T_{pol} 80+120ºC and T_{pol} 200ºC; the abrupt variation with a minimum at 310 ºC is due to thermal degradation; the inset shows the first run taken from -130 up to 70 ºC where no monomer's glass transition is detected.

All the dielectric data were fitted by a sum of the well-known Havriliak-Negami [17] (HN) functions:

$$\varepsilon^* = \varepsilon_\infty + \sum_j \frac{\Delta\varepsilon_j}{\left[1+\left(i\omega\tau_j\right)^{\alpha_{HNj}}\right]^{\beta_{HNj}}} \qquad \text{Equation 5.1}$$

The detailed description of this equation was given in Chapter 1. For temperatures higher than -70 ºC the data are influenced by low frequency conductivity contribution, and an additional term $i\sigma/\omega^c\varepsilon_0$ was added (see Chapter 1 for interpretation).

Looking at the results present now, a first important observation can be made: the β relaxation that was detected in the bulk monomer (remember Chapter 3) seems not to be present after polymerization. This remark was confirmed during the fitting procedure, where it was not necessary to introduce one relaxation between the well defined α and γ (see Figure 5.5.a and b where the isothermal data at -75 ºC are

represented including the individual and the total HN fitting functions employed). Nevertheless, it must be noted that at this moment we can not put completely apart the possible existence of this relaxation since it may exist merged under the α process of the remaining monomer.

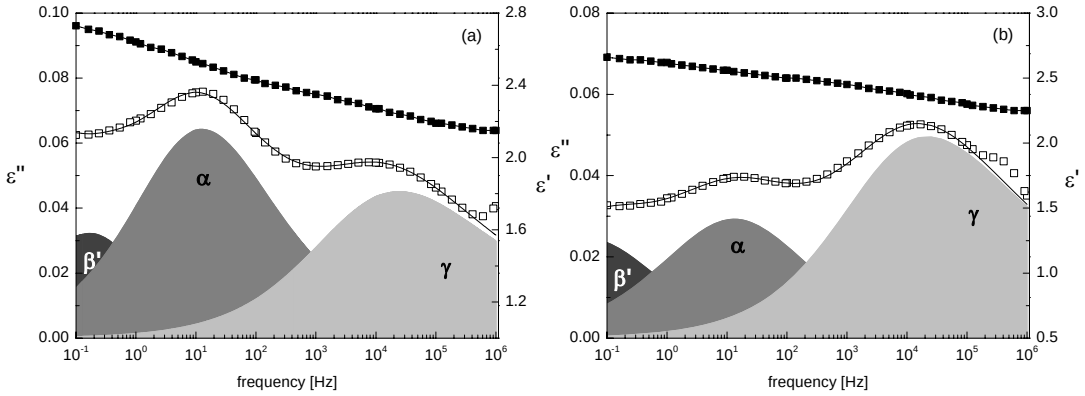

Figure 5.5 Real (full symbols and right axis) and imaginary parts (open symbols and left axis) of the complex permittivity obtained at -75 ºC for poly-TrEGDMA samples: a) T_{pol} 70ºC and b) T_{pol} 80ºC, and the corresponding individual HN fitting functions considered (filled area). The overall fitting curve is represented as solid line.

On the other hand, it is worth note that the experimental spectra shown in Figure 5.5 could not be fitted only by a sum of two relaxations functions and conductivity. In the low frequency side, all the curves show a contribution that is not originated from conductivity. Because of this, it is necessary to add a new HN function to reproduce ε'' data in the low frequency side of the α process of the remaining monomer. This relaxation process, which we will call hereafter β' is never resolved as a maximum in ε'' and its position in the frequency axis is consequently uncertain (consequently no numeric values could be determined accurately). Also in samples fully polymerized (*i.e.* samples named T_{pol} 80+120ºC and T_{pol} 200ºC) a different process must be considered to fit well the low frequency side of the spectra.

The dielectric strength, $\Delta\varepsilon$, obtained from the fittings for both the glass transition and secondary processes is presented *versus* the reciprocal of the temperature in Figure 5.6 for all the poly-TrEGDMA samples (full symbols - main process; open symbols - secondary process).

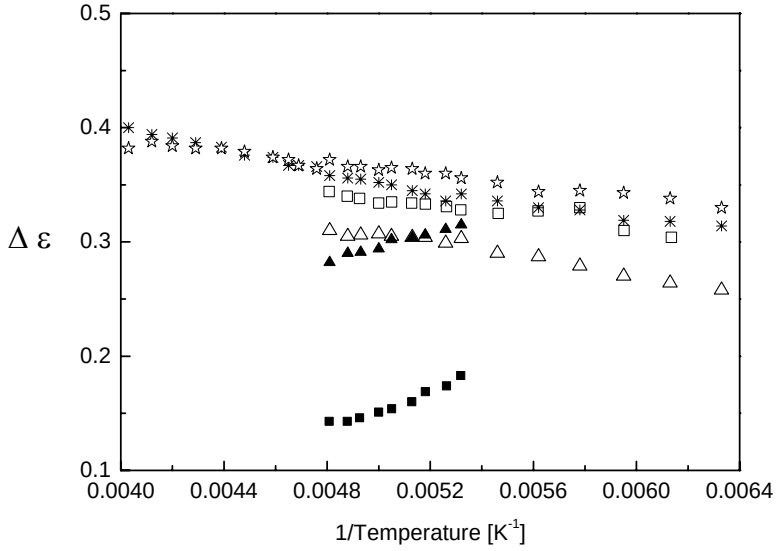

Figure 5.6 Dielectric strength, $\Delta\varepsilon$, in function of the reciprocal of temperature for all poly-TrEGDMA samples: full symbols – main process, open symbols – secondary process; T_{pol} 70ºC – triangles, T_{pol} 80ºC – squares, T_{pol} 80+120ºC – asterisks and T_{pol} 200ºC – stars.

The trends of the temperature dependence of the relaxation strengths for both main and secondary processes can be considered almost linear for all the systems represented.

The dielectric strength of the main process abruptly decreases in samples submitted to partial polymerization (T_{pol} 70ºC – triangles; T_{pol} 80ºC – squares) relatively to the bulk monomer (remember values of $\Delta\varepsilon_\alpha$ in Figure 3.6.a). Furthermore, this decrease is more accentuated with the increasing of T_{pol}, even vanishing for T_{pol} 80+120ºC and T_{pol} 200ºC. The dielectric strength of the main process for each sample slightly decreases with the temperature increase that permits to obtain the temperature onset as the extrapolation to $\Delta\varepsilon = 0$. The values so obtained are 118.7 ºC for T_{pol} 70ºC and 2.1 ºC for T_{pol} 80ºC. These very different results could be attributed to the low intensity of the main relaxation after polymerization at 80ºC and consequently, care must be taken in giving a physical meaning to this change in the T_{on}. For the γ process the increase of dielectric strength with temperature is observed in all the polymerized samples, as expected for secondary relaxations.

The α_{HN} and β_{HN} shape parameters remain approximately temperature independent for the main relaxation (values reported in Table 5.1). The α_{HN}, that in the unreacted monomer was 0.95±0.03, now takes the values 0.52 ± 0.09 and 0.45 ± 0.03 for T_{pol} 70ºC and T_{pol} 80ºC respectively. On the other side, the β_{HN} is 0.72 ± 0.05 and 0.94 ± 0.10, while in the pure monomer was 0.46 ± 0.03. This increase in the β_{HN} parameter can be due to the absence during the fitting procedure of the secondary β process. On the other hand, the decrease in the α_{HN} can be an indication of the inhomogenity of the polymer in formation.

	τ_0 [s]	B [K]	T_0 [K]	T_g [K]	m	$E_a(T_g)$ [kJ.mol^{-1}]	α_{HN}	β_{HN}
T_{pol} 70ºC	$(2\pm1)\times10^{-14}$	1219±115	153±2	186.7 (-86.4 ºC)	87	310	0.52±0.09	0.72±0.05
T_{pol} 80ºC	$(1\pm1)\times10^{-13}$	1120±113	153±2	187.9 (-85.2 ºC)	78	281	0.45±0.03	0.94±0.06
unreacted	$(3\pm1)\times10^{-16}$	1520±52	147±1	184.9 (-88.2 ºC)	85	303	0.95±0.03	0.46±0.03

Table 5.1 Glass transition temperatures (for τ = 10^2 s), activation energies at T_g ($E_a(T_g)$) and fragility indexes (m) estimated from the VFTH fittings (see text) for the partially poly-TrEGDMA samples, T_{pol} 70ºC and T_{pol} 80ºC, and for the monomer prior to polymerization. Also the shape parameters from the HN fitting of the main relaxation are included.

For the secondary γ_{pol} relaxation, no significant changes are detected on both shape parameters (see Table 5.2) despite of the different degree of polymerization. Only when compared to the corresponding γ of the unreacted monomer some differences are detected: the α_{HN} increases when the sample is polymerized and the opposite is true for the β_{HN}. This increase/decrease makes that the product $\alpha_{HN}\beta_{HN}$ keeps almost constant.

The final parameter obtained from the HN fittings is the relaxation time, τ_{MAX}. In Figure 5.7 we present the temperature dependence of the $-\ln\tau_{MAX}$ values for both main (α) and secondary (γ_{pol}) relaxation processes of all the studied polymerized

samples. The TrEGDMA/AIBN mixture after polymerization at 80+120 ºC and 200 ºC does not present the α process, therefore only data in the linear branch of the γ_{pol} process are represented in this activation plot.

	E_a [kJ.mol^{-1}]	τ_0 [s]	$T_{\alpha\gamma}$ [ºC]	α_{HN}	β_{HN}	$\alpha_{HN}\beta_{HN}$
T_{pol} 70ºC	39±1	$(3\pm2)\times10^{-16}$	-46.7	0.46±0.07	0.46±0.06	0.21±0.02
T_{pol} 80ºC	40±1	$(7\pm2)\times10^{-16}$	-53.7	0.47±0.07	0.47±0.04	0.22±0.03
T_{pol} 80+120ºC	36±1	$(2.2\pm0.2)\times10^{-15}$	---	0.46±0.06	0.50±0.09	0.23±0.04
T_{pol} 200ºC	36±1	$(2.2\pm0.6)\times10^{-15}$	---	0.47±0.06	0.48±0.08	0.23±0.6
unreacted	41±2	$(1.2\pm0.9)\times10^{-16}$	-54.5	0.42±0.06	0.55±0.07	0.26±0.05

Table 5.2 Activation energies and pre-exponential factor for the secondary γ relaxation for the poly-TrEGDMA samples and monomer prior to polymerization; estimated temperature for the intersection between the traces of the γ and α relaxations, $T_{\alpha\gamma}$; and shape parameters obtained from the HN fittings.

The secondary γ_{pol} process of all the polymerized TrEGDMA samples reveals Arrhenius behavior with the linear plots superimposed. The activation energy seems to decrease slightly from 40 to 36 kJ.mol^{-1} for samples partial and totally polymerized respectively. At the same time, the pre-exponential factor (τ_0) slightly increase, which probably indicates that the presence of the main relaxation process induces a certain degree of cooperativity in the molecular motions in the origin of this secondary process (see Table 5.2).

In what concerns the α process, the semi-polymerized samples present the typical departure from Arrhenius behaviour as it happens in the bulk monomer. In Figure 5.7 for facility of comparison, the results of the bulk monomer were included in grey symbols. The parameters for VFTH [18] curves are obtained jointly with the glass transition temperature, the fragility index and the apparent activation energy at T_g were calculated and the results are summarized in Table 5.1. Due to the deviation of the main relaxation for higher temperatures by the restrictions imposed by the

network formed, the glass transition temperature increases slightly. Also the apparent activation energy and the fragility index increase with polymerization.

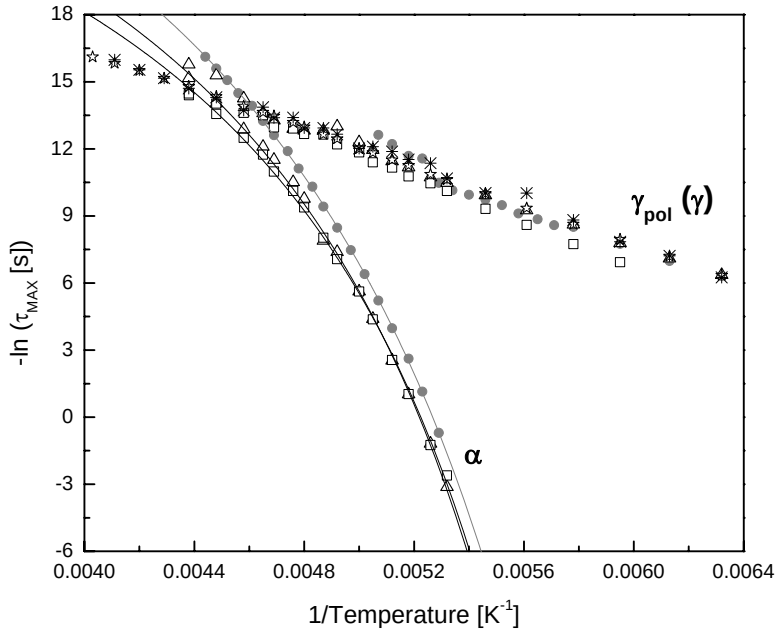

Figure 5.7 Activation plots for both main and secondary relaxation (γ_{pol}) processes for poly-TrEGDMA samples; solid lines represent the VFTH fittings of the main process. Symbols: T_{pol} 70ºC - triangles, T_{pol} 80ºC - squares, T_{pol} 80+120ºC - asterisks and T_{pol} 200ºC - stars; in grey full circles are represented the corresponding (α and γ) data for the monomer prior to polymerization.

5.3 Isothermal polymerization of DEGDMA and TeEGDMA

From the results obtained until now about the polymerization of TrEGDMA, it was the moment to continue with the remaining monomers, *i.e.* DEGDMA and TeEGDMA. From the tried different conditions it was decided to polymerize these systems using the isothermal procedure at 70 ºC during 2.5 hours.

5.3.1 Experimental conditions

The dielectric measurements were carried out in different increasing temperature steps from -120 up to 25 ºC: in the temperature range -120 ºC to -85 ºC and -55 ºC to 5 ºC, the dielectric spectra were recorded every 5 ºC; in the remaining temperature region the spectra were recorded every 2 or 3 ºC.

The polymerization was carried out in the same experimental conditions described in section 5.2.1.1, *i.e.* first keeping the sample at 70 ºC during 2.5 hours and then monitoring the changes induced in the mobility near the glass transition of the monomer (samples "T_{pol} 70ºC"). And after this, the polymerization continued until 120 ºC, samples "T_{pol} 70+120ºC" (see Scheme 5.1).

5.3.2 Results

Before specifying the results obtained for the polymerized systems, it is convenient to take in mind again the dielectric characterization of the monomers, presented in Chapter 3. The same samples studied in that chapter will be now polymerized.

In Figure 5.8 the loss curves collected at -100 ºC and -80 ºC are shown, for poly-DEGDMA (a) and c)) and poly-TeEGDMA (b) and d)) after polymerization (full symbols) where the loss curves measured at the same temperature prior to polymerization are also included in open symbols (these data are the same present in Chapter 3); solid lines represent the overall fitting achieved as a sum of the individual HN functions that are also illustrated by dashed and dotted lines (see legend).

In relation to the α process of each monomer after polymerization at 70 ºC, it vanishes in poly-TeEGDMA (Figure 5.8.d) but it is still observable in the relaxation spectrum of poly-DEGDMA, although with much less intensity (depletion of ε" peak in Figure 5.8.c presented in logarithmic scale). Something similar happened in the case of TrEGDMA polymerized under identical conditions (remember for example Figure 5.2). This fact indicates that the TeEGDMA monomer polymerizes faster than both DEGDMA and TrEGDMA that revealed incomplete polymerizations at this stage. It is worth noting that the position of the α relaxation in partially polymerized poly-DEGDMA nearly does not change to respect to that of the monomer, although a

small deviation to lower frequencies occurs (peak positions of unreacted and partially polymerized systems are indicated in Figure 5.8.c).

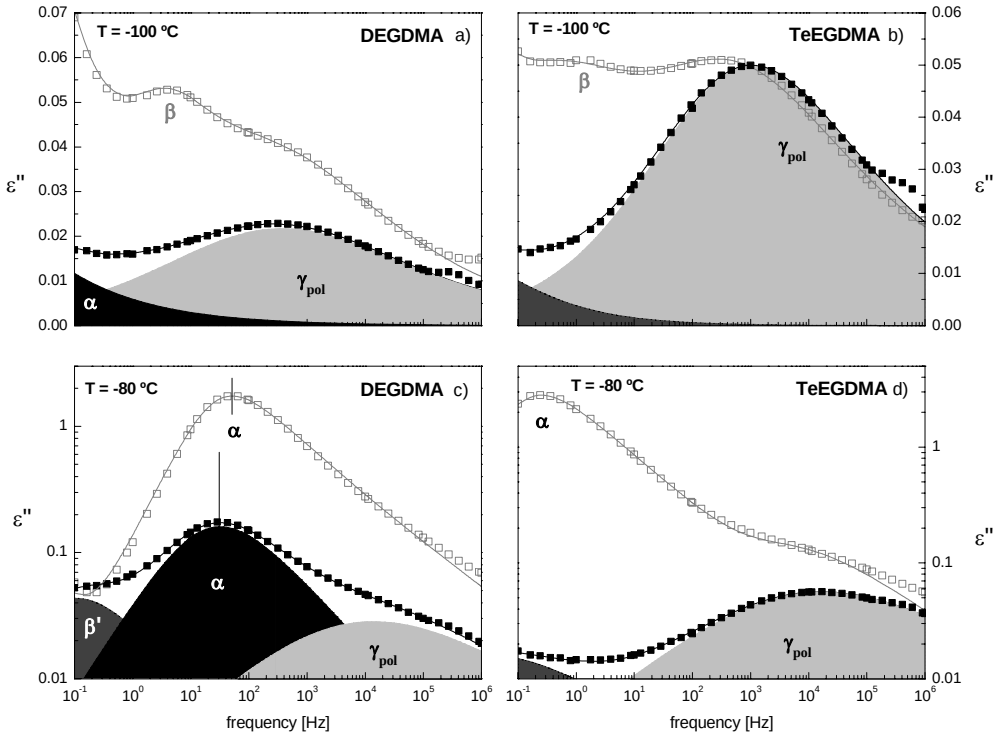

Figure 5.8 Dielectric loss spectra obtained at -100 and -80 ºC for: a) and c) poly- DEGDMA, and b) and d) poly-TeEGDMA, after polymerizing 2.5 hours at 70 ºC, *i.e.* T_{pol} 70ºC samples (full symbols). Grey open symbols correspond to unreacted mixtures. The individual HN curves (filled areas) for polymerized systems and the overall fittings (solid lines) are included.

Under isothermal polymerization induced at 70 ºC, the β process of the monomer is not detected in poly-TeEGDMA as it can be concluded from Figure 5.8.b and d. On the other hand, in poly-DEGDMA, as it was found in poly-TrEGDMA, it can not be concluded that does not exist since it may exist merged under the α process of the remaining monomer (full relative to open squares in Figure 5.8.a and c). Again, as it happened in poly-TrEGDMA, for poly-DEGDMA the isothermal data at -80 ºC (Figure 5.8.c) can not be fitted only by a sum of two relaxations (γ_{pol} and α) and conductivity, and thus another relaxation must be taken into account in the low frequency side of the α process of the remaining monomer (see Figure 5.9). Also the increase in the real part of the permittivity confirms the fact that this is not a d.c.

contribution (see inset in Figure 5.9). The use of this additional HN function, corresponding to the relaxation named β', was maintained in a limited temperature range to fit both poly-DEGDMA and poly-TeEGDMA data.

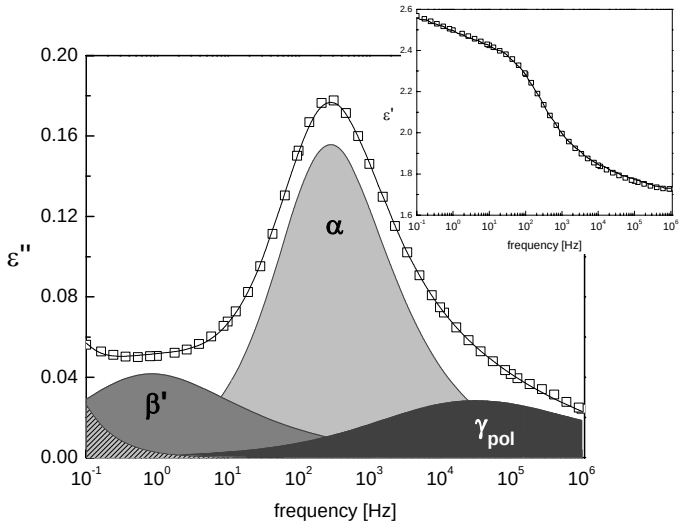

Figure 5.9 Dielectric loss spectra at -76 ºC collected for poly-DEGDMA partially polymerized, T_{pol} 70ºC. The individual HN and the overall fit curves are included. In the inset, real part of the complex permittivity and the corresponding fit line are represented.

In order to complete the polymerization process, the temperature was increased up to 120 ºC (path 5 described in section 5.2.1.1). As result (see Figure 5.10), the α relaxation completely disappears in poly-DEGDMA.

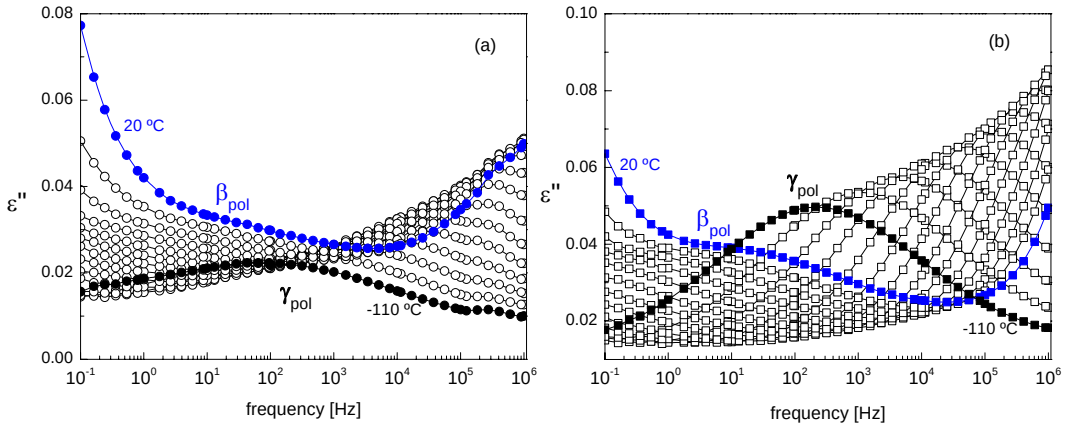

Figure 5.10 Dielectric loss represented every 10 ºC starting from -110 to 20 ºC for: a) poly-DEGDMA and b) poly-TeEGDMA after polymerization at 120 ºC, samples T_{pol} 70+120ºC. The isotherm at -110 ºC and 20 ºC are in full symbols.

It is so confirmed, as in poly-TrEGDMA, that the only relaxation process that remains in the final polymer is the secondary process γ, or more exactly γ_{pol} (see isotherm shown at -110 ºC in Figure 5.10, while α and β disappear due to the connectivity imposed by polymerization.

In the isochronal representation at 1 kHz Figure 5.11 the secondary relaxation β' is clearly detected in poly-DEGDMA after T_{pol} 70+120ºC (see inset of Figure 5.11.a) and it seems more depleted in sample T_{pol} 200ºC (see experimental procedure). This relaxation is not detected in poly-TeEGDMA at the same polymerization conditions, which can be explained taken into account that this monomer reacts quicker than the other one and this process is totally extinguished.

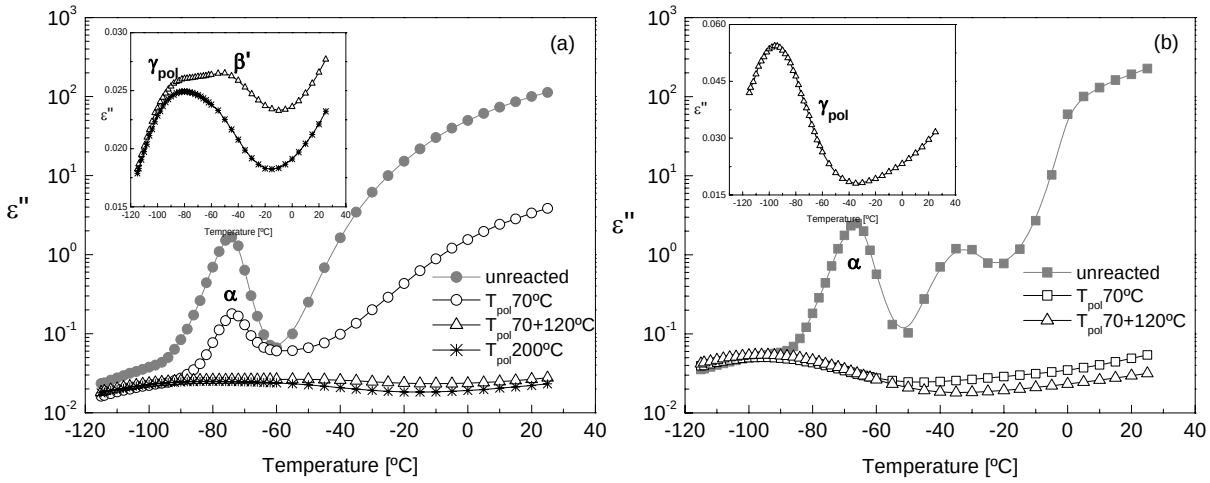

Figure 5.11 Isochronal representation of ε'' at 1 kHz taken from isothermal data for: a) poly-DEGDMA and b) poly-TeEGDMA. In the insets the series T_{pol} 70+120ºC and T_{pol} 200ºC for poly-DEGDMA and T_{pol} 70+120ºC for poly-TeEGDMA are enlarged. The results for the monomers prior to polymerization ("unreacted") were included for facilitating the comparison in grey full symbols.

If we pay attention to the polymer network originated after polymerizing the poly-TeEGDMA up to 120 ºC (sample T_{pol} 70+120ºC), besides γ_{pol} a secondary β_{pol} relaxation at higher temperatures can be clearly observed in the isochronal representation at 1 Hz (Figure 5.12). This polymerized sample was further measured

until 200 ºC in order to detect the glass transition process of the produced polymer. However the main relaxation process of the polymer network was not observed in this highly cross-linked system (Figure 5.12). The glass transition of these networks is expected above 190 ºC [19] (in TrEGDMA) but it is hardly detected in DSC as an extremely broad step in the thermogram with very small increment in heat capacity [20]. As a consequence it is not observable in dielectric measurements before the start of thermal degradation.

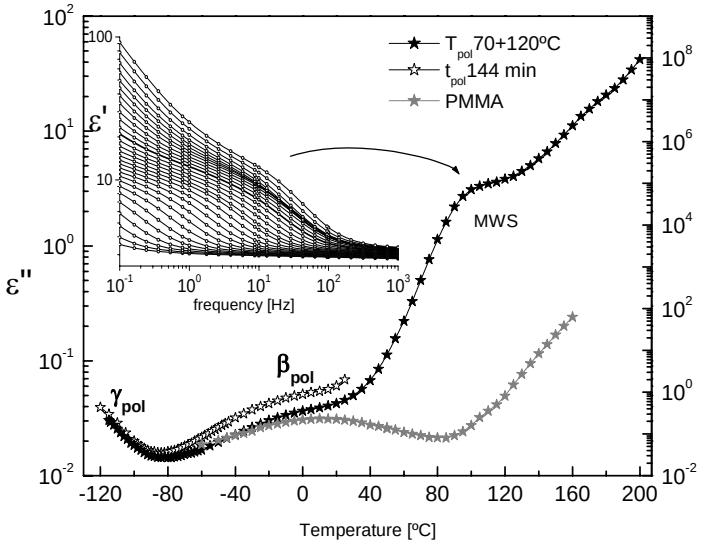

Figure 5.12 Isochronal plots of ε'' at 1 Hz taken from isothermal measurements for poly-TeEGDMA, sample T_{pol} 70+120ºC (black stars), together with the plot for poly-methyl methacrylate [25] (plotted using the right *y*-axis –gray stars) evidencing the similar location of the secondary relaxation detected in the two systems. The inset shows the isotherms of the real permittivity from 60 up to 200 ºC every 5 ºC, measured after polymerization at 120 ºC to illustrate interfacial polarization effect (MWS) at higher temperatures that is felt as a shoulder in the isochronal plot indicated by the arrow. The sample named t_{pol} =144 min (open stars) was polymerized in a cycling method described in next sections.

The isochronous representation of the relaxation spectrum of poly-TeEGDMA shows a rapid increase of ε'' with temperature after β_{pol} relaxation presenting a peak around 100 ºC. This is an unexpected phenomenon since no dipolar activity is predictable in this temperature range. The low frequency tail in the real permittivity as shown in the inset of Figure 5.12, points in the direction of an interfacial or

macroscopic polarization process related to some interfaces that develop under an heterogeneous polymerization as observed in polymeric samples of high molecular weight (Steeman and Turnhout in Chapter 13 in ref. 21).

The relaxation map for the systems polymerized after 2.5 h at 70 ºC (samples T_{pol} 70ºC) and after full conversion (samples T_{pol} 70+120ºC) is presented in Figure 5.13; gray lines show as a reference the position of the α relaxation of both monomers prior polymerization.

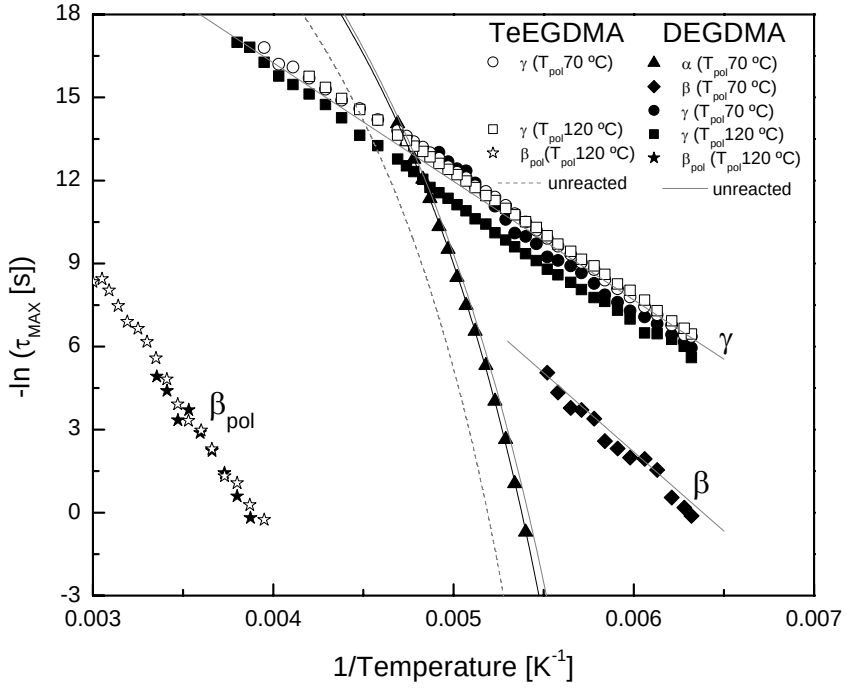

Figure 5.13 Relaxation map for both poly-DEGDMA and poly-TeEGDMA after polymerization 2.5 h at 70 ºC (T_{pol} 70ºC) and after polymerization at 120 ºC (referred here as T_{pol} 120ºC, see legend); solid line is the VFTH fitting for the main α -process for DEGDMA polymerized at 70 ºC. Temperature dependence for the α -process of unreacted monomers are shown as gray lines.

The γ process maintains almost the same activation energy prior and after full polymerization (γ_{pol}) for both DEGDMA and TeEGDMA (around 37 kJ.mol^{-1}), as denoted by the proximity of the straight lines' slopes (activation data included in Table 5.3). The small shift to high relaxation times of γ_{pol} for poly-DEGDMA (filled squares in Figure 5.13), was obtained as a result of the use of only one HN function to

fit ε'' data with a relatively broad shape (smaller α_{HN} value in Table 5.3 for the γ process of DEGDMA, T_{pol} 70+120ºC). However, if we use 2 HN functions assuming that a very small β process persists after polymerizing at 120 ºC, the estimated relaxation times will present slight deviations to lower τ values superimposing to the other γ plots. Nevertheless, because there is no evidence of bimodal character in the isothermal loss curves, we adopted the criterion of use only one fit function but it is not straightforward the validity of assuming the complete vanishing of the monomer's β process.

		$\Delta\varepsilon$ T = -100 ºC	α_{HN}	β_{HN}	E_a [kJ.mol^{-1}]	τ_0 [s]
DEGDMA	unreacted	0.194	0.45±0.07	0.49±0.07	36 ± 1	$(3.2\pm1.5)\times10^{-15}$
	T_{pol} 70ºC	0.160	0.42±0.05	0.54±0.09	42 ± 1	$(6\pm3)\times10^{-17}$
	T_{pol} 70+120ºC	0.241	0.26±0.05	0.94±0.12	38 ± 1	$(1.7\pm0.3)\times10^{-16}$
TeEGDMA	unreacted	0.347	0.44±0.14	0.49±0.08	37 ± 1	$(10\pm5)\times10^{-16}$
	T_{pol} 70ºC	0.384	0.46±0.12	0.52±0.15	37 ± 1	$(9\pm1)\times10^{-16}$
	T_{pol} 70+120ºC	0.397	0.47±0.10	0.47±0.09	36 ± 1	$(1.4\pm0.1)\times10^{-15}$
TeEGDMA cycles	unreacted (t_{pol}=0min)	0.324	0.40±0.08	0.50±0.06	36 ± 2	$(1.9\pm1.5)\times10^{-15}$
	t_{pol}=6min	0.300	0.43±0.09	0.63±0.14	36 ± 1	$(1.5\pm0.8)\times10^{-15}$
	t_{pol}=10min	0.328	0.34±0.03	0.75±0.11	37 ± 1	$(1.7\pm0.4)\times10^{-15}$
	t_{pol}=20 min	0.337	0.40±0.06	0.64±0.15	36 ±1	$(1.9\pm0.3)\times10^{-15}$
	t_{pol}=24 min	0.370	0.44±0.07	0.53±0.06	36 ± 1	$(2.0\pm0.2)\times10^{-15}$
	t_{pol}=144 min	0.454	0.47±0.12	0.53±0.07	37 ± 1	$(1.1\pm0.1)\times10^{-15}$

Table 5.3 HN shape parameters and $\Delta\varepsilon$ at -100ºC for the γ_{pol} process for poly-DEGDMA and poly-TeEGDMA are summarized. Activation energies and τ_0 are calculated from the Arrhenius fit. Data corresponding to the unreacted monomers are also included to facilitate the comparison. The sample named "TeEGDMA cycles" was polymerized in a different method described in next section.

The activation plot for the β process that still exists in the low frequency side of the γ process in partially polymerized DEGDMA (T_{pol} 70ºC), is presented in Figure 5.13 as filled diamonds, in coherence with the temperature dependence of the unreacted monomer (gray line); the estimated activation energy for this process is very close to the one obtained for the unreacted monomer, but with a significantly reduced intensity due to polymerization (see E_a and $\Delta\varepsilon$ at -100 ºC values in Table 5.4).

	$\Delta\varepsilon$ T = -100ºC	α_{HN}	β_{HN}	E_a [kJ.mol^{-1}]	τ_0 [s]
unreacted	0.139	0.78±0.03	0.42±0.02	48±1	$(1.4\pm0.7)\times10^{-17}$
T_{pol} 70ºC	0.023	0.70±0.03	0.47±0.04	49±2	$(4\pm3)\times10^{-17}$

Table 5.4 HN shape parameters obtained for the β process for poly-DEGDMA (T_{pol} 70ºC). Activation energies and τ_0 are calculated from the Arrhenius fit. Data corresponding to the unreacted monomer are also included to facilitate the comparison.

Concerning the temperature dependence of the main α relaxation in partially polymerized poly-DEGDMA respectively to the unreacted monomer, no significant changes are observed, nevertheless some slightly shift occurs mainly in the low temperature region where the polymerized system move to low frequencies (as already commented in analyzing Figure 5.8.c); respective VFTH fitting parameters are presented in Table 5.5. The apparent activation energy at T_g (T_g estimated using τ = 100 s criterion) and the fragility parameter (values included in Table 5.5) increase after polymerization as also happened with TrEGDMA.

	τ_0 [s]	B [K]	T_0 [K]	T_g [K]	$E_a(T_g)$ [kJ.mol^{-1}]	m	α_{HN}	β_{HN}
unreacted	7.5×10^{-17}	1691.9	139.1	179.5	276	80	0.92±0.04	0.52±0.03
T_{pol} 70ºC	9.4×10^{-16}	1375.1	146.3	181.4	306	88	0.72±0.07	0.71±0.04

Table 5.5 VFTH parameters calculated for α process, T_g (τ =100 s); activation energy at T_g and fragility index for poly-DEGDMA polymerized at 70 ºC (T_{pol} 70ºC); HN shape parameters are included. Data corresponding to the pure monomers are also incorporated to facilitate the comparison.

The activation energy of β_{pol} relaxation is nearly the same in poly-DEGDMA and poly-TeEGDMA, around 80 kJ.mol^{-1} (see E_a in Table 5.6 for samples T_{pol} 70+120ºC) as also denoted from the superposition of the activation plots (open and filled stars in Figure 5.13).

		α_{HN}	β_{HN}	E_a [kJ.mol^{-1}]	τ_0 [s]
DEGDMA	T_{pol} 70+120ºC	0.25±0.03	0.76±0.03	80 ± 3	(5.6±3.7)x10^{-17}
TeEGDMA	T_{pol} 70+120ºC	0.37±0.09	0.51±0.12	77 ± 1	(2.1±0.4)x10^{-17}
	t_{pol} =144 min	0.20±0.04	0.76±0.14	85 ± 2	(2.3±1.4)x10^{-17}

Table 5.6 HN shape parameters of the secondary process detected in the formed polymer, β_{pol}, after full polymerization (T_{pol} 70+120ºC). Activation energies and τ_0 are calculated from the Arrhenius fit. The sample named t_{pol} =144 min was polymerized in a cycling method described in next section.

5.4 Cyclying polymerization of TeEGDMA

An open question that remained after experiments described in the previous sections, was if β' process was really a new process or simply a deviation of the monomer's β relaxation. Thus, in order to understand better the changes of the detected processes in the molecular liquid undergoing polymerization, TeEGDMA was discontinuously polymerized at 70 ºC and data collected at different polymerization times, from the fresh TeEGDMA/AIBN mixture until maximum conversion.

5.4.1 Experimental conditions

A new sample of TeEGDMA/AIBN (the same mixture studied in section 5.2) was submitted to thermal cycling polymerization. Initially the mixture was monitored

in the low temperature region, *i.e.* from -115 to -50 ºC where the monomer's glass transition is comprised; after that, the sample was heated up to 70 ºC (the polymerization's temperature), kept there during 6 minutes, and next cooling down to -115 ºC in order to monitor the molecular mobility's changes in the glass transition region of the monomer. This procedure was repeated for different polymerization times (0, 6, 4, 10, 4 and 120 min). Data during this discontinuous polymerization will be designed using the accumulated polymerization time until this moment, *i.e.* t_{pol} = 0 min, t_{pol} = 6 (0+6) min, t_{pol} = 10 (0+6+4) min, t_{pol} = 20 min (0+6+4+10)…

5.4.2 Results

Figure 5.14 presents the loss spectra measured at -44 ºC, -80 ºC and -100 ºC after cooling the sample that was previously polymerized at different times (T_{pol} =70ºC) (see legend).

As a first observation, it is evident the vanishing of the α relaxation of the monomer in the right hand side of Figure 5.14.a at -44 ºC and Figure 5.14.b at -80 ºC, and the depletion of the β process (Figure 5.14.c at -100 ºC), that lefts over a longer time relatively to the glass transition process: while the α relaxation is no longer detected in the material polymerized for 20 minutes at 70 ºC, the β process is still observable after 20 and 24 minutes, only being absent after a total of 144 minutes of cycling polymerization.

Thus, the β process can act as a more sensitive probe to evaluate the polymerization progress comparing to the α process (see Table 5.7 further in the chapter, where the dielectric strength at -100 ºC for each t_{pol} are included). Both α and β processes are being extinguished without significant changes in their positions. This is pretty evident for the secondary process in Figure 5.14.c.

Concomitantly, the γ process increases its height which only becomes clear at the latest polymerization times (open stars relative to diamonds Figure 5.14.c); the same behavior is observed in $\tan\delta$, pulling apart thickness changes as the only origin of intensity raising (data not shown). Table 5.3 presents the dielectric strength values

at -100 ºC evidencing the increase of the γ_{pol} process intensity after polymerization (also shape parameters and activation energy is included in Table 5.3).

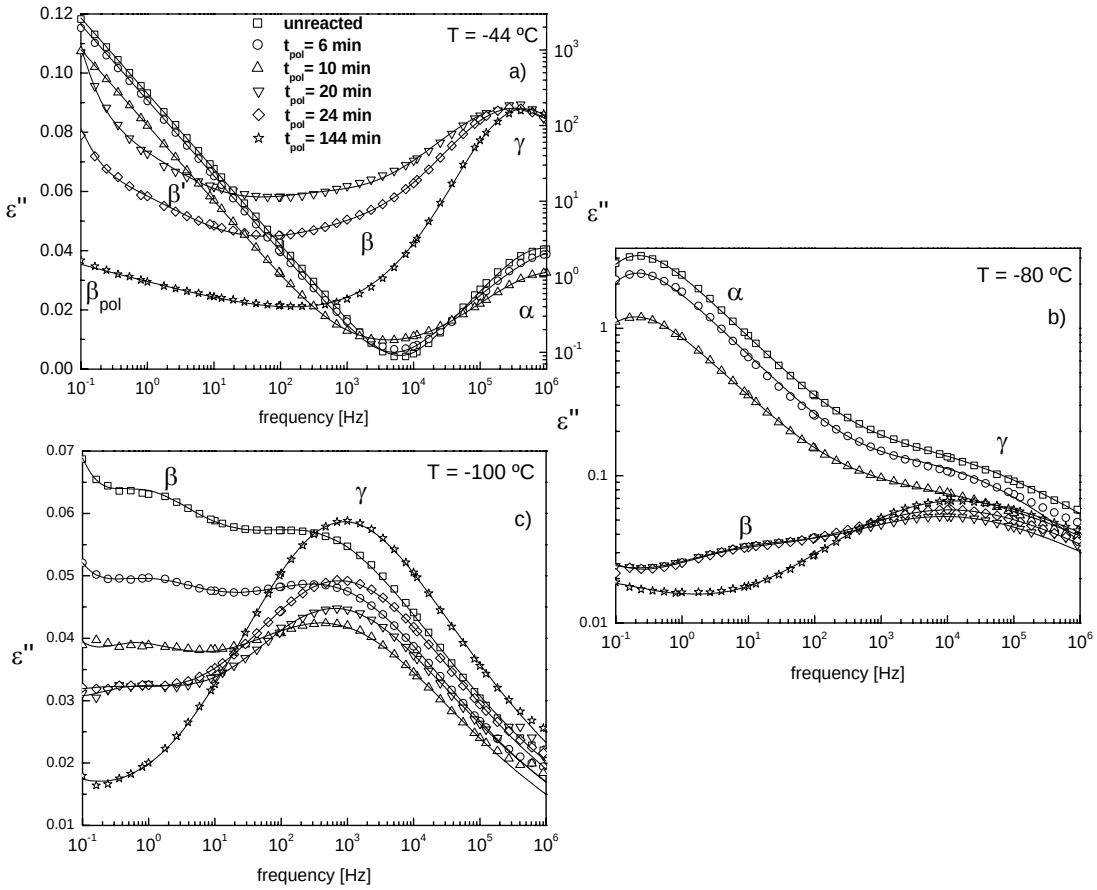

Figure 5.14 Loss curves collected after different polymerization times, t_{pol} (see legend inside) at T_{pol}=70ºC for poly-TeEGDMA at: a) -44 ºC, b) -80 ºC (ε'' in log scale) and c) -100 ºC; different ε'' scales are used due to the great intensity variation between the observed processes.

Meanwhile, a new relaxation process evolves after 20 minutes of polymerization, being noticeable in the low frequency side of the loss peaks detected after both 20 and 24 minutes: see Figure 5.14.a at -44 ºC where the individual relaxation process are depicted. This figure unequivocally demonstrate that this β' process, already commented in the previous sections, coexists with the monomer's β process discarding the hypothesis of being a consequence of a deviation to lower frequencies of the monomer's β relaxation. However it is never seen unambiguously as happened with β' process detected in the systems polymerized 2.5 h at 70 ºC

(samples T_{pol} 70ºC), being the reason why no fitting parameters concerning this process are given.

	$\Delta\varepsilon$ T = -100 ºC	α_{HN}	β_{HN}	E_a [kJ.mol^{-1}]	τ_0 [s]
Unreacted (t_{pol}=0min)	0.293	0.75→0.35 -120 →-86 ºC	0.45→0.86 -120 →-86 ºC	32±1	(4±2)x10^{-11}
t_{pol}=6min	0.259	0.71→0.31 -120→-84 ºC	0.48→0.90 -120→-84 ºC	33±2	(4±2)x10^{-11}
t_{pol}=10min	0.112	0.51±0.07	1	40±1	(3±1)x10^{-13}
t_{pol}=20min	0.101	0.49±0.05	0.99±0.01	45±1	(1.5±0.8)x10^{-14}
t_{pol}=24min	0.132	0.43±0.04	1	49±1	(1.4±0.4)x10^{-16}

Table 5.7 HN shape parameters and $\Delta\varepsilon$ at -100ºC for the β process for TeEGDMA polymerized at different times, t_{pol}. Activation energies and τ_0 are calculated from the Arrhenius fit.

A comparison of the results obtained at the different polymerization times studied are represented in Figure 5.15, where it is clearly visible how the main relaxation process disappear after 10 min and the relaxation behavior after 144 min presents similar profile to that found in the poly-TeEGDMA fully polymerized (T_{pol} 70+120ºC), *i.e.* the γ_{pol} and β_{pol} relaxations. Data concerning the β_{pol} relaxation are presented in Table 5.6.

The relaxation map in Figure 5.16 nicely illustrates the dynamical changes that undergo during polymerization.

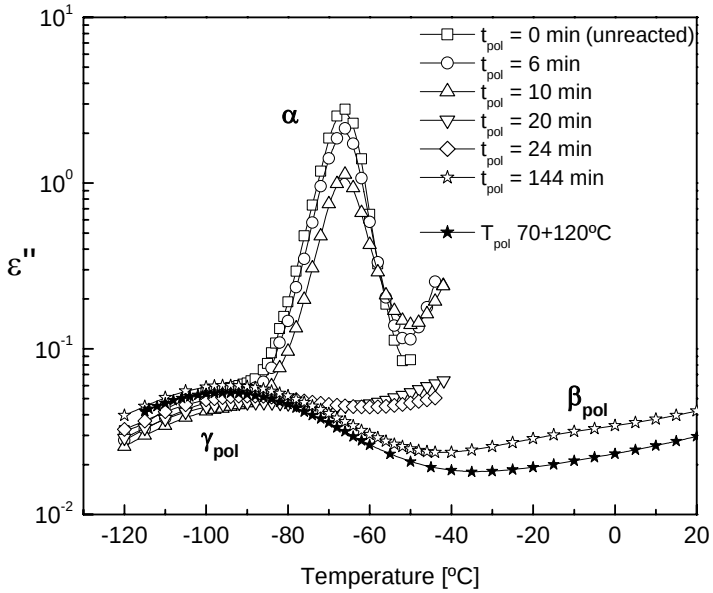

Figure 5.15 Isochronal plot of ε'' (log scale) at 1 kHz for TeEGDMA/AIBN at different polymerization times (t_{pol}). Data corresponding to the totally polymerized poly-TeEGDMA are included (T_{pol} 70+120ºC).

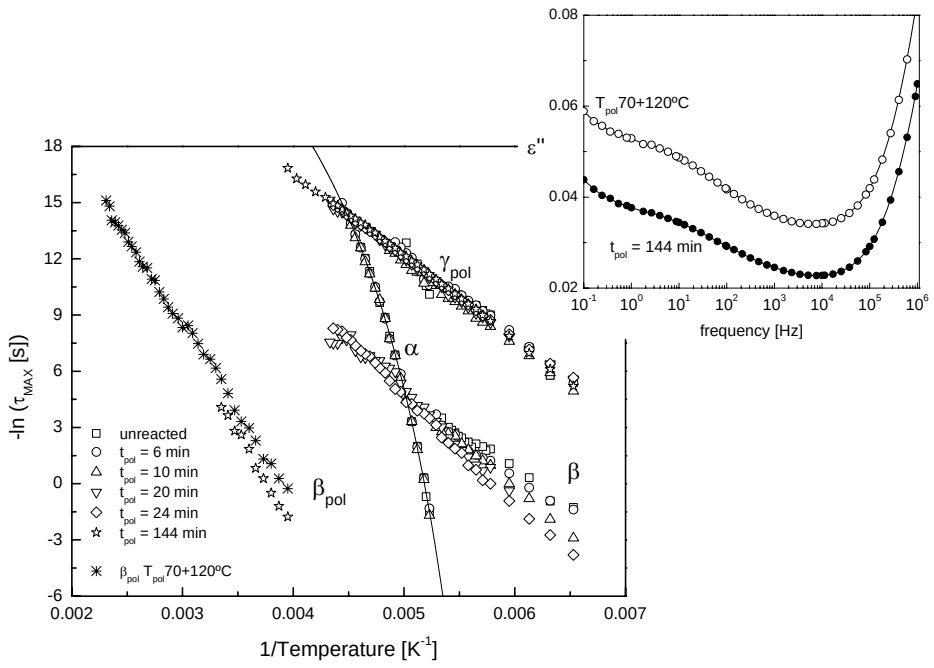

Figure 5.16 Relaxation map for TeEGDMA/AIBN polymerized by thermal cycling (see legend). The temperature dependence of the relaxation time of β_{pol} process detected in sample T_{pol} 70+120ºC (asterisks) is included. The inset shows the similarity between loss peaks for the final cycled sample (t_{pol}=144 min) and for the sample T_{pol} 70+120ºC.

In what concerns the α relaxation process of the unreacted TeEGDMA monomer, it is evident that keeps the same location in the earlier states of polymerization as can be seen by the overlap of the respective relaxation times: squares for monomer, circles and triangles after, respectively 6 and 10 minutes of polymerization, in Figure 5.16; solid line is the correspondent VFTH fitting (respective data included in Table 5.8). Nevertheless care must be taken in comparing this behavior with DEGDMA (and also TrEGDMA) where a small shift to longer times was observed since the VFTH plots were obtained for data collected prior and after a much longer polymerization time (2.5 hours).

Both γ and β processes maintain their positions upon TeEGDMA polymerization but largely extended due to the disappearance of the α process that allowed detection in an increased temperature range.

The activation plot of the β_{pol} process after 144 min superimposes that of the sample T_{pol} 70+120ºC (stars *vs.* asterisks in Figure 5.16).

t_{pol} [min]	τ_0 [s]	B [K]	T_0 [K]	T_g [K] (τ = 100 s)	$E_a(T_g)$ [kJ.mol^{-1}]	m	α_{HN}	β_{HN}
0	3.9x10^{-15}	1304.3	153.6	187.8	321	89	0.93±0.03	0.45±0.05
6	1.3x10^{-15}	1432.1	150.9	187.8	310	86	0.91±0.04	0.47±0.04
10	7.1x10^{-15}	1253.1	154.5	188.2	325	90	0.89±0.06	0.46±0.08

Table 5.8 VFTH parameters for the α process for TeEGDMA/AIBN polymerized at different times, t_{pol}. Glass transition temperature, activation energies calculated at T_g, fragility index and HN shape parameters are also included.

5.5 Discussion

Polymerization of TrEGDMA produces a polymer network with high cross-linking density and as a consequence with a limited ability to absorb a solvent. When polymerization takes place from the liquid monomer, at intermediate conversion degrees, the amount of liquid monomer that the polymer network is able to absorb is

smaller than the remaining unreacted solvent. Temperature modulated DSC studies (Chapter 4 and ref. 20) on the polymerization kinetics of TrEGDMA proved that phase separation occurs, *i.e.* one phase consisting of a monomer swollen highly cross-linked polymer network and the other one of unreacted liquid monomer. This conclusion was reached due to the observation that the glass transition of the system was much higher than expected for a homogeneous mixture of the growing polymer network and the remaining monomer.

Phase separation has as consequence on the one hand, that the main, α, dielectric relaxation of the monomer is observed at the same location as in the pure monomer, independently of the polymerization time (or conversion), although with decreasing relaxation strength since the number of monomer molecules decreases upon polymerization. On the other hand, the main dielectric relaxation corresponding to the swollen polymer network would appear at quite high temperatures from the first instant of polymerization, because the amount of liquid monomer that plasticizes it is limited. In fact the glass transition temperature observed by TMDSC was never below 50 ºC [20]. In addition to the monomer main relaxation, the dielectric relaxation spectrum of the system at intermediate conversion degrees, shows the secondary relaxations of the remaining monomer, β and γ and the secondary γ_{pol} relaxation of the polymer.

A new relaxation process that we have called β' appears only at intermediate stages of the polymerization process. After full conversion, a secondary relaxation process of the polymer network, β_{pol}, is detected. The different processes will be taken now for discussion.

5.5.1 Relaxation process already detected in the bulk monomers

From Chapter 3, it was demonstrated as the γ process was independent of the monomer's type and the β relaxation shifted downwards in frequency with increasing the size of the ethylene glycol moiety. Additionally, the polymerization studied in this chapter, leaves to extinction the β process and the γ keeps almost unaffected in the three polymers studied.

This fact is determinant in the assignment of the molecular mobility that is in the origin of such process owing the dipole types. The dipolar groups carried by the monomers can be of two kinds: *i*) the ones that lie in the ethylene glycol moieties and *ii*) that residing in the carboxylic groups. Upon polymerization, covalent bonds are formed between the methylene carbons adjacent to the *COOR* group leading to the chain growing.

Thus, the mobility associated with the rotation of the carboxylic groups should be more affected by polymerization than local twisting motions in the ethylene groups; moreover, the hindered rotations even in the monomer should have a higher relaxation time relatively to the twisting of $C-O-C$ bonds. Consequently, the process located at the highest frequencies, γ process, should be originated by dipolar motions of ethylene glycol moieties, while the β process must be attributed to the carboxylic groups (Figure 5.17).

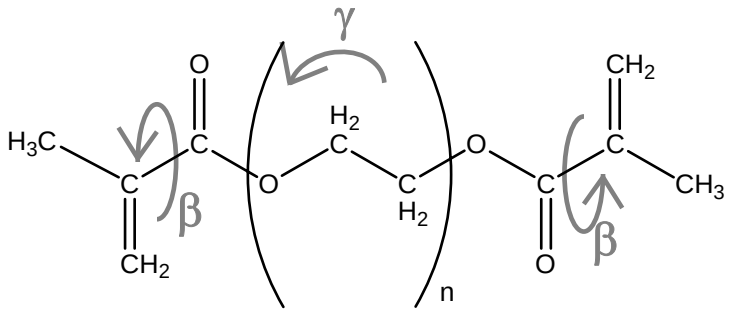

Figure 5.17 Chemical structure of n-ethylene glycol dimethacrylate monomer. The molecular motions that originate the secondary relaxation process, β and γ, are illustrated.

The fact that all the processes detected in monomers do not deviate continuously to lower frequencies as polymerization progresses, indicates that the mobility of the growing polymer does not derive from the monomer's mobility. The late simply depletes due to the number of dipoles that becomes gradually inactive owing to polymerization.

From the results discussed in section 5.3, where two samples of TrEGDMA were polymerized at 70 ºC and 80 ºC, an important feature was found: while the γ secondary process as already mentioned maintains its location independently of the polymerization degree (and also the monomer), the glass transition process of the left

unreacted monomer slightly deviates to lower frequencies/longer times in the partially polymerized mixtures relatively to the fresh mixture, with no significant changes in location between the two mixtures partially polymerized at 70 and 80 ºC (this fact was also detected in polymerization of DEGDMA/AIBN). Therefore, the merging of both α and γ process of the monomer that persists unreacted, changes upon partial polymerization.

This is a different splitting scenario relatively to the activation plots drawn by Parthun and Johari [22] for the isothermal cure process in thermosets taken at different cure times. The α and the secondary process plots are distinct for each cure time merging at the same frequency (10^7 Hz) and converging to the same pre-exponential factor of 10^{12} Hz corresponding to the vibrational frequency of atoms. That scenario implies a different location for the secondary process with the evolution of cure, by maintaining the same activation energy. In the present work, the secondary relaxation process is almost independent from the environment that is changing upon polymerization, preserving both location and activation energy. In what concerns the α process, we are monitoring the evolution of the monomer's glass transition rather than the evolution of the newly formed polymer's glass transition, therefore, being less sensitive to the structural changes upon polymerization as found for the thermoset that is being formed in the work of Parthun and Johari.

Comparing the three monomers, the rate of conversion increases with the increase of ethylene glycol moiety as revealed by a greater depletion of the α process at the same polymerization time (2.5 hours at 70 ºC), going from TeEGDMA where this process vanishes after 2.5 h at 70 ºC, to TrEGDMA and DEGDMA where it is still observed after the same polymerization time. Even the poly-TrEGDMA polymerized at 80 ºC during 2.5 h continues showing the α process, and in coherence with results of Chapter 4, this temperature leads to a network with less unreacted monomer at the end of the reaction.

The increase in intensity of the remaining γ process, the one detected in bulk monomers that persists after polymerization, can be analyzed in terms of the Fröhlich-Kirkwood equation (19, page 8 in ref. 21)

$$\varepsilon_s - \varepsilon_\infty = \frac{\mu_0^2 g \, N/V \, \varepsilon_s (\varepsilon_\infty + 2)^2}{3\varepsilon_0 k \, T 3(2\varepsilon_s + \varepsilon_\infty)} \qquad \text{Equation 5.2}$$

μ_0 is the dipolar moment of the isolated dipole, g takes into account the dipole-dipole correlation, ε_s and ε_∞ are the limits of the real part of the dielectric permittivity at low and high frequencies respectively, N/V is the number of dipoles per unit of volume and k is Boltzmann constant. Equation 5.2 can be transformed in

$$\frac{\mu_0^2 g \, N/V}{3\varepsilon_0} = \frac{3(2\varepsilon_s + \varepsilon_\infty)(\varepsilon_s - \varepsilon_\infty)}{\varepsilon_s (\varepsilon_\infty + 2)^2} k \, T = F(T) \qquad \text{Equation 5.3}$$

where the left hand side of the equation can be considered a measure of the reorientation ability of the permanent dipole moments responsible for the relaxation. The $F(T)$ function calculated for γ relaxation at any temperature between 150 K (-123 ºC) and 190 K (-83 ºC) for the TeEGDMA/AIBN mixture cyclically polymerized, continuously increases with increasing polymerization time, its value for the highest polymerization time is around a 36% higher than that calculated in the γ relaxation process of the monomer as can be seen in Figure 5.18.

At least a part of this increase comes from the increase in the density of the polymer with respect to monomer, which implies the same increase in the number of dipoles per unit volume or N/V in Equation 5.3. The rest of the increase of the relaxation strength could be due to a preferential alignment of the dipoles with crosslink that determines a more ordered structure relatively to states of lower conversion, in this polymer.

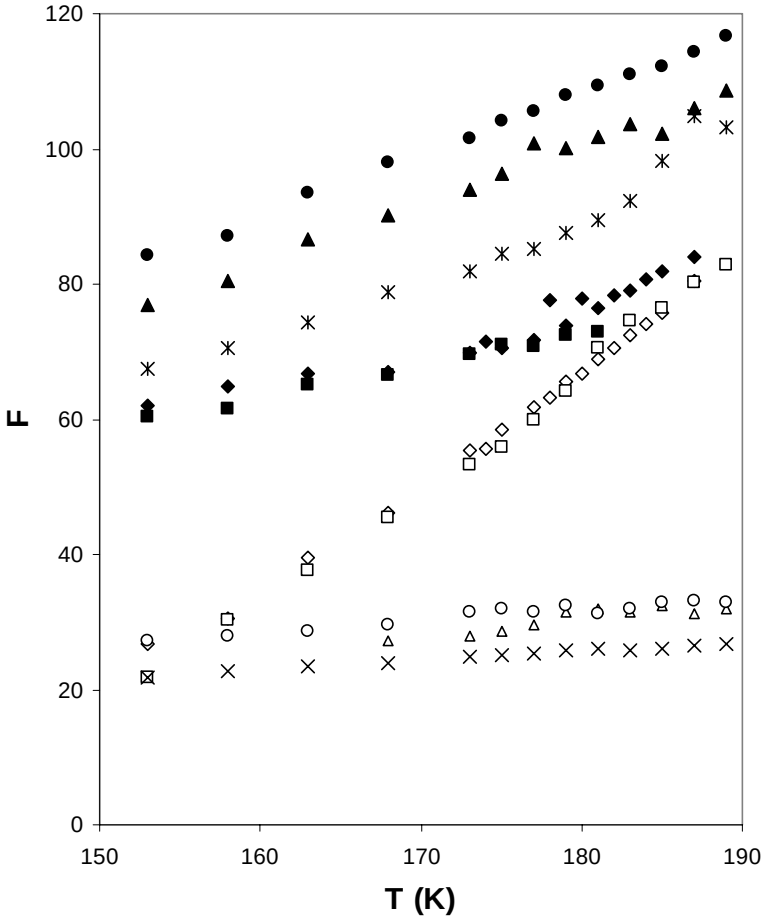

Figure 5.18 Plot of $F(T)$ against temperature in accordance with Equation 5.3 (see text) for the β and γ relaxations measured after different polymerization times t_{pol}, for TeEGDMA cyclically polymerized. β relaxation: (◊) unreacted (t_{pol} = 0 min), (□) t_{pol} = 6 min, (x) t_{pol} = 10 min, (Δ) t_{pol} = 20 min, (○) t_{pol} = 24 min; γ relaxation: (♦)unreacted, (■) t_{pol} = 6 min, (*) t_{pol} = 10 min, (▲) t_{pol} = 20 min, (●) t_{pol} = 24 min.

The $F(T)$ function (Equation 5.3) calculated for the monomer β relaxation suddenly drops during polymerization for reaction times between 6 and 10 minutes and then remains constant with a very small value (see Figure 5.18). This final contribution can be ascribed to a small amount of unreacted monomer when polymerization takes place at 70 ºC.

5.5.2 Molecular mobility in intermediate stages of polymerization and the full polymerized network

As explained in the first paragraphs of this discussion, only secondary relaxations can be observed in the polymer networks. The γ_{pol} process, the one observed at the lowest temperatures, comes out exactly in the same position than in the monomers, being also independent on the length of the n-ethylene glycol chain. It appears that the restriction imposed by the chain connectivity does not influence the local motions in this group. This is not surprising since the γ relaxation emerges in a temperature range below which the carboxyl groups, that are in the origin of the β relaxation, become active. Thus, the mobility of n-ethylene glycol groups, in the monomer is similar to that in the polymer network.

To assign the molecular origin of the β_{pol} process it is useful to bear in mind the type of polymer that is forming during polymerization. The covalent bonds establish adjacent to the carboxylic units in such a way that the main chain of the polymer under formation is similar to a poly(methyl methacrylate), with the ethylene glycol groups connecting different main chains (reference 19 presents a scheme of the growing of a similar polymer). Thus, the process observed at full conversion could correspond to the β relaxation observed in the lower poly(alkyl methacrylates), that is attributed in PMMA and PEMA, below but near T_g, to π flips of the carboxyl group (see Scheme 5.2) coupled to restricted rearrangements of the main chain (small angle $\approx$20º rocking motion of the main chain) [23,24].

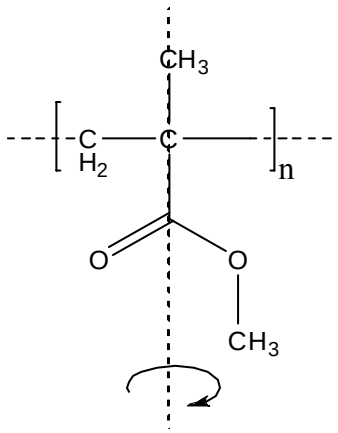

Scheme 5.2 Rotations of 180º around the $C-C$ bond connecting the side group to the backbone that is in the origin of the β relaxation of PMMA.

Figure 5.12 compares the isochronal plots of dielectric loss at 1 Hz of poly-TeEGDMA taken from the isothermal measurements obtained after polymerization at 120 ºC (dark stars), with the β relaxation of PMMA [25] (gray stars), being evident that both processes have exactly the same location (data relative to β process of PMMA is plotted in the right y-axis); also the activation energy for the different polymers studied, which is around 80 kJ.mol^{-1} (Table 5.6), is very similar to the values found for the lower members of the series of poly(n-alkyl methacrylates) (74 kJ.mol^{-1} [26], from 79 to 88 kJ.mol^{-1} by different authors cited in reference [27], 84 kJ.mol^{-1} [28] and 80 kJ.mol^{-1} [29]).

As seen before, the secondary β relaxation of the monomer does not shift in either the temperature or frequency axis as the liquid is polymerized, only its height decreases. So, the secondary relaxation process observed for the polymerized state neither involves the same modes of motion as the α relaxation of the respective unreacted monomer, nor correspond to the same sub-T_g relaxation observed for the molecular glass. This has been confirmed in several studies [30-32] involving different molecular substances forming either linear or network polymerized states. In our case, although the *COOR* dipole is involved in the secondary relaxation that emerges in the final polymer, its mobility is different from the motion in the molecular liquid.

At intermediate stages of polymerization another process coexists with the monomer β relaxation here designated β'. It is difficult to get conclusions about the origin of this β' process, due to the lack of precise data about the temperature and conversion dependence of its relaxation time and intensity. However it can be argued that no dipolar origin for this relaxation can be expected either from monomer or from the polymer both coexisting in the intermediate states of the polymerization. Let us analyze separately these two possibilities:

(a) in what concerns the possibility of this process being originated by the own monomer, since it appears at temperatures above the monomer's α relaxation, it seems unreasonable to conceive a dipolar relaxation that would take place at such high temperatures;

(b) concerning the possibility of being originated by molecular motions in either polymer or oligomers formed at intermediates degrees of polymerization, it also seems difficult to accept that it may arise from a main α relaxation or a secondary relaxation. Nevertheless, a α relaxation is due to cooperative conformational motions and its presence in the dielectric relaxation spectrum needs the existence of nanodomains (the length of cooperativity at the glass transition temperature is in ten orders of magnitude of some nanometers or even few tens of nanometers [33, 34]. But free radical polymerization hardly can produce these aggregates since chain growth is much faster than the initiator decomposition, thus, the initiation of the propagation of the reaction rapidly produces high molecular weight chains or networks [35]. Therefore it is not expected to have a significant contribution of an eventual main relaxation process of oligomers. On the other hand, the main relaxation of the high molecular weight networks would produce a main α relaxation at high temperatures due to the phase separation already probed by DSC experiments (Chapter 4 and ref. 19).

The possibility of being a secondary process of the oligomers, *i.e.* to consider that β' has the same origin than the β_{pol} process, can be pulled apart due to two main reasons: *i*) due to the small amount of molecular groups that will originate a process hardly detected by DRS; *ii*) it will imply an abnormal shift to lower temperatures of the β_{pol} due to plasticization by unreacted monomer, nevertheless accordingly several studies reported in literature [36,37] the secondary relaxation processes are insignificantly influenced by the presence of residual monomer. The same process is detected in the different systems polymerized after 70 and 80 ºC, when no full conversion is reached and thus, some unreacted monomer still remain.

Consequently one can speculate that space charges can accumulate in the interfaces between the liquid monomer and the newly formed polymer, originating the well known interfacial polarization phenomenon, *i.e.* a MWS process, which disappears after full conversion.

5.6 Conclusions

The polymerization of di-, tri- and tetra-ethylene glycol dimethacrylates monomers was dielectrically characterized monitoring principally the changes induced in the molecular mobility of the residual monomer.

Upon polymerization, the α and β relaxations deplete, however the later takes longer to be extinguish thus acting as a more sensitive probe to evaluate conversion. Simultaneously, the secondary γ process detected in bulk monomers still almost unaffected. All the detected processes reveal no significant shifts in either frequency or temperature axis when the monomer undergoes polymerization.

The different behavior found for the two secondary process of monomers allows us to assign the molecular motion in the origin of each one: the process located at the highest frequencies, γ, should be originated by dipolar motions of ethylene glycol moieties, while the β process must be attributed to the rotation of the carboxylic groups that due to the formation of covalent bonds upon polymerization are strongly influenced.

At intermediate stages of polymerization a new process evolves that could be related to space charge motions in the monomer/polymer mixture. The polymer network present, in addition to the γ_{pol} relaxation identical to the γ relaxation of the monomer, a β_{pol} relaxation with similar features to the β relaxation found in poly(n-alkyl methacrylates) originated by π flips of the carboxyl group coupled to restricted rearrangements of the main chain.

5.7 References

[1] J.E. Dietz, N.A. Peppas, Polymer 38 (1997) 3767-3781.

[2] K.S. Anseth, S.M. Newman, C.N. Bowman, Adv. Polym. Sci. 122 (1995) 177-217.

[3] "Radiation Curing in Polymer Science and Technology, Volume IV: Practical Aspects and Applications", J.P. Fouassier, J.F. Rabek, Elsevier, New York (1993).

[4] A.R. Brás, M.T. Viciosa, C. Rodrigues, C.J. Dias, M. Dionísio, J. Phys. Rev. E 73(6) (2006) 061709-061729 Part 1.

[5] M.T. Viciosa, C.M. Rodrigues, M. Dionísio, J. Non-Crystal. Solids 351 (2005) 14-22.

[6] M.T. Viciosa, A.R. Brás, M. Dionisio, J.L. Gómez Ribelles, Eur. Polym. J. (2007) in press.

[7] M.B.M. Mangion, G.P. Johari, J. Polym. Sci. Polym. Phys. 28 (1990) 1621-1639.

[8] M.B.M. Mangion, G.P. Johari, Macromolecules 23 (1990) 3687-3695.

[9] C. Cardelli, E. Tombari, J.P. Johari, J. Phys. Chem. B 105(44) (2001) 11035-11043.

[10] K. Venkateshan, G.P. Johari, J. Chem. Phys. B 108(39) (2004) 15049-15056.

[11] G. Williams, "Keynote Lectures in Selected Topics of Polymer Science", Eds. E. Riande, Instituto de Ciencia y Tecnologia de Polímeros, CSIC, Madrid (1995).

[12] M. Beiner, K.L. Ngai, Macromolecules 38 (2005) 7033-7042.

[13] M.B.M. Mangion, G.P. Johari, J. Polym. Sci. B 29 (1991) 437-449.

[14] D.A. Wasylyshyn, G.P. Johari, E. Tombari, G. Salvetti, Chem. Phys. 223 (1997) 313-322.

[15] I.K. Smith, S.R. Andrews, G. Williams, P.A. Holmes, J. Mater. Chem. 7 (1997) 203-209.

[16] B. Fitz B, S. Andjelić, J. Mijović, Macromolecules 30 (1997) 5227-5238.

[17] S. Havriliak, S. Negami, Polymer 8 (1967) 161-210.

[18] H. Vogel, Phys. Z. 22 (1921) 645; G. S. Fulcher, J. Am. Chem. Soc. 8 (1925) 339; G.Tammann, W. Hesse Z. Anorg. Allg. Chem. 156 (1926) 245.

[19] M.T. Viciosa, N. Rouzé, M. Dionísio, J.L. Gómez Ribelles, Eur. Polymer J. 43(4) (2007) 1516-1529.

[20] M.T. Viciosa, H.J. Quiles, M. Dionísio, J.L. Gómez Ribelles, J. Therm. Anal. and Calor., on-line (2007).

[21] "Broadband dielectric spectroscopy", A. Schönhals, F. Kremer, Springer-Verlag, Berlin (2003).

[22] M.G. Parthun, G.P. Johari, Macromolecules 25 (1992) 3254-3265.

[23] S.C. Kuebler, D.J. Schaefer, C. Boeffel, U. Pawelzik, H.W. Spiess, Macromolecules 30 (1997) 6597-6609.

[24] A.S. Kulik, H.W. Beckham, K. Schmidt-Rohr, D. Radloff, U. Pawelzik, C. Boeffel, W. Spiess, Macromolecules 27 (1994) 4746-4745.

[25] S. Soreto, "O efeito da cadeia polimérica nos parâmetros da caracterização vítrea", Master Thesis, Universidade de Aveiro, Portugal (2006).

[26] F. Garwe, A. Schönhals, H. Lockwenz, M. Beiner, K. Schröter, E. Donth, Macromolecules 29 (1996) 247-253.

[27] N.G. McCrum, B.E. Read, G. Williams, "Anelastic and Dielectric Effect in Polymeric Solids", Dover Publications, New York (1967), (reprinted 1991).

[28] M. Dionísio, J.J. Moura-Ramos, Polymer 35(8) (1994) 1705-1713.

[29] J.L. Gómez Ribelles, R.J. Díaz Calleja, J. Polym. Sci. Polym. Phys. Ed. 23 (1985) 1297-1307.

[30] M. Cassettari, G. Salvetti, E. Tombari, S. Veronesi, G.P. Johari, J. Mol. Liq. 56 (1993) 141-156.

[31] M. Cassettari, G. Salvetti, E. Tombari, S. Veronesi, G.P. Johari, J. Non-Cryst. Solids 172-174 (1994) 554-561.

[32] M.G. Parthurn, G.P. Johari, J. Chem. Phys 103(17) (1995) 7611-7617.

[33] E. Donth, "Relaxation and Thermodynamics in Polymers, Glass Transition", Berlin, Akademie Verlag (1992).

[34] J.L. Gómez Ribelles, A. Vidaurre, J.M.G. Cowie, R. Ferguson, S. Harris, I.J. McEwen, Polymer 40(1) (1998) 183-192.

[35] G. Odian, "Principles of Polymerization", Wiley (1991).

[36] A. Dubault, L. Bokobza, E. Gandin, J.L. Halary, Polym. Int. 52 (2003) 1108-1118.

[37] J.L. Ribelles, R. Díaz Calleja, Polym. Eng. and Science 24(15) (1984) 1202-1204.

CHAPTER 6 TrEGDMA/MA COPOLYMERS

6.1 Introduction

It is well-known that the properties of a polymeric material can be tailored by the combination of more soft with more rigid constituents. For instances, a cross-linked material can be softened combining with a monofunctional constituent (oppositely, a monomer that polymerizes linearly can be hardened by mixing with a polifunctional monomer that reticulates upon polymerization). That is the case of tri-ethyleneglycol dimetacrylate (TrEGDMA), studied in the present work which forms a dense network when polymerizing due to its bifunctionality, having glass transition temperatures of the order of 429 K (estimated from the best fit of calorimetric data in this work). On the other side, methyl acrylate, a monofunctional monomer, forms a linear chain upon polymerization, with a much lower glass transition temperature: 278 K [1], here estimated as 281 K (dielectric spectroscopy) and 284 K, calorimetrically. Thus, the wide temperature range that separates the glass state for every homopolymer, will allow, by mixing different proportions of each monomer, the formation of final products with significantly different mobility/glass transition temperatures. These changes in the physical properties of the polymers can be much appropriated for several applications; this is the case of polymer dispersed liquid crystals, where the combination of a cross-linker with a linear component can allow the formation of bigger domains to allocate the liquid crystal enhancing the electro-optical response [2-4].

It is well established that cross-linking increases the glass transition temperature of polymers [4-7] shifting the α relaxation to higher temperatures. Concomitantly, a lengthening of the temperature interval in which the glass transition occurs as cross-linking density increases, as also been reported [8-11] attributed to a heterogeneity increase where the macroscopic detected transition corresponds to the superposition of transitions that occur in different nanometric domains. Respectively to the monomers used in our work, the influence of cross links on the conformational mobility of PMA chain segments has already study by dielectric relaxation spectroscopy using ethyleneglycol dimethacrylate as cross-linking agent [10]. It was observed a broadening of the dielectric α relaxation spectrum with increasing cross-linking density, rationalized in terms of large and small-scale movements, accompanied by a shift to higher temperatures and a decrease of the dielectric strength.

The aim of this chapter, where MA/TrEGDMA copolymers with different composition ratios in the range 100/0 to 0/100 prepared by photochemical initiation are studied, is to investigate how the neat polymers dynamics are influenced by the softer/harder component (these results have been published in ref. 12). Thus, dielectric relaxation spectroscopy was used to monitor molecular mobility covering a wide temperature range, allowing the investigation of both cooperative and localized relaxation processes that are influenced differently by the co-monomer. Additionally, the glass transition was further studied by differential scanning calorimetry.

6.2 Experimental conditions

6.2.1 Sample preparation

Two initial solutions were prepared, one for every monomer (MA and TrEGDMA), with 0.2 % in weight of benzoin (Scharlau 98% pure) that will act as photoinitiator. Different networks were produced varying the quantity of the monomers[1]. The samples will be designed as MAXX, XX being the weight of MA. Also the linear PMA and the crosslinked TrEGDMA homopolymers were included in this study. Thus, copolymers ranging from 100/0 to 0/100 were prepared changing the percentage of co-monomer in steps of 10%. Besides homopolymers only the 30, 50, 70 and 80% in MA were measured by dielectric relaxation spectroscopy. All the samples were measured by differential scanning calorimetry (DSC).

Polymerization took place for 24 hr under ultraviolet (UV) light at room temperature to ensure full conversion. A sheet of around half-milimiter thick was obtained. Low molecular weight substances (like unreacted monomer) were extracted from the network by boiling in ethanol for 24 hours and then drying under vacuum at 80 ºC during 48 hours.

[1] The author would like to thank Nicolas Rouzé (Erasmus student in Biomaterials Center (U.P.V.), for the sample preparation.

6.2.2 Dielectric and thermal conditions

The samples were gold coated in order to get a better contact between de sample and the electrodes. Dielectric spectra were collected in successive exothermic sweeps starting at -120 ºC and finalizing between 100 and 150 ºC. The real and imaginary parts of the complex permittivity were collected in the frequency range between 0.1 and 10^6 Hz.

The MA:TrEGDMA films were placed between two gold-plated electrodes (diameter 20 mm) of a parallel-plate capacitor included in the sample cell BDS 1200. The dielectric measurements, as usually, were carried out using the ALPHA-N analyzer.

Mettler DSC823 was used for differential scanning calorimetry experiments. The calibrations of the temperature and the heat flow were performed using indium and zinc standards. Measurements were performed upon heating, at a rate of 10 ºC.min^{-1}. Samples were previously annealed for two minutes at a temperature well above the glass transition in order to erase the effect of the previous thermal history and then cooled at 10 ºC.min^{-1} to -50 ºC.

6.3 Results

6.3.1 Dielectric Relaxation Spectroscopy

The dielectric relaxation spectra obtained for the different samples of MA:TrEGDMA copolymers are shown in Figure 6.1 where the homopolymers are also included; the spectra presented correspond only to isothermal measurements for every ten degrees between -120 and 100 ºC.

As a first observation it is notorious the difference in magnitude of the dielectric response of each of the homopolymers a) PMA *vs.* f) poly-TrEGDMA; please note that different scales are used in y axis. While the α relaxation process of PMA has a strong dielectric loss, the equivalent process in poly-TrEGDMA is not detected due to the cross-link that hard increases the network density, hindering the mobility of active dipoles.

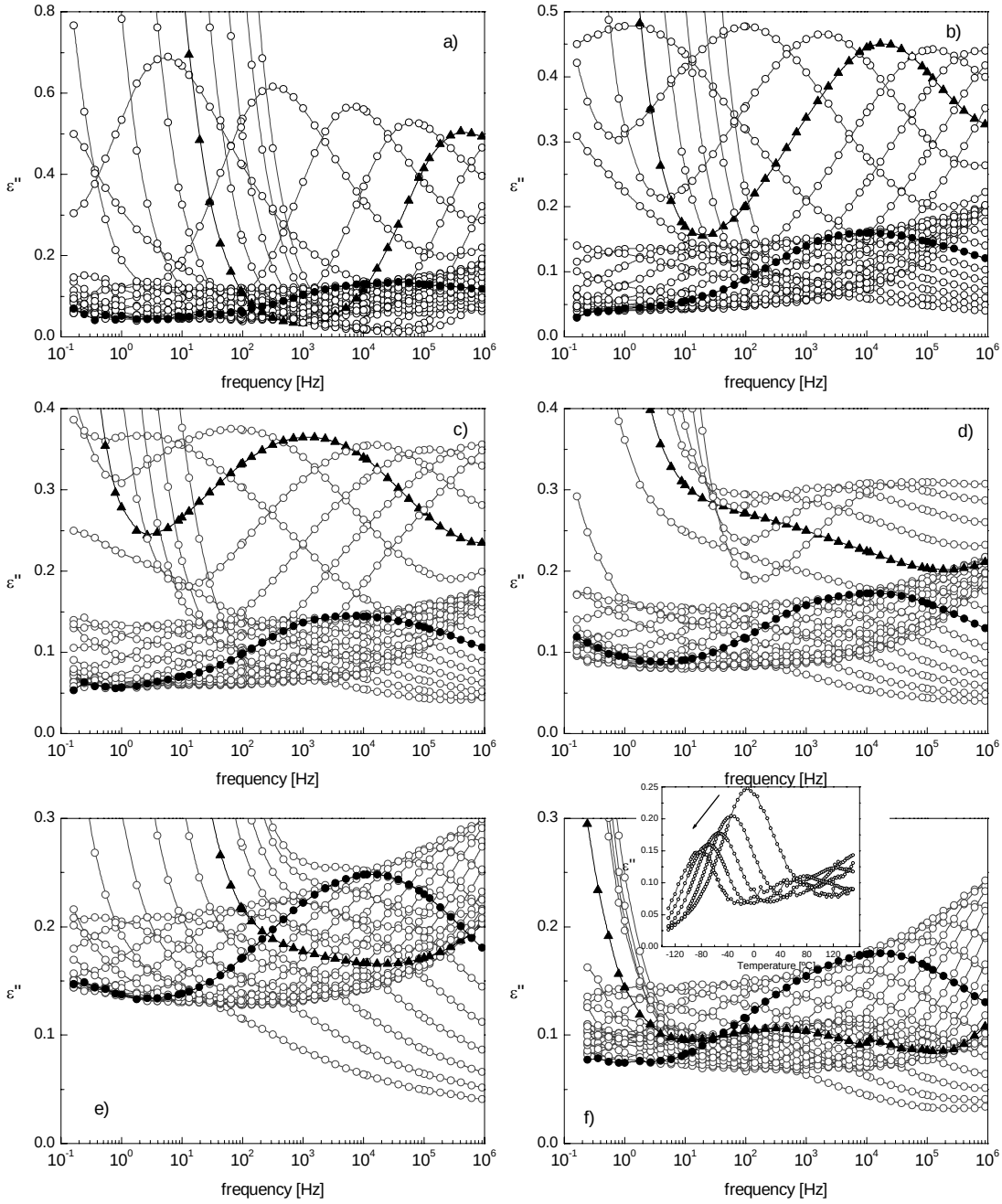

Figure 6.1 Loss curves in temperature region from -120 to 100 ºC every 10 degrees for a) PMA, b) MA80, c) MA70, d) MA50, e) MA30 and f) poly-TrEGDMA. Full symbols correspond to: circles, -60 ºC and triangles, 60 ºC. Inset in figure f) represents isochronal data taken from isothermal measurements for 1 MHz, 100, 10, 1 and 0.1 kHz in the arrow direction.

Secondly, as the proportion of TrEGDMA increases in the copolymer, *i.e.* increasing cross-linking, the loss peak deviates to lower frequencies; to help the

visualization of this effect each graph has the spectrum collected at 60 ºC presented in full triangles. The influence of the copolymerization with TrEGDMA is evident going from PMA (Figure 6.1.a) to MA50 (Figure 6.1.d), where the loss curve collected at 60 ºC is continuously shifted to lower frequencies while becomes broader. At MA70 the loss curve is much wider and at MA50 and MA30 the loss peak is masked by the conductivity. In homo poly-TrEGDMA, a different process is observed at this temperature, described later on.

In each graph the loss curve at -60 ºC is also differentiated (full circles in Figure 6.1) evidencing a secondary process associated with localized mobility. The influence of copolymerization in this secondary relaxation is less remarkable than for the α process; nevertheless there are some differences that can be better distinguished analyzing the isochronal plots of ε'' at fixed frequencies obtained from the isothermal measurements; the inset in Figure 6.1.f presents the isochronal plots for poly-TrEGDMA obtained at each decade of frequency (the arrows indicates increasing frequencies) and Figure 6.2 compares these plots at two different frequencies for all systems studied.

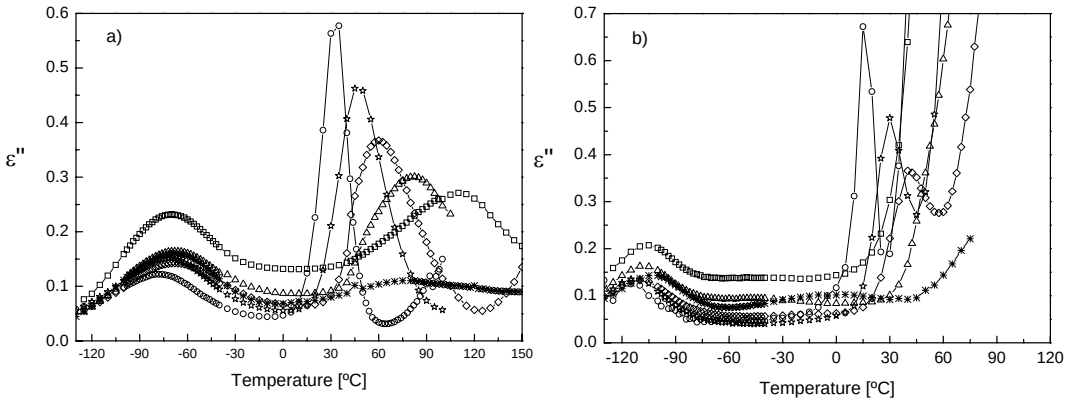

Figure 6.2 Temperature dependence of dielectric loss a) at 1 kHz and b) at 1Hz, taken from isothermal measurements: asterisks, poly-TrEGDMA; squares, MA30; triangles, MA50; diamonds, MA70; stars, MA80 and circles for PMA.

In Figure 6.2.a two temperature ranges are well distinguished, where dielectric processes are detected. At the lowest temperatures a secondary relaxation is observed while at higher temperatures the main relaxation or α process of PMA and copolymers is noticeable. The α process is more clearly seen at high frequencies

(1 kHz in Figure 6.2.a) due to a smaller influence of d.c. conductivity, while at low frequencies (1 Hz in Figure 6.2.b) the α peak is not observable for MA30 (squares) and MA50 (triangles) due to high conductivity (remember Figure 6.1.d and 1.e where high conductivity losses were observed at low frequencies). A close inspection of Figure 6.2.b shows two secondary relaxations appearing in all the copolymers and TrEGDMA. The one located at the lowest temperatures can be seen in all the copolymers and homopolymers at temperatures below -80 ºC. In the temperature range between -80 ºC and the α relaxation a broad and low intense process can be observed in TrEGDMA, MA30 and MA50, but the data treatment will show that it is present in the rest of copolymers as well. This process is also very well distinguished for pure poly-TrEGDMA at 1 kHz in Figure 6.2.a (asterisks), centered around 70 ºC, that should be not confused here with an α process.

The appearance of two secondary relaxations in homo poly-TrEGDMA, can be related to the presence of the permanent dipolar moments that reside in the carboxylic groups and in the ethylene glycol moieties. The rotation of the carboxylic groups must be responsible for the secondary relaxation appearing at the highest temperatures, in the same temperature range than the β relaxation of poly(alkyl methacrylates) [1,13,14], accordingly we will call it hereafter β. The relaxation appearing at lowest temperatures could be attributed to the local twisting motions of ethyleneglycol moieties as happens in the γ relaxation of poly(ethylene oxide) [1,15,16] and correspondingly we will label it γ relaxation of TrEGDMA. This relaxation is located at the same temperature range as the β relaxation of PMA, which corresponds to the hindered rotation of the carboxylic side group.

While the presence of TrEGDMA in the copolymers manifests mainly by a significant shift of the α process to higher temperatures with respect to that of PMA homopolymer and a considerable reduction of its intensity, the γ process shows almost no deviation in copolymers relative to homo poly-TrEGDMA. Interestingly, there is a significant intensity increase of this process in MA30; we will comment this further on. The β secondary relaxation shown by poly-TrEGDMA is shifted towards lower temperatures with the presence of MA segments in the copolymers. The process related with the rotation of carboxylic groups in homo PMA is detected at much lower temperatures, in the same temperature range that the γ process.

To allow for a clearer explanation, each process will be dielectrically characterized separately in the next sections.

6.3.1.1 γ relaxation process

This secondary process is located at the lowest temperatures in poly-TrEGDMA and copolymers (being absent in PMA). The respective loss curves can be fitted by the well-known empirical Havriliak-Negami [17] equation, described in detail in Chapter 1.

The characteristic relaxation times obtained from he HN fittings, τ_{HN}, were converted in frequencies of maximum loss, $2\pi f_{\max} = \tau_{\max}^{-1}$, according to Equation 6.1 [18].

$$2\pi f_{\max} = \frac{1}{\tau_{\max}} = \frac{1}{\tau_{HN}}\left[\sin\left(\frac{\alpha_{HN}\pi}{2+2\beta_{HN}}\right)\right]^{\frac{1}{\beta_{HN}}}\left[\sin\left(\frac{\alpha_{HN}\beta_{HN}\pi}{2+2\beta_{HN}}\right)\right]^{\frac{-1}{\beta_{HN}}} \qquad \text{Equation 6.1}$$

The activation energies estimated from the activation plots presented in Figure 6.3 are included in Table 6.1 showing a slight increase from MA80 (49 kJ.mol^{-1}) to neat poly-TrEGDMA (57 kJ.mol^{-1}).

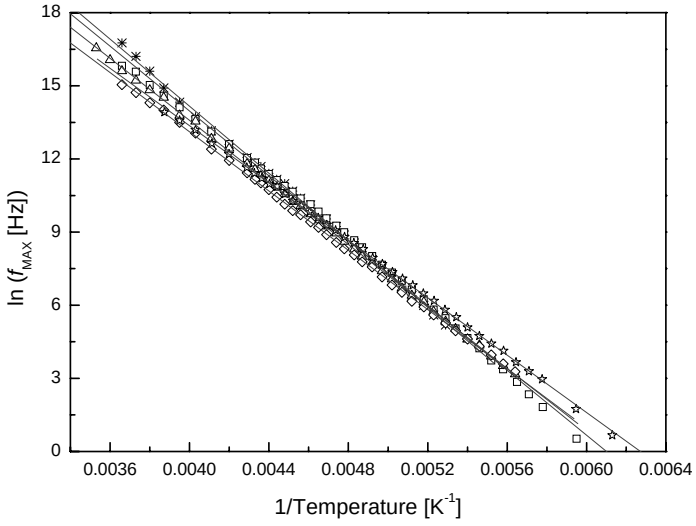

Figure 6.3 Temperature dependence of the relaxation times of γ process for: poly-TrEGDMA (asterisks), PMA30 (squares), PMA50 (triangles), PMA70 (diamonds) and PMA80 (stars).

In what concerns the shape parameters obtained from the HN fit for this secondary process, in the case of copolymers MA80, MA70 and MA50 there isn't significant temperature dependence; values of α_{HN} and $\alpha_{HN}\beta_{HN}$ are presented in Table 6.1 that also contains the dielectric strength thus obtained, which slightly increases with increasing temperature in these copolymers. Nevertheless, in the case of poly-TrEGDMA and MA30 copolymer, there are systematic dependence of α_{HN} and β_{HN} parameters with temperature, and the relaxation strength slightly decreases with increasing temperature.

	E_a (kJ.mol^{-1})	τ_0 (sec)	$\Delta\varepsilon$	α_{HN}	$\alpha_{HN}\beta_{HN}$
Poly-TrEGDMA	57±1	$(1.3\pm0.3)\times10^{-19}$	1.73 (-84ºC)-1.59 (-40ºC) 1.61 (-35ºC)-2.29 (0ºC)	0.31±0.08	0.22±0.03
MA30	55±1	$(3.9\pm0.8)\times10^{-19}$	2.46-2.00	0.31±0.09	0.25±0.06
MA50	53±1	$(1.9\pm0.1)\times10^{-18}$	1.68-1.97	0.39±0.06	0.13±0.01
MA70	50±1	$(9.2\pm0.9)\times10^{-18}$	1.45-1.57	0.44±0.04	0.12±0.01
MA80	49±1	$(1.5\pm0.1)\times10^{-17}$	1.48-1.83	0.50±0.02	0.11±0.01

Table 6.1 Activation energy, τ_0 and shape parameters from HN fitting for the γ relaxation. (Dielectric strength limit values obtained from isotherms collected respectively at the lowest and highest temperatures, except for poly-TrEGDMA)

The shape parameters temperature dependence means that for samples with lower TrEGDMA content it is possible to build a master curve in the Cole-Cole arc or ε'' plot, which is not possible for the high TrEGDMA content copolymers. Figure 6.4 shows the normalized Cole-Cole plots (the insets show the ε'' normalized curves) for a) homo poly-TrEGDMA, b) MA30 and c) MA70 for data measured at -70, -60 and -50 ºC. As expected, a single curve was obtained only for MA70 (Figure 6.4.c). For homo poly-TrEGDMA (Figure 6.4.a), the Cole-Cole plots become broader with the temperature decrease. In the inset, a master curve was built for each system containing the isothermal loss curves obtained at the same temperatures. The complete superposition was only achieved for MA70 and MA80 (not represented) confirmed by almost no variation on the shape parameters α_{HN} and β_{HN} (see Table 6.1**)** while the biggest deviation is verified for MA30 and homo poly-TrEGDMA. A close inspection of Figure 6.4.a shows that the Cole-Cole plot of homo poly-TrEGDMA at the lowest

temperatures, has a peculiar shape that could indicate the overlapping of two different processes. To clarify this point more work is needed.

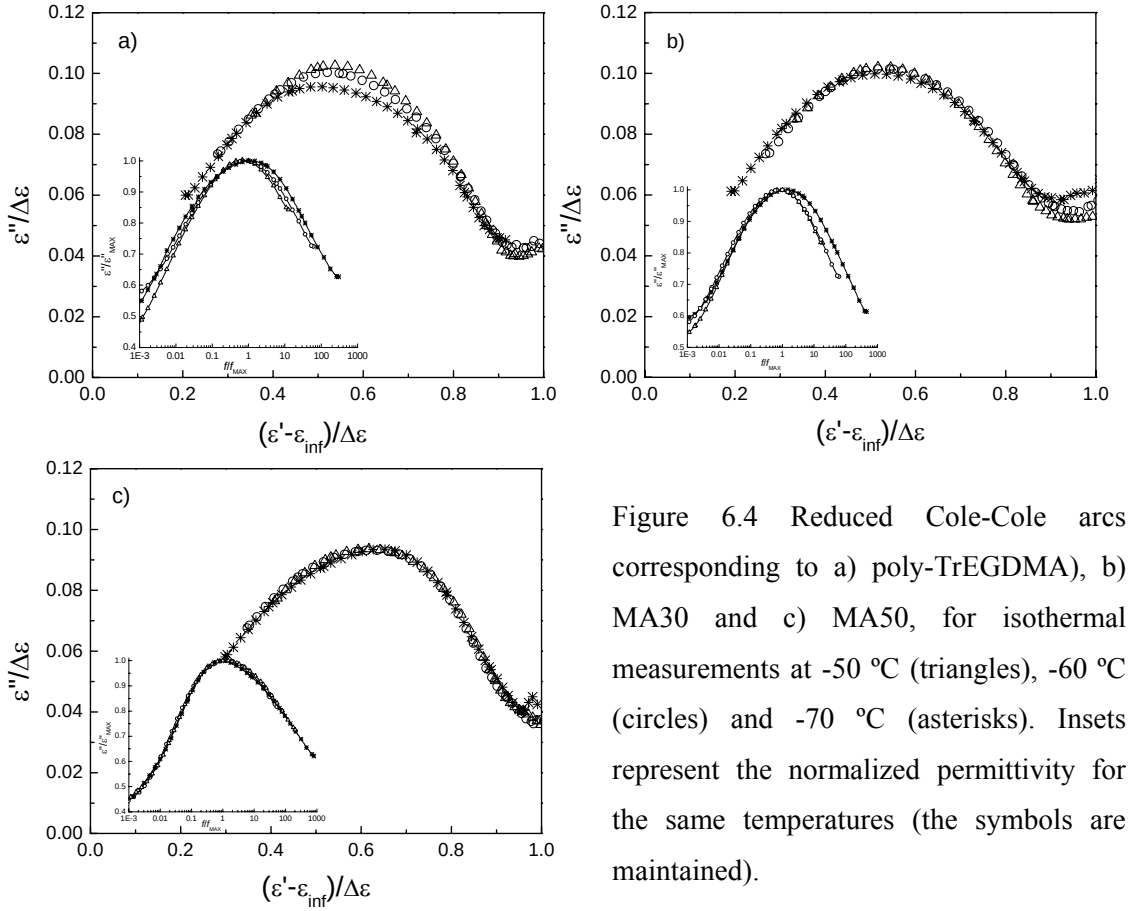

Figure 6.4 Reduced Cole-Cole arcs corresponding to a) poly-TrEGDMA), b) MA30 and c) MA50, for isothermal measurements at -50 ºC (triangles), -60 ºC (circles) and -70 ºC (asterisks). Insets represent the normalized permittivity for the same temperatures (the symbols are maintained).

6.3.1.2 β relaxation process

As previously mentioned, homo poly-TrEGDMA, MA30 and MA50 clearly exhibit a relaxation process at intermediate temperatures (remember Figure 6.2), attributed to rotations of the carboxylic group. This process is also felt in the fitting procedure of the remaining materials. The characteristic relaxation times obtained from the HN fits, were converted to f_{MAX} by using Equation 6.1. Figure 6.5 shows the resulting activation plot.

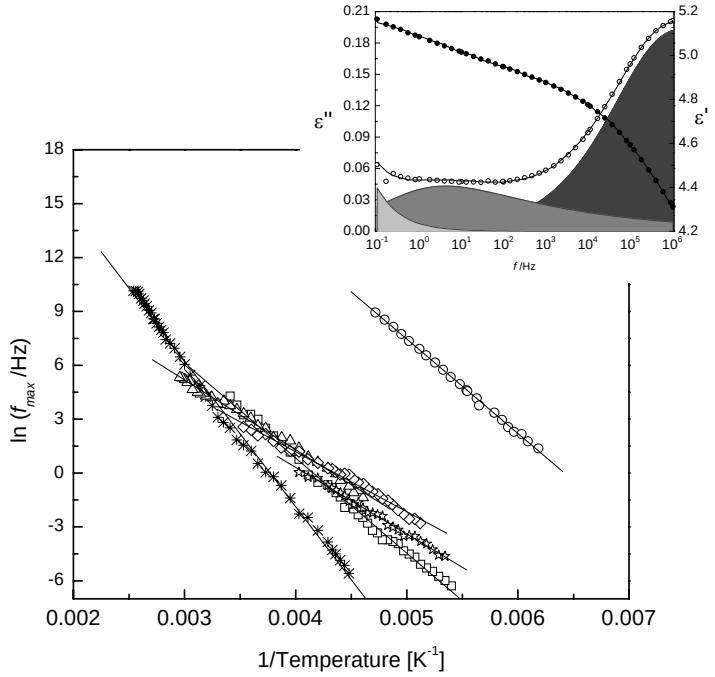

Figure 6.5 Arrhenius plot for the β relaxation: asterisks, poly-TrEGDMA, squares, MA30; triangles, MA50; diamonds, MA70; stars, MA80 and circles for PMA (data for the later obtained from isochronal data). The inset shows the individual and overall HN fitting functions for ε'' at -10 ºC for MA80 (left axis), and the corresponding ε' data and overall fitting (right axis).

The inset presents an isothermal spectrum at -10 ºC for MA80 with the three HN individual relaxation functions: the incoming α process at the lowest frequencies, the low-temperature secondary process at the highest frequencies and this third relaxation function at intermediate frequencies.

In what concerns neat PMA, the loss curves didn't allow for a reliable fit, thus its activation plot (circles in Figure 6.5) was built from the isochronal plots, *i.e.* the representation of $\log(f)$ *vs.* the reciprocal of the temperature at which the maximum of ε'' occurs, $1/T_{\max}$, that revealed to be an advantageous method allowing to distinguish between multiple processes [19].

Log(*f*) *vs.* $1/T_{\max}$ fits were performed using TableCurve 2D Version 5.01 Systat Software Inc., Richmond, California, USA.

Table 6.2 resumes the shape parameters, dielectric strength and activation energies obtained for this process. In the copolymers, the activation energy is more or

less independent of cross-linking except for the highest concentrations of TrEGDMA monomer where it increases together with an intensity increase quantified by the dielectric strength. The β process of homo PMA appears at temperatures much lower than TrEGDMA, emerging in the same temperature region where the γ relaxation is detected for the other systems, since the $-COOCH_3$ rotations do not suffer the hindrance imposed by either cross-link or the $\alpha - CH_3$ group present in poly-TrEGDMA.

	E_a [kJ.mol^{-1}]	τ_0 [s]	$\Delta\varepsilon$	α_{HN}	$\alpha_{HN}\beta_{HN}$
Poly-TrEGDMA	67±1	(8±2)×10^{-15}	0.94±0.22	0.33±0.05	0.23±0.05
MA30	44±1	(4±1)×10^{-11}	0.64—1.72	0.75—0.21	0.75—0.21
MA50	32±1	(8±1)×10^{-9}	0.32—2.94	0.49—0.20	0.47—0.19
MA70	28±1	(8±2)×10^{-8}	0.16—0.66	0.67—0.25	0.58—0.24
MA80	31±1	(4±1)×10^{-8}	0.25—0.50	0.32±0.11	0.26±0.09
PMA*	44±1	(4±1)×10^{-16}	---	---	---

Table 6.2 Activation energy, τ_0 and HN fitting parameters for the β relaxation. (Limits values obtained from isotherms collected respectively at the lowest and highest temperatures)

* Results obtained from $\log(f)$ *vs* $T_{\max}^{-1}$ procedure.

6.3.1.3 α relaxation process

Figure 6.6 shows the relaxation map for the main dielectric relaxation process. Since the α relaxation in some copolymers is highly influenced by conductivity (MA30 and MA50) the described activation plot, $\log(f)$ *vs.* $1/T_{\max}$ (open symbols in Figure 6.6) was adopted for all copolymers and homo PMA. For PMA (asterisks), MA80 (stars), MA70 (diamonds) and MA50 (triangles), the isothermal loss curves allow also the HN fit (remember Figure 6.1.a to 1.d). A term $-i\sigma/\omega^c\varepsilon_0$ was added to HN equation to take into account the d.c. conductivity contribution in the low frequency side for temperatures higher than around 50 ºC, (see Chapter 1 for an explanation).

For these systems the shape parameters were independent of the temperature, making possible to build a master curve for ε''. The values of the shape parameters are presented in Table 6.3.

The τ_{HN} values such obtained were converted in $f_{\max}$ according Equation 6.1, and are included in Figure 6.6 (full symbols) revealing excellent agreement. The main dielectric relaxation of neat poly-TrEGDMA was not observed in the studied temperature range.

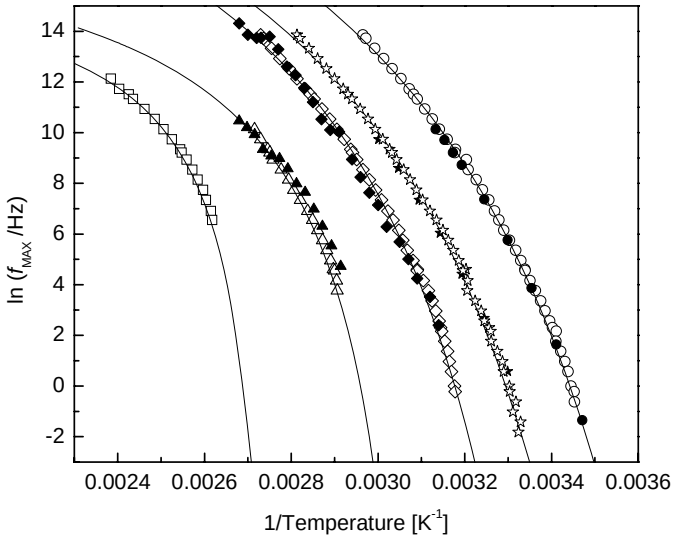

Figure 6.6 Temperature activation energy plots for α relaxation: squares, MA30; triangles, MA50; diamonds, MA70; stars, MA80 and circles for PMA. Full symbols obtained from HN procedure, and open symbols obtained from $\log(f)$ *vs* $T_{\max}^{-1}$. Solid lines correspond to linear fit for secondary and MWS relaxation and, to VFTH fit for data obtained from the last method proposed for the main relaxation (see text).

The activation plots in Figure 6.6 show the characteristic curvature of the temperature dependence of the relaxation times of cooperative processes, that obeys the Vogel-Fulcher-Tamman-Hesse (VFTH) law [20-22]. The pre-exponential factor, τ_0, B and T_0 are listed in Table 6.3. The resulting curves obtained from the parameters estimated from log(*f*) *vs.* $1/T_{\max}$ plots, are shown as solid lines in Figure 6.6. Also included in Table 6.3, are the glass transition temperatures, T_{gDRS}, estimated by

replacing τ = 100 s in VFTH equation [23] and the respective activation energies at T_{gDRS}, determined by Equation 1.2. Both T_{gDRS} and activation energy at T_{gDRS} decrease with increasing MA content.

	B [K]	τ_0 [sec]	T_0 [K]	T_{gDRS} [ºC]	$E_a(T_{gDRS})$ [kJ.mol^{-1}]	m	α_{HN} (m')	$\alpha_{HN}\beta_{HN}$ (n')	MWS $\Delta\varepsilon$
MA30	266 ±25	$(1.8\pm0.5)\times10^{-8}$	353 ±2	92.1	2102	301	---	---	27.4 (90ºC)
MA50	443 ±97	$(3\pm2)\times10^{-9}$	312 ±4	56.8	1199	190	---	---	14 (90ºC)
MA70	1047 ±77	$(3\pm1)\times10^{-12}$	272 ±2	32.1	716	122	0.31	0.18	0.32 (70ºC)
MA80	1262 ±79	$(7.0\pm0.1)\times10^{-13}$	255 ±2	20.3	602	107	0.41	0.22	0.97 (50ºC)
PMA	1322 ±73	$(1.7\pm0.7)\times10^{-13}$	242 ±2	7.7	574	107	0.79	0.24	---

Table 6.3 VFTH parameters calculated for α process from $\log(f)$ *vs* $T_{\max}^{-1}$ procedure; T_g obtained from substitution of $\tau = 100s$ in the VFTH equation, activation energy at T_g and fragility index, m. Also the shape parameters from HN fitting for the samples where this procedure was reliable are included. Finally, dielectric strength for MWS process at the indicated temperature is presented.

6.3.2 Differential Scanning Calorimetry

Figure 6.7 shows the DSC thermograms obtained after cooling the samples from equilibrium at a cooling rate of 10 ºC.min^{-1}. The glass transition shifts towards higher temperatures and broadens as the TrEGDMA content of the copolymer increases. The glass transition temperatures were determined as the temperature of the mid point of the rise of the heat capacity in the transition (presented later on Figure 6.10). It is worth noting that the temperature interval of the glass transition in the TrEGDMA copolymers arrives to be more than 50 ºC. It was not possible to distinguish the heat flow increment in the glass transition of pure TrEGDMA network.

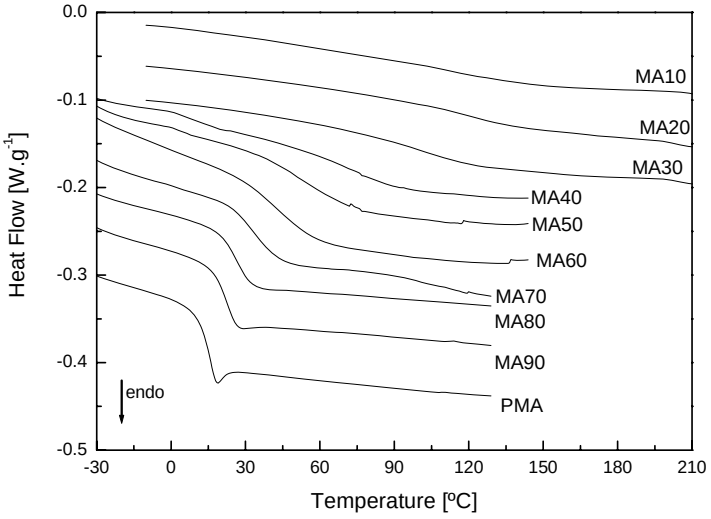

Figure 6.7 DSC heating curves obtained at 10 ºC.min^{-1} for all prepared mixtures except poly-TrEGDMA.

6.4 Discussion

6.4.1 Secondary relaxations

In what concerns homo PMA, it is well known from literature [10], that it presents only a sub-glass relaxation process, called β process, having an activation energy ranging from 38-59 kJ.mol^{-1} [1], in accordance with our results (44 kJ.mol^{-1}). This process is attributed to the rotation of the ester side groups [1].

The process with the same molecular origin in homo poly-TrEGDMA, is located at a much higher temperature due to the hindrance imposed by $\alpha - CH_3$ as in poly(n-alkyl methacrylates) [1]. These molecular motions are exemplified in Scheme 6.1.

In the copolymers, this β relaxation tends to approach the β relaxation of homo PMA, nevertheless highly influenced by TrEGDMA monomeric units as illustrated in Figure 6.5 where the activation plots of all copolymers are closer to homo poly-TrEGDMA comparing to PMA. The random succession of acrylate monomeric units among methacrylate monomers along the polymer chain, lowers the

energy barriers that opposes the rotation of the carboxylic side group in homo-TrEGDMA. Consequently the apparent activation energy measured in the β relaxation of TrEGDMA segments decreases with increasing MA contents up to MA50 copolymer although it remains constant for higher MA contents, as shown by the slopes of the linear plots of Figure 6.5 and the values listed in Table 6.2. On the other hand in all the copolymers only a peak appears in the temperature region of the β relaxation of PMA segments and γ relaxation of TrEGDMA (from -120 to -30 ºC at 1 kHz). It is reported that in random copolymers of PMA and poly(methyl methacrylate) [1] both β relaxation processes are detected and tend to approach each other. If this kind of behavior happens in the actual copolymers, that will indicate that the β process characteristic of PMA is perfectly merged on the γ process, since neither in ε'' plots or fitting procedure we felt the evidence of bimodal character.

In what concerns the γ process, it is related with the mobility of ethyleneglycol moieties thus, being absent in PMA (see Scheme 6.1). This process was characterized in Chapter 5 [24] in homo poly-TrEGDMA but with somewhat different results, namely a narrower spectrum was obtained and inferior activation energy estimated (36-39 kJ.mol^{-1}). The higher E_a value (57 kJ.mol^{-1}) in the photopolymerized material could be an indication of higher cross linking while a broader spectrum is related with a wider distribution of relaxation times due to different microenvironments that surround the relaxing units. Such density fluctuations occurs as a result of the cross-linking [25] formation kinetics that is faster in photo initiated polymerization relatively to thermal polymerization. The loss peak shape of this relaxation process seems to be dependent of the polymerization process as well. This behavior can be due to differences in the topology of the polymer network. This point deserves further attention with a systematic experimental study.

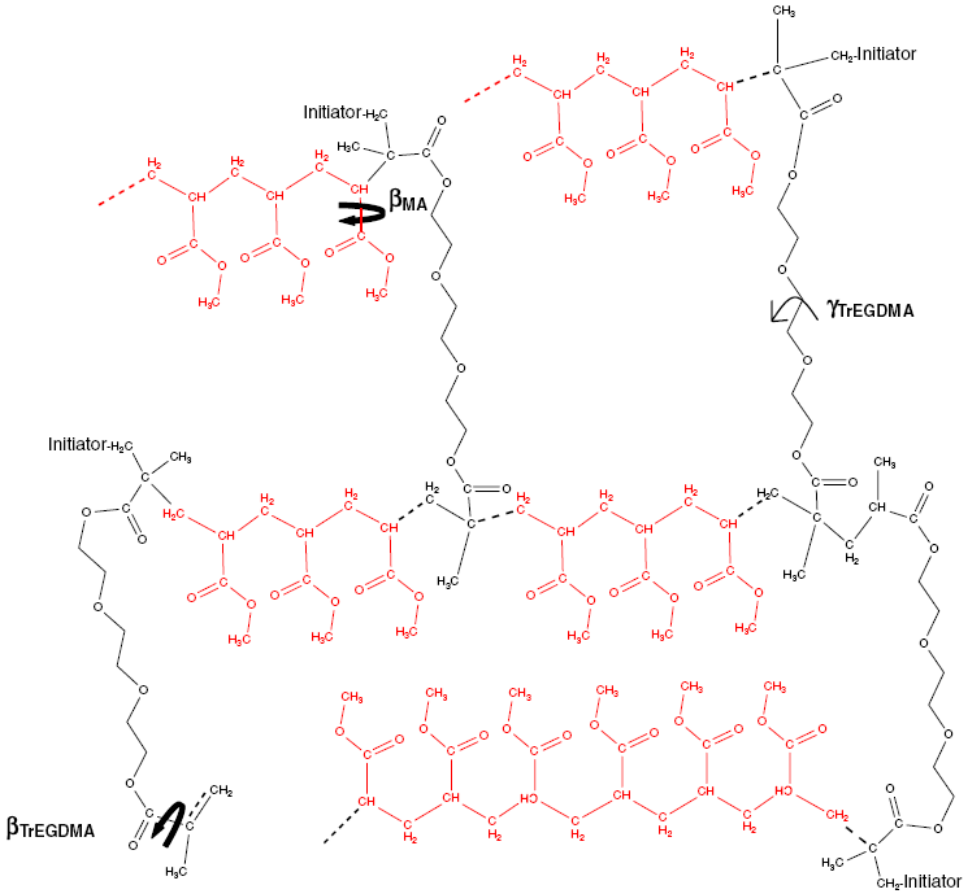

Scheme 6.1. Oversimplified structure of the network formed by MA (red) and TrEGDMA (black) monomers, evidencing the molecular motions that are in the origin of sub-glass relaxations [12].

The intensity of this secondary process decreases with MA increase but passes through a maximum in the MA30 copolymer (see $\Delta\varepsilon$ in Table 6.1) which could represent a join effect of both high TrEGDMA concentration and enhanced mobility due to some softening originated by the MA monomer that increases distance between cross-links.

6.4.2 α relaxation process

This process was also studied by dynamical mechanical analysis in ref. 12. As in dielectric measurements the temperature of the main, α, relaxation increases with increasing TrEGDMA content of the copolymer. Two causes are in the origin of this behavior: on the one hand the copolymerization of a two monomers whose respective homopolymers have very different glass transition temperatures (a polyacrylate and a

polymethacrylate) and on the other hand the increase on the cross-linking density of the network with increasing TrEGDMA. The presence of a shoulder in the low-temperature side of the DMA loss tangent peak for high TrEGDMA contents denounces a phase separation in the polymer network, probably due to different reactivity of the two comonomers. In that case polymerization initially produces a polymer network richer in the more reactive monomer than the average, and consequently at the end of the reaction the remaining less reactive monomer incorporates to the network forming domains rich in this monomer. Dielectric measurements do not allow observing clearly the overlapping of more than one process in the α relaxation region of rich TrEGDMA copolymers, because at low frequencies where more resolution can be achieved, the high d.c. conductivity masks the dipolar relaxation. Nevertheless fitting procedures give more information.

To fit the experimental curves in addition to HN model for the α relaxation one has to include not only the conductivity term but also a Maxwell-Wagner-Sillars [26-28] mechanism, that was confirmed by an increase of ε' at low frequencies. As an example, Figure 6.8 shows the complete relaxation map of MA70 copolymer. The later effect is originated by the accumulation of interfacial charges. The strength of this relaxation is one order of magnitude higher in MA50 and MA30 than in the rest of copolymers what can be interpreted in the sense that phase separation takes place in these materials (dielectric strength values for the MWS process estimated from the fitting procedure, are presented in last column of Table 6.3 at a temperature that is roughly 30 ºC higher than the glass transition, except for MA30 where $\Delta\varepsilon$ was estimated near below T_g, predicting a much higher value for the same reference temperature comparing with the other copolymers).

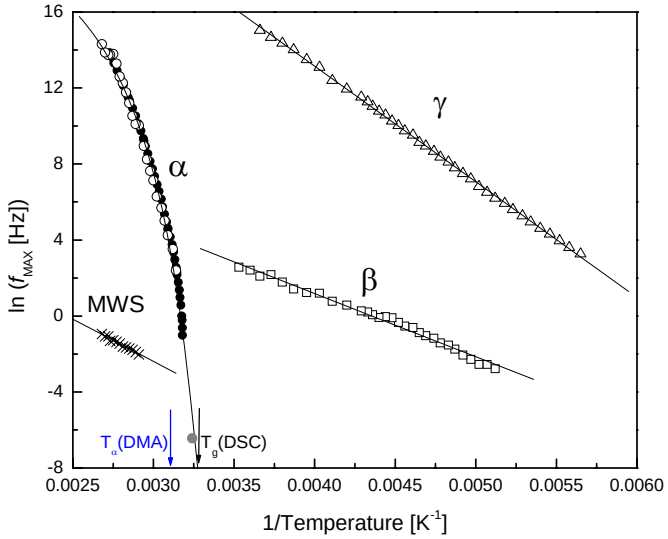

Figure 6.8 Activation plot for all the processes detected in sample MA70: triangles, γ; squares, β; circles, α (open for HN procedure, and full for $\log(f)$ *vs.* $T_{\max}^{-1}$); cross symbols for MWS. The arrows indicate the T_g values measured by DSC and by DMA [12].

The shift of the α relaxation to higher temperatures with increasing TrEGDMA content is accompanied by a broadening of the relaxation curves even for the copolymers richest in MA units. The broadening of the glass transition can be interpreted as an increase in heterogeneity, where the transition corresponds to the superposition of transitions in different nanodomains. The changes in the α relaxation spectrum can be related with changes in intra- and inter-molecular interactions in the cooperative conformational movements that originate this relaxation process [10]. In a model proposed by Schönhals and Schlosser [29,30] two parameters, m' and n', related respectively with large and small scale movements can be related with the α_{HN} and β_{HN} shape parameters: $m' = \alpha_{HN}$ and $n' = \alpha_{HN}\beta_{HN}$. These values in the systems that were unequivocally fitted by HN equation, respectively, neat PMA, MA80 and MA70, vary in an opposite manner, *i.e.* m' decreases while n' increases with the reduction of MA content (Table 6.3). Thus, the broadening effect quantified by the decrease in m' with increasing cross-linking density can be rationalized in the framework of Schönhals and Schlosser's theory as a consequence of the increase in the intermolecular interaction as chain connectivity increases, effect noticed in other polymer networks [10,31,32] as well.

The effect in the n' parameter depends on the chemical structure of the polymer chain since it is strongly related with local intra-chain dynamics, varying with cross-linking density in different manners (see ref. 10 and references therein). Our results, in spite of an increase of the β_{HN} parameter with cross-linking, show a decrease of n' due to the more abrupt decrease in α_{HN}. The difference between m' and n' decreases with cross-link density increase, meaning that the relaxation becomes more symmetric as shown in Figure 6.9 for the three systems at 55 ºC, where the curve for MA70 (diamonds) is more symmetrical than the correspondent loss curve for PMA (circles). These results are consistent with the behavior reported for cross-linked networks of PMA and EGDMA [10].

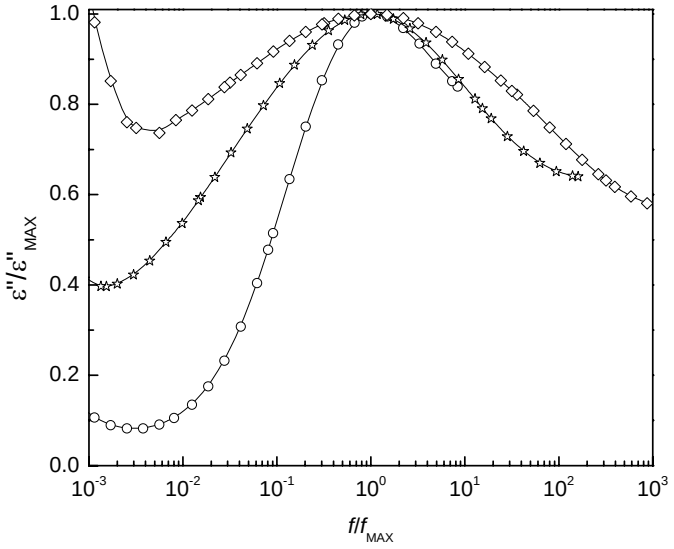

Figure 6.9 Normalized loss curves at 55 ºC for:
diamonds, MA70; stars, MA80 and circles for PMA.

From the activation plots, the glass transition temperatures T_{gDRS}, defined as the temperature for which the dielectric relaxation time equals 100 seconds, were predicted being presented in Figure 6.10. These values agree with those determined by DSC, also included. The experimental values of the glass transition temperature where fitted by the well known Fox relation [33] (solid line in Figure 6.10):

$$\frac{1}{T_g} = \frac{W_{MA}}{T_{gPMA}} + \frac{1 - W_{MA}}{T_{gTrEGDMA}} \qquad \text{Equation 6.2}$$

where W_{MA} and T_{gPMA} are, respectively, the weight fraction of MA units and the glass transition temperature determined by DSC for the PMA network in this work; $T_{gTrEGDMA}$ is the glass transition temperature of TrEGDMA estimated by the best fit of Fox's equation as 429 K (156 ºC). In spite of using an equation that only describes homogeneous mixtures, which is not the case since there is evidence of phase separation at least in MA30 and MA50, the T_g value such obtained seems to be reasonable when compared with the glass transition temperature reported in the literature [34] for poly-DEGDMA (466 K, 193 ºC) that has a shorter ethylene glycol moiety and consequently higher T_g.

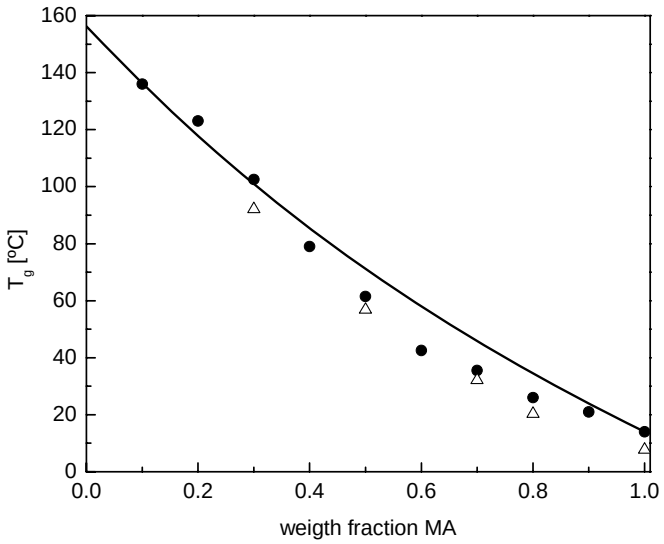

Figure 6.10 Glass transition temperature measured by DSC (full circles), and calculated from VFTH curve for τ =100 sec obtained from dielectric measurements (triangles). The solid line represents the glass transition temperature of a homogeneous mixture of monomer and the polymer network according to Fox's equation (see text).

The apparent activation energy at T_g significantly increases with TrEGDMA increase, revealing the hindrance to segmental mobility. Its value at T_g allows the estimation of the fragility index, m, according to reference 35, $m = E_a(T_g)/RT_g \ln 10$.

The fragility indexes thus estimated were included in Table 6.3, decreasing significantly with MA increase. Typical fragility indexes for polymers lay between 80 and 160 [36]. Neat PMA presents a fragility index of the order of polyvinyl acetate ($m = 95$) [35,36] lower than other amorphous polymer such as PMMA or PS [35,36,37]; MA30 presents the highest fragility index (remember that neat TrEGDMA was not able to be fitted and thus neither E_a or m were estimated) being the material that shows a more pronounced departure from Arrhenius behavior as Figure 6.6 shows (squares), characteristic of fragile glass formers.

6.5 Conclusions

The relaxation properties of MA/TrEGDMA copolymers covering the complete composition range have been characterized both by dielectric relaxation spectroscopy and differential scanning calorimetry.

The main relaxation broadens, becomes more symmetric and shifts towards higher temperatures with increasing TrEGDMA content. The strong dependence of the HN shape parameters with the composition of the richest MA copolymers was analyzed in relation to changes in intra- and inter-molecular interactions in the co-operative conformational movements that are in the origin of this relaxation process.

In the copolymers richest in TrEGDMA a phase separation can be detected in the DMA results by the presence of a shoulder in the low temperature side of the loss tangent peak [12]; dielectrically this effect is felt by the occurrence of a strong Maxwell-Wagner-Sillars process.

In what concerns the secondary relaxations of the homopolymers detected dielectrically, they are also present in the copolymers: the β relaxation process related with the rotations of the carboxylic units and the γ process due to twisting motions of ethyleneglycol moieties (except for PMA where the γ is absent). The β relaxation lie in between the homopolymers but highly influenced by TrEGDMA monomeric units. The γ relaxation is observed in all the copolymers at the same temperature interval as the β relaxation of PMA remaining almost invariant. Although the detected γ relaxation has a unimodal character, it is not clear up to know

if it results from a superposition of both TrEGDMA γ and PMA β relaxations, since in random copolymers of acrylate and methacrylate monomers both β relaxations are perceived.

6.6 References

[1] N.G. McCrum, B.E. Read, G. Williams, ‘‘Anelastic and Dielectric Effect in Polymeric Solids’’, Dover Publications, New York (1967) (reprinted 1991).

[2] U. Maschke, X. Coqueret, M. Benmouna, Macromol. Rapid Commun. 23 (2002) 159-170.

[3] R.T. Pogue, L.V. Natarajan, S.A. Siwecki, V.P. Tondiglia, R.L. Sutherland, T.J. Bunning, Polymer 41 (2000) 733-741.

[4] J.L. Gómez Ribelles, M. Monleón Pradas, J.M. Meseguer Dueñas, C. Torregrosa Cabanilles, J. Non-Cryst. Solids, 307–310 (2002) 731-737.

[5] J.L. Gómez Ribelles, M. Monleón Pradas, J.M. Meseguer Dueñas, C. Torregrosa Cabanilles, J. Phys. Cond. Matter. 15 (2003) S1149-S1161.

[6] L.E. Nielsen, “Mechanical Properties of Polymers and Composites”, Vol. 1, Marcel Dekker, New York (1974).

[7] P. Mason, Polymer, 5 (1964) 625-635.

[8] C.M. Roland, Macromolecules 27(15) (1994) 4242-4247.

[9] A.R. Kannurpatti, J.W. Anseth, C.N. Bowman, Polymer 39 (1998) 2507-2513.

[10] J.M. Meseguer Dueñas, J. Molina Mateo, J.L. Gómez Ribelles, Polym. Eng. Sci. 45 (2005) 1336-1342.

[11] V.Y. Kramarenko, T.A. Ezquerra, I. Šics, F.J. Baltá-Calleja, V. Privalko J. Chem. Phys., 113 (2000) 447-452.

[12] M.T. Viciosa, N. Rouzé, M. Dionísio, J.L. Gómez Ribelles, Europ. Pol. J. 43 (2007) 1516-1529.

[13] M. Beiner, Macromol. Rapid Commun. 22(12) (2001) 869-895.

[14] M.S. Dionísio, J.J. Moura-Ramos, Polymer 35(8) (1994) 1705-1713.

[15] X. Jin, S. Zhang, J. Runt, Macromolecules 37 (2004) 8110-8115.

[16] X. Jin, S. Zhang, J. Runt, Polymer 43 (2002) 6247-6254.

[17] S. Havriliak, S. Negami, Polymer 8 (1967) 161-210.

[18] "Broadband Dielectric Spectroscopy", F. Kremer, A. Schönhals, Springer-Verlag, Berlin Heidelberg (2003).

[19] I.K. Smith, S.R. Andrews, G. Williams, P.A. Holmes, J. Mater. Chem. 7(2) (1997) 203-209.

[20] H. Vogel, Phys. Z. 22 (1921) 645-646.

[21] G.S. Fulcher, Am. Ceram. Soc. 8 (1925) 339-355.

[22] G. Tammann, W. Hesse, Z. Anorg. Allg. Chem. 156 (1926) 245-257.

[23] "Disorder Effects on Relaxational Processes", R. Richert, A. Blumen, Springer, Berlin (1994).

[24] M.T. Viciosa, C.M. Rodrigues, M. Dionísio, J. Non-Cryst. Solids 351 (2005) 14-22.

[25] R.A. Vaia, D.W. Tomlin, M.D. Schulte, T.J. Bunning, Polymer 42(3) (2001) 1055-1065.

[26] K.W. Maxwell, "Electricity and Magnetism", Vol. 1; Clarendon: Oxford, UK (1982).

[27] K.W. Wagner, Arch. Elektrotech. 2 (1914) 371-387.

[28] R.W. Sillars, J. Inst. Electr. Eng. 80 (1937) 378-394.

[29] A. Schönhals, E. Schlosser, Colloid. Polym. Sci. 267(2) (1989) 133-138.

[30] A. Schönhals, E. Schlosser, J. Non-Cryst. Solids 131-133 (1991) 1161-1163.

[31] V.Y. Kramarenko, T.A. Ezquerra, I. Šics, F.J. Baltá-Calleja, V.J. Privalko, J. Chem. Phys. 113(1) (2000) 447-452.

[32] J.K.W. Glatz-Reichenbach, L.J. Sorriero, J.J Fitzgerald, Macromolecules 27(6) (1994) 1338-1343.

[33] T.G. Fox, Bull. Am. Phys. Soc. 1 (1956) 123-135.

[34] A. Kannupartti, A. Bowman, J. of Polymer Science: Part B: Polymer Physics 35 (1997) 2297-2307.

[35] R. Böhmer, K.L. Ngai, C.A. Angell, D.J. Plazek, J. Chem. Phys. 99(3) (1993) 4201-4209.

[36] E. Hempel, G. Hempel, A. Hensel, C. Schick, E. Donth, J. Phys. Chem. B 104v (2000) 2460-2466.

[37] N. Alves, J.F. Mano, J.L. Gómez Ribelles, J.A. Gómez Tejedor, Polymer 45(3) (2004) 1007-1017.

CHAPTER 7 | INFLUENCE OF CRYSTALLIZATION ON THE MOLECULAR MOBILITY OF THE AMORPHOUS PHASE IN EGDMA

7.1 Introduction

EGDMA monomer by showing high dielectric relaxation intensity for the α-relaxation and easiness to crystallize, is thus a good candidate to study simultaneously the crystallization process and the mobility of the coexistent supercooled state.

Therefore, one of the objectives of the work reported in the present chapter is to investigate the influence of crystallization on the α-relaxation of the remaining amorphous fraction. With this purpose, isothermal crystallization was promoted at different temperatures allowing establishing a correlation between molecular dynamics and the kinetics of isothermal crystallization. The later was characterized by calorimetric studies reproducing the same thermal histories than in dielectric experiments. This kind of studies can give relevant information on the dynamical behavior of the remaining amorphous region under spatial confinement, since the amorphous matrix in advanced stages of crystallization subsists in dimensions of the order of nanometers. This work envisages being a further contribution in literature concerning the crystallization of low molecular weight materials, since related studies are scarce and different behaviors are reported as will be explored in more detail in the *Discussion* section.

Furthermore, concerning the secondary processes detected in this family of monomers, their isothermal polymerization ended to be a strategy to resolve those low intense processes from the dominating α relaxation, as reported in previous chapters. Now, the crystallization of EGDMA with a concomitant decrease in the magnitude of the α process will put in evidence the two secondary processes, in particular the β-relaxation.

7.2 Characterization of the amorphous state

For obtaining EGDMA monomer in amorphous state at temperatures below the melting point, the sample was cooled down from 25 ºC to -120 ºC without any programming setup, only setting the temperature to -200 ºC in order to maximize the cooling rate reached by the DRS equipment. The dielectric loss spectra were taken at different increasing temperatures steps from -115 up to 0 ºC (in the temperature range

-115 ºC ≤ T ≤ -95 ºC and -40 ºC ≤ T ≤ 0 ºC, the dielectric spectra were recorded every 5 ºC; in the remaining temperature region the spectra were recorded every 2 or 3 ºC). This procedure was, thus, the same than in the study of the other monomers. The values of ε'' collected isothermally between -100 and -78 ºC are shown in Figure 7.1. The spectra show a strong relaxation process, similar to the other monomers, associated with the dynamic glass transition. This α-process dominates at the lowest temperatures. DSC experiments show that with this thermal treatment EGDMA is nearly fully amorphous, although enthalpy calculations indicates that the presence of a small fraction of crystals cannot be discarded even for the fastest cooling. The intensity of the main relaxation is comparable to the magnitude of this process in the other members of the series (see Chapter 3, Figures 3.2 and 3.3). On the other hand, the height of the ε'' peaks slightly increases up to -86 ºC. For temperatures higher than -86 ºC, the α-peak decreases abruptly due to crystallization. If we assume that the monomer circumvented crystallization upon cooling and only starts crystallizing in this further heating mode, the type of crystallization observed is called cold crystallization [1,2]. The curves collected from -76 to -55 ºC are presented in the inset of Figure 7.1 (ε'' values in a different scale), putting in evidence that the main relaxation process, still visible at -76 ºC, vanishes at -75 ºC. At higher temperatures, only secondary relaxations are left.

It is important to point out that the onset of crystallization and the rate at which the intensity of the α peak decreases, vary with the number of isothermal spectra collected. This fact was not surprising since the thermal profile during crystallization depends of the number of isotherms measured. An isothermal measurement takes around 10 minutes (in which it is included the time necessary to stabilize the sample).

At temperatures below -90 ºC, the spectra seems to exhibit only one secondary relaxation as shown at -115 ºC in Figure 7.2, that also includes the isothermal data for all the monomers taken at the same temperature.

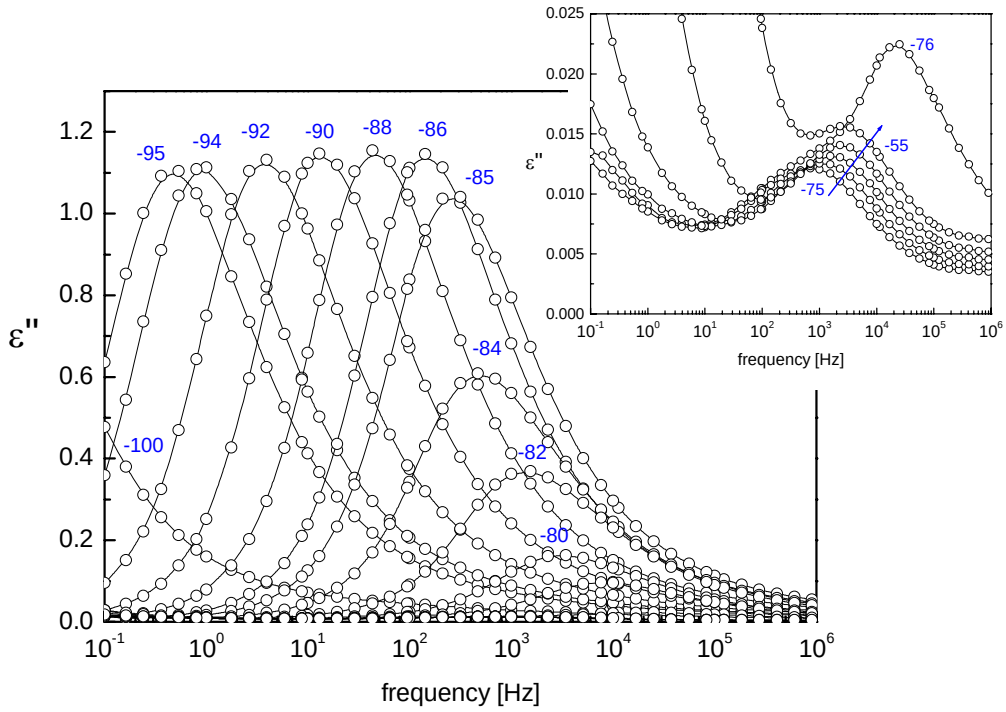

Figure 7.1 Dielectric loss spectra for EGDMA between -100 and -78 ºC.
Inset: dielectric loss spectra from -76 to -55 ºC.

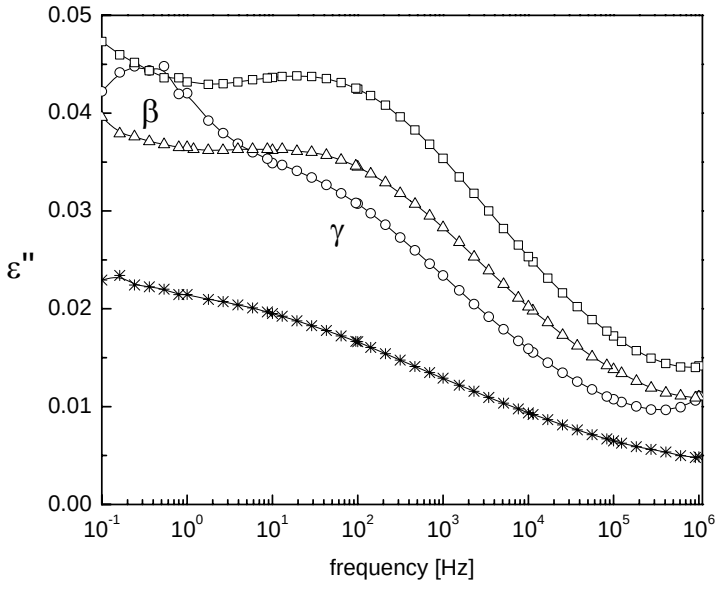

Figure 7.2 Dielectric loss spectra obtained at -115 ºC for: EGDMA (asterisks), DEGDMA (circles), TrEGDMA (triangles) and TeEGDMA (squares).

At higher temperatures, around -20 ºC, the dielectric spectra shows an abrupt increment of intensity, fact that can be attributed to the fusion of the crystalline phase previously formed. This behavior will be commented further in the text.

The data treatment was carried out using the empirical Havriliak-Negami function described in Chapter 1. For the lowest temperatures, where only the high frequency tail of the main relaxation process is shown up in the frequency window of the experiments, the dielectric spectra can be well reproduced by considering either one or two HN functions. In next figure the two options are presented for the isothermal data collected at -115 ºC. Taking into account the spectra corresponding to the other studied monomers, it seems easy to accept the existence of two secondary relaxations, nevertheless in next sections this fact will become clearer.

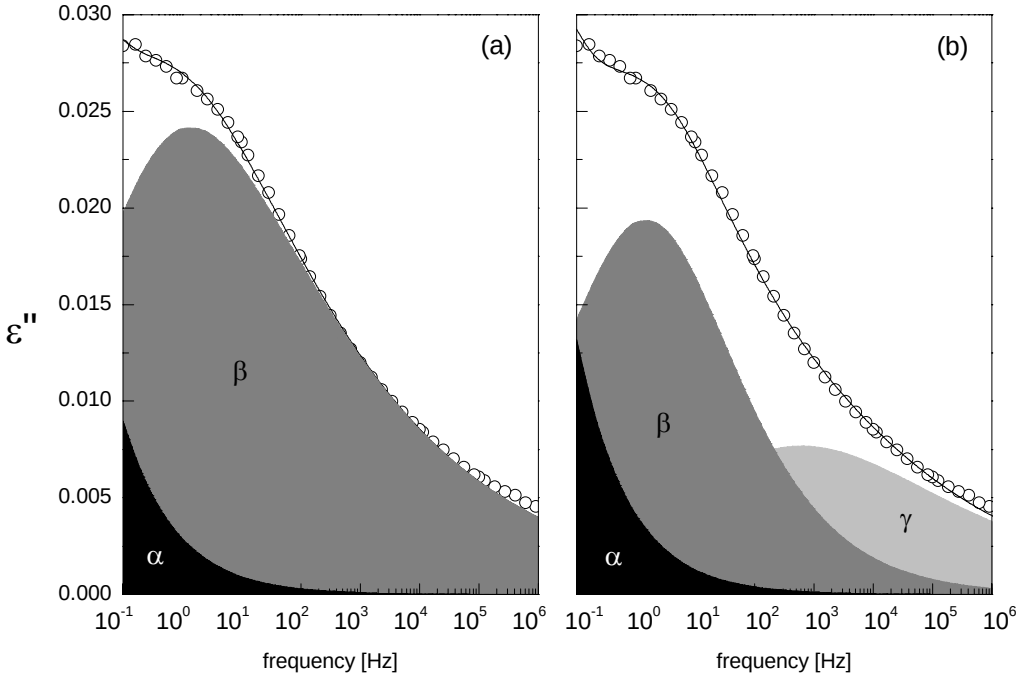

Figure 7.3 Dielectric loss spectra for EGDMA collected at -115 ºC and the respective overall HN fitting curve (solid line). The individual HN functions employed during fitting procedure are shown as filled areas: a) one HN function corresponding to the secondary β process, and b) two HN functions for the β and γ secondary relaxations. In both cases the high frequency tail of the α relaxation is felt in the low frequency side of the spectrum.

7.2.1 The α process

The peak corresponding to the α relaxation is detected in a narrow temperature range, from -95 to -76 ºC. It appears as a well defined process, that can be fitted by the HN function with the following shape parameters: $\alpha_{HN} = 0.92 \pm 0.02$ and $\beta_{HN} = 0.51 \pm 0.03$, in perfect agreement with those of the already studied monomers (Chapter 3). As it happens in the other members of the family, the almost invariance in the shape of the α-peak allows constructing a master curve. During the non-isothermal cold-crystallization process, the shape parameters associated to the isotherms where the α-peak is still detected although with decreasing intensity, do not suffer significant changes, which can indicate that the distribution of the relaxation times of the conformational large scale motions associated to the glass transition is not affected by the restrictions imposed by crystallization (we will see later that this is not strictly true under isothermal cold-crystallization).

Few temperatures are available for the analysis of the temperature dependence of the characteristic relaxation time, but they are enough to allow us localizing without any doubts its position relatively the other systems. In Figure 7.4 the activation plot for EGDMA monomer in the amorphous state is presented; the respective plots of the others monomers in grey symbols and lines are included for comparison purposes.

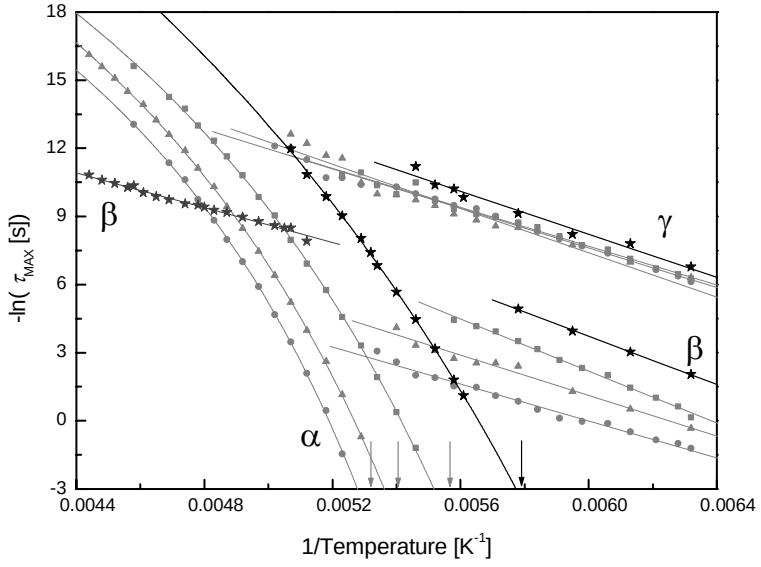

Figure 7.4 Relaxation map for the four monomers studied in this work: black stars correspond to EGDMA, grey squares, triangles and circles correspond to DEGDMA, TrEGDMA and TeEGDMA already studied in Chapter 3. Solid lines are the VFTH and Arrhenius fittings.

The curvature of the plot of $-\ln \tau_{max}$ *vs.* reciprocal of temperature, *i.e.* the departure from the Arrhenius behavior, is smaller than in the other polymers of the series as can be seen in Figure 7.4. The relatively narrow temperature interval in which isothermal spectra are available increases the uncertainty in the fit of the VFTH equation to the experimental points. The parameters obtained from the VFTH function are listed in Table 7.1 that also includes the glass transition temperature, apparent activation energy and fragility index estimated accordingly Equations 3.2 and 3.3 respectively. Table 7.1 includes two set of data that revealed different crystallization onsets. The activation plots although being fitted with distinct VFTH parameters, led to glass transition temperatures, apparent activation energies and fragility indexes with very reasonable agreement.

	τ_0 [s]	B [K]	T_0 [K]	T_g [K]	m	$E_a(T_g)$ [kJ.mol^{-1}]
Data from Fig. 7.4	$(5\pm5)\times10^{-21}$	2820±586	117±7	171.4 (-101.7 ºC)	70	229
Different set of isothermal data	$(2\pm2)\times10^{-25}$	4252±1391	103±13	171.7 (-101.4 ºC)	67	219

Table 7.1 VFTH fitting parameters for the main relaxation process of EGDMA, glass transition temperature (T_g) at 100s, activation energy at T_g and fragility index, m. Two different series of isothermal data (considering different list of temperatures) are shown.

7.2.2 The secondary relaxations β and γ

The secondary relaxations, as already mentioned, were detected since the very beginning of measurements at the lowest temperatures, but they do not show up well resolved in the dielectric spectra in the wholly amorphous state. The proximity of the main relaxation process reduces to four the number of spectra available for fitting the β relaxation before the onset of crystallization. In this narrow temperature range, the α_{HN} changes from 0.41 at -115 ºC to 0.56 at -100 ºC, and the β_{HN} keeps constant as 0.94±0.02. After cold crystallization, *i.e.* above -78 ºC, this process is observed much more clearly, allowing an unequivocal determination of its position and shape. In this situation, while β_{HN} is basically insensitive to crystallization (0.95±0.03), α_{HN}

increases to 0.61±13 given of course, an increase in $\alpha_{HN}\beta_{HN}$ from 0.47±0.07 in the amorphous state to 0.61±0.17 in the semi-crystalline state.

The activation energy before crystallization was estimated in 44±1 kJ.mol^{-1} in agreement with the values found for the other monomers (remember Table 3.3). After crystallization E_a decreases to 32±1 kJ.mol^{-1}. The pre-exponential factor that initially takes the value of (5±2)×10^{-16} s increases to (9±4)×10^{-13} s (the regression coefficient is 0.99 in both cases).

The γ relaxation always arises merged in the more intense β relaxation (remember Figure 7.3.b) making difficult to characterize it. However, the shape parameters obtained are 0.41±0.09 and 0.44±0.04 for α_{HN} and β_{HN}, respectively. The Arrhenius fit let us estimate the activation energy as 39±3 kJ.mol^{-1} and τ_0 as (1.2±0.9)×10^{-16} s. This relaxation is very close to that of the other monomers as it can be seen in Figure 7.4.

After crystallization, this process seems to be present in the high frequency side of the spectra (see inset in Figure 7.1) however no reliable location of its maximum can be provided, so no data can be reported.

7.3 Real time dielectric measurements during isothermal cold-crystallization

A fresh sample was cooled down to -120 ºC at the maximum rate allowed by the instrument (around -10 ºC.min^{-1}), to prevent crystallization, and at the same time data were collected in isochronal procedure. Then the sample was rapidly heated up to the cold crystallization temperature, T_{cr}, -86, -84, -82, -80, -78 and -76 ºC, to avoid (or at least to minimize) the growth of crystals. At T_{cr} successive frequency sweeps from 0.7 Hz to 1 MHz were collected every 90 seconds during a total time of 2 hours (the reason why no lower frequencies than 0.7 Hz were chosen to collect data was to guarantee that during the frequency scan the change in crystallinity was significantly small). Between different isothermal crystallization measurements, the sample was heated up to the molten state at 25 ºC to erase its thermal history and eliminate all crystalline nuclei. The isochronal plots of both ε' and ε'' collected in the following

descending step to -120 ºC allowed to check the status of the sample confirming that no crystallization occurred. The ε' trace is particularly sensitive to crystallization showing a pronounced discontinuity to lower values [3] (besides the normal jump associated with the manifestation of the relaxation process); no such feature was found during the different isothermal crystallization analyses.

Figure 7.5 shows the real time evolution of the dielectric loss during the isothermal crystallization process at T_{cr} = -80 ºC.

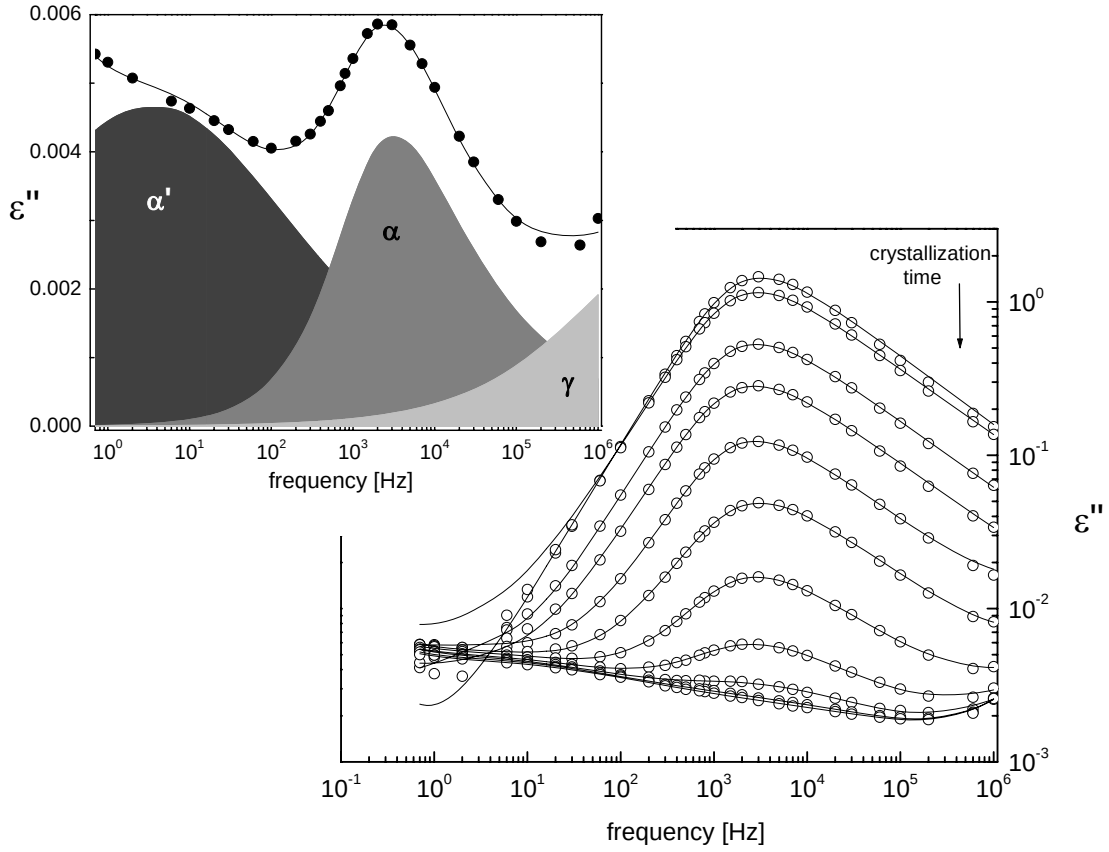

Figure 7.5 Dielectric loss for EGDMA collected during real time isothermal cold crystallization at -80 ºC. The solid lines are the overall fitting to the experimental data obtained at different times using the sum of three HN functions. Only the loss curves collected each 12 minutes are shown in a total collecting time of 2 hours. The graphic in inset represents the spectrum collected at 84 min (points) and the overall HN fit (solid line); the corresponding HN individual curves are also included (filled areas).

Dielectric spectra were fitted with the empirical Havriliak-Negami equation considering three relaxations (as exemplified in the inset of Figure 7.5): *i*) the main

relaxation, which is the major contribution from the first stage of the crystallization process, *ii*) the γ relaxation, whose contribution becomes important when the α-relaxation is significantly depleted and its $\Delta\varepsilon_\alpha$ is low, and *iii*) a relaxation located in the low frequency side of the α process identified as α'.

The fitting was carried out fixing the shape parameters and the relaxation time, τ_{HN}, of both γ and α' processes. For the main α-relaxation, a first tentative was made allowing all the parameters to vary. It was concluded that no significant changes occur in both location and β_{HN} parameter. Thus, τ_{HN} and β_{HN} were fixed. By this way only the dielectric strength, $\Delta\varepsilon$, corresponding to the three relaxations and the α_{HN} shape parameter of the α-process, were let to change during the fitting procedure. The fixed parameters for each crystallization temperature are summarized in Annex II.

While crystallization progresses, four features are observed: *i*) a reduction of the intensity of the α process with increasing crystallization time; *ii*) the α peak does not suffer any significant change either in position or shape in the first stages of crystallization, however a broadening is observed when high crystallization degrees were attained (loss curves collected at the final times for samples crystallized at -80 and -78 ºC), *iii*) the magnitude of the final spectrum after 2 hours of crystallization depend on T_{cr} and *iv*) another relaxation process in the low-frequency flank of the α-peak evolves at high crystallization degrees, designated as α'.

The dielectric strength for the main relaxation process, $\Delta\varepsilon_\alpha$, is represented as a function of crystallization time in Figure 7.6.a. When isothermal crystallization is carried out at temperatures above -80 ºC, the extinction of the α relaxation is complete, while it persists when the crystallization process is monitored at lower temperatures.

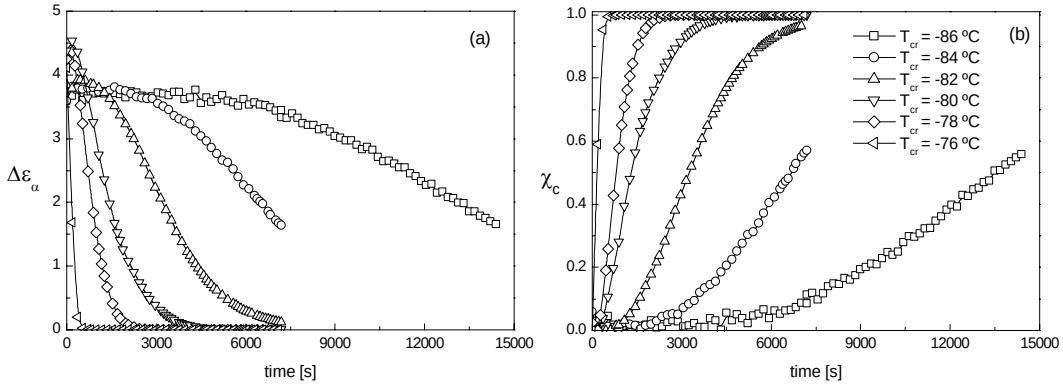

Figure 7.6 a) Dielectric strength for the α -relaxation, $\Delta\varepsilon_\alpha$, obtained from the HN fitting and b) crystallization degree, χ_c, as a function of crystallization time for the isothermal cold-crystallization at temperatures, T_{cr}, indicated.

The variation of $\Delta\varepsilon_\alpha$ with the crystallization time can be used to estimate the crystalline fraction, χ_c, considering that the relaxation strength is proportional to the non-crystalline part. This approximation is based in the fact that low-molecular-weight compounds present only two phases during the crystallization process, *i.e.* the amorphous and the crystalline one [4]. The time dependence of the degree of crystallinity for each T_{cr} between -86 and -78 ºC was estimated from the normalized dielectric strength of the α -relaxation according to Equation 7.1 [4]:

$$\chi_c(t) = 1 - \frac{\Delta\varepsilon(t)}{\Delta\varepsilon(t=0)} \qquad \text{Equation 7.1}$$

Thus, χ_c, changes from 0 at the first experimental point (thus the sample is assumed to be fully amorphous after cooling) to 1 when the main relaxation is not observed (Figure 7.6.b). The crystallinity degree attains the value of 1 for the three highest temperatures (being also very close after cold-crystallization at -82 ºC), but only reaches 0.6 for the two lowest temperatures, -84 and -86 ºC.

The time dependence of the crystallinity degree, allows extracting kinetic information. A widespread treatment in literature to analyze the transformation from the disordered, amorphous phase into the ordered, polycrystalline phase [5] at a fixed temperature, is the Avrami model [6-8]. In this treatment of the isothermal

crystallization kinetics, different nucleation and growth mechanisms have correspondingly different time dependences of the crystallization rate that can be modelled by the Avrami law [6]:

$$\chi_c(t) = 1 - \exp(-kt^n) \qquad \text{Equation 7.2}$$

or

$$\ln[-\ln(1-\chi_c(t))] = n\ln t + \ln k \qquad \text{Equation 7.3}$$

where χ_c indicates the crystalline fraction as defined above, k the rate constant, and n the Avrami exponent which relates to the nucleation rate, growth mechanism, and crystal shape. From Equation 7.3, a plot of $\ln[-\ln(1-\chi_c(t))]$ *vs.* $\ln t$ yields a linear line whose slope is *n* and the intercept is related to k.

To determine at each temperature a characteristic time for the isothermal crystallization, the Avrami equation has been rewritten as a phenomenological Kohlraush-Williams-Watts (*KWW*) equation [9]:

$$\chi_c(t) = 1 - \exp\left[-\left(\frac{t}{\tau_{cr}}\right)^{\beta}\right] \qquad \text{Equation 7.4}$$

where τ_{cr} is the characteristic crystallization time and β is a constant. These parameters are connected to the Avrami parameters by the relationships $\tau_{cr} = k^{-1/n}$ and $\beta = n$ (the crystallization times thus estimated are plotted in Figure 7.11 presented later on).

The double logarithmic representation according to Equation 7.3 is shown in Figure 7.7. Data concerning the highest temperatures at which isothermal crystallization was monitored, reveal a change of slope; the flat region at longer times corresponding to full crystallization. So a linear regression analysis was carried out taking only in account data concerning the first stages of crystallization (*i.e.* excluding

data collected after a change in the slope); the respective estimated values of τ_{cr} and n are summarized in Table 7.2.

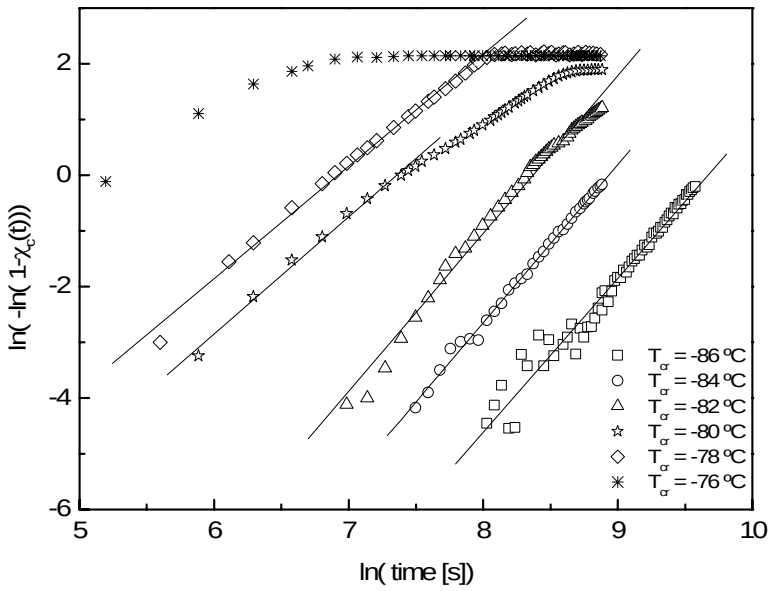

Figure 7.7 Avrami plot according to Equation 7.3 and corresponding regression line (see text) for each crystallization temperature (T_{cr}) studied.

T_{cr} [ºC]	k	τ_{cr} [s]	n	R
-86	2.5×10^{-12}	1.58×10^{4}	2.8	0.985
-84	9.4×10^{-12}	7.57×10^{3}	2.8	0.998
-82	5.0×10^{-11}	4.31×10^{3}	2.8	0.993
-80	1.9×10^{-7}	1.56×10^{3}	2.1	0.996
-78	8.9×10^{-7}	1.01×10^{3}	2.0	0.997

Table 7.2 Parameters obtained from the Avrami's fit for the crystallization temperatures, T_{cr}, indicated. The corresponding linear regression coefficient, *R*, is included.

The value of the exponent *n* has been related in the literature to the mechanism of nucleation and growth: values of n = 0.54 - 0.62, have been reported for a diffusion controlled growth mechanism, while a phase-boundary, *i.e.* interface, controlled mechanism is indicated by n = 1 - 1.24. A mechanism involving simultaneous nucleation and growth yields n = 2.0 - 3.0 (10 and 11, in ref. 12). Thus

we can deduce that crystallization progresses in the EGDMA system with simultaneous nucleation and growth since all n values are comprised between 2 and 3 (Table 7.2).

A more detailed interpretation of Avrami's exponent has been proposed [13,14] according to which n can be expressed in terms of nucleation and growth parameters, $n = a + bc$, where a is the nucleation index which governs the time dependence of the number of nuclei per unit volume (N) of untransformed material $N \alpha t^a$ ($a = 0$ for nucleation rate 0, $a = 1$ for constant nucleation rate, $a > 1$ for increasing and $0 < a < 1$ for decreasing nucleation rates, respectively). b is the dimensionality of the growth ($b = 1, 2, 3$ for 1D, 2D, 3D growth, respectively). c is a growth index depending on the type of transformation (typically $c = 1$ for a linear growth, as in interface-controlled growth, and $c = 1/2$ for a parabolic growth, as in diffusion-controlled growth). For instance an Avrami exponent of 2.5 (close to our mean value) is explained by Wang and co-workers [15], as corresponding to diffusion-controlled growth ($c = 1/2$), a constant nucleation rate during transformation ($a = 1$) and a 3-dimensional ($b = 3$) growth. However, it is difficult to realistically determine three parameters (*a, b* and *c*) only from one (n).
We recognize that this is only a raw data analysis acting as starting point to future work that certainly will need further development.

7.4 Mobility in the semi-crystalline material

At the end of each isothermal cold-crystallization monitoring, reported in the previous section, the semicrystalline sample was cooled down to -120 ºC and successive dielectric spectra were measured while increasing temperature.

Additionally, in order to study the remaining mobility for a different crystalline state, melt-crystallization was induced by slowly cooling down a fresh sample of EGDMA from room temperature to -120 ºC (cooling rate of -1 ºC.min^{-1}); during the cooling process data were acquired non-isothermally at some frequencies. Then, isothermal measurements in increasing temperature steps were performed, following the protocol described above for the cold-crystallization experiments.

An interesting feature was observed comparing measurements obtained after crystallization from the melt and after cold-crystallization: while in the former, the intensity of the relaxation processes that are still detected in the amorphous fraction, does not suffer any changes by further temperature increase and superimposes in both cooling and further heating runs (in the temperature range from -120 to -60 ºC), the different crystalline states reached after cold-crystallization are not completely stable, *i.e.* during the heating procedure in which isothermal data are collected, the crystalline fraction formed until that moment increases by the effect of the temperature. The mobility remaining in the supercooled state (above the glass transition) is enough to molecules diffuse to the crystal surfaces inducing a new crystallization. These results are discussed in detail in the following sections.

At this moment it is important to refer how dielectric permittivity monitors crystallization and melting of EGDMA on cooling and heating scans respectively, as illustrated in Figure 7.8. Equilibrium melting temperature of EGDMA is around -10 ºC as determined by the onset of the melting endotherm peak in DSC heating thermograms. The real part of the dielectric permittivity measured on heating also shows at this temperature the onset of the transition reflected by a sharp step. On cooling EGDMA easily supercools, crystallization is monitored by the sharp decrease of ε' that takes place around -45 ºC, at temperatures significantly below the melting temperature, *i.e.* following paths 2 and 2'' of Figure 1.1 presented in the *Introduction* in Chapter 1; it is also worth note that the temperatures at which both crystallization and fusion occur are frequency independent given their 1st order transition character, while the kinetic nature of the glass-liquid "transition" is obvious by the frequency dependence of ε' and ε'' traces. These results (Figure 7.8) nicely illustrate that DRS is a very sensitive tool to probe phase transitions/transformations through both ε' and ε'' traces.

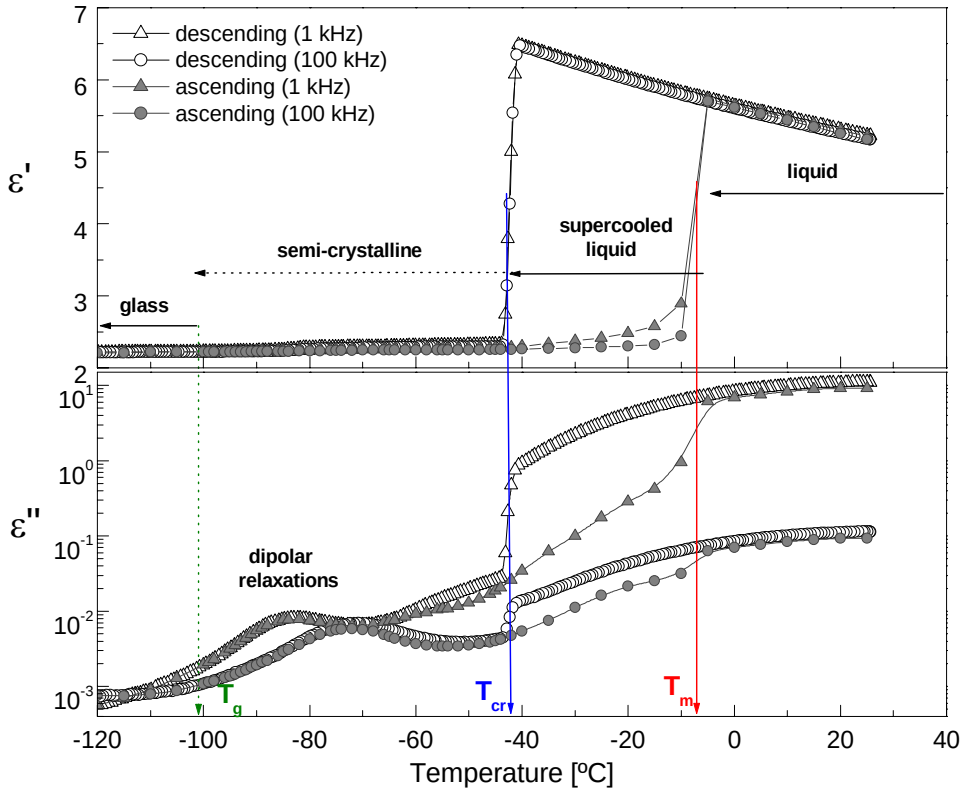

Figure 7.8 Isochronal plots of ε' and ε'' revealing frequency-independent sharp steps at melting (T_m) and crystallization (T_{cr}), and frequency-dependent liquid to glass "transition" (T_g); all of them are indicated by the vertical arrows. The horizontal arrows indicate the different states attained by the sample upon cooling.

Finally, the comparison between the amorphous and the semi-crystalline states of EGDMA, when amorphous and crystalline phases co-exist, can bring new information to the previous characterization of both main and secondary relaxation processes. The mobility remaining in each state obtained after cold crystallization and crystallization from the melt will be analyzed separately.

7.4.1 Mobility in the amorphous phase after non-isothermal crystallization from the melt

Figure 7.9 presents some representative loss curves of EGDMA previously crystallized from the melt. The spectra are dominated by a sharp although low intense process that shows up since the very beginning of measurements, far below the glass transition temperature ($T_{g\,DRS}$ = -102 ºC), thus it is ascribed to the β relaxation. This peak remains clearly visible at temperatures above T_g, splitting in two at higher temperatures. This could mean either that the α-relaxation extinguishes and only local motions remain, or the α-relaxation strongly depletes being merged under the secondary relaxation processes. To clarify this, a detailed analysis of the spectra is now provided.

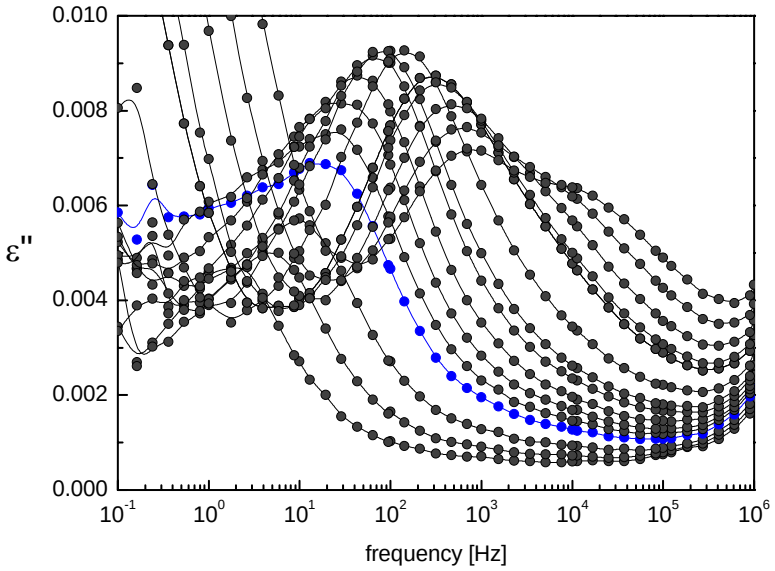

Figure 7.9 Dielectric loss spectra for EGDMA obtained after non-isothermal melt-crystallization for temperatures between -115 to -100 ºC every 5 ºC, and after until -76 ºC every 2 ºC. The spectrum collected at -100 ºC is represented in blue colour to help the visualization of the β process and the incoming α process in the low frequency side.

The complex spectra obtained for the melt-crystallized sample need the consideration of several individual HN curves as it is shown in Figure 7.10 (the

increase of ε'' above 10^5 Hz has not real meaning, since the low values of ε'' lye in the limit the operability of the Alpha-N analyzer at those frequencies [16]).

At -110 and -99 ºC, the presence of the γ relaxation at the high frequency side of the β-process is clearly shown. In spite of its low intensity, the γ relaxation is now more visible than in the fully amorphous sample, where its presence could be doubtful (remember Figure 7.3).

At -99 ºC (Figure 7.10) another process emerges in the low frequency side of the β relaxation being well fitted, although it is clearly visible in only few isothermal spectra.

At -90 ºC (Figure 7.10), it becomes submerged in the slowest β-peak, widening its low frequency side. It over passes the β-process at -80 ºC swelling the weak γ relaxation. From its rapid shift in the frequency axis with the temperature increase it looks like the α-relaxation. This will be confirmed below with the analysis of the relaxation times obtained from the HN fittings.

Finally, for temperatures above -90 ºC, the strong ε'' increase at low frequency corresponds to a new relaxation process assigned to charge accumulation in the interface of crystalline/amorphous fractions, *i.e.* a Maxwell-Wagner-Sillars effect (MWS), confirmed by an increase in the real part of the complex permittivity, ε' (not shown).

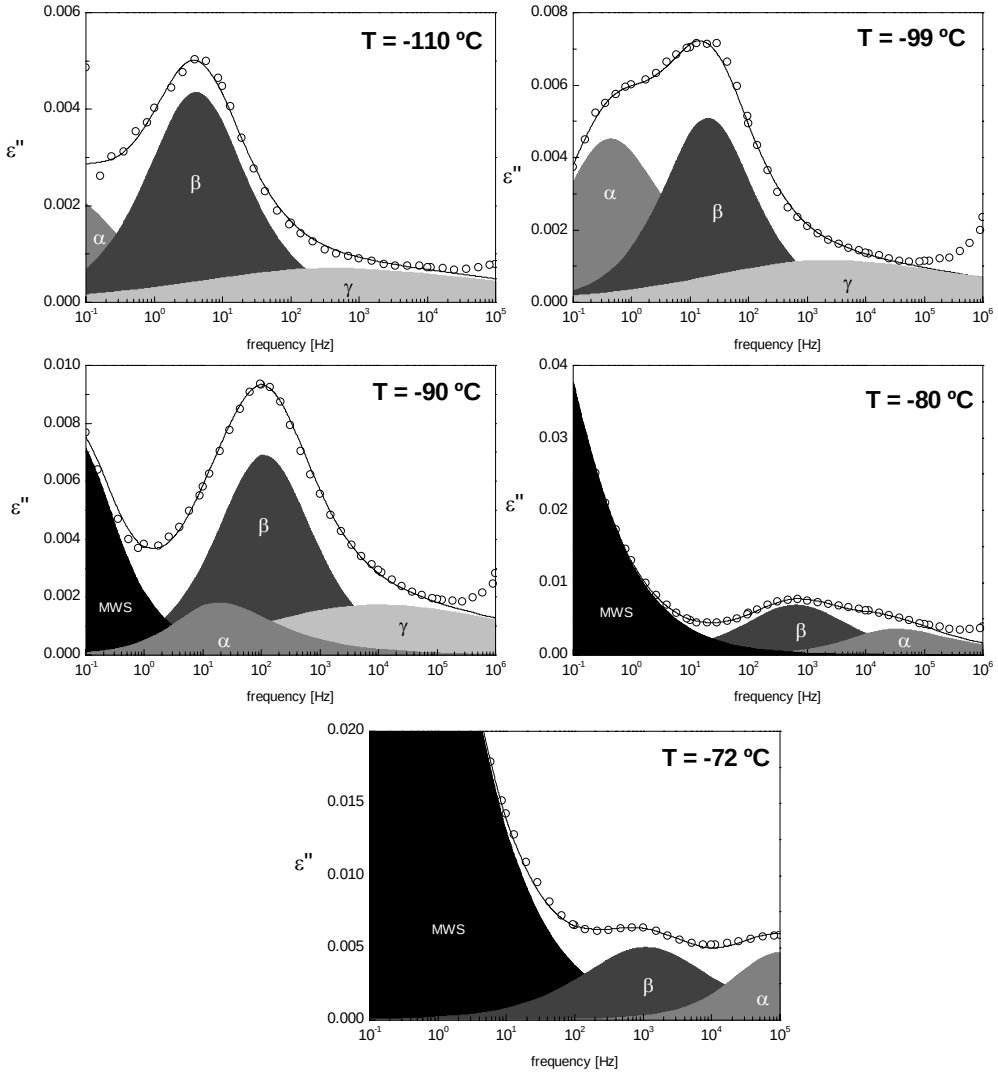

Figure 7.10 Isothermal loss spectra for the EGDMA after non-isothermal crystallization from melt (at -1 ºC.min^{-1}) at the temperatures indicated. The overall fit (black line) and the corresponding individual HN functions (filled areas) employed to reproduce the complete ε'' spectra are included.

	α_{HN}	β_{HN}	E_a [kJ.mol^{-1}]	τ_0 [s]
β	0.72±0.09	0.98±0.01	41±1	(4±2)x10^{-15}
γ	0.32→0.55	0.53±0.04	38±1	(3±2)x10^{-16}
MWS	0.55±0.05	0.96±0.03	71±3	(2±1)x10^{-18}

Table 7.3 Shape parameters obtained from the HN fit (α_{HN} and β_{HN}) for the relaxation processes, β, γ and MWS, detected after non-isothermal crystallization from the melt. The corresponding activation energies (E_a) and pre-exponential factors (τ_0) calculated from Arrhenius fit are also included.

The HN shape parameters used to fit the isothermal loss curves are summarized in Table 7.3. It is important to note that the α_{HN} shape parameter obtained for the β relaxation denote a narrower distribution of relaxation times than the one found in the amorphous state (α_{HN} is 0.72 in the semi-crystalline sample, while in the amorphous sample α_{HN} takes values around 0.41-0.57). However, its temperature dependence overlays the one observed in the amorphous state allowing confirming that this relaxation process is really the β-relaxation. Also the activation plot of the γ-process superimposes to the corresponding in the amorphous state. This secondary relaxation seems to be more insensitive to the changes imposed by the crystalline phase, since their respective shape parameters keep constant.

The trace of the third relaxation process is not well defined due to its low intensity and overlapping with the β and γ secondary processes. However, from the activation plot presented in Figure 7.11, where it can be seen that its temperature dependence nearly follows the α-relaxation process of the amorphous state proving that it is the cooperative relaxation process although highly depleted due to crystallization. The very low magnitude of this process attests that a high crystallization degree was achieved; however no full conversion was reached. Its α_{HN} shape parameter shows a decrease from 0.92 in the amorphous sample to 0.79 in this melt-crystallized EGDMA, as also detected during isothermal cold-crystallization after a high crystallization degree being attained.

The α trace in the relaxation map (Figure 7.11) suffers no influence from the β secondary relaxation as they approach each other. On the contrary, the temperature dependence of the relaxation time of the β process undergoes a deviation to lower times, being somehow accelerated by the merging with the α-process. It is difficult to reach conclusions relative to the evolution of the γ-relaxation since it becomes completely swollen under the α-relaxation.

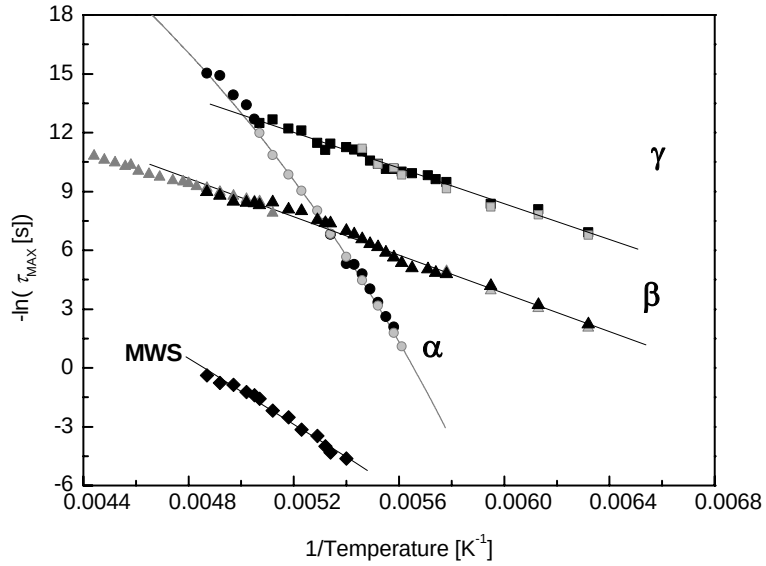

Figure 7.11 Arrhenius plot of the semicrystalline state attained after non-isothermal crystallization from the melt. The relaxations detected in the amorphous state are included in grey symbols (the grey line is the VFTH fit for the main relaxation process). Black lines correspond to the linear fits.

The activation energy and pre-exponential factor obtained from the linear fit in the Arrhenius plot are 41±1 kJ.mol^{-1} and $(4\pm2)\times10^{-15}$ s for the β relaxation and 38±1 kJ.mol^{-1} and $(2\pm1)\times10^{-16}$ s for the γ relaxation. The inaccuracy in the determination of the parameters of the main relaxation does not allow a reliable VFTH fit.

The pre-exponential factor of the β (~10^{-15} s) seems clearly affected by the presence of the main relaxation process. When the α-relaxation is far enough from the β-process, τ_0 tends to coincide with that we identified as "amorphous" sample

(section 7.2) that crystallized during the data acquisition in heating steps (grey symbols in Figure 7.11), which presents a pre-exponential factor of around 10^{-13} s.

The relaxation time for the process due to MWS for which the activation energy is estimated as 71±3 kJ.mol^{-1} and τ_0 of $(2\pm1)\times10^{-18}$ s are included in Figure 7.11 as well.

7.4.2 Mobility in the amorphous phase after isothermal cold-crystallization

To complete the characterization of the semi-crystalline state, the final state achieved after isothermal cold-crystallization at -82 ºC was also analyzed (samples crystallized at -84 and -86 ºC show similar characteristics). Concerning the final states achieved after isothermal cold-crystallization at the highest temperatures (-76, -78 and -80 ºC) the main observation is the complete extinction of the main α process. The increase in the low frequency side of the last spectrum when monitoring isothermal cold-crystallization (see Figure 7.5 for T_{cr} = -80 ºC) denotes the presence of the highly constrained α' relaxation significantly shifted to lower frequencies when compared with the position of the α bulk like process. Whether the secondary relaxations still exist or also vanish is not straightforward from the spectrum. However if the location and shape of the rigid α' process are considered temperature independent in the HN fit, another process, with the characteristics of the γ relaxation, would have to be considered to reproduce the experimental spectra. Data collected after isothermal crystallization from -120 ºC to -80 ºC does not help to clarify this feature, since no maximum is perceptible.

Several relaxation are still detected in the sample cold-crystallized isothermally at a lower temperature, -82 ºC, resulting in very complex dielectric spectra. From the results presented in section 7.3 concerning isothermal cold-crystallization, it was concluded that two hours at -82 ºC is not enough time to form a fully crystalline material, since the main α-relaxation process is clearly detected in the last stage of crystallization (crystallization degree around 0.6).

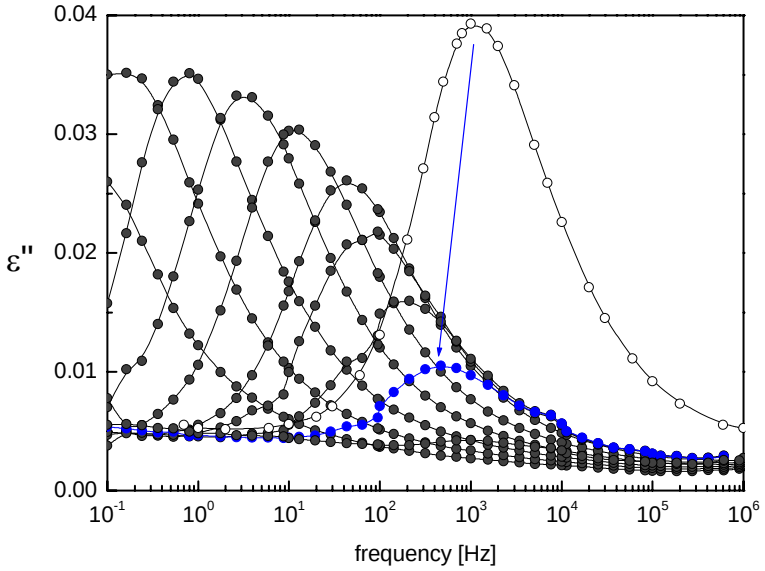

Figure 7.12 Dielectric loss spectra for EGDMA obtained after isothermal cold-crystallization at T_{cr} =-82 ºC for temperatures between -98 and -80 ºC every 2 ºC (full symbols); the isothermal at -82 ºC is shown in blue color. The ε'' curve measured at the end of the isothermal crystallization at -82 ºC (*i.e.* after 120 min) is also included (open symbols).

Figure 7.12 presents, in the temperature range from -98 to -80 ºC, the relaxation spectra of the sample previously cold-crystallized during 2 hours at -82 ºC (full symbols). Superimposed is the last loss curve collected in real time isothermal crystallization (after 2 hours at -82 ºC). The continuous disappearance of the α-process with the temperature increase (full symbols) and the big difference in the intensity of the isothermal spectrum taken at -82 ºC (blue symbols) and that collected at the end of cold-crystallization (open symbols), indicates that the sample is suffering additional cold-crystallization that leads to the extinction of the amorphous fraction. It is important to note that in these experiments each spectrum is collected every 1 ºC which favors crystallization to occur. We could not discard completely the hypothesis that also some crystallization occurred during the cooling process from -82 ºC, after isothermal crystallization, and -120 ºC.

In order to obtain a good fit of the overall spectra, multiple individual HN relaxations are needed as illustrated in Figure 7.13 At -90 ºC, the α-relaxation is the dominating process that is influenced by the γ-process at the highest frequencies. In the low frequency side a new relaxation (α') seems to emerge that becomes clearer at

higher temperatures although accompanied by a 4th process (MWS-1, plots at -70 and -60 ºC in Figure 7.13). It is important to point out that the main relaxation process detected at -90 ºC suffers a strong decrease from this temperature up to -80 ºC (Figure 7.13) due to the additional cold-crystallization. Finally at -40 ºC a 5th process (MWS-2) shows up.

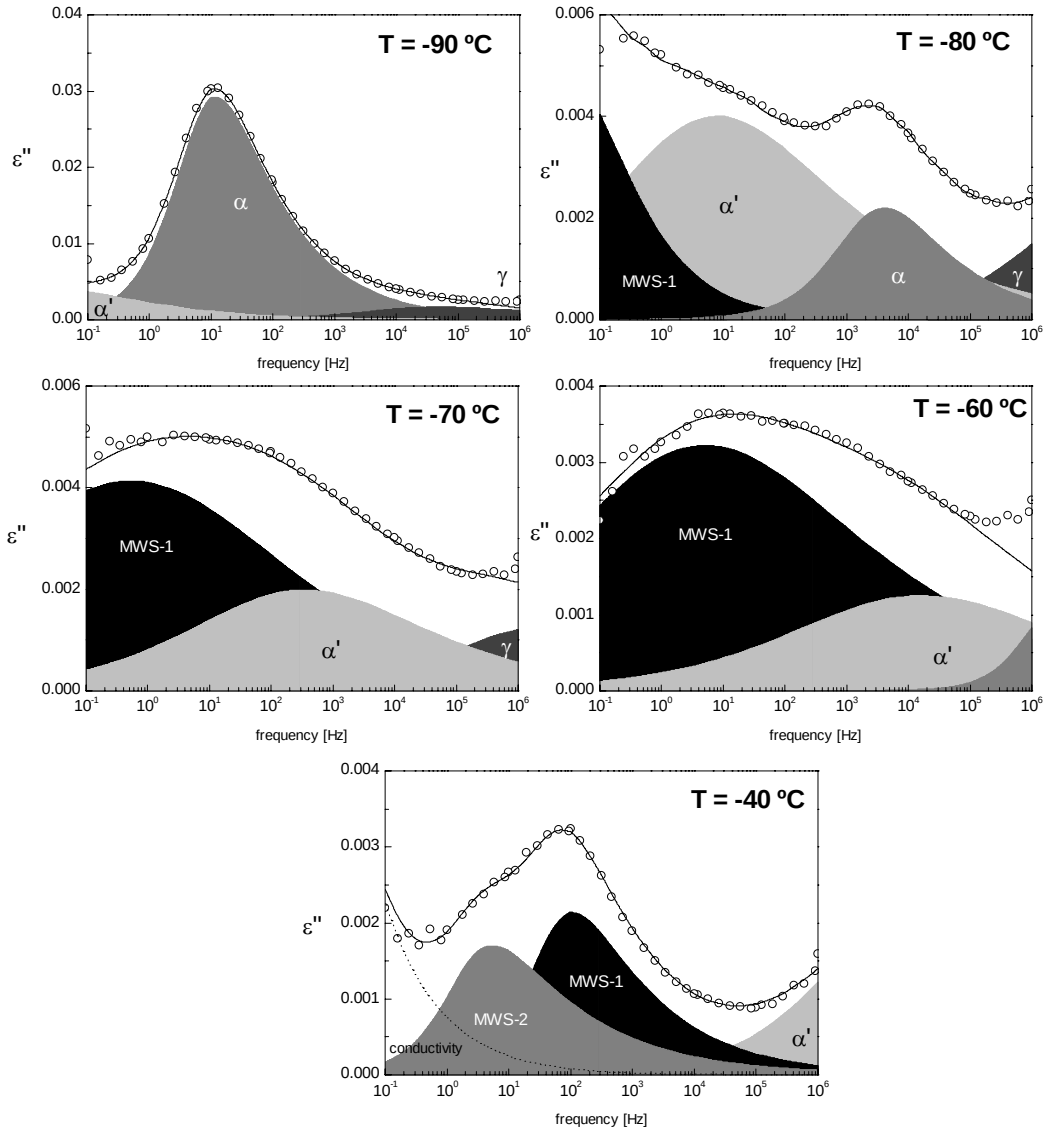

Figure 7.13 Dielectric loss spectra for EGDMA collected after isothermal cold-crystallization at -82 ºC. The overall fit (black line) and the corresponding individual HN functions (filled areas) employed to reproduce the complete ε'' spectra are included. Note a strong depletion of the α process from -90 to -80 ºC due to additional cold-crystallization.

The assignment of all these relaxations is not an easy task to do without some speculation. Nevertheless some possible explanations could be provided. At -80 ºC the 3rd relaxation process shows up as a broad shoulder on the low-frequency side of the glass transition loss peak, the later being strongly depleted as already mentioned due to further crystallization. This is exactly the same profile found by Shafee [17] for semi-crystalline poly(3-hydroxybutyrate) where the additional relaxation was attributed to eventual mobilization of the remaining amorphous material at higher temperatures.

Although the appearance of a rigid amorphous phase upon crystallization has been reported mainly in polymeric materials as PLLA [18], PPS [19], PEEK [20,21], a constrained amorphous phase is also found at an advanced crystallization degree in a low molecular weigh compound (acid dipropyl ester [4]). For this compound, the measured dielectric loss curves were able to be fitted by a superposition of two processes: the α-relaxation due to the amorphous matrix and a low frequency process related to the interface between the lamellae-like crystals within a layer thickness of less than 2 nm and thus, influenced by spatial confinement. Furthermore, in our case, the rate at which this process (α') moves in the frequency window with the temperature increase is similar to that followed by the α process, as illustrate in the relaxation map presented in Figure 7.14.

So probably it corresponds to the relaxation of a more hindered amorphous phase that, as already mentioned, gained mobility at higher temperatures as compared with the bulk-like α-relaxation. The other two processes could be related with interfacial polarization. This kind of polarization phenomenon was expected since the amorphous and crystalline phases co-exist in the material. Maybe the existence of different inter-phases due to different morphologies built in the semi-crystalline material will cause distinct Maxwell-Wagner-Sillars processes. The estimated activation energies by a linear fit of the time dependence of the respective relaxation times (presented in Table 7.4) are similar to the values found for the sample crystallized at -1 ºC.min^{-1} (melt crystallization) where such MWS effect is present and the activation energy estimated was 70 ± 2 kJ.mol^{-1}.

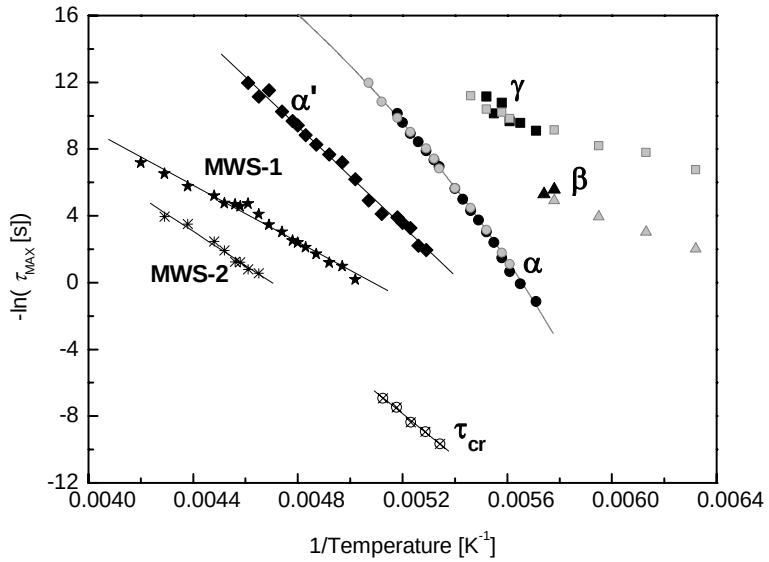

Figure 7.14 Arrhenius plot of the semicrystalline state attained after isothermal cold-crystallization at T_{cr} = -82 ºC during 2 hours. The relaxations detected in the amorphous state are included in grey symbols (the grey line is the VFTH fit for the main relaxation process). Black lines correspond to the linear fits. The crystallization time, τ_{cr} calculated from the Avrami's method in asterisks and its linear fit.

	α_{HN}	β_{HN}	E_a [kJ.mol^{-1}]	τ_0 [s]
α' (-84→-56 ºC)	0.34±0.06	0.68±0.20	134±4	(2±1)x10^{-44}
MWS-1 (-74→-35 ºC)	0.28→0.94	1→0.4	71±2	(2±1)x10^{-19}
MWS-2 (-56→-35 ºC)	0.58→0.89	0.89→0.53	70±4	(9±7)x10^{-18}

Table 7.4 Shape parameters obtained from the HN fit (α_{HN} and β_{HN}) for the different relaxation processes detected after isothermal cold-crystallization at -82 ºC (2 hours). The corresponding activation energies (E_a) and pre-exponential factors (τ_0) are also included.

At -35 ºC a huge increase of conductivity occurs impairing any further fit.

The shape parameters obtained from the HN fittings and the activation energy and pre-exponential factors are summarized in Table 7.4.

7.4.3 Comparison between different crystallization procedures

Figure 7.15 shows the normalized ε'' values at -90 ºC taken from the isothermal measurements after the different conditions of crystallization. This temperature was chosen since it is too low to induce further crystallization, and in this way it is possible to compare the final states attained. Figure 7.15 also includes the corresponding data obtained in the amorphous state (full circles).

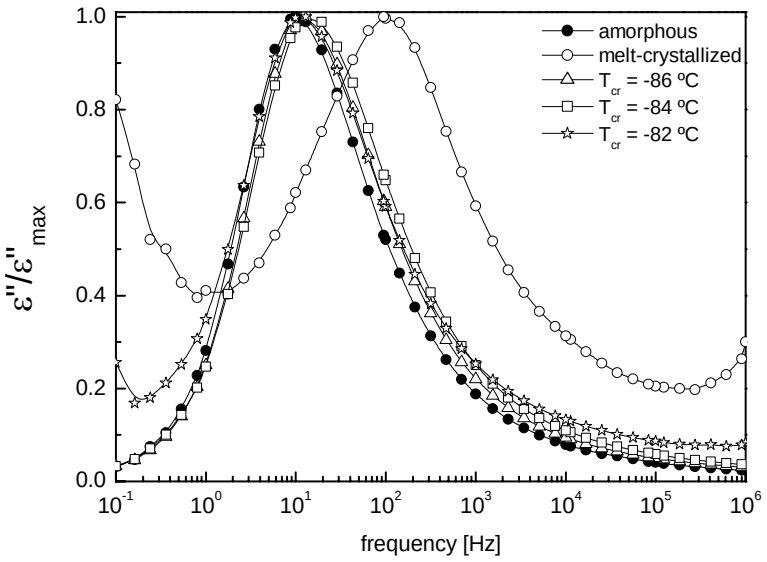

Figure 7.15 Normalized dielectric loss spectra collected at -90 ºC for EGDMA: amorphous state (full circles), after non-isothermal melt-crystallization (open circles) and after isothermal cold crystallizations at different T_{cr} (2 hours), whose symbols are indicated in figure.

One can observe that the main relaxation process keeps the same shape for the fully amorphous sample and after cold-crystallization at -86 and -84 ºC (if we also normalize the frequency axis those curves completely superimpose (not shown)).

While maintaining the same location, it increases slightly its asymmetry when detected after cold-crystallization at -82 ºC, probably due to a greater influence of the secondary relaxation processes that merge under the high frequency side with similar features to an excess wing; remember that EGDMA cold-crystallized at -82 ºC

reached a crystalline degree higher than 0.9 meaning that the intensity of the α-process that leftovers is really low (remember Figure 7.6.b). Also, there is an increase in the heterogeneity of micro-environments explored by active dipoles while suffering conformational changes.

Now it is a good opportunity to stress the sensitivity of dielectric relaxation spectroscopy that still probes the mobility in the amorphous regions under so high crystalline degrees. However, it should be emphasized that the estimation of the crystalline degree can be affected by some error since its calculation assumes a two-phase model and in cold-crystallization monitoring, an additional hindered amorphous phase was detected (α'-process). Moreover, χ_{cr} is determined through the value of the dielectric strength assuming that only the effective dipole moment is changing due to crystallization. However the density can vary and the correlation factor, g, could also change due to extra-correlations that establish under continuous crystallization.

The more evident process detected in the sample crystallized from the melt is the secondary β-relaxation but widened in the low frequency side by the submerged α-process. It is hard to verify if further crystallization occurred in this sample since, by analogy to the sample measured after cold-crystallization, is mainly the α-relaxation that felts the influence of crystallization. Given that, in this sample, the α-process is difficult to resolve from the secondary relaxations, it is complicated to conclude anything about the variation of its magnitude with the temperature increase. However since no significant changes occur in the magnitude of the single peak that accounts for the superposition of both α and β-relaxations: if the α-process would decrease due to crystallization, this would mean that the dielectric strength of the β-peak was increasing in order to compensate the α-peak decrease, which seems unreasonable. Thus it seems acceptable to conclude that no further crystallization occurred in the sample previously melt-crystallized.

7.5 Calorimetric studies

DSC was performed using a Pyris 1 apparatus (Perkin Elmer). Temperature was calibrated by using zinc and indium. The melting heat of indium was used for calibrating heat flow.[1]

The thermogram obtained by DSC at a heating rate of 10 ºC.min^{-1} (curve A in Figure 7.16) clearly shows the glass transition signature. The T_g determined as the temperature of the mid point of the heat capacity increment in the transition, is -97.5 ºC and the $\Delta c_p(T_g)$ = 114.9 J.(K.mol)$^{-1}$. The glass transition is quite narrow, covering just ΔT_g = 3.5 ºC (determined, as usual, by the temperature difference between the intersection of the tangent in the inflection point of the heat flow curve with the liquid and glassy lines respectively). The onset of the crystallization peak is -71.2 ºC and the maximum of the crystallization exotherm is at -70.5 ºC. Melting starts at -8.4 ºC and the maximum of the endotherm is at -2.0 ºC. The enthalpy increment of crystallization is 13.6 kJ.mol^{-1} while that of melting is 21.1 kJ.mol^{-1}.

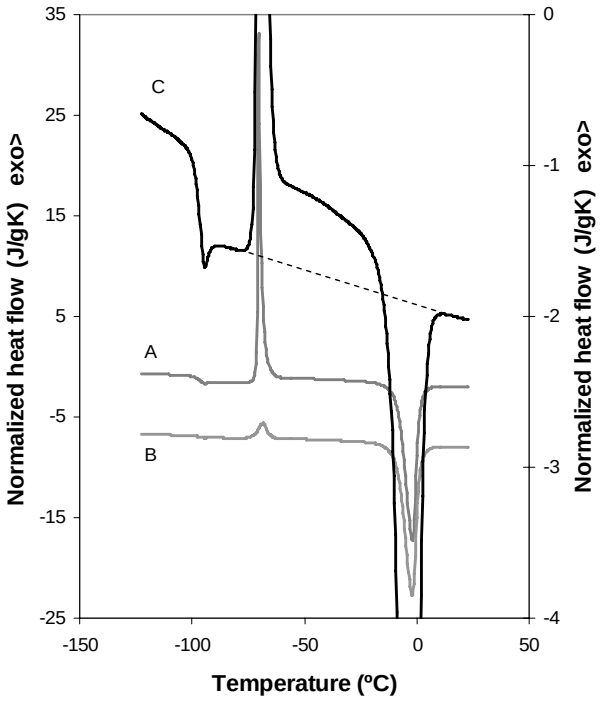

Figure 7.16 DSC thermograms recorded on heating at 10 ºC.min^{-1} measured in the sample previously cooled from 25 to -140 ºC: curve A, at 20 ºC.min^{-1} and curve B at 1 ºC.min^{-1} (left axis). The curve C is a detail in an amplified scale of curve A (right axis).

[1] The author would like to thank to C.M. Rodrigues from Chemical Department (U.N.L.) for preliminary studies and to Dr. M. Salmerón from Biomaterials Center (U.P.V.) for these measurements.

The DSC thermogram recorded on heating with a sample previously cooled at 1 ºC.min^{-1} (curve B in Figure 7.16) shows a small crystallization peak that proves that crystallization on cooling, even at this quite small rate, was not complete and the sample at the beginning of the heating scan, at -140 ºC, was a semicrystalline material. This fact is in accordance with dielectric results where melt-crystallized sample obtained in similar conditions still shows the α process (remember for example Figure 7.10). Nevertheless, contrary to dielectric measurements, the amount of amorphous phase was insufficient to show the glass transition in the calorimetric runs. The melting peak exactly matches that recorded after cooling at 20 ºC.min^{-1}.

Isothermal crystallization from melt was conducted at different temperatures between -85 and -55 ºC. The sample was cooled at 20 ºC.min^{-1} from 25 ºC to the crystallization temperature and the heat flow was recorded isothermally as a function of time. Only some of these curves are shown in Figure 7.17 for clarity. The exothermal heat flow against time shows a symmetric peak in the temperature range between -85 and -60 ºC but above this temperature the shape of the exotherm is quite irregular as shown in Figure 7.17 for the -55 ºC curve. The time at which the peak shows up shifts towards lower times between -85 ºC and -60 ºC, and then start increasing again up to -54.5 ºC. The isothermal treatment at -54 ºC showed no crystallization peak, in fact the heat flow was constant in a 200 minutes experiment, and the same result was found for higher temperatures. The position of the maximum and onset of the isothermal crystallization peak are shown in Figure 7.18.

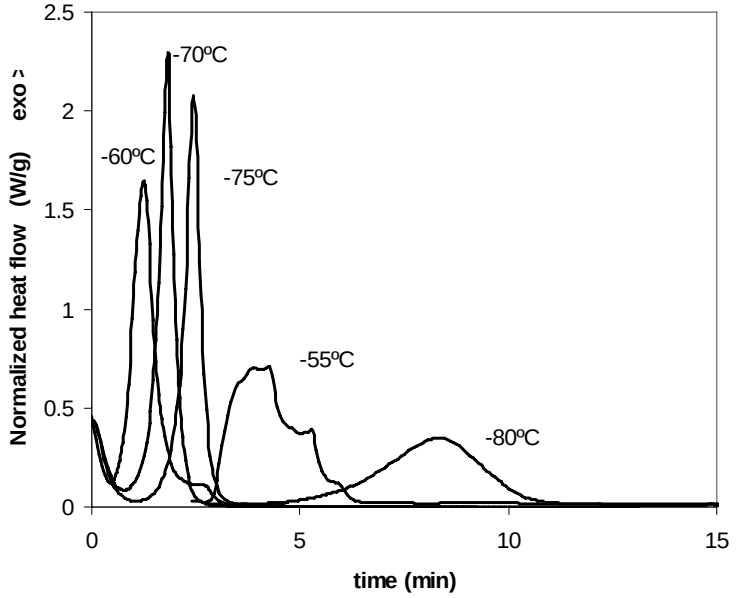

Figure 7.17 Crystallization isotherms of EGDMA melt-crystallized at several temperatures indicated next to the curve.

The crystallization enthalpy increments as a function of the crystallization temperature as shown in Figure 7.19. The points corresponding to crystallization at -65 and -70 ºC were not included since the exotherm was not complete due to the lack of heat flow stabilization before the onset of crystallization and integration of the peak is very uncertain. A heating scan recorded at 10 ºC.min^{-1} after the isothermal treatment showed the melting peak (Figure 7.20) with a shape independent of the crystallization temperature for those temperatures in which the crystallization was shown in the isothermal treatment, and no melting endotherm in the sample subjected to an isothermal annealing at temperatures equal or higher than -54 ºC, as shown in Figure 7.20.

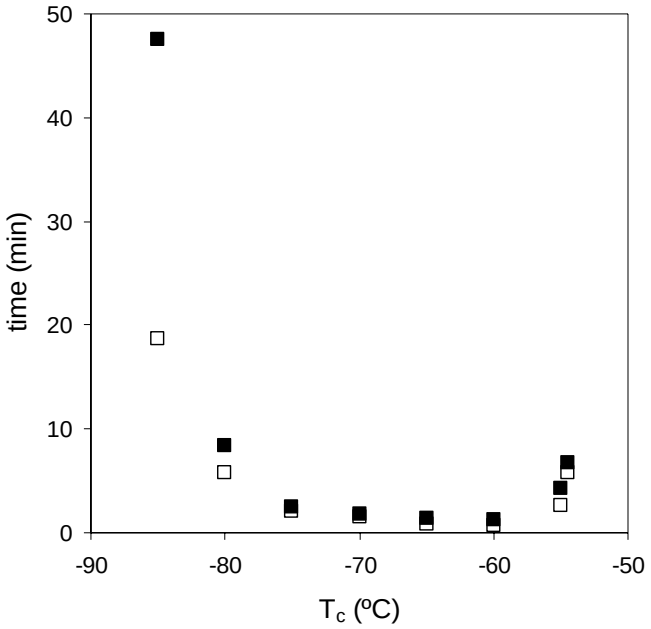

Figure 7.18 Time of the onset (□) and the maximum (■) of the isothermal crystallization peak as a function of crystallization temperature (T_c).

In order to show the role of nucleation on the crystallization kinetics of this material, the sample was cold-crystallized at -80 ºC after cooling at 20 ºC.min^{-1} from 25 to -120 ºC and then heating to the crystallization temperature (-80 ºC). Figure 7.21 compares the thermogram obtained after this nucleation treatment with the one recorded after direct cooling from 25 to -80 ºC. This figure shows as in the last treatment (cold-crystallization – curve B) there is an increment of the number of crystallization nuclei at he beginning crystallization relatively to the other one.

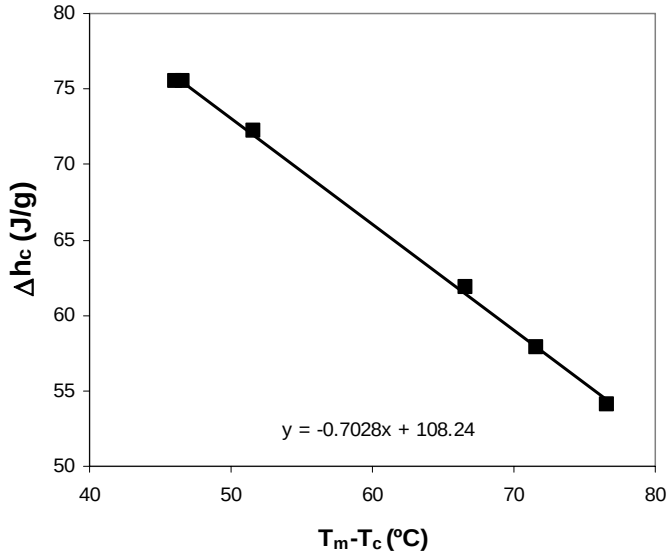

Figure 7.19 Crystallization enthalpy increment (Δh_c) *vs.* the difference between the melting (T_m) and crystallization (T_c) temperatures, determined for isothermal crystallizations from the melt.

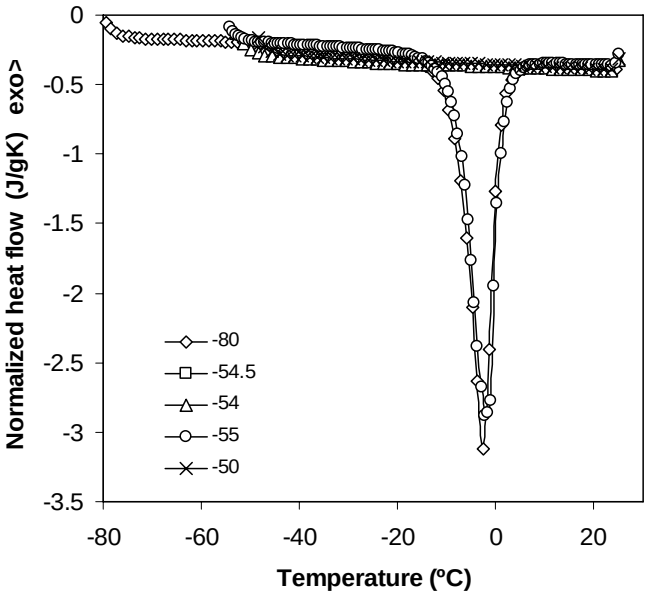

Figure 7.20 Heating scans measured at 10 ºC.min^{-1} after isothermal crystallization at different temperatures indicated inside.

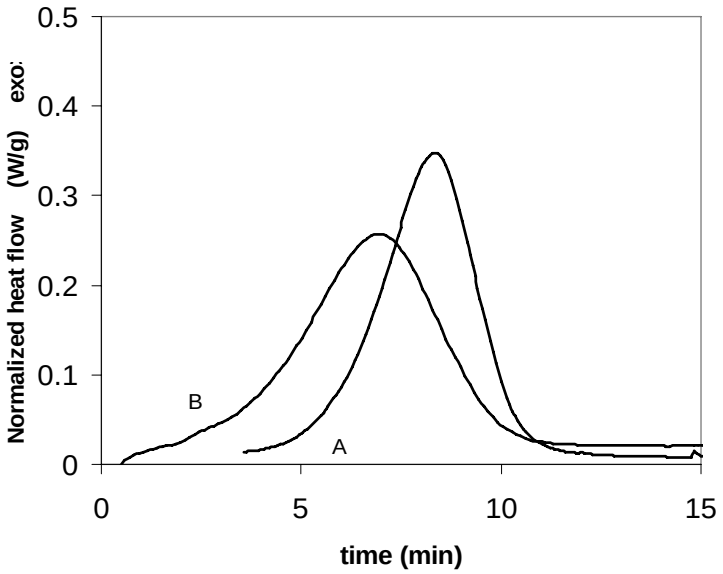

Figure 7.21 Crystallization isotherms at -80 ºC: curve A, for a sample cooled from 25 ºC to the crystallization temperature (melt-crystallized) and curve B, for another one previously cooled to -120 ºC and then heated to the crystallization temperature, *i.e.* a sample cold-crystallized.

7.6 Discussion

The mobility in the amorphous state of ethylene glycol dimethacrylate was studied in heating mode after a rapid cooling to low temperatures in order to avoid melt-crystallization since this monomer reveals a high tendency to crystallize in both cooling and heating runs. From calorimetric studies it was concluded that even at relatively high cooling rates as -20 ºC.min^{-1} some crystallization is observed.

Even so, we believe that meaningless crystallization occurred during the fast cooling of the sample, prior to the dielectric measurements, allowing characterizing the different relaxation processes detected at the lowest temperatures, as belonging to a fully amorphous material.

One of the questions addressed in the beginning of the study of this first member of the series was how their relaxation processes will fit in the trend of the other studied monomers. Essentially the same tendency was found that is: *i*) the location of the γ-relaxation looks independent of the monomer size, while its magnitude decreases with the increase of that validating the attribution of this

relaxation process to dipolar fluctuations within the ethyleneglycol moiety, *ii*) the β-process shifts to higher frequencies when compared with the its location in the other members of the series, so the β-relaxation shifts to lower times with the decrease of the size of the ethylene glycol sequence, *iii*) the mobility of the α-process increases with the decrease in the molecule size.

The available data before cold-crystallization allowed the temperature dependence of the relaxation times to be fitted by a VFTH law. The estimated T_g for τ = 100 s was -101.4 ºC very close to the value measured by DSC, -97.5 ºC, where the sample was previously rapidly cooled in order to avoid crystallization (as discussed below, some crystallization occurred but we assume that it didn't affect meaningfully the determination of the glass transition temperature).

Thus the glass transition temperature decreases with the decrease of the ethylene glycol size confirming the behavior observed for the other members of the series.

The heat capacity increment in the glass transition is quite high, $\Delta C_p(T_g)$ = 114.9 J.(K.mol)$^{-1}$, that allows us to situate this material as a thermodinamically fragile system according to the strong/fragile classification of Angell [22]. Although elevated, the variation in the heat capacity at the glass transition is inferior to the values determined for the other monomers. The same happened to the fragility index estimated from dielectric results that lead to a value of 70 slightly lower than those estimated for the other members of the series (80, 85 and 90 for n = 2, 3 and 4 respectively) revealing a less fragile behavior as also denoted by the lower curvature of the activation plot. Furthermore, the apparent activation energy is in sequence with the other systems increasing with the increase of the monomer's size (220, 276, 303, and 325 kJ.mol^{-1}, for n =1, 2, 3 and 4 respectively).

The dielectric strength before crystallizing is around 3.4 (see Annex II), value that confirms the tendency to decrease as the molecular weight decreases ($\Delta\varepsilon_\alpha$ in between 9.3-7.8 for TeEGDMA, 8.8-7, for TrEGDMA and 5.8-4.8 for DEGDMA).

If we take an average value of $\Delta\varepsilon_\alpha$ for each monomer, the increment between the three first members of the series is nearly constant (around 2) which can be attributed to the contribution of the additional ethylene glycol polar moiety, meaning that conformational arrangements of these molecules are similar. The difference

decreases when comparing to TeEGDMA, probably because the superior number of the ethylene glycol groups (n = 4) confers higher flexibility to the molecule that arranges differently in such a way that the effective dipole moment is not anymore proportional to n.

The shape parameters obtained from the HN fitting indicate that the distribution of the relaxation times in EGDMA is very similar to DEGDMA, TrEGDMA and TeEGDMA allowing constructing a master curve for the four monomers studied.

In what concerns crystallization, the first observation refers to the transitions' characteristics temperatures of EGDMA. During the DSC heating scan, measured at 10 ºC.min^{-1}, around 25 degrees above the glass transition, the liquid crystallizes (the onset of crystallization is at -71.2 ºC) and the formed crystals melt around 63 degrees above (onset of melting is at -8.4 ºC). It is interesting to note the step in the measured heat flow in the crystallization transition (curve C in Figure 7.16) that indicates the difference between the heat capacity of the liquid (at temperatures in the interval between the glass transition and the onset of crystallization) and the solid phase (at temperatures above the exothermic peak). A straight line has been drawn in Figure 7.16 joining the liquid states just above the glass transition and just above melting showing that the thermogram in the temperature interval when the sample is in the solid phase is above this line. The difference between the heat capacity of the solid and the liquid seems to be in the order of magnitude of the heat capacity increment in the glass transition as it should, since the heat capacity of the glass should be not very different form that of the crystal. The area measured in the thermogram from a temperature just above the glass transition (-85 ºC) to 20 ºC, taking the straight dashed line of Figure 7.16 as baseline for integration is slightly endothermal, around 0.8±0.4 kJ.mol^{-1} while the area of the melting peak is 20±1 kJ.mol^{-1}. This could mean that during cooling at 20 ºC.min^{-1} a few percent of the mass of the sample crystallized. Thus the sample can be not completely amorphous before the glass transition and the heat capacity increment determined from the thermogram can be slightly underestimated.

It is noteworthy the dependence of the position of the exothermal peaks measured in the isothermal crystallization (*i.e.* from melt) experiments on the

crystallization temperature. In the high temperature side of the crystallization window (Figure 7.18), the crystallization time rapidly changes with temperature, in fact the time of the maximum of the exothermic peak takes place at 5 min at -55 ºC, 7 min at -54.5 ºC but no sign of crystallization can be detected in a 200 min experiment at -54 ºC or higher temperatures. This means that crystallization nuclei are not stable above -54 ºC, *i.e.* 46 degrees below the melting temperature. In the low crystallization temperatures side of the plot of Figure 7.18, the crystallization time also increases rapidly with temperature due to the rapid decrease of the molecular mobility as the glass transition approaches.

The crystallization enthalpy decreases with undercooling as shown in Figure 7.19, and is always lower than the melting enthalpy. The reason for that is obviously the temperature dependence of the enthalpy of the liquid and the solid according to their respective heat capacity $c_{p,l}$ and $c_{p,s}$ respectively. Thus, assuming that the difference $\Delta c_p = c_{pl} - c_{ps}$ is independent of temperature, the enthalpy increment of the crystallization at temperature T_{cr} can be written as

$$\left|\Delta h_{cr}(T_{cr})\right| = h_l(T_{cr}) - h_s(T_{cr}) = h_l(T_m) - h_s(T_m) - (c_{pl} - c_{ps})(T_m - T_{cr}) \qquad \text{Equation 7.5}$$

where T_m is the equilibrium melting temperature. Equation 7.5 explains the linear dependence of Δh_{cr} with temperature and allows to determine $\Delta c_p = c_{pl} - c_{ps}$ from the experimental results, obtaining a value of $\Delta c_p = c_{pl} - c_{ps} = 139$ J.(K.mol)$^{-1}$, slightly higher than the heat capacity difference between the liquid and the glass. The fit of Equation 7.5 to the experimental values yields $h_l(T_m) - h_s(T_m) = 21$ kJ.mol^{-1} close to the values determined by integration of the melting endothermic peak in the heating scans.

The heat flow traces in the isothermal crystallization experiments stabilizes before 10 minutes for temperatures above -80 ºC (Figure 7.17), nevertheless the rapid increase of the crystallization times at lower temperatures makes that crystallization could be incomplete in crystallization times of 200 minutes in good agreement with the dielectric experiments.

Figure 7.21 shows that the influence of the nucleation treatments is significant. Cooling at 20 ºC.min^{-1} to a temperature below T_g increases the number of crystallization nuclei in the sample what accelerates the isothermal crystallization at -80 ºC. This was the thermal treatment performed to study cold crystallization in the dielectric experiments.

Isothermal cold-crystallization was also followed in real time at different temperatures by DRS, however only the low temperature side of the time-temperature diagram (Figure 7.18) was covered when compared with DSC measurements.

The main observation is the decrease of the intensity of the α process, as it would be expected, but without any significant changes in position. However the rate of the decrease of this magnitude varies with the temperature at which the isothermal crystallization undergoes. In dielectric results it was observed a continuous increase of the crystallization rate with increasing T_{cr} from -86 to -76 ºC. During the crystallization time of two hours, those accomplished at highest T_{cr} (-76, -78 and -80 ºC) attained the maximum crystallization degree. Since the crystalline phase does not show up in the dielectric measurements, it is reasonable to assume (as usual in literature [4,23,24]) a proportionality between the intensity of the α process (amorphous phase) and crystallization degree. Based in this assumption, the final states attained at those T_{cr} correspond to the full crystallization (χ_c=1). For the temperatures of -82, -84 and -86 ºC the α peak is still detected so the crystallization time was not enough to assure full crystallization.

The way how the main relaxation process evolves undergoing isothermal cold-crystallization is an important point of discussion in literature. Studies involving low molecular weigh compounds are scarce and some different results are reported. For instance, Alie *et al.* [23] found that both shape and frequency position of the α-relaxation are weakly time dependent during isothermal crystallization of a drug substance, while real-time dielectric spectroscopy of alcohols [25,26] and of an acid dipropyl ester [4] reveal a shift of the α-loss peak to lower frequencies. However, in the later, the shift only starts at a degree of crystallinity above 90%. In EGDMA neither the position nor the shape of the α-relaxation vary during the first stages of crystallization. Only at very high crystallization degrees, a slight broadening of the α peak is observed, meaning that the distribution of the large scale motion relaxation

times is enlarged as result of more heterogeneous environments originated by the crystalline phase.

The evolution of χ_{cryst} *vs.* the crystallization time was fitted by the Avrami relation giving an exponent around 2.5 which is compatible with a diffusion-controlled growth, a constant nucleation rate during transformation and a 3-dimensional growth; however this point deserves more attention in the future.

Dielectric measurements revealed a distinct mobility of the remaining amorphous phase in the semi-crystalline samples obtained under different thermal conditions.

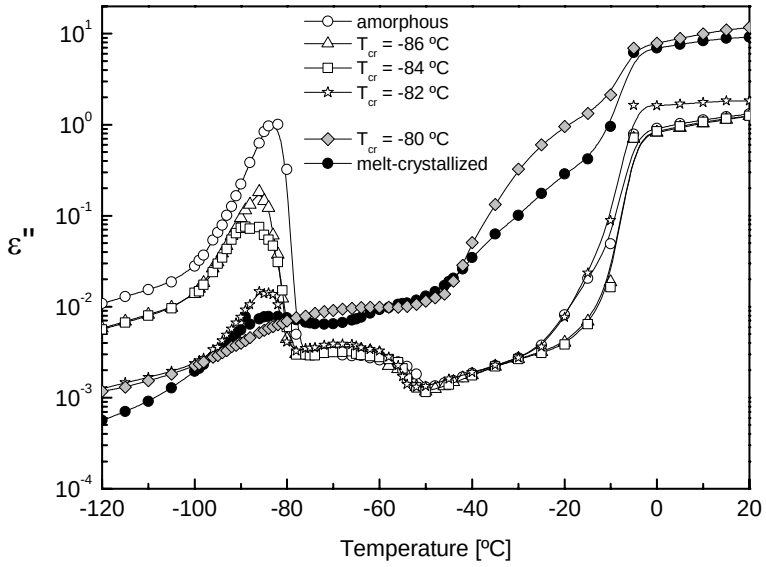

Figure 7.22 Isochronal plot of ε'' at 1 kHz taken from isothermal ascending data for amorphous and crystalline states indicated inside.

Figure 7.22 will help to differentiate the several behaviors, where the temperature dependence of ε'' is presented at 1 kHz. Two main groups can be differentiated concerning the evolution of both the α process and conductivity. The group that includes the amorphous material and samples cold-crystallized isothermally at -86, -84 and -82 ºC, and the set constituted by the sample crystallized at -80 ºC and the one melt-crystallized. In the former group, we observe an increasing depletion of the α process with the T_{cr} increase, with no change in position, followed by a broad high-temperature shoulder due to a hindered amorphous phase. At higher

temperatures two inflexions occur (at -50 ºC and -20 ºC) originated by two different MWS processes followed by a sharp increase around 0 ºC due to fusion. The sample cold-crystallized at -80 ºC no exhibits the α process, instead a very broad relaxation process that probably results from the merging of the α' hindered relaxation with the γ relaxation. A very intense MWS process follows and fusion occurs near below 0 ºC as found for the other samples. Finally, the sample melt-crystallized shows at lower temperatures a peak mainly due to the β process, although hiding the very low α relaxation, followed by MWS and fusion.

The different MWS processes observed namely between cold and melt-crystallized samples, and the narrowing of the β process in the later, lead us to conclude that different morphologies were built upon the distinct crystallization procedures or at least they were established following different steps. However, the sharp jump in ε'' (shown in Figure 7.22) due to fusion occurs at the same temperatures far all crystallization procedures.

It is interesting to point out that also the melting temperature detected by DSC (endothermic peak in Figure 7.20) is independent on the thermal history followed during the crystallization process and close to the value found by DRS (sharp jumps in ε'' shown in Figure 7.8 and Figure 7.22). From the former the onset of melting is -8.4 ºC, and from the later is around -7 ºC. According to Gibbs-Thomson equation [27,28], this fact means that the crystals formed are large enough to make insignificant their surface free energy when compared with volume free energy, since the former is responsible for the dependence of melting temperature on the crystal size. However, the sensibility of the DRS technique lets us to assume that the microstructure of the semicrystalline materials formed is different (Figure 7.22).

The relaxation strength of the main dielectric α-relaxation denotes the presence of small fractions of EGDMA molecules remaining in the liquid state at low temperatures. The small contribution of this relaxation process to the dielectric spectra shows that even in the sample crystallized from the melt by a slow cooling, at -1 ºC.min^{-1}, a fraction of the material remains in the amorphous state, as can be seen in Figure 7.10. This result agrees with that observed for the cold crystallization in a heating DSC scan recorded after the same thermal history. Something similar can be

said with respect to cold crystallization in which crystallization kinetics can be monitored by the strength of α relaxation.

But perhaps more important is the significant differences between the relaxation spectra measured after slow cooling from the melt and after cold crystallization at the highest crystallization temperatures. In both cases the material is nearly fully crystalline. As mentioned in the former paragraph only a small fraction of EGDMA remains in the liquid or amorphous state. Nevertheless after cold-crystallization a new relaxation process, we have called α', appears. It is important to remember that while in crystallization from the melt nucleation and growth occur simultaneously, in the cold-crystallization these mechanisms take place separately. In the later, a huge number of nuclei start growing simultaneously until they consume the liquid molecules, resulting in a microstructure with a great number of small crystals and a large surface of grain borders. On the contrary, during crystallization from the melt, a small number of large crystals is quickly formed leading to less number of interfaces between them.

Two possibilities arise to explain the presence of the α' peak:

i) Considering that in cold-crystallized samples fully conversion is never attained even when the α relaxation completely disappears; thus the sample can be described as composed of stable crystalline phase coexisting with a non-transformed supercooled liquid [29]. This situation was found in triphenyl phosphite where the existence of nanocrystals in the supercooled matrix was confirmed by Raman and X-ray spectroscopies [29,30]. In this case, α' can be due to the molecular mobility of the amorphous or the crystalline parts: in one hand, the liquid molecules confined in the interstitial volume between crystals present a highly restricted mobility. Therefore, its cooperative conformational motions would take place at higher temperatures relative to the liquid sample, thus the relaxation process will be detected shifted towards higher temperatures. As we have seen before, the independence of melting temperature with thermal history proves that crystal surfaces are not significant with respect to volume free energy of the crystal. Thus, the presence of liquid EGDMA molecules must be related to grain borders, and so their presence can be more important in cold-crystallized samples than in those crystallized from the melt. On the

other hand, the observed α'-relaxation could be assigned to slow motions of nanocrystals as a whole [29], which consist in the possible sliding in the grain borders. This kind of motions, possible in small crystals, would be impossible in large crystals. We must note that similar movement has been detected in semicrystalline polymers, where the polymeric lamellae slide in respect to each other providing the opportunity of additional relaxation process [31].

ii) Assuming that at the end of cold-crystallization the sample is fully crystallized (for T_{cr} higher than -80 ºC), then the α' peak could be attributed to rotational motions of the molecules in their fixed crystalline positions, as it is observed in plastic-crystals [32-34] (remember Figure 1.1).

The other interesting feature shown by the dielectric spectra is the appearance of MWS peaks in the cold-crystallized samples that are not observed in the sample crystallized from the melt reflecting the presence of larger interfaces in the former.

It will be very interesting to investigate the type of crystalline morphologies thus formed, however the X-ray analysis is not trivial since crystallization and fusion occur at sub-ambient temperatures.

The β-process in EGDMA is more defined when comparing to the other members of the series and even narrows by the effect of melt-crystallization (higher α_{HN}). This is an indication of a narrow distribution of relaxation times and thus of a more homogeneous surrounding medium. This effect has been found also in secondary relaxations of liquid crystalline polymers [35] when these pass to a higher ordered phase.

On the other hand, if we pay attention to the main relaxation process, the opposite seems to occur since the corresponding peak broadens when the crystalline fraction constrains the amorphous phase (remember that during isothermal crystallization a slight decrease in the α_{HN} parameter was found). In these terms, it is important to distinguish the origin of the main and the secondary relaxations. While the α-process deals with long-range mobility (cooperative conformational motions), the β-process is associated with short-range motions. By this way, while long-range

mobility explores different environments (bulk-like and constrained amorphous regions) the micro-environment felt by each relaxing dipole involved in local motions, such as hindered rotations, could be very similar.

Also the activation energy of the β-process after crystallization decreases from 44 to 32 kJ.mol^{-1} and the pre-exponential factor, initially estimated as 5×10^{-16} s increases to 9×10^{-13} s. These findings could be a consequence of the narrowing of the distribution of relaxation times reached after confinement induced by crystallization, as quantified by a higher α_{HN} parameter. A larger distribution of relaxation times, as found prior to crystallization, can be associated to a broader asymmetric distribution of energy barriers [36], *i.e.* in our case comprising higher energy barriers in such a way that the average value is shifted to upper ones.

In fact, the activation energy estimated by DRS is an average value and its decrease could reflect a narrower distribution of activation energies instead reflecting an easier movement. Concerning the pre-exponential factor, we could doubt about its physical meaning since the intercept is usually affected by significant error, however if we assume that its increase has a real meaning (given that it was already observed in DEGDMA (see Table 3.4)), this could be also a consequence of the change in the distribution of relaxation times.

We cannot discard the hypothesis that upon crystallization with the extinction of the α relaxation, the β process becomes less influenced by the main relaxation and consequently its activation energy would decrease and the τ_0 value would approach the expected value for local and non-cooperative processes, *i.e.* 10^{-13} s [36]. Thus the presence of the α process would induce a cooperative nature to the secondary β relaxation, lowering the pre-exponential factor and increasing the activation energy.

On the other hand, the TrEGDMA and TeEGDMA show τ_0 values about 10^{-13} s already in the amorphous state, revealing a more local and non-cooperative origin of the molecular motion behind the β relaxation. This lower sensitivity to the presence of the main relaxation process can be due to the ethylene glycol units which, acting as spacers, would facilitate the rotation that is in the origin of the β-process.

Finally we can speculate that the better resolution of the β relaxation relative to the other members of the series could be in the origin of the great tendency of EGDMA to crystallize. In fact, several authors [3,23,37,39] attribute the tendency to crystallize to the presence of a secondary relaxation whose molecular motions will be involved in the mechanism of crystallization.

Since the β relaxation keeps the same Arrhenius dynamics over the entire temperature range investigated above and below T_g (see Figure 7.11) we can accept that molecular movements involved in that secondary relaxation participate in the mechanism of crystallization as it was suggested by Menegotto *et al.* [23,38]. The authors strengthen their suspicions comparing with the temperature dependence of τ_{cr} that it is also Arrhenius type (see Figure 7.14) excluding any direct correlation with the cooperative motions in the origin of the α process. Also Hikima *et al.* [39] following isothermal crystallization in triphenylethylene, arrived to the conclusion that the β-molecular rearrangements control the growth rate of embryo/nucleus and not the α-one.

7.7 Conclusions

EGDMA monomer presents a higher tendency to crystallize than the other members of the series. However, it is easy to obtain a semi-crystalline material in both cold and melt crystallizations, but never 100% crystalline as confirmed by calorimetric measurements. Nevertheless, it seems reasonable to assume that the eventual crystallization occurred previously to dielectric measurements didn't affect the dynamical behavior of the amorphous material. Accepting this, the EGDMA monomer fits in the overall tendency of the family of n-EGDMA, where a concomitant decrease of the relaxation time for the dynamic glass transition with the molecular size is observed; the same happened with the relaxation times associated with the secondary β-relaxation, while the γ-process relaxes independently of the molecular size.

By DSC experiments the T_g obtained was -97.5 ºC, in agreement with that estimated from DRS results (-101.7 ºC). The $\Delta C_p(T_g)$ jump, although very

pronounced as found in fragile glass formers, decreases with decreasing size of ethylene glycol moiety.

Upon isothermal cold-crystallization monitored by DRS, the α-process depletes continuously with neither changing position nor shape. Only at advanced stages of crystallization a slight broadening of the relaxation process is observed and a new process evolves in the low-frequency side of the main α-peak, however well separated.

The interfacial polarization effect manifested differently in cold- and melt-crystallized samples leads to conclude that different crystalline morphologies were attained: the interfaces between crystal grains is much larger in cold-crystallized samples than in those crystallized from the melt.

The appearance of a new dipolar relaxation process α' in cold-crystallized samples can be ascribed to hindered motions taking place in amorphous molecules confined in the crystal borders. Nevertheless, reorientations of small crystals as a whole, or rotational motions of the molecules in their fixed crystalline positions, cannot be ruled out. More experiments must be done in order to further clarify the origin of this relaxation.

The calorimetric studies allow establishing a relation between the role of nucleation on the crystallization kinetics of EGDMA. The previous thermal treatment highly influences the number of crystallization nuclei, the lower the temperature attained before the isothermal crystallization the higher number of nuclei formed, diminishing the induction time to crystallization. A maximum crystallization rate was determined at -60 ºC.

Finally, if it is assumed that the secondary β-process plays a crucial role in crystallization, the higher resolution of this process relative to the γ-relaxation, could be in the origin of a superior tendency to crystallize of EGDMA relative to the other members of the series.

7.8 References

[1] B. Wunderlich, J. Chem. Phys. 29(6) (1958) 1395-1404.

[2] H.P. Diogo, J.J. Moura Ramos, J. Chem. Ed. 83(9) (2006) 1389-1392.

[3] G.P. Johari, S. Kim, R.M. Shanker, J. Pharm. Sciences 96(5) (2007) 1159-1175.

[4] J. Dobbertin, J. Hannemann, C. Shick, M. Pötter, H. Dehne, J. Chem. Phys. 108(21) (1998) 9062-9068.

[5] S.M. Dounce, J. Mundy, H-L Dai, J. Chem. Phys. 126 (2007) 191111(1-4).

[6] M. Avrami, J. Chem. Phys. 7 (1939) 1103-1112; 8 (1940) 212-224; 9 (1941) 177-184.

[7] R.H. Doremus, "Rates of Phase Transformations", Academic, Orlando (1985).

[8] I. Gutzow, J. Schmelzer, "The Vitreous State: Thermodynamics, Structure, Rheology, and Crystallization", Springer-Verlag, Berlin (1995).

[9] M.D. Ediger, C.A. Angell, S.R. Nagel, J. Phys. Chem. 100 (1996) 13200–13212.

[10] J. D. Hancock, J. H. Sharp, J. Am. Ceram. Soc. 55(2) (1972) 74-77.

[11] S.Y. Chen, C.M. Wang, S.Y. Cheng, J. Am. Ceram. Soc. 74 (1991) 2506-2512.

[12] J. Zhai, H. Chen, J. Appl. Phys. 94(1) (2003) 589-593.

[13] S. Ranganathan, M. von Heimendahl, J. Mater. Sci. 16 (1981) 2401.

[14] G. Ruitenberg, A.K. Petford-Long, R.C. Doole, J. Appl. Phys. 92 (2002) 3116.

[15] X.P. Wang, G. Corbel, S. Kodjikian, Q.F. Fang, P. Lacorrea, J. Solid State Chem. 179 (2006) 3338–3346.

[16] "Alpha high resolution dielectric/impedance analyzer", Novocontrol (2003).

[17] E. El. Shafee, Eur. Polym. J. 37 (2001) 1677-1684.

[18] M. Dionísio, M.T. Viciosa, Y. Wang, J.F. Mano, Macromol. Rap. Commun. 26 (2005) 1423–1427.

[19] P. Huo, P. Cebe, J. Polym. Sci. Part B: Polym. Phys. 30 (1992) 239-250.

[20] B. Sauer, P. Avakian, J. Starkweather, B.S. Hsiao, Macromolecules 23(24) (1992) 5119-5126.

[21] E. Schlosser, A. Schönhals, Colloid. Polym. Sci. 267 (1989) 963-969.

[22] C.A. Angell, J. Non-Cryst. Solids 13 (1991) 131-135.

[23] J. Alie, J. Menegotto, P. Cardon, H. Duplaa, A. Caron, C. Lacabanne, M. Bauer, J. Pharm. Sci., 93 (1) (2004) 218-233.

[24] M. Massalska-Arodz, G. Williams, I.K. Smith, C. Conolly, G.A. Aldridge, R. Dabrowskic, J. Chem. Soc., Faraday Trans. 94 (1998) 387-394.

[25] M. Jiménez-Ruiz, T.E. Ezquerra, I. Sics, M.T. Fernández-Díaz, App. Phys. A-Mat. Science & Process. 74: S543-S545 Part 1 Suppl. S, Dez 2002.

[26] M. Jiménez-Ruiz, A. Sanz, A. Nogales, T.A. Ezquerra, Rev. of Scient. Instr. 76 (4): Art. No. 043901 Apr 2005.

[27] B. Wunderlich, "Macromolecular Physics", Vol. 3, Academic Press, London (1980).

[28] H. Zhou; G.L. Wilkes, Polymer 38(23) (1997) 5735-5747.

[29] A. Hédoux, Y. Guinet, P. Derollez, O. Hernandez, L. Paccou, M. Descamps, J. Non Crystal. Sol 352 (2006) 4994-5000.

[30] A. Hédoux, T. Denicourt, Y. Guniet, L. Carpentier, M. Descamps, Sol. State Comm. 122 (2002) 373-378.

[31] "Viscoelastic properties of polymers", J.D. Ferry, Eds. John Wiley and Sons (1980).

[32] R. Brand, P. Lunkenheimer, A. Loidl, J. Chem. Phys. 116(23) (2002) 10386-10401.

[33] M. Descamps, N. T. Correia, P. Derollez, F. Danede, F. Capet, J. Phys. Chem. B. 109 (2005) 16092-16098.

[34] M. Dionísio, H.P. Diogo, J.P.S. Farinha, J.J.M. Ramos, J. Chem. Ed. 82 (9) (2005) 1355-1360.

[35] A. Schönhals, D. Wolff, J. Springer, Macromolecules, 28 (1995) 6254-6257.

[36] N.T. Correia, J.J. Moura Ramos, Phys. Chem. Chem. Phys. 2 (2000) 5712-5715.

[37] K. Kamiński, M. Paluch, J. Ziolo, K.L. Ngai, J. Phys.:Condens. Matter 18 (2006)5607-5615.

[38] J. Menegotto, J. Alié, C. Lacabanne, M. Bauer, Dielectric Newsletter, Novocontrol GmbH (2004).

[39] T. Hikima, M. Hanaya, M. Oguni, J. Mol. Struct. 479 (1999) 245-250.

CHAPTER 8 CONCLUSIONS

By the first time in literature a detailed dielectric characterization of the set of n-EGDMA monomers for n = 1 to 4 is provided. Both dielectric and thermal measurements show that these materials easily avoid crystallization, being classified as molecular glass-formers.

The glass transition temperatures, T_g, detected by DSC and estimated from dielectric data, are in very good agreement. It was shown that the corresponding value increases with the number of ethylene-glycol unities from around -98 ºC for EGDMA to -83 ºC for TeEGDMA.

The dielectric spectra for the four monomers present, beside the α relaxation process ascribed to cooperative motions associated to the glass transition, two more secondary relaxations due to local motions: the β process related to the rotation of the carboxyl groups, and the γ process, associated to the ethylene glycol twisting motions. While the size of the ethylene glycol group clearly influences the temperature location of the α and β relaxations, the γ process seems to be indifferent to it.

In the relaxation map, the relaxation time temperature dependence of the dominating α process presents the curvature assigned to fragile glass formers, while the dependence of the relaxation times of both secondary relaxations follows Arrhenian behavior.

Monitoring the isothermal free radical polymerization of TrEGDMA (n = 3) by TMDSC and dielectric experiments, it was possible to verify that the phase separation between the unreacted monomer and the network formed occurs from the early stages of the reaction. This result was determinant to study the influence of the polymerization on the relaxation processes detected in bulk monomers. Also following the polymerization, the moment where vitrification occurs was easily detected by a sharp decrease in the measured C_p', without any previous peak as discussed in literature.

The formation of covalent bonds by the isothermal polymerization of the n = 2 to 4 monomers leaded to the progressive extinction of the α and β relaxation processes detected in pure monomers, and the increase of the intensity of the γ secondary process, possibly due to a preferential orientation of the dipole residing in the ethylene glycol moieties in the polymer. However, no significant changes in

frequency/temperature location were found in any of the relaxation process, independently the monomer employed. This is the principal feature that allows us to conclude that the new relaxation process detected in the partial or full polymerized samples, does not derive directly from that of the monomers, *i.e.* its mobility is independent of that presented in the original monomers.

The relaxation process detected in the full polymerized networks named β_{pol}, seems to be similar to that detected in other poly-alkyl methacrylates, related to reorientational process of the side group involving some coordination with the main chain.

Since a dense network is formed upon full polymerization, no glass transition relaxation was detected either by dielectric relaxation or by DSC. Thus, TrEGDMA monomer was copolymerized with methylacrylate, a softer constituent, allowing the detection of T_g in a large composition range. By extrapolating the composition dependence of the glass transition temperature to neat poly-TrEGDMA, it was possible to estimate a value of the glass transition temperature of 160 ºC.

Additionally, EGDMA, the smallest monomer studied, apart from vitrifying also shows a high tendency to crystallize by coming from both, melt and glassy states. In both cases, the onset of the melting and crystallization peaks appear markedly displaced.

The isothermal crystallization in the supercooled state was analyzed in terms of Avrami's method where a exponent comprised between 2 and 2.8 was found. Calorimetric measurements allowed establishing a dependence of the crystallization time on the crystallization temperature which passes through a maximum at -65 ºC.

Crystallization pathway, and consequently morphology, is affected by nucleation and crystal growth that in turn depends on the thermal history in the formation of the crystal phase. Depending on this morphology amorphous molecules are entrapped between crystals and dielectric relaxation is sensible to their mobility. In determined circumstances, it was possible to obtain a crystalline material where the cooperative motions are completely suppressed while the secondary β process is detected. This finding let us to hypothesize that the molecular motions in the origin of this local process, can play an important role in this different behavior of this monomer regarding amorphous/crystalline transformation when compared with the other ones. This point opens a way through future work.

ANNEXES

Annex I.

a) HN fitting parameters for the main (α) and secondary processes (β and γ) of DEGDMA monomer in the bulk state.

	α - relaxation			β - relaxation				γ - relaxation			
Temp. [°C]	Δε	α	β	τ_{max} [s]	Δε	α	β	τ_{max} [s]	Δε	α	β	τ_{max} [s]
-115	---	---	---	---	0.16	0.81	0.40	8.60E-01	0.18	0.44	0.45	1.92E-03
-114	---	---	---	---	0.14	0.81	0.40	5.35E-01	0.18	0.44	0.45	1.57E-03
-112	---	---	---	---	0.14	0.81	0.40	3.63E-01	0.19	0.44	0.45	1.22E-03
-110	---	---	---	---	0.14	0.80	0.42	2.33E-01	0.19	0.45	0.46	8.01E-04
-108	---	---	---	---	0.14	0.78	0.43	1.35E-01	0.19	0.45	0.46	5.34E-04
-106	---	---	---	---	0.14	0.77	0.43	9.89E-02	0.19	0.46	0.46	4.36E-04
-104	---	---	---	---	0.14	0.77	0.43	6.85E-02	0.19	0.46	0.46	2.98E-04
-102	---	---	---	---	0.15	0.75	0.43	4.31E-02	0.19	0.46	0.46	1.98E-04
-100	---	---	---	---	0.14	0.76	0.43	3.00E-02	0.19	0.47	0.46	1.65E-04
-98	---	---	---	---	0.14	0.77	0.44	1.95E-02	0.20	0.48	0.46	1.28E-04
-96	---	---	---	---	0.14	0.77	0.44	1.56E-02	0.21	0.48	0.47	1.11E-04
-94	---	---	---	---	0.14	0.77	0.44	1.17E-02	0.22	0.48	0.47	8.92E-05
-92	---	---	---	---	---	---	---	---	0.24	0.50	0.48	6.20E-05
-90	5.85	0.90	0.51	3.32E+00	---	---	---	---	0.34	0.51	0.50	2.80E-05
-88	5.79	0.91	0.52	6.89E-01	---	---	---	---	0.37	0.46	0.57	4.66E-05
-86	5.74	0.91	0.49	1.46E-01	---	---	---	---	0.38	0.40	0.59	3.14E-05
-84	5.66	0.91	0.51	3.67E-02	---	---	---	---	0.41	0.38	0.59	1.80E-05
-82	5.60	0.91	0.51	1.04E-02	---	---	---	---	0.43	0.43	0.59	1.94E-05
-80	5.56	0.92	0.49	3.18E-03	---	---	---	---	---	---	---	---
-78	5.50	0.89	0.53	9.89E-04	---	---	---	---	---	---	---	---
-76	5.46	0.89	0.53	3.51E-04	---	---	---	---	---	---	---	---
-74	5.39	0.89	0.54	1.18E-04	---	---	---	---	---	---	---	---
-72	5.34	0.89	0.54	5.28E-05	---	---	---	---	---	---	---	---
-70	5.28	0.90	0.54	2.03E-05	---	---	---	---	---	---	---	---
-68	5.23	0.91	0.54	8.82E-06	---	---	---	---	---	---	---	---
-66	5.16	0.92	0.54	4.41E-06	---	---	---	---	---	---	---	---
-64	5.10	0.95	0.51	2.27E-06	---	---	---	---	---	---	---	---
-62	5.03	0.95	0.53	1.07E-06	---	---	---	---	---	---	---	---
-60	4.99	0.96	0.52	6.47E-07	---	---	---	---	---	---	---	---
-55	4.88	0.97	0.52	1.66E-07	---	---	---	---	---	---	---	---

b) HN fitting parameters for the main (α) and secondary processes (β and γ) of TrEGDMA monomer in the bulk state.

	α - relaxation				β - relaxation				γ - relaxation			
Temp. [°C]	Δε	α	β	τ_{max} [s]	Δε	α	β	τ_{max} [s]	Δε	α	β	τ_{max} [s]
-115	---	---	---	---	0.12	0.44	0.75	1.39E+00	0.25	0.36	0.56	1.81E-03
-110	---	---	---	---	0.12	0.51	0.76	6.00E-01	0.27	0.38	0.55	9.21E-04
-105	---	---	---	---	0.11	0.51	0.77	2.76E-01	0.28	0.38	0.56	4.31E-04
-100	---	---	---	---	0.12	0.54	0.79	8.96E-02	0.29	0.42	0.48	2.02E-04
-98	---	---	---	---	0.11	0.55	0.79	7.83E-02	0.31	0.38	0.58	1.87E-04
-96	---	---	---	---	0.14	0.48	0.83	7.86E-02	0.32	0.37	0.60	1.43E-04
-94	---	---	---	---	0.15	0.47	0.77	6.44E-02	0.33	0.38	0.54	1.10E-04
-92	---	---	---	---	0.18	0.45	0.81	4.49E-02	0.32	0.42	0.49	7.60E-05
-90	---	---	---	---	0.22	0.41	0.83	3.56E-02	0.33	0.40	0.54	5.94E-05
-88	---	---	---	---	0.25	0.45	0.83	1.64E-02	0.37	0.42	0.51	4.77E-05
-86	---	---	---	---	---	---	---	---	0.42	0.40	0.51	3.92E-05
-84	8.76	1.00	0.45	2.01E+00	---	---	---	---	0.44	0.47	0.64	2.81E-05
-82	8.64	0.94	0.49	3.18E-01	---	---	---	---	0.46	0.53	0.55	9.47E-06
-80	8.57	0.92	0.51	7.28E-02	---	---	---	---	0.46	0.54	0.57	8.44E-06
-78	8.49	0.93	0.49	1.87E-02	---	---	---	---	0.47	0.48	0.57	4.94E-06
-76	8.30	0.95	0.48	5.43E-03	---	---	---	---	0.49	0.48	0.50	3.28E-06
-74	8.28	0.95	0.47	1.66E-03	---	---	---	---	---	---	---	---
-72	8.16	0.95	0.47	5.67E-04	---	---	---	---	---	---	---	---
-70	8.04	0.95	0.47	2.09E-04	---	---	---	---	---	---	---	---
-68	8.03	0.95	0.46	8.12E-05	---	---	---	---	---	---	---	---
-66	7.92	0.94	0.47	3.33E-05	---	---	---	---	---	---	---	---
-64	7.82	0.95	0.47	1.48E-05	---	---	---	---	---	---	---	---
-62	7.77	0.95	0.46	6.79E-06	---	---	---	---	---	---	---	---
-60	7.70	0.95	0.45	3.33E-06	---	---	---	---	---	---	---	---
-58	7.64	0.97	0.43	1.76E-06	---	---	---	---	---	---	---	---
-56	7.64	0.94	0.48	8.90E-07	---	---	---	---	---	---	---	---
-54	7.56	0.97	0.43	5.07E-07	---	---	---	---	---	---	---	---
-52	7.50	0.96	0.44	2.84E-07	---	---	---	---	---	---	---	---
-50	7.44	0.97	0.44	1.69E-07	---	---	---	---	---	---	---	---
-48	7.37	0.96	0.44	1.00E-07	---	---	---	---	---	---	---	---

c) HN fitting parameters for the main (α) and secondary processes (β and γ) of TeEGDMA monomer in the bulk state.

	α - relaxation				β - relaxation				γ - relaxation			
Temp. [°C]	Δε	α	β	τ_{max} [s]	Δε	α	β	τ_{max} [s]	Δε	α	β	τ_{max} [s]
-115	---	---	---	---	0.17	0.79	0.40	3.34E+00	0.32	0.40	0.44	2.17E-03
-114	---	---	---	---	0.17	0.75	0.41	2.73E+00	0.32	0.40	0.44	1.73E-03
-112	---	---	---	---	0.19	0.66	0.50	2.33E+00	0.32	0.40	0.46	1.28E-03
-110	---	---	---	---	0.19	0.61	0.57	1.64E+00	0.33	0.40	0.48	8.78E-04
-108	---	---	---	---	0.20	0.58	0.61	1.12E+00	0.33	0.42	0.45	6.32E-04
-106	---	---	---	---	0.22	0.50	0.73	1.04E+00	0.34	0.40	0.50	4.58E-04
-104	---	---	---	---	0.23	0.46	0.80	8.98E-01	0.34	0.39	0.51	3.33E-04
-102	---	---	---	---	0.24	0.44	0.81	6.05E-01	0.35	0.42	0.46	2.42E-04
-100	---	---	---	---	0.25	0.42	0.85	4.29E-01	0.35	0.41	0.48	1.67E-04
-98	---	---	---	---	0.27	0.40	0.87	3.34E-01	0.34	0.41	0.49	1.24E-04
-96	---	---	---	---	0.28	0.40	0.86	2.29E-01	0.35	0.42	0.48	8.78E-05
-94	---	---	---	---	0.29	0.40	0.87	2.19E-01	0.35	0.43	0.47	7.61E-05
-92	---	---	---	---	0.30	0.36	0.87	1.49E-01	0.35	0.42	0.49	5.76E-05
-90	---	---	---	---	0.33	0.40	0.85	1.35E-01	0.36	0.43	0.48	4.59E-05
-88	---	---	---	---	0.32	0.43	0.75	7.53E-02	0.37	0.44	0.46	3.32E-05
-86	---	---	---	---	0.33	0.45	0.67	4.66E-02	0.41	0.42	0.50	3.06E-05
-84	---	---	---	---	---	---	---	---	0.44	0.39	0.57	3.19E-05
-82	9.32	0.96	0.51	4.30E+00	---	---	---	---	0.46	0.47	0.60	2.22E-05
-80	9.24	0.90	0.49	6.39E-01	---	---	---	---	0.47	0.65	0.49	2.20E-05
-78	9.10	0.89	0.50	1.24E-01	---	---	---	---	0.47	0.62	0.55	1.06E-05
-76	8.99	0.92	0.47	3.10E-02	---	---	---	---	0.48	0.55	0.50	6.12E-06
-74	8.81	0.93	0.46	9.33E-03	---	---	---	---	0.49	0.57	0.44	5.46E-06
-72	8.70	0.94	0.44	2.70E-03	---	---	---	---	0.50	0.37	0.50	2.28E-06
-70	8.63	0.95	0.43	9.00E-04	---	---	---	---	---	---	---	---
-68	8.52	0.94	0.44	3.45E-04	---	---	---	---	---	---	---	---
-66	8.47	0.95	0.52	1.46E-04	---	---	---	---	---	---	---	---
-64	8.37	0.96	0.42	5.90E-05	---	---	---	---	---	---	---	---
-62	8.21	0.94	0.44	2.48E-05	---	---	---	---	---	---	---	---
-60	8.12	0.95	0.43	1.17E-05	---	---	---	---	---	---	---	---
-55	7.89	0.92	0.46	2.16E-06	---	---	---	---	---	---	---	---

Annex II.

a) HN fitting parameters that were fixed (except for T_{cr} = -80 and -78 ºC where the α_{HN} parameters varies) during the fitting procedure of data corresponding to the isothermal cold-crystallization of EGDMA at the temperatures indicated inside.

T_{cryst} [ºC]	α	α'	γ
-86	α_{HN} = 0.95 β_{HN} = 0.49 τ_{HN} = 2.5x10^{-3}	α_{HN} =0.50 β_{HN} =0.94 τ_{HN} =1.0 x 10^{-5}	α_{HN} =0.78 β_{HN} =0.53 τ_{HN} =2.2 x 10^{-8}
-84	α_{HN} =0.95 β_{HN} =0.48 τ_{HN} =8.4 x 10^{-4}	α_{HN} =0.50 β_{HN} =0.94 τ_{HN} =5.0 x 10^{-2}	α_{HN} =0.78 β_{HN} =0.53 τ_{HN} =2.9 x 10^{-8}
-82	α_{HN} =0.94 β_{HN} =0.48 τ_{HN} =2.8 x 10^{-4}	α_{HN} =0.40 β_{HN} =0.75 τ_{HN} =2.9 x 10^{-2}	α_{HN} =0.78 β_{HN} =0.53 τ_{HN} =2.0 x 10^{-7}
-80	α_{HN} =0.98→0.59 β_{HN} =0.45 τ_{HN} =1.0 x 10^{-4}	α_{HN} =0.36 β_{HN} =0.95 τ_{HN} =5.2 x 10^{-2}	α_{HN} =0.45 β_{HN} =0.61 τ_{HN} =3.0 x 10^{-8}
-78	α_{HN} =0.99→0.87 β_{HN} =0.48 τ_{HN} =(3.8±1.3) x 10^{-5}	α_{HN} =0.40 β_{HN} =0.44 τ_{HN} =8.0 x 10^{-2}	α_{HN} =0.52 β_{HN} =0.61 τ_{HN} =1.0 x 10^{-7}
-76	α_{HN} =0.97 β_{HN} =0.35 τ_{HN} =2.8 x 10^{-5}	α_{HN} =0.23 β_{HN} =0.99 τ_{HN} =1.0 x 10^{-1}	α_{HN} =0.52 β_{HN} =0.65 τ_{HN} =2.0 x 10^{-8}

b) HN fitting parameters for the main (α) and secondary processes (β and γ) of EGDMA starting in the amorphous state.

Temp. [°C]	α - relaxation				β - relaxation				γ - relaxation			
	Δε	α	β	τ_{max} [s]	Δε	α	β	τ_{max} [s]	Δε	α	β	τ_{max} [s]
-115	---	---	---	---	0.108	0.41	0.92	1.31E-01	0.090	0.32	0.44	1.15E-03
-110	---	---	---	---	0.097	0.45	0.94	4.82E-02	0.090	0.39	0.40	4.09E-04
-105	---	---	---	---	0.068	0.56	0.95	1.93E-02	0.109	0.44	0.44	2.74E-04
-100	---	---	---	---	0.097	0.56	0.95	7.26E-03	0.127	0.45	0.42	1.08E-04
-95	3.410	0.92	0.53	3.33E-01	---	---	---	---	0.205	0.47	0.44	5.37E-05
-94	3.448	0.92	0.52	1.68E-01	---	---	---	---	0.225	0.39	0.45	3.71E-05
-92	3.486	0.92	0.53	4.23E-02	---	---	---	---	0.210	0.43	0.47	3.09E-05
-90	3.400	0.94	0.53	1.15E-02	---	---	---	---	0.245	0.40	0.44	1.37E-05
-88	3.518	0.92	0.53	3.48E-03	---	---	---	---	---	---	---	---
-86	3.484	0.92	0.53	1.09E-03	---	---	---	---	---	---	---	---
-85	3.190	0.92	0.53	6.01E-04	---	---	---	---	---	---	---	---
-84	1.934	0.93	0.49	3.28E-04	---	---	---	---	---	---	---	---
-82	1.110	0.91	0.53	1.20E-04	---	---	---	---	---	---	---	---
-80	0.487	0.91	0.53	5.20E-05	---	---	---	---	---	---	---	---
-78	0.291	0.93	0.47	1.94E-05	0.063	0.37	0.96	3.67E-04	---	---	---	---
-76	0.050	0.95	0.47	6.32E-06	0.055	0.55	0.69	2.06E-04	---	---	---	---
-75	---	---	---	---	0.051	0.52	0.98	2.07E-04	---	---	---	---
-74	---	---	---	---	0.050	0.53	1.00	1.84E-04	---	---	---	---
-72	---	---	---	---	0.049	0.55	0.89	1.55E-04	---	---	---	---
-70	---	---	---	---	0.048	0.57	0.90	1.27E-04	---	---	---	---
-68	---	---	---	---	0.046	0.58	0.96	1.03E-04	---	---	---	---
-66	---	---	---	---	0.054	0.53	1.00	9.49E-05	---	---	---	---
-65	---	---	---	---	0.048	0.59	0.89	8.19E-05	---	---	---	---
-64	---	---	---	---	0.049	0.58	1.00	7.57E-05	---	---	---	---
-62	---	---	---	---	0.049	0.61	0.99	7.09E-05	---	---	---	---
-60	---	---	---	---	0.051	0.60	0.99	5.95E-05	---	---	---	---
-58	---	---	---	---	0.048	0.63	1.00	5.17E-05	---	---	---	---
-56	---	---	---	---	0.047	0.65	0.97	4.37E-05	---	---	---	---
-55	---	---	---	---	0.040	0.70	0.83	3.22E-05	---	---	---	---
-54	---	---	---	---	0.040	0.69	1.00	3.43E-05	---	---	---	---
-52	---	---	---	---	0.032	0.78	1.00	2.877E-05	---	---	---	---
-50	---	---	---	---	0.033	0.74	0.99	2.50E-05	---	---	---	---
-48	---	---	---	---	0.022	0.86	0.98	2.00E-05	---	---	---	---